Dissertation zur Erlangung des Doktorgrades
der Fakultät für Chemie und Pharmazie
der Ludwig-Maximilians-Universität München

Ionic Hyaluronic Acid Coating and cRGD Modification of siRNA Polyplexes

Victoria Caroline Vetter
aus Leverkusen, Deutschland

2025

Erklärung

Diese Dissertation wurde im Sinne von § 7 der Promotionsordnung vom 28. November 2011 von Herrn Prof. Dr. Ernst Wagner betreut.

Eidesstattliche Versicherung

Diese Dissertation wurde eigenständig und ohne unerlaubte Hilfe erarbeitet.

München, 27.03.2025

.....

Victoria Vetter

Dissertation eingereicht am	27.03.2025
1. Gutachter:	Prof. Dr. Ernst Wagner
2. Gutachter:	Prof. Dr. Stefan Zahler
Mündliche Prüfung am	08.05.2025

Meiner Familie

Table of Contents

1 Introduction 7

1.1 Nucleic acid-based therapeutics: an overview 7

1.2 siRNA therapeutics: advancements and mechanisms 7

1.3 Nucleic acid delivery: from viral to non-viral vectors 8

1.4 Design of oligoaminoamide-based polyplexes for nucleic acid delivery 10

1.5 Optimizing siRNA polyplexes for tumor therapy 11

1.6 Aim of the thesis 13

2 Targeting nucleic acid-based therapeutics to tumors: challenges and strategies for polyplexes 15

2.1 Abstract 16

2.2 Introduction 16

2.3 Overview of barriers 18

2.4 Blood circulation and protein corona 19

2.5 Vascular barrier 20

2.5.1 Mechanisms of extravasation 20

2.5.2 Active targeting of tumor vasculature 25

2.5.3 Active targeting of the Blood-Brain-Barrier (BBB) and Blood-Brain-Tumor-Barrier (BBTB) 29

2.6 Tumor microenvironment and stroma 35

2.7 Tumor cell targeting 38

2.7.1 Transferrin receptor 45

2.7.2 Epidermal growth factor receptor 47

2.7.3 Folate receptor 48

2.7.4 Integrin $a_v\beta_3$ 49

2.7.5 Antibodies 50

2.7.6 c-Met 51
2.7.7 Anionic polymers 51
2.7.8 Dual targeting 51
2.8 Molecular therapeutic strategies 52
2.8.1 Therapeutic pDNA polyplexes 58
2.8.2 Therapeutic siRNA polyplexes 61
2.8.3 Therapeutic miRNA polyplexes 62
2.8.4 Other therapeutic RNA polyplexes 63
2.9 Conclusion 65

3 Ionic coating of siRNA polyplexes with cRGD–PEG–hyaluronic acid to modulate serum stability and in vivo performance 67

3.1 Abstract 68
3.2 Introduction 68
3.3 Materials and Methods 71
3.3.1 Materials 71
3.3.2 Methods 72
3.4 Results and Discussion 82
3.4.1 Design of a tunable ionic HA coating for siRNA polyplexes 82
3.4.2 Cell association and gene silencing efficiency of HA-coated polyplexes 86
3.4.3 Physicochemical characteristics and functionality of HA-coated polyplexes after serum incubation 93
3.4.4 *In vivo* biodistribution of HA-coated polyplexes 100
3.4.5 *In vivo* gene silencing efficiency 102
3.5 Conclusions 105

4 Summary 107

5 Appendix 109

5.1 Supplementary information..... 109

5.1.1 Analytical methods 109

5.1.2 Supporting tables..... 110

5.1.3 Supporting figures and schemes 119

5.2 Abbreviations..... 128

6 References 132

7 Publications 159

7.1 Review article 159

7.2 Research articles..... 159

8 Acknowledgments.....160

1 Introduction

This chapter briefly introduces the research field of polyplex-based nucleic acid delivery to tumors. It does not aim to cover the entire scientific area but serves to contextualize the data presented in this thesis.

1.1 Nucleic acid-based therapeutics: an overview

Nucleic acids have emerged as a revolutionary class of therapeutic agents, providing innovative approaches for treating diseases such as genetic disorders, cancers, and viral infections—many of which were once considered 'undruggable'. Unlike conventional therapies that primarily target proteins and often yield only transient therapeutic effects, nucleic acid-based therapeutics act at the molecular level by modulating the expression of disease-associated genes through mechanisms such as gene replacement, repair, or downregulation. By directly targeting the underlying causes of these diseases, nucleic acid-based therapies offer the potential for more durable therapeutic outcomes and, in some instances, even curative interventions.

The concept of using nucleic acids as therapeutic agents was first proposed in the early 1970s when Friedmann and Roblin introduced the groundbreaking idea that gene therapy could be employed to treat human genetic diseases [1]. This vision came to fruition several decades later with the approval of Glybera in 2012 [2]. Glybera, which uses an adeno-associated virus (AAV) vector encoding for lipoprotein lipase (LPL), became the first nucleic acid-based product to receive marketing authorization from the European Commission (EC). Since then, the field has seen remarkable growth, with more than 32 gene therapeutics and 34 RNA-based therapeutics currently approved globally and over 4000 in development [2].

Therapeutic nucleic acids used in gene and RNA therapies encompass a diverse range of molecules, including plasmid DNA (pDNA), messenger RNA (mRNA), small interfering RNA (siRNA), guide RNA (gRNA), and antisense oligonucleotides (ASOs). The choice of a specific nucleic acid for therapeutic application depends on the underlying disease mechanism and the intended therapeutic strategy—whether to restore, enhance, or suppress gene function.

1.2 siRNA therapeutics: advancements and mechanisms

siRNA has emerged as a vital therapeutic tool for addressing diseases caused by the overexpression of specific genes. As of today, six siRNA-based therapies have been

authorized for clinical use by both the U.S. Food and Drug Administration (FDA) and the EC: Patisiran, Givosiran, Lumasiran, Inclisiran, Vutrisiran, and Nedosiran [2]. These therapeutics leverage the ability of siRNA to downregulate gene expression through the RNA interference (RNAi) pathway, a mechanism first discovered in 1998 [3, 4].

Upon delivery to the cytosol of a target cell, siRNA—a double-stranded molecule typically 21 nucleotides in length—integrates into the RNA-induced silencing complex (RISC). The siRNA duplex is unwound within RISC, and the passenger (sense) strand is discarded. The remaining guide (antisense) strand then directs RISC to complementary sequences within the disease-associated mRNA. Argonaute-2, a key protein of RISC, subsequently catalyzes the cleavage of the target mRNA [5-7], thereby suppressing protein translation and mitigating the expression of the disease-related gene, as illustrated in **Scheme 1**.

Despite the remarkable progress achieved with siRNA therapeutics, their current clinical application is restricted to diseases originating in the liver. This limitation highlights the predominant challenge of achieving efficient and targeted delivery to a broader range of tissues and cells. To fully unlock the therapeutic potential of siRNA and enable extension to a larger spectrum of diseases, overcoming these delivery barriers through innovative technologies is critical.

1.3 Nucleic acid delivery: from viral to non-viral vectors

In the bloodstream, unprotected nucleic acids are highly susceptible to rapid degradation by nucleases. Furthermore, their charge, large size, and hydrophilicity hinder their efficient uptake into target cells by impeding passage through the lipid bilayer of cell membranes. Therefore, encapsulating therapeutic nucleic acids within delivery systems is crucial for clinical application. These systems must protect nucleic acids from degradation, ensure effective delivery to target cells via the bloodstream, facilitate cellular uptake, and enable intracellular release of the therapeutic payload by promoting endosomal escape (**Scheme 1**). Ideally, these systems should also exhibit high biocompatibility and low immunogenicity.

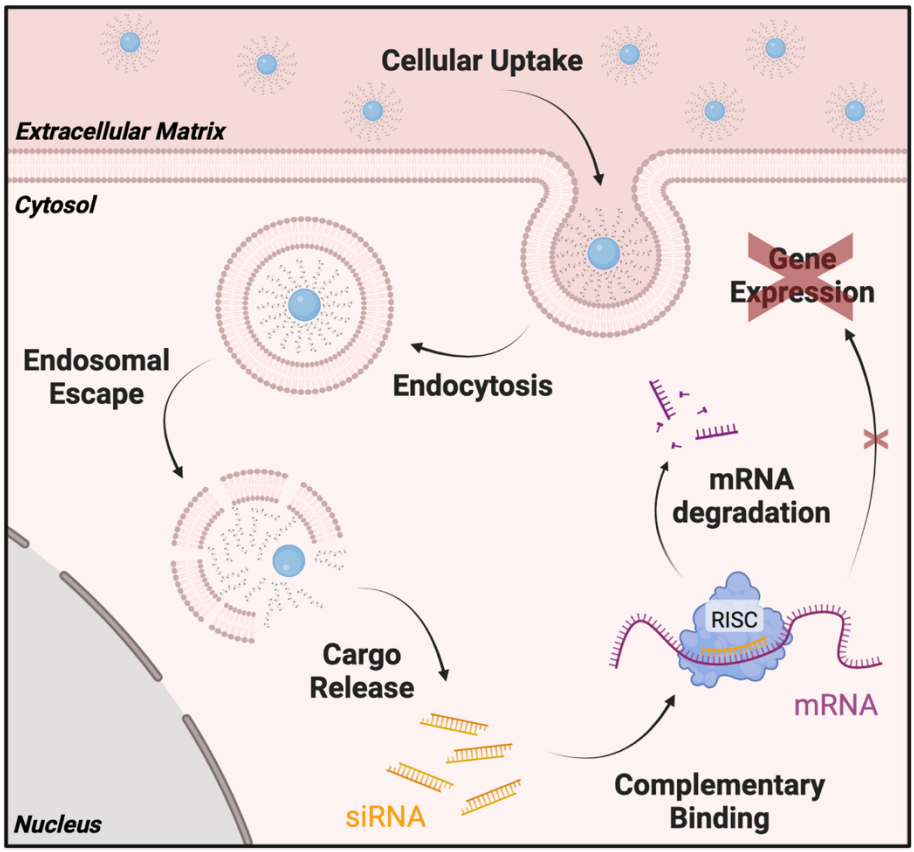

Scheme 1. Schematic representation of siRNA transfection via non-viral delivery systems and the subsequent gene silencing mechanism. Delivery to the target cell is followed by the cellular uptake of delivery systems (e.g., polyplexes) via endocytosis, after which endosomal escape enables the release of siRNA. The guide strand of siRNA is incorporated into the RNA-induced silencing complex (RISC), which binds to complementary mRNA, inducing its degradation and suppressing gene expression. Created with BioRender.com.

Historically, viral vectors have been the most widely applied delivery systems, given their natural ability to transport nucleic acids into host cells. Consequently, viral vectors currently account for most gene therapeutics that have received market approval [2, 8]. However, there has been a noticeable shift towards using non-viral delivery systems in recent years, particularly evident among approved RNA-based therapeutics [2, 9]. For instance, most siRNA products employ chemically modified nucleic acids conjugated with N-Acetyl-D-Galactosamine (GalNAc) to enhance stability and facilitate targeted delivery [10]. Furthermore, the encapsulation of RNA within lipid nanoparticles (LNPs) has proven highly effective. Notable examples include Onpattro (Patisiran), the first approved siRNA therapeutic for hereditary transthyretin amyloidosis [11], and the mRNA-based COVID-19 vaccines, which have immunized millions worldwide [12-14].

This paradigm shift towards non-viral delivery systems is primarily driven by several limitations of viral vectors, including immunogenicity—which precludes repeated dosing—limited cargo capacity, restricted cell tropism, and the complexity of production

and quality control. In contrast, non-viral vectors offer advantages such as higher encapsulation efficiency, greater adaptability, more effortless scalability, and reduced production costs [15].

Non-viral vectors can be broadly divided into two main categories: lipid-based carriers including lipoplexes, lipo-polyplexes, liposomes, and LNPs; and polymer-based carriers, such as polymeric micelles, polyplexes, and hydrogels [15-20]. While LNPs have demonstrated notable clinical success, as previously mentioned, each carrier type presents unique advantages concerning stability, encapsulation capacity, biocompatibility, and delivery efficiency.

Among these non-viral delivery systems, polyplexes—nanoscale complexes formed through entropy-driven electrostatic interactions of polycations with anionic nucleic acids—are particularly valued for their high encapsulation efficiency, stability, efficient cellular delivery, and ability to facilitate endosomal escape. In addition, polyplexes offer substantial flexibility in modulating circulation time and biodistribution, as their size, charge, and surface properties can be readily customized.

To optimize nucleic acid delivery using polyplexes, a variety of cationic polymers has been investigated, including poly-L-lysine (PLL) [21-23], polyethylenimine (PEI) [24-27], poly-N-oligoethylenimino-aspartamides [28], methacrylates [29-31], dendrimers [32-34], and, as utilized in this thesis, sequenced-defined artificial oligoaminoamide (OAA) peptides [35-38].

1.4 Design of oligoaminoamide-based polyplexes for nucleic acid delivery

Sequence-defined OAAs are synthesized using standard solid phase supported synthesis (SPSS). This precise method enables the generation of OAA libraries with diverse structural topologies by combining natural and artificial amino acids, such as the cationizable polyaminoamide motif succinoyl tetraethylene pentamine (Stp) [36].

Since polyplex-based nucleic acid delivery does not adhere to a “one-size-fits-all” approach, carriers must be designed to meet the specific requirements of each payload type and application. By modifying the amino acid sequence, key polyplex properties—such as stability, encapsulation capacity, cellular uptake, and endosomal escape efficiency—can be systematically refined for optimal performance.

Polyplex stability is crucial for effective nucleic acid delivery to cells, with the choice of stabilization strategies varying based on the specific nucleic acid type. For instance, cationizable hydrophilic structures are particularly effective in promoting pDNA compaction and delivery, while siRNA delivery benefits from stabilizing elements such

as lipidic residues (e.g., oleic acid), tyrosines, and disulfide-forming cysteines, which enhance structural integrity and functionality [19, 35, 39-44].

Polyplex stability is also highly dependent on the nitrogen-to-phosphate (N/P) ratio, which represents the ratio of protonatable amines (N) in the carrier to phosphate groups (P) in the nucleic acid. Positively charged (cationic) polyplexes, achieved at higher N/P ratios, are generally preferred as they ensure complete cargo encapsulation, enhance particle stability, and facilitate cellular uptake through electrostatic interactions with the negatively charged cell membrane [45-47].

In addition to stability, the intracellular release of the nucleic acid payload is essential for achieving therapeutic efficacy. OAA carriers can address this challenge by incorporating buffering elements, such as the polyaminoamide motif Stp or imidazole-containing histidines (with a pKa of 6) [41, 48]. While the buffering amines remain unprotonated at physiological pH, they become protonated in the acidic environment of late endosomes (pH 5.5). This protonation facilitates endosomal escape via mechanisms such as the proton sponge effect or membrane destabilization by the polycations [49], ultimately releasing the cargo into the cytosol.

Optimizing OAA-based polyplexes requires a thorough understanding of structure-activity relationships. Despite significant advancements in the field, systematic *in vitro* and *in vivo* screenings of OAA libraries remain crucial for identifying carriers suited to specific therapeutic applications. However, recent progress in methodologies, such as Design of Experiments (DoE) and *in silico* approaches leveraging artificial intelligence, has the potential to streamline and accelerate the complex optimization process, providing powerful tools that may support researchers in the future [50-52].

1.5 Optimizing siRNA polyplexes for tumor therapy

Cancer remains a significant global health challenge and is one of the leading causes of mortality worldwide [53-56]. Despite advancements in treatment, conventional therapies—such as radiotherapy, surgery, and chemotherapy—often fail to provide definitive cures and are frequently associated with severe side effects. In recent years, nucleic acid therapeutics, particularly siRNA, have emerged as a promising alternative due to their ability to target and modulate tumor-promoting gene expression specifically. However, the clinical application of these therapeutics is still limited by the challenges associated with their efficient delivery to tumor cells.

Given the necessity of systemic administration, tumor-targeted siRNA therapeutics must navigate several biological obstacles, including circulation in the bloodstream,

interactions with blood components, binding to and penetrating tumor endothelial cells (TECs), migrating through the extracellular matrix (ECM), and ultimately being taken up by tumor cells. One promising approach to address these challenges is the encapsulation of siRNA into polyplexes with engineered surface modifications for shielding and targeting.

Shielding strategies aim to neutralize the positive surface charge of polyplexes, reducing undesirable interactions in the bloodstream, non-specific cellular uptake, rapid clearance by the reticuloendothelial system (RES), and associated toxicity [26, 57-59]. By prolonging circulation time, shielding also facilitates polyplex accumulation in the tumor vasculature, which serves as a critical entry point into the tumor microenvironment. Additionally, modifications related to shielding—such as alterations in surface charge and particle size—have enhanced polyplex penetration through the dense and heterogeneous ECM that separates tumor cells from the vasculature [60, 61].

Various molecules have been investigated for shielding purposes, including the widely used polymer polyethylene glycol (PEG) [26, 62-64] and polyanions such as hyaluronic acid (HA), poly-L-aspartate, poly-L-glutamate, and polyacrylate [65-69].

In addition to shielding, targeting strategies—either active or passive—can enhance the delivery efficiency of polyplexes by increasing tumor specificity. Passive targeting leverages the enhanced permeability and retention (EPR) effect, allowing polyplexes with optimized physicochemical properties and prolonged circulation to extravasate through the characteristic leaky tumor vasculature into the ECM [70-74]. Conversely, active targeting involves functionalizing the polyplex surface with ligands such as peptides [75, 76], antibodies [77, 78], proteins [23, 79], or carbohydrates [80-82] that selectively bind to receptors overexpressed on cancer cells or TECs.

The formulation development of shielded and targeted polyplexes is a complex process that requires meticulous optimization to overcome the various *in vivo* barriers. A key challenge in this process is the accurate evaluation of polyplex formulations *in vitro*, as currently available *in vitro* models often fail to mimic the dynamic and multifactorial nature of *in vivo* conditions [65, 83, 84]. While specific factors, such as blood-polyplex interactions, can be studied *in vitro*, a holistic assessment of polyplex performance still necessitates testing in living organisms. Although *in silico* modeling techniques are increasingly utilized to predict the *in vivo* behavior of optimized formulations [85], these approaches are not yet fully capable of capturing the complexity of biological systems and, therefore, cannot entirely replace animal models. Consequently, while advancements in *in vitro* and *in silico* approaches contribute to developing polyplex

formulations, comprehensive *in vivo* testing remains essential for ensuring the successful implementation of nucleic acid delivery strategies.

1.6 Aim of the thesis

Nucleic acid-based therapeutics have markedly advanced modern medicine, offering innovative treatment strategies for diseases that were previously challenging to manage. Among these, small interfering RNA (siRNA) has emerged as a potential modality in tumor therapy due to its capacity to selectively target and modulate the expression of tumor-promoting genes. However, despite advancements in delivery systems, the clinical translation of siRNA therapeutics remains hindered by substantial challenges in achieving efficient and tumor-specific delivery.

Polyplexes, promising non-viral nucleic acid carriers known for their stability, high encapsulation efficiency, and endosomal escape capability, still face limitations *in vivo*. In particular, their positive surface charge, while beneficial for nucleic acid complexation and cellular uptake, can also trigger immune system activation, toxicity, and non-specific accumulation. To overcome these limitations, developing strategies for surface shielding and ligand modification is essential to enhance the targeted delivery of polyplexes and thereby enable the clinical application of siRNA in tumor therapy.

The aim of this thesis was to enhance the systemic delivery of OAA-based siRNA polyplexes to tumors by implementing strategies for both shielding and targeting. Building on prior successful studies, hyaluronic acid (HA), an endogenous polyanion, was chosen as the shielding agent. The cationic core polyplexes were to be ionically coated with HA to mitigate key delivery obstacles. The HA coating was expected to mask the positive surface charge of polyplexes, thereby reducing non-specific interactions in the bloodstream, preventing rapid clearance, prolonging circulation, and minimizing potential toxicity. Furthermore, HA was to function as a targeting ligand due to its binding affinity for CD44, a receptor commonly overexpressed on cancer cells and tumor endothelial cells (TECs).

The initial objective was to develop the ionic HA coating by systematically varying the HA-to-polyplex ratio. Physicochemical parameters, including particle size, siRNA compaction, and zeta potential, were to be analyzed to identify the optimal ratio of HA disaccharide units per Stp.

After selecting an optimal HA unit/Stp ratio, the HA-coated polyplexes were to be functionalized with a secondary targeting ligand to further enhance tumor-specific

accumulation. For this purpose, cyclic RGDfK (cRGD), a peptide with high affinity for integrin αvβ3—another receptor commonly overexpressed on TECs—was to be utilized. To facilitate the conjugation of cRGD to the HA coating via strain-promoted alkyne-azide cycloaddition (SPAAC), HA was to be modified with dibenzocyclooctyne (DBCO) moieties. Correspondingly, the targeting ligand was to be equipped with a terminal azide, either directly or via a short PEG spacer, to improve its presentation on the polyplex surface. HA modified only with azido-PEG was to serve as a negative control in all experiments.

The newly developed HA- and cRGD-modified polyplexes were to be characterized in dynamic light scattering (DLS) and gel shift studies to assess whether the additional ligand modification affected their physicochemical properties.

Subsequently, a series of *in vitro* studies were to be conducted. These studies aimed to evaluate cell association, uptake, gene silencing efficiency, endocytosis pathways, and cytotoxicity across multiple cell lines, focusing on assessing potential shielding and targeting effects.

To evaluate the integrity and functionality of the HA- and cRGD-modified polyplexes under physiological conditions, further physicochemical and *in vitro* studies were to be performed following prolonged incubation in full serum. These studies were to assess particle size, siRNA compaction, and transfection efficiency. In addition, fluorescence cross-correlation spectroscopy was to be employed to confirm the stable association of the ionic HA coating with the polyplex during serum incubation.

Finally, in collaboration with veterinarians of our research group, the HA- and cRGD-functionalized polyplexes were to be evaluated *in vivo* in a Neuro2A tumor-bearing mouse model, again focusing on potential shielding and targeting effects. First, Cy7-labeled polyplexes were to be injected intravenously to assess the biodistribution of the various formulations. Following this, the *in vivo* gene silencing efficiency of the systemically administered shielded and targeted polyplexes, encapsulating siEG5, was to be assessed in tumors.

2 Targeting nucleic acid-based therapeutics to tumors: challenges and strategies for polyplexes

*Victoria C. Vetter,[1] Ernst Wagner[1,2]**

[1]Pharmaceutical Biotechnology, Center for System-Based Drug Research, Ludwig-Maximilians-Universität (LMU), Munich 81377, Germany

[2]Center for NanoScience (CeNS), Ludwig-Maximilians-Universität, Munich 81377, Germany

* Corresponding author at: Pharmaceutical Biotechnology, Center for System-Based Drug Research, Ludwig-Maximilians-Universität, Munich 81377, Germany. E-mail address: ernst.wagner@cup.uni-muenchen.de (E. Wagner)

This chapter is adapted from a review article published in the **Journal of Controlled Release in June 2022, volume 346, pages 110-135, [86] Copyright Elsevier.**

Graphical Abstract

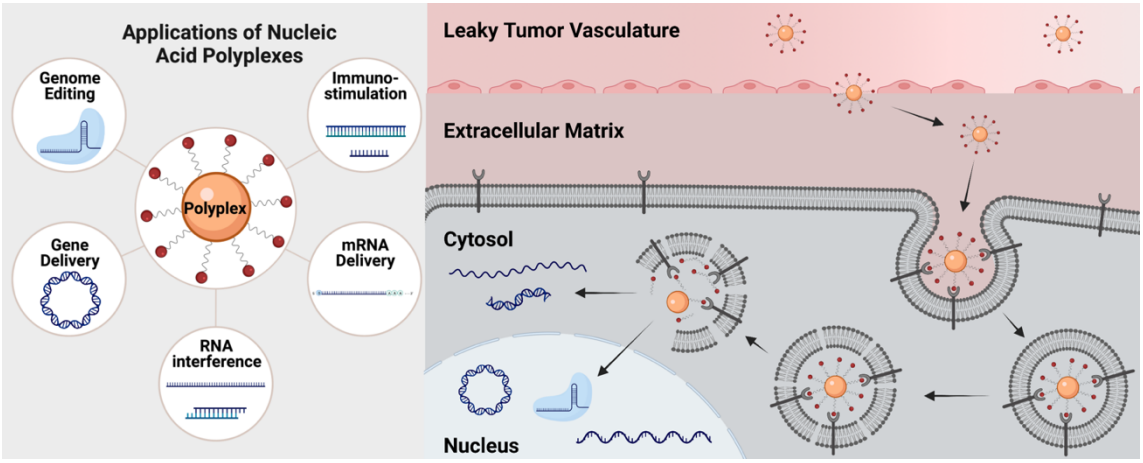

Created with BioRender.com

Keywords

Cancer, nanoparticle, pDNA, polyplex, siRNA, targeting

2.1 Abstract

The current medical reality of cancer gene therapy is reflected by more than ten approved products on the global market, including oncolytic and other viral vectors and CAR T-cells as ex vivo gene-modified cell therapeutics. The development of synthetic antitumoral nucleic acid therapeutics has been proceeding at a lower but steady pace, fueled by a plethora of alternative nucleic acid platforms (from various antisense oligonucleotides, siRNA, microRNA, lncRNA, sgRNA, to larger mRNA and DNA) and several classes of physical and chemical delivery technologies. This review summarizes the challenges and strategies for tumor-targeted nucleic acid delivery. Focusing primarily on polyplexes (polycation complexes) as nanocarriers, delivery options across multiple barriers into tumor cells are illustrated.

2.2 Introduction

Nucleic acid therapy is an exciting novel approach for cancer therapy and a promising alternative to the common tumor treatment regimen. Irradiation, surgery, and chemotherapy come along with severe side effects due to a lack of specificity towards tumor cells, or reduced efficacy due to development of chemoresistance. As cancer remains one of the deadliest diseases worldwide [55, 56], finding efficient, selective, and non-toxic drugs or drug combinations is of great interest. Nucleic acid therapies are expected to meet this challenge enabling specific modification of gene expression in tumor cells. Using viral vectors, several cancer gene therapies have reached the medical market (Gendicine in 2004, Oncorine in 2005, Imlygic in 2015, Delytact in 2021). In addition, between 2017 and 2021 six CAR T-cell products (Kymriah, Yescarta, Tecartus, Breyanzi, Abecma, Relma-cel) have been approved as most successful representatives of *ex vivo* cancer gene therapeutics [87]. The lower gene transfer efficacy of nonviral approaches hampered their clinical development into *in vivo* cancer gene therapies. Early research with plasmid DNA (pDNA) focused on the delivery of antitumoral or immunostimulatory genes and cancer vaccinations [88]. Subsequently, the clinical research focus shifted towards the delivery of short interfering RNA (siRNA), a short double-stranded RNA that can knock down tumor-promoting gene expression through sequence-specific degradation of messenger RNA (mRNA). Antitumoral effects of single or combinations of siRNAs have preclinically proven the effectiveness, and first clinical studies have been conducted [89-91]. Outside the cancer area, the first siRNAs have already been approved for genetic diseases that can be ameliorated by gene silencing in hepatocytes. Patisiran is the first siRNA drug on market formulated into lipid

nanoparticles (LNPs), followed by Givosiran, Lumasiran and Inclisiran, which are tri-GalNAc (N-Acetylgalactosamine) conjugates of chemically stabilized siRNAs [11, 92, 93]. Most recently other RNA formats, including messenger RNA (mRNA) [94-96] or CRISPR Cas9/single guide RNA (sgRNA) [97-99], have entered the therapeutic area. The world-wide use of Comirnaty and Moderna COVID-19 mRNA LNP vaccines proved their potency for vaccination [100-102] and paved the way also for cancer mRNA vaccines and related immunotherapies [103, 104]. Although the abovementioned therapeutic achievements sound very promising, they are primarily based on well-established technologies for *ex vivo*, local, or hepatic nucleic acid transfer.

Intravenous delivery of nucleic acid-based drugs to tumors remains challenging. Trying to meet the needs, in the last three decades a multitude of non-viral nucleic acid carriers have been developed, dividable into two major groups – lipid-based and polymer-based carrier systems [20]. Lipid based carriers include lipoplexes [88, 105-108], lipo-polyplexes [109, 110] and the now medically established class of LNPs [11, 97, 111]. Polymer-based carriers [19, 112-116] include polymeric micelles/polyplexes and hydrogels [18]. In this report, we summarize the continuous evolution of polyplexes for tumor-targeted nucleic acid delivery. Polyplexes consist of anionic nucleic acid complexed with cationic polymers by electrostatic and other interactions into spherical, often positively charged nanoparticles. A variety of cationic polymers have been investigated for this purpose, including poly-L-lysine (PLL) derivatives [21-23], polyethylenimine (PEI) and derivatives [24-27], poly-N-oligoethylenimino-aspartamides [28], methacrylates [29-31], dendrimers [32-34] and, in our recent own work, synthetic amino ethylene-based peptide-like sequences [35-38]. For a detailed description of polyplexes the reader is referred to other published work [19, 114-116]. Unmodified polyplexes are prone to interactions with blood components and tend to accumulate in tissues non-specifically. Consequently, functionalizing polyplexes with targeting and shielding moieties is essential to increase tumor accumulation, eliminate adverse effects and reduce required therapeutic doses. An ideal polyplex will provide the right balance between preferential nanoparticle size of 20-200 nm, stability and circulation in blood, protection of nucleic acid against degradation, extravasation, and specific uptake into target cells, and facilitating endosomal escape with release of cargo at the proper intracellular location. Most importantly, biocompatibility and absence of toxicity must always be maintained. Here we review current strategies along the delivery path of a polyplex from its intravenous injection to the tumor, pointing out the extracellular and intracellular barriers, possibilities to overcome them, potential targeting approaches and required polyplex specifications for every step of delivery.

2.3 Overview of barriers

Nucleic acid delivery is a versatile process involving many limiting extracellular and intracellular barriers, ranging from the macroscopic patient level to the microscopic tissue level to the nanoscopic organelle and supramolecular level (**Figure 1**). DNA/RNA nanoagents must comprise special features to overcome all of these hurdles [117], optionally in a dynamic pre-programmed fashion as stimuli-responsive nanorobots [118-120]. When polyplexes are first injected to blood, ideally intravenously, they are rapidly distributed to the body through blood vessels, where they are confronted by prevailing blood conditions and components. While circulating in the bloodstream, polyplexes will eventually flow through tumor vasculature where they must cross the lining tumor endothelial cells to enter tumor tissue.

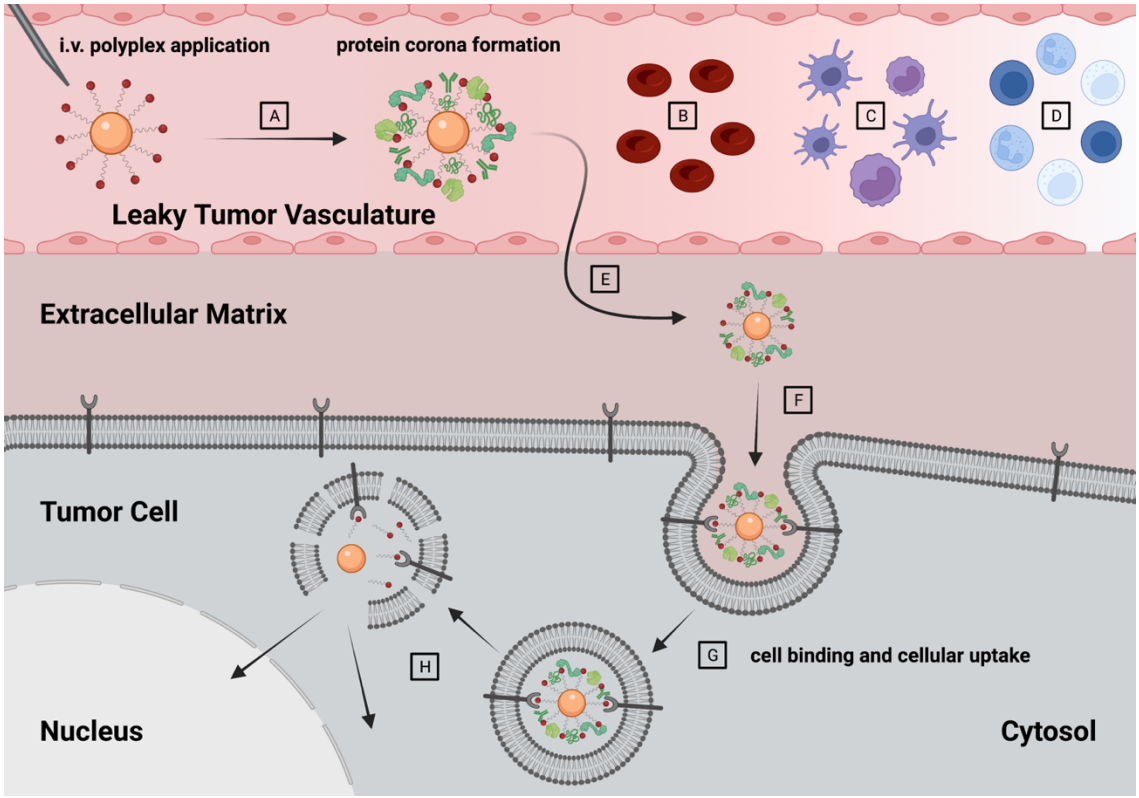

Figure 1. Extra- and intracellular obstacles for systemically applied polyplexes. In the blood stream, systemically applied polyplexes may be opsonized by blood components and/or proteins forming a biomolecular/protein corona (A). The protein corona may alter the delivery efficiency of polyplexes by masking targeting ligands or by hampering endosomal escape. Interaction of polyplexes with blood cells, especially erythrocytes (B), may lead to the formation of aggregates which can cause severe toxicity. The mononuclear phagocyte system (C) may eliminate polyplexes from the blood stream and the recognition by immune cells (D) may lead to the induction of immune reactions. To deliver nucleic acids to tumor cells, intravenously applied polyplexes must extravasate from tumor vasculature (E), penetrate the tumor extracellular matrix (F), bind to the tumor cell and be internalized via endocytosis (G), and finally escape the endosome and release the cargo to the proper intracellular compartment (H). Created with BioRender.com.

After extravasation, polyplexes face the extracellular matrix (ECM) of tumors, which surrounds and connects tumor cells and tumor vasculature. Penetration deep into the ECM is necessary to reach the tumor cell membrane, where active uptake *via* endocytosis and encapsulation into endosomes is initiated upon arrival. Endosomal escape, one of the most critical processes in nucleic acid delivery, is the major strategy after internalization to avoid endo/lysosomal degradation or recycling back to the cell membrane. Polyplexes must support the release of their nucleic acid cargo at the proper intracellular compartment in functional form. In doing so, siRNA and mRNA should remain in the cytosol, pDNA, splicing-modulating oligonucleotides or genome-editing RNPs (ribonucleoproteins) must enter the nucleus. Taken together, numerous limiting barriers on the way to the tumor cell may hamper nucleic acid delivery, yet some tumor-specific distinct characteristics provide unique favorable delivery options which polyplexes can be addressed to for specific cancer targeting.

2.4 Blood circulation and protein corona

When a polyplex upon injection enters the blood stream (**Figure 1**), it is confronted by enzymes, plasma proteins, the reticuloendothelial system (RES), phagocytic cells and many other components present in blood [26, 62, 84, 121]. Polyplexes are rapidly opsonized by layers of these proteins. Such a protein corona can alter polyplex characteristics [84], it may enhance or reduce subsequent interactions such as cell binding, cellular uptake, and transport (**Figure 1**) [84, 122, 123]. The protein composition can vary depending on the physicochemical properties, the material, and the surface charge of a polyplex, but also on the physiological environment and the duration of exposure. In the worst case opsonization by negatively charged plasma proteins such as IgM, fibrinogen, fibronectin or complement C3, may lead to formation of aggregates. Moreover, cationic polyplexes may even lead to aggregation of erythrocytes [26]. Such corona-coated nanoparticles and aggregates are recognized by the innate immune system resulting in rapid elimination by the mononuclear phagocyte system (MPS). Importantly, aggregates are also prone to induce severe toxic effects by accumulating in small lung capillaries [124].

To reduce these unwelcome interactions with blood components and to stay invisible for eliminating factors, cationic charges on polyplex surfaces can be shielded with hydrophilic ‘stealthing’ polymers. The most common and widely used shielding agent is polyethylene glycol (PEG) [26, 62, 125], but other hydrophilic polymers such as hyaluronic acid (HA) [66, 126, 127] have also shown good shielding effects . In addition

to the reduction of toxic side effects, shielding prolongs blood circulation time which positively affects nucleic acid delivery. Unfortunately, shielding cationic charges may also weaken polyplex interaction with tumor cell surfaces, which reduces uptake into tumor cells. This is known as the 'PEG-dilemma' [128]. Insertion of pH-responsive linkers between polyplexes and their hydrophilic shielding polymers is one of the options to circumvent this issue. As soon as the shielded polyplex enters the slightly acidic conditions of the ECM, the shielding agent is shed from the polyplex surface revealing the cationic charges [129-131]. Although surface shielding can reduce protein corona formation, it cannot completely avoid it. In some cases this might even be favorable [132].

2.5 Vascular barrier

2.5.1 Mechanisms of extravasation

The tumor vessel wall, lined with tumor endothelial cells (EC) on the luminal side, represents the first biological barrier that polyplexes must overcome to reach the tumor. Due to their large size and hydrophilic surface charge, polyplexes cannot simply cross the vessel wall by diffusion like small molecule drugs. Basically, two options exist for extravasation, either through inter-endothelial junctions or *via* transcellular transport mechanisms. Both of these pathways can be further subclassified, including a distinction between active and passive transport processes. Although investigations have been ongoing for several decades, the exact extravasation mechanisms of nanoparticles are still not fully understood and may differ for various tumors and patients. Multiple reliable mechanistic models have been presented over the past years and are under continuous refinement (**Figure 2**) [45-47, 70-74, 123, 125, 133-141]. The polyplex type and its physicochemical properties, including size, charge, shielding, and surface modifications (e.g., targeting ligands), but also the type and stage of tumor is expected to have a large impact. For tumors within the brain, which is additionally protected by the tight blood-brain barrier (BBB), transcellular transport mechanisms across the tightly arranged brain endothelial lining is required for polyplex delivery, unless the blood-brain tumor barrier (BBTB) is leaky as in high-grade gliomas and brain metastases [142].

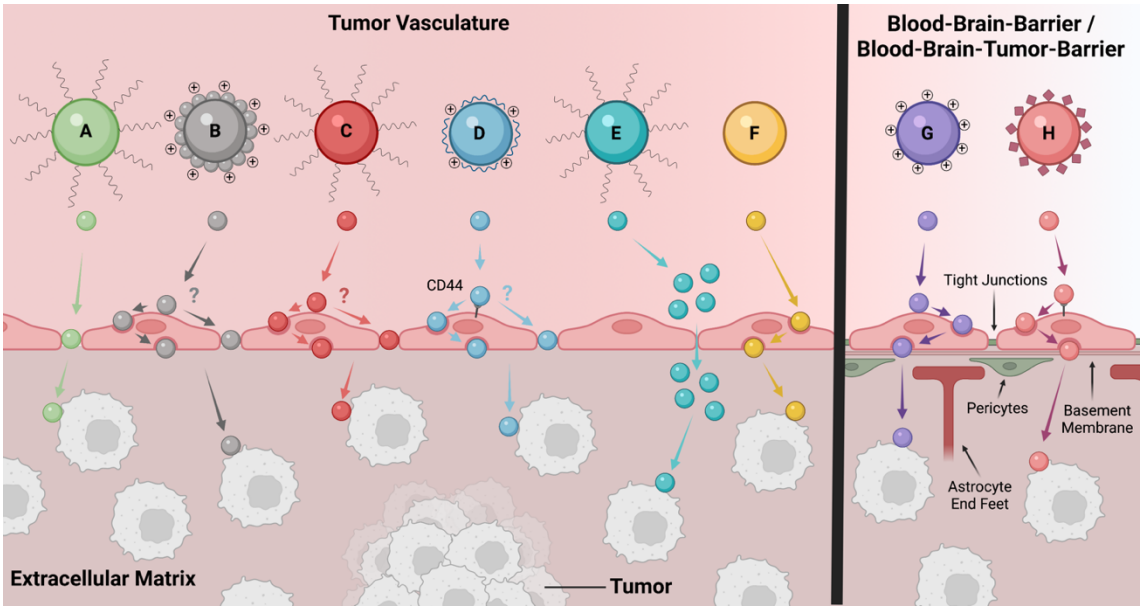

Figure 2. Mechanisms of extravasation. A, EPR effect/passive targeting; B, positive charge dependent attachment to tumor vessels; C, endothelial binding and extravasation of cationic PEG-coated nanoparticles; D, endothelial binding and extravasation of cationic HA-shielded polyplexes; E, vascular bursts via dynamic vents; F, active trans-cellular transport via caveolae-mediated transcytosis; G, H, active transfer across BBB / BBTB (G, adsorption-mediated transcytosis; H, receptor- and carrier-mediated transcytosis). Created with BioRender.com.

*2.5.1.1 EPR effect/passive targeting (**Figure 2A**)*

Tumor tissue, including its surrounding environment and supplying vasculature, is different from normal tissue. To list some examples, there are differences in the type and number of receptors on cell surfaces, pH and composition of the interstitial space and the architecture of vasculature. Because of rapid angiogenesis, tumor blood vessels contain large interendothelial junctions and discontinuous or absent basement membranes. These properties make tumor vasculature leaky, allowing plasma proteins and other blood components to access the interstitial space passively through diffusion or convection [70, 125].

Researchers recognized this as an excellent opportunity to target nanoparticles specifically to tumors and thereby increase their delivery efficiency. In pioneering work in 1986, Maeda et al. [74] reported passive nanoparticle accumulation in tumors. They discovered that SMANCS, conjugates of the polymer polystyrene-co-maleic acid (SMA) with neocarzinostatin (NCS), accumulated selectively in breast cancer tissue, while normal tissues were not penetrated. This early work also proved that conjugating low molecular weight drugs to a polymer considerably increased *in vivo* half-life and passive accumulation in human solid tumors. This effect requires an extended circulation of macromolecular conjugates or nanoparticles; its foundation was shown to be the leaky,

hyperpermeable architecture of tumor vasculature in combination with poor lymphatic drainage in tumors, which in combination leads to increased accumulation of nanoparticles specifically in tumors. These findings were also confirmed independently by Jain et al. and others [70-73]. The effect was named the *Enhanced Permeation and Retention (EPR)* effect and since then is considered the basis for passive tumor targeting. Ongoing investigations of the EPR effect revealed that passive targeting is dependent on several criteria and cannot be applied universally. The EPR effect is limited to polymers and nanoparticles within the size range from as small as 4 nm / 15-70 kDa to as large as about 400 nm. Smaller polymers diffuse in and out of tumors freely without accumulating and are cleared by the kidney, while larger nanoparticles are not able to cross the vessel wall due to the limited junction size. Blood circulation of a minimum of three hours, which can be achieved by surface shielding, is an essential requirement to permit nanoparticles to circulate tumor vasculature several times before extravasation [125, 135]. Apart from nanocarrier characteristics, tumor properties such as tumor type, tumor stage and the degree of vascularization were shown to influence polyplex accumulation *via* passive targeting [71], which can even differ in two patients with the same tumor type [71]. Now, >35 years after its discovery, the EPR effect remains the fundamental strategy for macromolecular tumor targeting [133, 134, 143, 144]. Research on the EPR effect is continuing and recent innovative strategies such as the use of ultrasound or hyperthermia, or applications using bubble liposomes to further improve passive targeting are being explored [135, 136].

*2.5.1.2 Charge dependent extravasation (**Figure 2B-D**)*

Another extravasation mechanism was discovered by both Thurston et al. and Dellian et al., who observed cationic molecules to specifically attach to tumor vasculature *via* negatively charged glycoproteins on the luminal side of tumor endothelium [45-47]. Thurston and coworkers demonstrated that increasing cationic surface charges (from 10 to 50 mol%) enhances (in this case doubles) accumulation in tumors. Tumor specificity was proven by a 15-33-fold increased uptake of cationic liposomes into angiogenic endothelial cells compared to healthy endothelial cells. Internalization of cationic molecules occurs mainly *via* clathrin-mediated endocytosis after active attachment to tumor endothelium, and less *via* leaky vasculature [46, 145]. Moreover, cationic molecules were shown to extravasate faster than their anionic or neutral counterparts [47], due to the negatively charged glycocalyx that forms an electrostatic barrier for anionic nanoparticles [45]. In more recent work, Wang et al. compared PEGylated cationic, anionic, and neutral nanoparticles for tumor accumulation, penetration, and

antitumor efficacy in different tumor models (**Figure 2C**). Although the cationic nanoparticles were slightly inferior regarding blood circulation time and tumor accumulation, they were significantly more effective in tumor penetration and inhibiting tumor growth. Overall, cationic nanoparticles have proven superior tumor accumulation and antitumor efficacy in comparison to their neutral or anionic analogues [45, 46, 123]. In recent work by our own group, Luo et al. demonstrated enhanced *in vivo* tumor accumulation and gene silencing of cationic HA-shielded polyplexes compared to analogous negatively charged HA polyplexes (**Figure 2D**) [40]. Rapid polyplex attachment to tumor endothelial cells within five minutes after polyplex application was observed *via* 3D confocal microscopy. However, cationic charge alone did not lead to the anticipated fast attachment, HA-coating was an additional requirement. Although HA was primarily used as a shielding agent, it is also a ligand to the CD44 receptor, widely expressed on tumor and tumor endothelial cells. The combination of cationic charge, shielding and receptor-ligand interaction most probably led to the observed tumor accumulation. Despite cationic nanoparticles being superior in tumor accumulation and growth inhibition, they have some limitations compared to neutral and anionic nanoparticles (as discussed in *Section 3*) [117, 146]. Their high zeta potential makes them subject to toxicity, liver accumulation and rapid plasma clearance [146]. However, these limitations can efficiently be compensated by shielding the cationic charges with hydrophilic polymers such as PEG [123].

*2.5.1.3 Vascular bursts (**Figure 2E**)*

An alternative, versatile and transient permeation route for molecules was recently discovered by the group of Kataoka [147]. Vascular bursts are dynamic vents, different from static pores, that open and close intermittently up to 10 hours after drug injection and thereby enhance blood vessel permeability for nanoparticles. The vents, with an estimated size of ~600nm, are frequently found in the tumor periphery and less in healthy blood vessels. By following a library of different particles (dextran, polymeric nanoparticles, liposomes, and microspheres) covering a wide range of sizes with intravital confocal laser scanning microscopy, Igarashi et al. demonstrated that vascular bursts especially enhance nanoparticle delivery for molecules smaller than 300 nm, independent of their material [147]. Moreover, transport of antibodies, platelets and in some cases molecules with sizes up to 1µm was demonstrated [148]. Although the exact mechanisms are still unknown and more investigation is needed, vascular bursts may provide a suitable, targetable pathway to increase nanoparticle extravasation.

*2.5.1.4 Active transcellular transport (**Figure 2F**)*

Active transport *via* caveolae-mediated transcytosis was reported for the plasma protein albumin in early pioneering work by Schnitzer [137]. The glycoprotein gp60, expressed by endothelial cells, was identified as the specific binding domain that can initiate the active transport process upon binding of albumin. This mechanism has successfully been translated to a number albumin-based nanoparticles for tumor therapy to enhance their efficacy [149]. Another option to initiate active transport through tumor endothelium is to directly target caveolae. Oh et al. generated an antibody (mAnnA1) that specifically recognizes the caveolae protein annexin A1, a protein expressed selectively in tumor caveolae, but not by normal cells, and therefore allows specific tumor penetration [138]. *In vitro* and *in vivo* studies demonstrated rapid attachment and active caveolae-based uptake of antibody labelled molecules, dependent on both annexin A1 and caveolin 1 proteins [149]. Evidence that active transport may play a role in tumor accumulation of nanoparticles was given by Sindhwani et al. who reported that 97% of nanoparticles in their study entered tumors via an active process through tumor endothelial cells [150].

*2.5.1.5 Transfer across BBB / BBTB (**Figure 2G-H**)*

Targeting brain tumors for gene therapy requires special considerations. As the most critical system in our body, the central nervous system (CNS) is strictly regulated by the BBB. The BBB represents the boundary between blood circulation and neural tissue and is responsible for nutritional supply and homeostasis of the brain and protects it from toxins. It consists of a single layer of brain capillary endothelial cells (BCECs), thoroughly sealed by tight junctions, a continuous basement membrane and surrounding astrocyte end feet and pericytes (**Figure 3)** [151, 152]. Due to its structure and function, only small lipophilic molecules <500 Da are capable of diffusing across the BBB [153]. All other substances, including hormones and nutrients, are dependent on selective carriers and receptors that initiate active transport across the BCECs. Moreover, efflux pumps (e.g., MDR (multi-drug resistant protein) or P-gp (P-glycoprotein)) eliminate potentially harmful substances such waste or drug products from the CNS *via* outward directed transport. In high-grade gliomas and brain metastases the BBTB can be leaky [142] and different from healthy BBB. Nevertheless, the BBTB presents an additional barrier for systemic treatment of brain tumors, most importantly gliomas, the most common and aggressive form of brain cancer [154]. Since active transport across BCECs is the preferential route for nanoparticle drugs into the CNS, research has focused on specifically targeting these active transport mechanisms to exploit them for drug delivery. There are three possible endocytosis pathways through which macromolecules can enter the CNS: 1) *via* carrier

mediated transcytosis (CMT), 2) *via* adsorptive-mediated transcytosis (AMT) or 3) *via* receptor-mediated transcytosis (RMT) [155]. All three pathways have been investigated for their ability to transport therapeutic nucleic acid polyplexes.

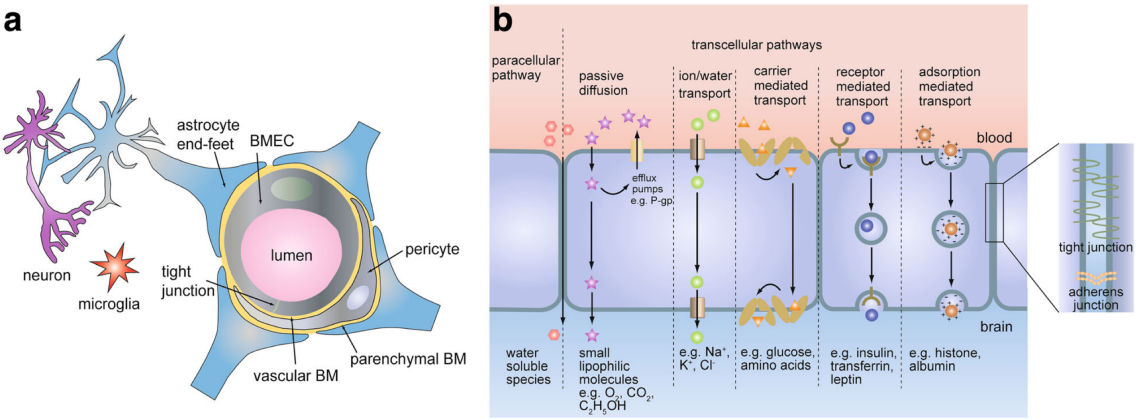

Figure 3. The BBB: structure and possible transport pathways. a, overview of cell types involved in the formation of the highly regulated BBB in a cross-section schematic; **b**, possible trans- and paracellular transport pathways for molecules across the BBB. Reproduced without changes from Jamieson, J.J., Searson, P.C., Gerecht, S., J Biol Eng, 11, 2017, ref. [151]. Licensed under a Creative Commons Attribution (CC BY) license. Copyright 2017 The Authors.

2.5.2 Active targeting of tumor vasculature

Functionalizing a polyplex with targeting ligands enables, after blood circulation, specific binding to tumor vasculature which ideally initiates its uptake *via* an active transcytosis pathway [137]. Enhanced attraction to tumor vasculature reduces non-specific accumulation in healthy tissue and thereby lowers the risk for side-effects and reduces required therapeutic doses. Equipping polyplexes with ligands for active targeting is especially suitable in cases where passive accumulation is unlikely or not sufficient such as in particular tumor types lacking fenestrations and leaky vasculature (e.g., pancreatic ductal adenocarcinoma) [156], or for short circulating polyplexes, respectively, as accumulation *via* the EPR effect takes time [157]. Research has identified multiple receptors overexpressed specifically on tumor vasculature, many of them being involved in tumor angiogenesis, tumor progression and metastasis. Often, receptors are expressed by both tumor cells and tumor endothelial cells, providing corresponding ligands with dual-targeting capabilities (see *Section 6* for targeting of tumor cells). Receptor-ligand interactions may initiate endocytosis of bound molecules. Utilizing this mechanism for polyplexes has shown enhanced transcellular transport and tumor accumulation compared to non-targeted polyplexes. Investigated ligands include proteins, peptides and antibodies that are often derived from naturally occuring

substances or fragments of such, peptide sequences identified *via* phage display, or recombinant antibodies (see **Table 1**).

Table 1. Receptors and ligands for targeted delivery of nucleic acid polyplexes to tumor vasculature.

Receptor	Ligand	Polyplex/Cargo	Major Findings	Ref.
Integrin avβ3	RGD	Oligolysine/pDNA	Integrin dependent 10-fold enhanced uptake,100-fold increased transfection	[158]
		PEI/pDNA	Replacement of aspartic acid by glutamic acid (RGE) reduced transfection efficiency, proving integrin dependent internalization	[159]
		PEG-PEI/siRNA	Selective tumor uptake, targeting enhanced inhibition of protein expression, tumor angiogenesis and growth rate	[160]
	cRGD	PEG-ECO/siRNA PEG-ECO/ miR-200c	Gene silencing, therapeutic efficacy, suppressed tumor growth (*see Section 7/Table 4*)	[161] [162] [163]
		PEG-PAsp(DET)/ pDNA	Adding the targeting ligand restored transfection efficiency that was lost by removing free cationic polymers	[164]
		PEG-PAsp(DET)/ pDNA	Enhanced PEG shielding prolonged blood circulation; cRGD improved tumor accumulation and tumor growth suppression	[165]
NRP-1	iRGD	PMDM/siRNA	Conjugation of iRGD to non-charged polyplexes enhanced tumor penetration and cellular uptake in vitro and in vivo	[166]

	Lyp-1	TPN/siRNA	Treatment of tumor bearing mice with Lyp-1 targeted polyplexes supressed growth and improved survival	[167]
	KHHK	HK/pDNA	Gene delivery was mediated by NRP-1	[168]
CD13 (amino-pepti-dase N)	NGR	PEG-PEI/DNA	Targeting resulted in increased tumor-specific gene expression; competition with free ligand led to loss of transfection efficiency	[169]
	cNGR	PEG-PEI/pDNA	Enhanced tumor specific and aminopeptidase dependent gene delivery mediated by cNGR	[170]
Unknown	APRPG	PEG-PEI/siRNA	Tumor growth inhibition by VEGF siRNA	[171]

Abbreviations: NRP-1, neuropilin-1; PEI, polyethylenimine; PEG, polyethylene glycole; ECO, (1-aminoethyl)- iminobis[N-oleicylcysteinyl-1-aminoethyl)propionamide]; PAsp(DET), poly(N′-[N-(2-aminoethyl)-2-aminoethyl]aspartamide); PMDM, mal-PEGMA-b-PDPA-b-PDMA; TPN, tumor-penetrating nanocomplex; HK, histidine-lysine

Integrin $\alpha v\beta 3$, closely associated to cell proliferation, metastasis, and cell survival of many cancers, is one of the best known and investigated receptors overexpressed on tumors and tumor endothelial cells. It is not surprising that scientists have identified integrins as ideal receptors for targeting tumor therapeutics to enhance their delivery and therapeutic efficacy [172-177].

In a phage display study, Ruoslahti et al. identified the peptide sequence arginine-glycine-aspartic acid (RGD) as the specific integrin binding motif [172]. RGD-presenting molecules specifically bind to integrin expressing tumor endothelium (and tumor cells) and initiate endocytosis [159]. Depending on the ligand density, exposure time and RGD-molecule concentration uptake kinetics may vary [178, 179]. Moreover, the RGD peptide structure (i.e., linear or cyclic form) influences integrin specificity and internalization rates. For RGD, the constrained cyclic peptide has been found superior [179]. Since its identification, RGD peptides have been used to target nucleic acid loaded polyplexes to tumors. Early integrin targeting approaches for DNA delivery were investigated by conjugating RGD to oligolysine [158] and polyethylenimine (PEI)-based

polyplexes [159]. RGD-targeted PEG-PEI polyplexes for siRNA delivery followed later [160].

More sophisticated cationic polymers for targeted siRNA delivery were recently developed by the group of Zheng-Rong Lu. The amino lipid ECO ((1-aminoethyl)-iminobis[N-oleicylcysteinyl-1-aminoethyl)propionamide]) was conjugated to cyclic RGD *via* a PEG spacer to deliver multiple types of siRNA (siDANCR, siβ3) and miRNA (miR200c) to triple-negative breast cancer (TNBC) xenograft bearing mice, in all cases leading to effective tumor growth inhibition [161-163]. High efficiency of RGD as a tumor targeting ligand was also proven in work by Kataoka et al., who demonstrated that RGD is even capable of restoring transfection efficiency that was initially lost due to the removal of free cationic polymers from a polyplex formulation [164, 165].

Although RGD-functionalized polyplexes demonstrated enhanced attachment to tumor vasculature, extravasation and especially deep penetration into tumor parenchyma against the elavted interstitial pressure in tumors remains challenging. In a later, further phage display screening by Ruoslahti et al., searching for novel peptides that bind to tumor vasculature led to the discovery of a RGD peptide derivative [180, 181]. The cyclic tumor-homing peptide iRGD (internalizing RGD), containing the distinct R/KXXR/K motif, can bind and activate the Neuropilin-1 (NRP-1) receptor, but only if the relevant motif is presented at the c-terminal end of the peptide (= *C-end Rule*) [182]. Tumor-homing of iRGD occurs is a three-step process in which the integrated RGD sequence first mediates binding to integrins, which is then followed by a proteolytic cleavage of the peptide, leading to the loss of affinity to integrins and revealing of the terminal R/KXXR/K motif, which finally enables binding to NRP-1 and the initiation of transcytosis. In contrast to RGD, which primarily accumulates in and around tumor blood vessels, iRGD can penetrate extensively into tumor interstitium and spread within the tumor more effectively [180]. Consequently, iRGD and other tumor-homing peptides containing CendR sequences such as iNGR [183-185], LyP-1 [186], F3 [187] or CGKRK [188] have been conjugated to antitumoral drugs to enhance their efficacy [180, 189-192]. For instance, pH-sensitive siRNA polyplexes were targeted with covalently bound iRGD to lung carcinoma cells, resulting in effective intratumoral delivery and gene silencing [166]. A special characteristic of iRGD is that it does not necessarily require covalent conjugation, co-administration with the drug carrier molecule facilitates tumor delivery in equal manner [156]. A different tumor-penetrating peptide targeting NRP-1, namely Lyp-1, was used to deliver siRNA polyplexes to ovarian tumor-bearing mice and thereby reduce tumor growth and enhance survival time [167]. Lyp-1, also containing the CendR motif, binds to p32, a mitochondrial protein expressed by tumor endothelium [186]. Mixson and

colleagues designed linear and branched HK (histidine-lysine) peptides for pDNA delivery [168]. Such HK peptides share the common -KXXK- (CendR) sequence with tumor penetrating peptides, enabling binding to NRP-1 and subsequent transendothelial transport of targeted polyplexes.

Two further options to target tumor vasculature for nucleic acid delivery are conjugating the peptidic ligands APRPG (Ala-Pro-Arg-Pro-Gly) or NGR (Asn-Gly-Arg) [193] to polyplexes. APRPG, also a tumor-homing peptide that was found by Oku et al. *via* phage display specifically binds to tumor neovasculature, but not to tumor cells or healthy cells [194]. APRPG targeted PEI-PEG-APRPG/siRNA polyplexes, but also other antitumoral drugs [171, 195-197] achieve superior therapeutic efficacy compared to their non-targeted equivalents.

2.5.3 Active targeting of the Blood-Brain-Barrier (BBB) and Blood-Brain-Tumor-Barrier (BBTB)

To systemically treat brain cancer with nucleic acid therapeutics, it is inevitable to conquer the BBB/BBTB. To increase neural tissue accumulation and augment therapeutic efficacy, research has concentrated on active targeting of the three endocytosis pathways CMT, AMT and RMT (compare **Figure 3**) using optimized, surface-modified polyplexes. A selection of examples is listed in **Table 2**.

Table 2. Targeted nucleic acid polyplexes to enhance transport across the BBB/BBTB

Receptor/ Target	Ligands	Polyplex/ Cargo	Major Findings	Ref.
TfR	Tf	PEG-PAMAM/pDNA	Tf increased uptake compared to unmodified PAMAM polyplexes; polyplex concentration dependent cellular uptake; efficient non-invasive gene delivery to the brain	[198]
	T7	PEG-DGL/pDNA	T7-polyplexes showed enhanced gene silencing compared to unmodified polyplexes and did not compete with transferrin	[199]

LfR	Lf	DAB/pDNA	Lactoferrin enhanced gene expression in the brain and reduced expression in other major organs	[200]
AChR	RVG	RVG9R/siRNA	RVG9R polyplexes exhibited specific gene silencing in the brain after i.v. injection	[201]
	RVG29	PEG-PAMAM/pDNA	Uptake into BCEC through clathrin- and caveolae dependent endocytosis which could be inhibited by free RVG29 and GABA, but not by nAchR: RVG29 uptake depends on GABA and AChR	[202]
	RVG	SSPEI/miRNA	RVG is capable of transporting miRNA to the brain in vivo; RVG polyplexes showed less toxicity; mannitol (disruptance of BBB) further enhanced transfection	[203]
	RVG29	RVG29-9R/pDNA	Efficient brain accumulation and reporter gene expression after intravenous application	[204]
	RVG	PEG-PIC/siRNA	Proof of brain targeting ability of RVG-PICs; enhanced gene silencing efficiency	[205]
LRP1	ANG-2	PEG-PAMAM/pDNA	LRP1-mediated endocytosis is the main transport mechanism; targeted polyplexes exhibited increased brain accumulation and gene expression compared to untargeted polyplexes	[206]
		PEG-PAMAM/pDNA	Cellular internalization through endo/lysosomal pathway; increased survival time of treated mice	[207]
		Angiopep-PEG-oligomer/siRNA	Efficient gene silencing both in glioma cells and in a glioma tumor model after systemic administration	[208]

	ANG-2 (TG1)	PF14/siRNA	Conjugating the CPP-siRNA carrier to TG1 (hexaglutamated ANG-2) led to two-fold increase in gene silencing	[209]
AMT	CPP LNP	PEG-DGL/pDNA	LNP targeted polyplexes induced strong apoptosis at the tumor site and increased survival time	[210]
Trans-cytosis mechanism unknown	CPP TAT	TAT-$(LLHH)_3$/pDNA	Clathrin- and caveolin-mediated endocytosis and macropinocytosis; enhanced transfection and gene expression in vitro and in the brain of zebrafish	[211]
GLUT1 (CMT)	Glucose	PEG-PLL/ASO	Endocytosis of GLUT1 during a fasting period can be exploited to enhance brain delivery of glucose-coated polyplexes; efficient accumulation in the brain 1h after i.v. administration along with significant knockdown of long non-coding RNA	[212]

Abbreviations: TfR, transferrin receptor; LfR, lactoferrin receptor; AChR, acetylcholin receptor; LRP-1, low-density lipoprotein receptor-related protein; Tf, transferrin; Lf, lactoferrin; ANG, angiopep; PAMAM, polyamidoamine; DGL, dendrigraft poly-l-lysine; DAB, 3-diaminobutyric polypropylenimine; RVG9R, RVG-arginine nonamer; PIC, polyion complex; PF14, CPP PepFect 14; LLHH, endosomal escape segment; LNP = nuclear translocation signal sequence of the LIM Kinase 2 protein; ASO, antisense oligonucleotide

*2.5.3.1 CMT (**Figure 2H**)*

Hormones, carbohydrates, amino acids, and other nutrients traverse the BBB *via* carrier-mediated transcytosis. As glucose is the brain's main energy source, the glucose transporter GLUT1 is one of the most abundant carriers on the BBB, expressed on both the apical and basal side of BCECs [213] and on glioma cells [214]. In standard function, GLUT acts as passive carrier translocating the small glucose cargo across the cell membrane into the cytosol. Although adding carbohydrate ligands to nanoparticles has provided GLUT1-mediated brain targeting potential [215-218], transcytosis and accumulation levels were mostly limited [219] and less encouraging for nucleic acid based therapeutics. However, Kataoka et al. recently developed a strategy to efficiently

transport glucose-modified polyplexes to the brain [80]. In a period of fasting, GLUT1 receptors are transported from the apical to the basal side of BCECs through endo/exocytosis mechanisms as a measure of glycaemic control. Hence, by actively targeting GLUT1 during a fasting period, this mechanism can be exploited to transport carrier-bound glycosylated polyplexes across the BBB. Although this mechanism has not specifically been used to deliver antitumoral nucleic acid to the brain, the capability of GLUT1-mediated endocytosis for gene therapy was recently proven by successful CNS delivery of PEG-PLL polyplexes carrying antisense oligonucleotides to treat central nervous disorders [212].

*2.5.3.2 AMT (**Figure 2G**)*

AMT is an energy-, receptor- and transporter-independent pathway across the BBB that is activated either by cell-penetrating peptides (CPPs) or cationic molecules [220] through their electrostatic interactions with BCEC membranes. However, the exact mechanisms of AMT remain unclear [221, 222].

CPPs are short amphipathic or cationic peptides of less than 30 amino acid residues with high capacity to cross the BBB without inducing cytolytic effects [222]. Hence, CPPs have been used to enhance brain accumulation of multiple antitumoral drugs [209, 210, 221, 223-225]. Recently, Wang et al. designed peptide-based vectors consisting of an endosomal escape segment ($(LLHH)_3$) and TAT, a cationic CPP derived from HIV, to compact pDNA into polyplexes and to trigger their transport across the BBB *via* clathrin- and caveolin-mediated endocytosis and macropinocytosis for glioma treatment [211]. The AMT-mediating carrier-peptides demonstrated high transfection efficiency and specificity with low cytotoxicity proven in both an *in vitro* BBB model and in the brain of zebrafish. Beside CPPs, glycosylated amphipathic peptides have shown the capability to increase accumulation of nanoparticles in the CNS. Tosi et al. conjugated g7, a glucosylated heptapeptide, to the surface of nanoparticulate carriers which achieved enhanced brain delivery and sustained release of the encapsulated drug. Although the exact mechanisms of the enhanced, g7-mediated brain accumulation were unknown, a similar mechanism as the one used by the parent opioid peptides was suggested, which cross the BBB *via* AMT due to their amphipathic and helical structure [226]. Nonetheless, other endocytosis routes such as carrier-mediated endocytosis via GLUT1, mediated by the incorporated glucose residue in g7, are conceivable.

*2.5.3.3 RMT (**Figure 2G**)*

RMT presents the third and most frequently targeted route across the BBB/BBTB for glioma therapeutics. To target RMT, polyplexes are equipped with ligands that are capable of initiating active transcytosis mechanisms through their specific binding to receptors expressed on BCECs. Receptors that have been targeted for this purpose include the transferrin (Tf) receptor (TfR), folate receptor, LDL (low density lipoprotein) receptor (LDLR), insulin receptor (IR), lactoferrin receptor, glutathione receptor and diphteria toxin receptor [152, 222, 227, 228]. Among these, the TfR belongs to the receptors that have attracted most attention for BBB targeting. Its physiologic function is to transport transferrin-bound iron, an essential molecule for DNA synthesis, cell division and cellular metabolism [229], across the BBB *via* RMT [230, 231]. A detailed overview of the TfR functions and structure is described elsewhere [232-234]. To benefit from this physiologic function for cancer therapy, nanoparticles have been functionalized with TfR-selective ligands such as the natural serum protein Tf, artificial peptides targeting either Tf (Tf_2, T_{10}) [235, 236] or the TfR [237-240], or monoclonal antibodies [232, 241-246]. Monoclonal antibodies and artificial peptides, which were identified *via* phage display or *via* in silico simulations [235, 240], were found to have the great advantage not to interfere with free serum Tf due to their distinct binding sites. Independent of the ligand, TfR-targeted nanoparticles have demonstrated enhanced, concentration dependent transport across the BBB *via* clathrin- and caveolin-mediated endocytosis. Compared to untargeted nanoparticles, this resulted in increased drug accumulation within the brain [198, 235, 247-250]. *In vivo* studies investigating Tf- and T7- modified polyplexes, T7 being an artificial TfR targeting peptide derived from phage display [240], revealed a more than two-fold increase in gene delivery and gene silencing, respectively, proving the superiority of targeted polyplexes in systemic applications [198, 199]. Nevertheless, standard peptides like T7 are often subject to proteolytic degradation and their targeting ability directly correlates with their stability in serum. Thus, Prades et al. synthesized optimized enantio and retro-enantio proteolysis-resistant peptide ligands made of *(D)*-amino acids. These novel products demonstrated enhanced permeability across the BBB and higher accumulation in the CNS compared to their parental peptide. Moreover, especially the retro-enantio derivative showed advanced properties to transport small, medium sized and large cargo across the BBB, demonstrating its potential for brain cancer treatment [238].

To create an affinity of intravenously injected nanoparticles to the TfR and thereby increase transcytosis across the BBB, Santi et al. developed a strategy to generate an artificial Tf protein corona. For this purpose a peptide ligand (Tf_2) with specific affinity for

free serum transferrin was designed [235]. Later on, applying the same decapeptide (then called T_{10}), the group of Huang applied this strategy for Tf opsonized doxorubicin-loaded COF (covalent organic framework) nanoparticles. Overall, Tf enhanced transport across the BBB and significantly increased survival times of glioma bearing mice [236].
Lactoferrin, another member of the iron-transporting transferrin family, has also exhibited the ability to increase polyplex transport across the BBB. Somani et al. functionalized polyplexes with the lactoferrin ligand to specifically target the lactoferrin receptor, a low-density lipoprotein receptor-related protein (LRP) that is also overexpressed on the BBB. The targeted polyplexes demonstrated a two-fold increase in cellular uptake *in vitro* and a more than six-fold increase in gene expression in the brain after intravenous injection. Moreover, Somani et al. could show that gene expression mediated by lactoferrin-polyplexes was limited to the brain without unspecific expression in all other major organs [251].
RVG is a short peptide derived from rabies virus glycoprotein that specifically binds to acetylcholine and as later discovered to GABA receptors [202], both expressed by neuronal cells. Targeting nucleic acids and polyplexes with RVG has been reported to enhance brain accumulation and gene expression compared to unmodified equivalents [201-205].
Angiopep-2 (ANG-2) is a further peptide with great BBB targeting and penetration ability that has reached clinical evaluation for the treatment of gliomas [252]. The angiopep series of peptides that were detected by sequence alignment of aprotinin with other human proteins containing a Kunitz domain [253] interact with LRP1 (low-density lipoprotein receptor-related peptide), a member of the low-density lipoprotein receptor (LDLR) family [253, 254]. ANG-2 has been used to transport peptides [255], small molecule drugs [256-259], and nucleic acid delivery systems [207, 260-262]. This resulted in BBB penetration ability, accumulation and retention in glioblastoma and, most importantly, growth inhibition and survival benefits. ANG-2 functionalized polyplexes exhibited specific internalization *via* LRP1-induced clathrin- and caveolin-mediated endocytosis [206]. Enhanced gene silencing and survival rates of treated tumor-bearing mice proved ANG-2 to be a favorable targeting ligand for systemically administered polyplexes [207-209].
As a consequence to successful BBB targeting with angiopeps, novel ligands for LRP1 were investigated to further increase brain accumulation of functionalized nanoparticles. L57 was identified as the first artificial LRP1 ligand that showed enhanced cellular uptake and BBB permeability accompanied by stability in mouse plasma [263, 264]. The peptide L57 actively targets the cluster 4 of LRP1 although it does not show homology with

angiopeps [263]. In a recent study Rodrigues et al. investigated cellular uptake and cytotoxicity of L57 compared to angiopep-7 (A7) and octaarginine (R8), which are both peptides known for their capability to cross the BBB. L57 showed enhanced, concentration dependent cellular uptake and higher biocompatibility compared to A7 and R8. Hence, L57 may present a potenital novel targeting ligand to improve brain accumulation i*n vivo* [264]. The identification of L57 also demonstrated that active targeting of a specific receptor may be enhanced by identifying novel artificial peptide-based ligands.

Overall, several BBB-targeted polyplexes have shown great potential for systemic brain tumor therapy with reduced toxicity and side effects. Classical approaches for brain tumor gene therapy involve either local injection or disturbing the BBB's integrity with physical or chemical stimuli [265-267], which both have high risks and potential severe side-effects. With progress in BBB-targeting, systemic administration of gene therapeutics is made possible which will ideally avoid invasive classical approaches in future.

2.6 Tumor microenvironment and stroma

When nanoparticles extravasate from tumor vasculature they reach the tumor stroma, the connecting tissue between tumor cells, lymphatic vessels, and tumor vasculature. Hence, before nanoparticles may perform their therapeutic effect in tumor cells, they must overcome the tumor interstitial space. The tumor stroma (**Figure 4**) strongly differs from the stroma in normal tissues [268] regarding its structure, composition, stiffness, interstitial fluid pressure (IFP) and its pH, which is slightly shifted towards acidic conditions [269] – altogether forming a physical barrier that hinders nanoparticle penetration deep into the tumor [270].

Large parts of the tumor stroma are comprised of the ECM, which consists of collagen, hyaluronic acid, elastin fibers, proteoglycans and glycosaminoglycans which form a dense cross-linked network [271]. The increased density of the ECM, which is mainly due to higher amounts of collagen, is one of the main barriers that hinder nanoparticle diffusion across tumor tissue. Thus, the capability of nanoparticles to penetrate the dense ECM is highly dependent on their size, charge, and shape [272, 273]. Kataoka et al. demonstrated that smaller, 30nm sized nanoparticles exhibited higher tumor penetration ability than their larger 100nm sized equivalents [61].

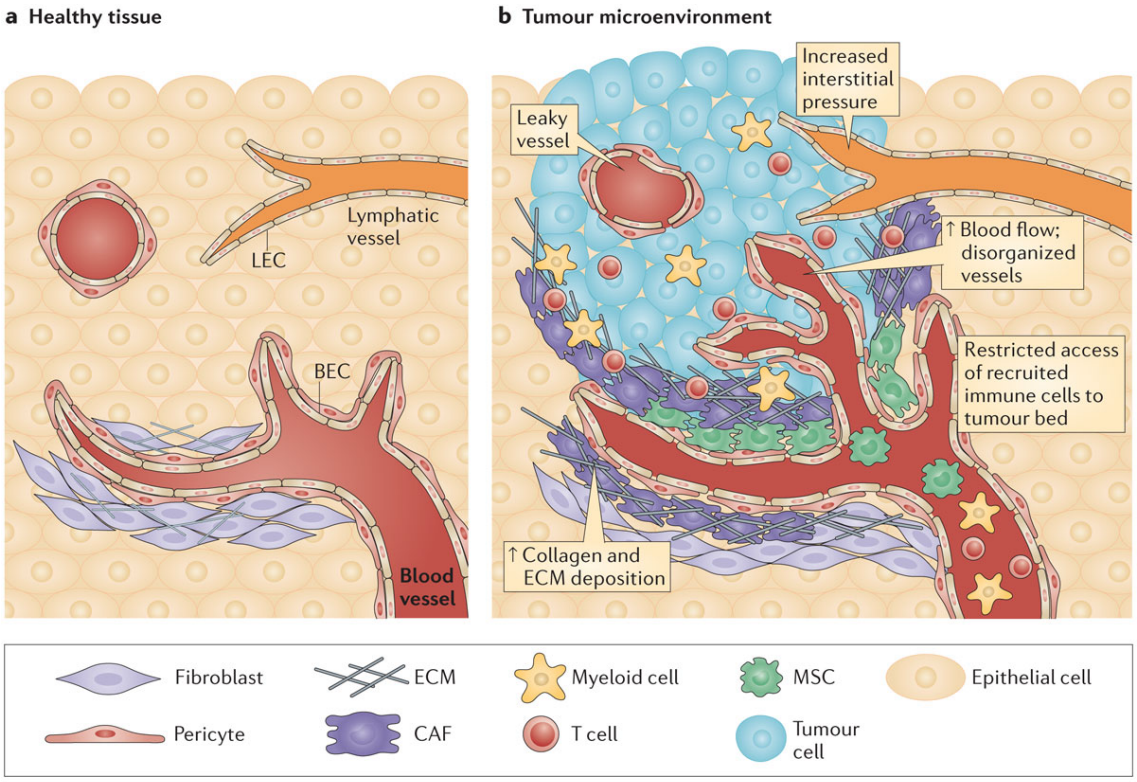

Figure 4. Structural and cellular changes in the tumor microenvironment (TME)/stroma. In comparison to healthy tissue (a), the structure and composition of the TME (b) is highly disorganized. Due to pro- and antiangiogenic factors tumors exhibit reduced, abnormal vascularization and leaky blood vessels. In combination with decreased lymphatic drainage, this leads to increased interstitial fluid pressure (IFP). The tumor extracellular matrix (ECM) exhibits increased density due to a high deposition of collagen. Tumor secreted molecules (not shown) recruit mesenchymal stem cells (MSC) and cancer associated fibroblasts (CAF), secreted cytokines attract activated T cells and myeloid cells to the TME. The high IFP, the increased ECM density and the reduced vascularization hinder tumor penetration of recruited cells (and nanoparticles). Reprinted with permission from Springer Nature, Nature Reviews Immunology, ref. [268]. Copyright 2015 Nature Publishing Group.

Due to the large proportion of anionic polymers (hyaluronan and collagen) in the ECM, diffusion of charged nanoparticles is additionally hampered through electrostatic attraction and repulsion [60, 269]. Therefore, to shield surface charges of cationic nanoparticles from unspecific interactions with the ECM by PEGylation or other means is a necessary measure to increase their travelling distance through stroma [274, 275]. Alongside the ECM, the tumor microenvironment (TME) consists of a heterogenous composition of stromal cells, including cancer-associated fibroblasts (CAFs), blood- and lymphatic endothelial cells, pericytes, mesenchymal cells and immune cells [268, 276]. Among these, CAFs play a major role in tumor progression by secreting growth factors like VEGF (vascular endothelial growth factor), EGF (epidermal growth factor), and other cytokines and by initiating remodeling of the ECM [268]. The elevated number of macrophages in TME are known to facilitate tumor progression by creating an immunosuppressive environment. Kircheis et al. reported that high tumor infiltration

through tumor-associated macrophages (TAM) in certain solid tumor types can lead to the elimination of administered pDNA polyplexes, resulting in reduced gene expression [277].

Nanoparticle penetration into tumors is additionally impeded by the elevated interstitial fluid pressure within tumor tissue. Increased IFP is caused by a combination of a) rapidly proliferating tumor cells in a limited space, b) replaced lymphatic vessels (through rapidly proliferating cells) causing reduced lymphatic drainage and c) leaky tumor vasculature with enhanced permeability [269]. Apart from hindering nanoparticle penetration into tumor tissue, high interstitial fluid pressure can reduce nanoparticle extravasation or even cause outward directed flow back into tumor vasculature.

To enhance nanoparticle penetration, despite the unfavorable conditions of the tumor stroma, diverse strategies have been developed. The main focus has been on adapting the physicochemical properties of nanoparticles, including their size, charge, and surface modifications to the conditions in the TME. A promising strategy was the introduction of size-switching nanoparticles. As diffusion across the dense ECM network preferably requires small sized nanoparticles, but larger nanoparticles are favorable in systemic applications to prolong blood circulation and avoid rapid renal filtration, size-switching nanoparticles allow ideal nanoparticle sizes for both situations. To induce size-switching, various trigger mechanisms have been investigated, including endogenous stimuli, matrix metalloproteases and light (reviewed by Zhang et al. [278] and Sun et al. [279]).

Functionalizing nanoparticle surfaces with tumor penetrating peptides presents a second strategy for optimizing nanoparticles to enhance their tumor penetration capability. iRGD, a ligand for the neuropilin-1 receptor that has demonstrated the ability to increase extravasation of nanoparticles from tumor vasculature (compare *Section 4.2*) has also been found to significantly increase the tumor penetration of functionalized nanoparticles. Sugahara et al. demonstrated that iRGD-functionalized nanoparticles increased drug delivery to tumor cells more than tenfold compared to unmodified nanoparticles [180].

Recently, Liu et al. demonstrated that tumor penetration and distribution of nanoparticles is not limited to diffusion but can also be achieved *via* an active trans-cell transportation process [139]. Cationic charges on nanoparticles were shown to initiate caveolae-mediated endocytosis and transcytosis in tumor cells, enabling uniform distribution throughout tumor tissue [280]. To avoid adverse effects through positively charged nanoparticles in blood circulation, Zhou et al. conjugated enzyme-cleavable γ-glutamyl camptothecin-polymers to nanoparticle surfaces, which enabled site specific presentation of the required cationic charges. Only when the nanoparticles entered the

tumor stroma the γ-glutamyl transpeptidase overexpressed on cell membranes cleaved the γ-glutamyl moieties and exposed the cationic charges [280].

As an alternative to nanoparticle functionalization, modulation of the TME presents an encouraging strategy to restore normal-tissue conditions and thereby increase tumor penetration of nanoparticles. Degradation of the dense tumor ECM was achieved by treating tumors with bacterial collagenases or the hormone relaxin. The degradation of the ECM network led to significantly increased diffusion rates of investigated molecules [281, 282]. Alternatively, degrading enzymes have been directly conjugated to nanoparticle surfaces to enable in vivo applications. Nanoparticles with conjugated hyaluronan exhibited increased tumor penetration ability and, moreover, led to an enhanced vessel density and perfusion in the treated tumor [283, 284]. Restoring normal vascularization and tissue perfusion was also achieved by both antiVEGF2 [285] and anti-TGF-β antibodies [286], which also significantly improved tumor penetration of nanoparticles [286].

In summary, the tumor stroma represents an additional barrier for tumor therapeutics and requires special consideration in nanoparticle drug design. Several strategies to overcome and modulate the tumor stroma have been investigated, however, more research is required to further enhance efficacy and to fully understand the limiting factors. Moreover, when developing strategies to enhance tumor penetration, one must consider that different tumor types and stages exhibit distinct stroma compositions and characteristics, which may demand distinct solutions [281].

2.7 Tumor cell targeting

Abundant efforts to enhance the efficacy of nucleic acid polyplexes for antitumoral therapy have focused on active tumor cell targeting. Once polyplexes have reached the tumor cell, they must cross the cell membrane to exert their activity (**Figure 5**).

For a macromolecule or nanoparticle, the most common way to enter the cell is *via* active endocytosis, which can be triggered by the interaction of a polyplex with the plasma membrane. Therefore, active targeting of polyplexes through surface modification with ligands that exhibit high affinity to tumor cell receptors can increase the internalization rate and specificity. The interaction of conjugated ligands and cellular receptors subsequently may initiate polyplex internalization *via* clathrin- or caveolae-mediated endocytosis [110, 287-289].

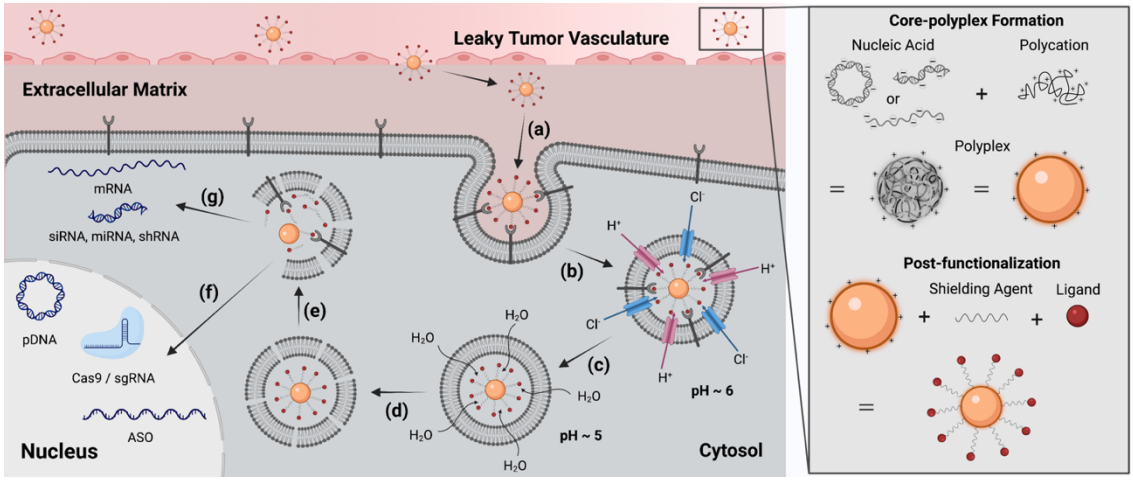

Figure 5. Tumor-targeted polyplexes: Cellular uptake and intracellular barriers. (a) active receptor targeting, (b) receptor-mediated endocytosis, (c) proton-sponge effect (in the case of PEI-polyplexes), (d) endosomal membrane disruption, (e) endosomal escape, (f) nuclear entry, (g) cytosolic cargo release. Created with BioRender.com.

Over the past decades it has been the objective to identify suitable receptors that efficiently initiate such a cellular uptake (**Table 3**). Research has led to the identification of multiple ligand types with high receptor affinity and optimized structures for high quality formulations. In the following, a selection of these receptors and ligands is presented.

Table 3. Targeted tumor cell receptors for polyplex delivery

Receptor	Ligand	Polyplex/cargo	Major findings	Refs.
TfR	Tf	PLL/pDNA	First targeted polyplexes for gene delivery to tumor cells *via* receptor-mediated uptake; PLL polyplexes required addition of endosomolytic agent	[23, 290-292]
		PEI/pDNA	Endosomolytic agents are not strictly required for high transfection efficiency; in vivo tumor targeted gene transfer	[293, 294]
		PEG-PEI/pDNA	PEGylation of Tf polyplexes influenced biodistribution, toxicity and in vivo gene transfer	[26, 295]

		PEG-PEI/pDNA	Targeted polyplexes delivering TNF-α inhibited tumor growth in all investigated tumor lines without toxicity	[296, 297]
		OEI-HD/siRNA	Efficient siRNA mediated gene silencing and reduction of tumor growth without signs of toxicity	[298]
		CDP/pDNA	Monofunctionalized transferrin conjugates maintained high receptor binding affinity	[299]
		CDP/siRNA	TfR-mediated endocytosis enhanced therapeutic efficacy; absence of abnormalities in major organs after systemic administration in xenograft mice	[300]
		CDP/siRNA	No signs of toxicity after repeated systemic administration to non-human primates	[301]
		CDP/siRNA	RNAi-mediated gene silencing in tumor after systemic administration in a Phase I study in melanoma patients	[302, 303]
		OAA/pDNA	Histidines in the formulation were required for endosomal escape; post-functionalized polyplexes exhibited highest transfection efficiency	[304]
		Lipo-OAA/siRNA	TfR specific cellular uptake; further optimization required for systemic delivery	[305]
	reTfR	PEG-Lipo-OAA/ pDNA or siRNA	Retro-enantio peptides proved efficient pDNA and siRNA delivery to tumor cells	[75]
EGFR	MAb B4G7	PLL/pDNA	Gene delivery to EGFR overexpressing cells via receptor-mediated endocytosis	[306]

EGF	PLL/pDNA	The ratio of polyplex components and EGF-ligands were critical for efficient gene delivery	[307]
	PEG-PEI/DNA	EGF-modified PEGylated polyplexes were 10-100 fold more efficient than polyplexes without EGF	[308]
		EGFR-mediated cellular uptake allowed high specific in vivo gene expression in tumors	[309]
		Cellular uptake and gene expression depend on tumor vascularization and macrophage infiltration	[277]
	PEG-PEI/PolyIC	Effective treatment of gliomas, breast cancer and adenocarcinomas in xenograft mice	[310]
EGF vs. GE11	PEG-PEI/pDNA PEG-PEI	EGFR specific targeting and gene transfer by both EGF and GE11; uptake kinetics depend on the type of ligand; EGF activates EGFR, GE11 does not	[311] [312]
GE11	PEG-PEI/polyIC	Free GE11 does not exhibit strong affinity to EGFR, but conjugation to PEG-PEI strongly increases it, similar transfection efficiency as EGF polyplexes	[313]
	PEG-Lipo-OAA/siRNA and miRNA	Ligand-dependent gene silencing and tumor growth inhibition	[314]
	PEG-PEI/pDNA	Tumor specific accumulation and reduction of tumor growth	[27]

		PEG-lipo-OAA/siRNA + MTX	EGFR-targeted polyplexes enhanced anti-tumoral activity	[315]
		PEG-lipo-OAA(454)/pDNA	Post-integration of bivalent GE11 ligand exhibited superior gene delivery ability to monovalent ligand	[316]
		PEG-lipo-OAA/siRNA + pretubulysin	EGFR-targeted polyplexes enhanced anti-tumoral activity; co-delivery of siRNA + pretubulysin resulted in superior antitumoral activity	[317]
		PEG-lipo-OAA/siRNA	Bivalently superior to monovalently attached ligands	[318]
FR	Folate	PLL/ODNs	Targeting enhanced down-regulation of gene expression and inhibition of tumor cell proliferation	[319]
		PLL/pDNA	Folate-dependent internalization via endo/lysosomal pathway; chloroquine required for endosomal escape	[320]
		PEG-PLL/pDNA	pDNA content, size, surface charge, PEG-spacer length and polyplex concentration influenced cellular uptake; uptake was saturable	[321]
		PEG-PEI/pDNA	FR-mediated uptake; targeting increased transfection efficiency and reduced toxicity	[322] [323]
		OAA/siRNA	Small (≈6nm) siRNA nanoplexes; integrated endosomolytic agent required; gene silencing in vitro and after i.t. injection of targeted polyplexes	[324]
		HP-β-CD-PEI/ siRNA + DOX	Targeting reduced gene expression and enhanced apoptosis and therapeutic efficacy	[325]

		PEI-PCL-PEG/siRNA	Targeted polyplexes exhibited less toxicity and increased gene knock-down; high stability in vivo, efficient tumor accumulation and gene silencing	[326]
		TCP/siRNA	Targeting increased transfection efficiency; Inf7 as endosomolytic agent necessary	[327]
		TLPs /siRNA	Targeting enhanced transfection efficiency; tyrosine and oleic acid containing lipo-oligomer was found the best performer and capable of endosomal escape	[328]
		Lipo-oligomer/ siRNA	Bivalent ligands with bioreducible linkers (for disessembly in reductiv cytosol conditions)	[157]
		PDP/shRNA + DOX	Targeted polyplexes showed superior antitumor efficacy in vitro and in vivo; co-delivery enhanced therapeutic efficacy through synergistic effects	[329]
		PPFR/siRNA	In vitro and in vivo efficient cellular uptake and gene silencing, more efficient than comercial transfection agents	[330]
		PEI/TMC-SH/pDNA	Folate targeting enhanced transfection of multifunctional ternary polyplexes; enhanced endosomal escape due to pH-sensitive bonds and effective redox-responsive release of pDNA	[331]
		NFP/siRNA	Targeting enhanced gene silencing and antitumor effects	[332]
Integrins	cRGD	PEG-PLL/pDNA	cRGD led to rapid (3h) accumulation in the perinuclear region of tumor cells and	[333] [334]

			to efficient gene silencing by caveolae-mediated endocytosis	
	RGD	PEG-PEI/siRNA	RGD-mediated in vivo siRNA delivery	[160]
OA3	OA3-TL16 *Antibody*	PEG-PEI/pDNA	Antibody-modified polyplexes showed tumor specificity and low toxicity in vitro	[335]
HER2/ neu	Anti-HER2 *Antibody*	PEI/pDNA	Targeted polyplexes achieved HER2-specific gene transfer	[336]
		PEI/pDNA	Antibody-mediated gene delivery was proven by comparing HER2/neu positive and negative cell lines	[337]
		PLI/siRNA	Herceptin led to significant increase in transfection, mRNA down-regulation, cancer cell apoptosis and therapeutic efficacy in vitro and in vivo	[338]
		PEI-PEG/pDNA	Effective targeting of HER2/neu led to increased cancer cell death	[339]
MSLN	antiMSLN scFv	LGA-PEI/miRNA and pDNA	Antibody conjugation increased binding affinity, internalization into PC cells, and miRNA/pDNA delivery efficiency	[340]
c-Met	cMBP2	OAA-PEG/DNA	Targeted polplexes showed high efficacy, stability in serum and tumor specificity in vivo; implementation of histidines promoted endosomal escape	[48]
CD44 + HER2	HA + HER2 *antibody*	PLL/siRNA	Additive effects of two ligands; uptake via both CD44- and HER2- receptor-mediated endocytosis	[341]
CD44	HA	Lipo-OAA/siRNA	HA for both shielding and targeting; only cationic and HA-modified polyplexes exhibited rapid cellular attachment and efficient gene silencing	[40]

GRP40	LA	LA-CCD/siRNA	LA for both shielding and targeting; specific targeting, enhanced gene silencing, low cytotoxicity	[342]

Abbreviations: TfR, transferrin receptor; EGFR, epidermal growth factor receptor; FR, folate receptor; MSLN, mesothelin; PLL, poly-L-lysine; PEG, polyethylene glycol; PEI, polyethylenimine; OEI, oligoethylenimine; CDP, β-cyclodextrin polymers; OAA, oligoaminoamide; reTfR, retro-enantio transferin receptor targeting peptide; EGF, epithelial growth factor; PolyIC, polyinosine/cytosine; miRNA, microRNA; ODN, oligodeoxynucleotides; HP-β-CD-PEI, hydroxypropyl-β-cyclodextrin; MTX, methotrexate; PCL, polycaprolactone; TCP, targeted combinatorial polyplex; TLP, targeted lipoplexes; PDP, pullulan-desoxycholic acid-PEI; shRNA, short hairpin RNA; PPFR, poly(citric acid)-polymine-folic acid-rhodamine B; TMC-SH, thiolated trimethylated chitosan; NFP, FA-N-Ac-L-Leu-PEI; SPPP, N-succinimidyl-3-(2-pyridyldithio)proprionate; SMCC, N-succinimidyl-4-(maleimidomethyl)-cyclohexan-carboxylate; IBFP, 3-(2-(2-(vinylsulfonyl)ethylthio)ethyl)quinazoline-2,4(1H,3H)-dione; PLI, mPEG-b-PLL-g-(ss-lPEI); LGA, lactic-co-glycolic acid; CCD, cyclic PAsp(-N=C-PEG)-PCys-PAsp(DETA); HA, hyaluronic acid; LA, lauric acid

2.7.1 Transferrin receptor

The transferrin receptor (TfR, CD71), which is overexpressed on most tumor cells [343], was the first tumor cell receptor to be targeted by polyplexes for gene therapy. The PLL based polyplexes were conjugated to the serum protein Tf to target the TfR and increase polyplex accumulation *via* receptor-mediated endocytosis [23, 290]. Since then, the TfR has been used to deliver various cargos selectively to tumors in preclinical and clinical studies [303, 343-346]. Modifying the PLL polyplexes with Tf led to significantly enhanced gene delivery and expression compared to unmodified polyplexes while maintaining high cell viability post-transfection [23]. Due to its great potential for nucleic acid delivery, Tf was also used to enhance delivery of the next polyplex generation, which was based on the cationic polymer PEI [293, 295-298]. The advantage of PEI-based polyplexes, in contrast to PLL, was that they did not require the inclusion of endosomolytic agents to achieve high gene expression levels [293]. When polyplexes are internalized *via* transferrin-receptor mediated endocytosis, they accumulate in cell internal endosomes. Endosomolytic agents such as chloroquine or peptides including influenza HA-2 N-terminus or melittin aid polyplexes to escape these endosomes to avoid degradation in lysosomes or recycling to cell surface, and to deliver the encapsulated cargo to the cytosol or nucleus. PEI, as opposed to PLL, is not completely

protonated at physiologic pH (only 1/6 of amino nitrogens) enabling it to act as a proton sponge in the acidic conditions of endosomes, with its protonation leading to chloride influx, osmotic swelling and ultimately, rupture of the endosomal membrane (**Figure 5**). Transferrin-conjugation to PEI-polyplexes enabled a 10-100-fold increase of gene transfer intratumorally. For systemic applications, shielding of polyplexes with either sufficient density of Tf [294] or PEG [45, 264] was inevitable to avoid toxicity through aggregation and accumulation in lung, liver, and spleen, and to enable tumor gene transfer. Systemic application of transferrin-modified PEG-PEI/pDNA polyplexes into xenograft mice bearing different types of tumors led to preferential gene expression in tumors and upon TNF-α gene delivery an inhibition of tumor growth [296, 297]. Conjugating Tf to oligoethylenimine (OEI)-based polyplexes later enabled systemic delivery of siRNA to tumors, which led to efficient gene silencing and reduction of tumor growth without any signs of toxicity [298]. The capability of Tf to specifically deliver pDNA and siRNA polyplexes to tumors in systemic applications and its value for tumor treatment was emphasized in a series of preclinical and clinical studies with cyclodextrin-oligocation-based carriers. These multifunctional carriers were developed by Davis et al. to further enhance biocompatibility in systemic applications for siRNA and pDNA delivery, while maintaining the targeting efficiency mediated by Tf ligands [299-301, 303]. The cationic residue was designed to compact nucleic acid, while the cyclodextrin motifs served as an anchor for adamantyl-PEG-Tf ligands. The efficiency of this TfR-targeted polyplex regarding gene silencing/gene delivery after systemic administration was evaluated in mice, non-human primates and later in a Phase I clinical trial in humans [299-303].

Conjugation of Tf also increased efficacy of novel oligoaminoamide (OAA)-based delivery systems for pDNA and siRNA *in vitro* and *in vivo*. OAAs are low molecular weight precise sequence-defined oligocations based on amino ethylene, the favorable domain in PEI that enables nucleic acid complexation and endosomal buffering [35, 36]. Solid-phase assisted synthesis (SPSS) was utilized to develop OAAs by combining artificial oligoamino acids, natural α-amino acids, and fatty acid residues. This resulted in a variety of topological structures allowing stepwise optimization for nucleic acid binding, extracellular stability, transfection efficiency, cell tolerability, and endosomal escape and cytosolic nucleic acid release capability [39, 48]. Compared to previous formulations and unmodified polyplexes, TfR-mediated endocytosis of Tf-PEG-OAA polyplexes achieved an up to a 100-fold increase in gene expression [304]. 80% gene silencing and reduced tumor growth were achieved by repeated systemic applications of Tf post-functionalized PEG-OAA/siRNA polyplexes, without inducing toxic effects or causing significant

changes in blood parameters [305]. However, the large size of the Tf protein (80kDa), in combination with the PEG spacer, shielded the OAA/siRNA polyplexes in such a way that its endosomal escape capability was hampered, leading to the requirement of an additionally incorporated endosomal release agent [305].

To optimize polyplex formulations and to further enhance their binding affinity to the TfR the incorporation of artificial ligands as an alternative to the natural serum protein transferrin was investigated. Smaller synthetic peptides enable precise, sequence-defined, and high-quality pharmaceutical grade formulations, which presents a challenge for the serum protein Tf. Lee et al. identified synthetic TfR-specific targeting peptides *via* phage display, which have also been used to target the BBB (compare *Section 4.3*). The peptidic ligands exhibited similar affinity to the TfR as serum Tf, but avoided their competition by attaching to distinct binding sites [240]. Peptide-based ligands may be subject to rapid degradation by proteolytic enzymes, which led to the development of protease-resistant TfR ligands containing all amino acids in *D*-configuration and in reversed order [238, 347]. The efficacy of one of these peptides, reTfR (H-pwvpswmpprht-NH_2), was also proven for both siRNA and pDNA delivery in a study by Benli-Hoppe et al., who post-functionalized lipo-OAA polyplexes with the protease resistant bivalent reTfR peptide *via* a PEG spacer and thereby achieved efficient gene silencing and gene delivery *via* receptor mediated endocytosis in different cell lines [75].

2.7.2 Epidermal growth factor receptor

The epidermal growth factor receptor (EGFR) represents another receptor overexpressed on tumor cells that has long been in the focus of research. Like the TfR, the EGFR has been targeted by multiple ligand-functionalized polyplexes to initiate their endocytosis [348, 349]. The first approach to deliver pDNA to EGFR expressing cells in 1994 was to conjugate a monoclonal anti-EGFR antibody to PLL-based polyplexes for uptake *via* receptor mediated endocytosis [306]. Similar results were subsequently obtained by conjugating the natural epithelial growth factor (EGF), a 53- amino acid polypeptide, to polyplexes [307, 350]. Here, EGFR-mediated uptake was shown to be dependent on the number of EGF-ligands presented on the polyplex surface. Moreover, the study exhibited that EGF leads to an increase in polyplex size, which may influence its physicochemical properties [307]. The efficiency of EGF as a targeting ligand for tumor treatment was demonstrated by the efficient gene delivery *in vitro* and *in vivo* to multiple tumor types [277, 308-310]. Depending on the transfected cell line EGF-conjugation led to an 10-100-fold increase in transfection efficiency of PEG-shielded

PEI/DNA polyplexes compared to polyplexes lacking EGF [308]. Furthermore, pronounced tumor accumulation of PEG-PEI/DNA polyplexes was also observed after intravenous injection into xenograft mice [277, 309]. As an alternative to the natural EGF peptide, phage display revealed the short EGFR specific targeting peptide GE11 [351]. A comparison of gene delivery efficiency of PEG-PEI/pDNA polyplexes functionalized with either EGF or GE11 *via* live-cell imaging demonstrated that the two ligands use distinct internalization pathways [312]. EGF-functionalized polyplexes were internalized *via* an accelerated EGFR-mediated endocytosis pathway within minutes, while GE11 promoted clathrin-dependent uptake with much slower kinetics and independent of EGFR activation [312]. Thus, accumulation of the majority of EGF polyplexes occurred within ten minutes after application, whereas it took GE11-modified polyplexes four hours to achieve similar intracellular concentrations. Nevertheless, both ligands accomplished comparable transfection efficiency. A possible advantage of GE11 might be a missing EGFR activation as it circumvents the induction of cell proliferation and mitotic activity of targeted tumor cells. In addition, the activation of EGFR through EGF exhibited a reduction of EGFR expression on cell surfaces for four hours after its administration [311]. Although the affinity of free GE11 is less pronounced than the affinity of free EGF to the EGFR, GE11-conjugated polyplexes achieved similar antitumor effects as corresponding EGF polyplexes [313]. Compared to polyplexes without targeting ligands, conjugation of GE11 to siRNA and miRNA polyplexes has shown EGFR-mediated cellular internalization, gene silencing and increased antitumoral effects, proving its potential for RNAi-based therapeutics [314, 315, 317, 318]. In later studies with lipo-OAA based polyplexes a comparison of different GE11 ligands with varying linkers revealed the superiority of bivalently over monovalently attached ligands [316, 318]. Finally, significant tumor specific accumulation and reduced tumor growth after intravenous injections of therapeutic PEG-PEI/pDNA polyplexes proved the potential of the GE11 ligand for systemic tumor therapy [27].

2.7.3 Folate receptor

The folate receptor (FR) is a receptor overexpressed on tumor cells to cover its increased requirement of folate/folic acid (FA), an essential vitamin for the proliferation and metabolism of cells [352]. The high affinity of folic acid to its receptor has been employed to enhance the efficacy of cancer therapeutics [352, 353]. Conjugated to polyplexes, folic acid has achieved enhanced accumulation of both RNAi (siRNA, antisense oligonucleotides and shRNA) [157, 319, 323-330] and DNA [320-322] therapeutics in

tumor cells. Early FR-targeted PLL-based DNA polyplexes exhibited a 6-fold higher gene expression than polyplexes without folate [320]. Their uptake was evidently mediated by the folate receptor and followed a lysosomal pathway, shown by the requirement of chloroquine for endo/lysosomal escape [320]. Although polyplexes attached to the folate receptor, uptake of free folic acid was not inhibited [319]. Leamon et al. demonstrated that folate-receptor mediated endocytosis is a concentration dependent and saturable process, which can be blocked by free excess ligands [321]. The study also demonstrated that transfection efficiency of folic acid-targeted polyplexes was dependent on the spatial distance between the ligand and the polyplex. Moreover, a favorable biocompatibility of the targeted polyplexes was proven through high cell viability after polyplex exposure [321]. Folate-receptor mediated endocytosis was proven for FA-modified PEI- and OAA-based polyplexes *via* competition assays, near-infrared fluorescence imaging and immuno-TEM measurements [322, 324, 328]. Both PEI- and OAA- based FA-modified polyplexes were superior to non-FA corresponding polyplexes regarding their transfection efficiency [322]. FR targeting has predominantly been applied for siRNA delivery. Targeted siRNA (and shRNA) polyplexes have exhibited higher gene silencing specifically in FR-positive tumors both *in vitro* and *in vivo* compared to polyplexes lacking a folic acid residue [323-327, 329, 330]. Furthermore, accumulation in other tissues could not be observed for FA-polyplexes [324] and their cytotoxicity was reduced compared to non-FA-polyplexes [326]. Ternary PEG-PCL (polycaprolactone)-PEI polyplexes exhibited a decreased zeta potential as a result of FA conjugation [326]. This contributed to *in vivo* stability and prolonged blood circulation, which together with the targeting ligand led to a recovery of 17% of the i.v. injected siRNA dose per gram in the tumor 24 hours after injection [326]. Approximately 65% gene silencing and reduced tumor proliferation were demonstrated by Lee et al. and Klein et al., who thus confirmed the efficacy of folic acid-modified siRNA polyplexes for systemic tumor treatment [157, 327, 328]. For this achievement, Klein et al. observed that bivalently attached ligands were superior to monovalent ligands, corresponding to observations that were also made for the GE11 ligand [157, 316, 318].

2.7.4 Integrin $a_v\beta_3$

As presented in ***Section 2.4.3***, the receptor integrin $\alpha_v\beta_3$ is known to be expressed predominantly on tumor vasculature. Hence, research has mainly focused on targeting the active integrin-mediated endocytosis pathway to increase tumor accumulation. However, integrins are also expressed by numerous tumor cells, providing the earlier

presented RGD-targeted polyplexes with dual-targeting capabilities. Therefore, integrin targeting will not be discussed here in detail. Nonetheless, research on integrin targeting has exhibited that RGD-functionalization of polyplexes does not only affect tumor accumulation and cellular internalization, but also the intracellular trafficking mechanisms. Kataoka et al. observed that RGD polyplexes preferentially accumulate in the perinuclear region of cells within three hours after incubation, which could not be observed for unmodified polyplexes [333, 334]. Confocal laser scanning microscopy revealed that this was due to the distinct internalization pathways of the two polyplex types: RGD-polyplexes were internalized *via* caveolae-mediated endocytosis, while polyplexes lacking the RGD ligand were internalized *via* clathrin-mediated endocytosis which resulted in the endo/lysosomal degenerative pathway [334]. This explained that RGD polyplexes demonstrated enhanced transfection efficiency, compared to untargeted polyplexes, in integrin positive cells, but not in integrin negative cells [333, 334].

2.7.5 Antibodies

An alternative approach to active tumor receptor targeting, instead of using natural or synthetic receptor-ligands, has been the usage of receptor-directed monoclonal antibodies which enables targeting to a tumor specific surface antigen. PEG-PEI polyplexes that were functionalized with the antigen binding fragment of OV-TL16, an antibody directed to the surface antigen OA3, which is expressed by many human ovarian carcinoma cell lines, exhibited a 6-fold increased binding affinity and an up to 80-fold higher gene expression compared to untargeted polyplexes. The antibody led to a specific transfection of OA3 expressing cells, while it did not influence polyplex stability [335]. An antibody that has attracted much attention in the past years is trastuzumab, an HER2/neu specific monoclonal antibody, directed to the human endothelial growth receptor (HER2/neu) that is overexpressed on many tumor cells, but especially plays a role in breast and ovarian cancer. Depending on the ligand : PEI ratio, trastuzumab enhanced HER2/neu-specific transfection efficiency of PEI polyplexes up to 20-fold, which was maintained in serum containing medium and was in line with increased number of cell deaths triggered by induced gene expression [336, 337, 339]. Li et al. applied HER2 antibodies to siRNA polyplexes and demonstrated high transfection efficiency to HER2 positive cell lines *in vitro* and *in vivo* leading to enhanced gene silencing, tumor cell apoptosis, and therapeutic efficacy while containing low cytotoxicity [338]. Recently, two different antibodies, either a single-chain variable fragment antibody

(scFv) against mesothelin (MSLN), a biomarker for pancreatic cancer, or an anti-EGFR antibody (Cetuximab), were conjugated to polyplexes based on lactic-co-glycolic acid-polyethylenimine (LGA-PEI). This antibody-polyplex construct confirmed the capability of antibodies by significantly increasing binding affinity and internalization into tumor cells and enabling the efficient delivery of miRNA and pDNA therapeutics [340].

2.7.6 c-Met

The c-Met proto-oncogene, the receptor for the hepatocyte growth factor, is another receptor overexpressed by many tumor cells and was first used for non-viral tumor-targeted gene delivery by Kos et al. [48]. The c-Met specific peptide ligand cMBP2, which was identified earlier *via* phage display, was conjugated to shielded OAA-based polyplexes. The targeted polyplexes achieved enhanced cellular uptake and gene transfer compared to non-targeted polyplexes specifically in c-Met expressing tumors *in vitro* and *in vivo*.

2.7.7 Anionic polymers

Anionic polymers such as HA present an option to both shield cationic surface charges and target polyplexes at once. HA, when used for targeting, acts as a ligand for the CD44 receptor, an adhesion molecule that is expressed on many tumor and tumor endothelial cells, where CD44 activation promotes angiogenic processes [242, 354]. HA modification has shown to enhance the delivery of siRNA polyplexes to CD44 overexpressing cells [40, 66, 355] and to improve therapeutic efficacy of antitumoral nanoparticles through CD44 specific targeting [355-358]. In a recent study by Liu et al. lauric acid (LA) was incorporated into an anionic polymer used to coat positively charged polyplexes to, firstly, reduce the zeta potential of siRNA polyplexes and to achieve prolonged blood circulation and reduced cytotoxicity [342]. Secondly, specific targeting and efficient growth inhibition of tumor cells overexpressing the fatty acid receptor GRP40 was achieved through LA-mediated active targeting [342].

2.7.8 Dual targeting

To further enhance transfection efficiency dual-targeting approaches have been investigated. Nie et al. combined the targeting peptide B6, a ligand that was identified *via* phage display, and the peptide RGD for integrin targeting on the surface of PEG-PEI polyplexes. Both ligands exhibited specific binding to their receptors. A clear synergistic

effect of the both ligands could be observed, resulting in a higher transfection efficiency than corresponding single-targeted polyplexes. This derived from the utilized biphasic mechanism in which cell binding was predominantly mediated by integrins, while cellular uptake was initiated by other receptors [359]. In a recent study by Kim et al., HA and an anti-HER2 antibody were combined to enhance siRNA delivery with anionic PLL nanoparticles. These dual-targeted carriers were also superior to single-targeted equivalents, mediated through both CD44 and HER2 receptor-mediated endocytosis. Moreover, the dual-targeted nanoparticles exhibited enhanced biostability due to a reduced accessibility for degradative enzymes [341].

Taken together, the past decades have revealed numerous receptors with high potential to enhance polyplex activity in tumor cells *via* receptor-mediated endocytosis. For this purpose, natural peptides and proteins, synthetic peptides, monoclonal antibodies, and anionic polymers have been conjugated to polyplexes; these have been investigated regarding their optimal ligand/polyplex ratios, their biocompatibility and their influence on biophysical properties. The combination of more than one ligand may provide synergistic dual targeting or cascade targeting effects.

2.8 Molecular therapeutic strategies

Achieving high antitumor efficacy of nucleic acid-based therapeutics comprises both efficient delivery to tumor cells and the therapeutic potency of a nucleic acid to interfere with tumor growth and eliminate the treated tumor. Instead of only affecting survival of the transfected tumor cells, strategies focusing on broader regional antitumoral effects (via paracrine and other by-stander actions) or even systemic effects such as triggered antitumoral immunity, are preferred. Technically, nucleic acid therapy may occur on different levels of endogenous gene expression (**Figure 6**), for example by re-introducing tumor suppressing genes, by silencing or knocking down tumor-promoting genes, or by modulating the tumor microenvironment by stimulating antitumoral immune cells or suppressing protumoral angiogenesis and other tumor-promoting cells. **Table 4** provides selected examples of nucleic acid cargos (pDNA, siRNA, microRNA and other RNA types) introduced as polyplexes to act at the different antitumoral molecular biology levels.

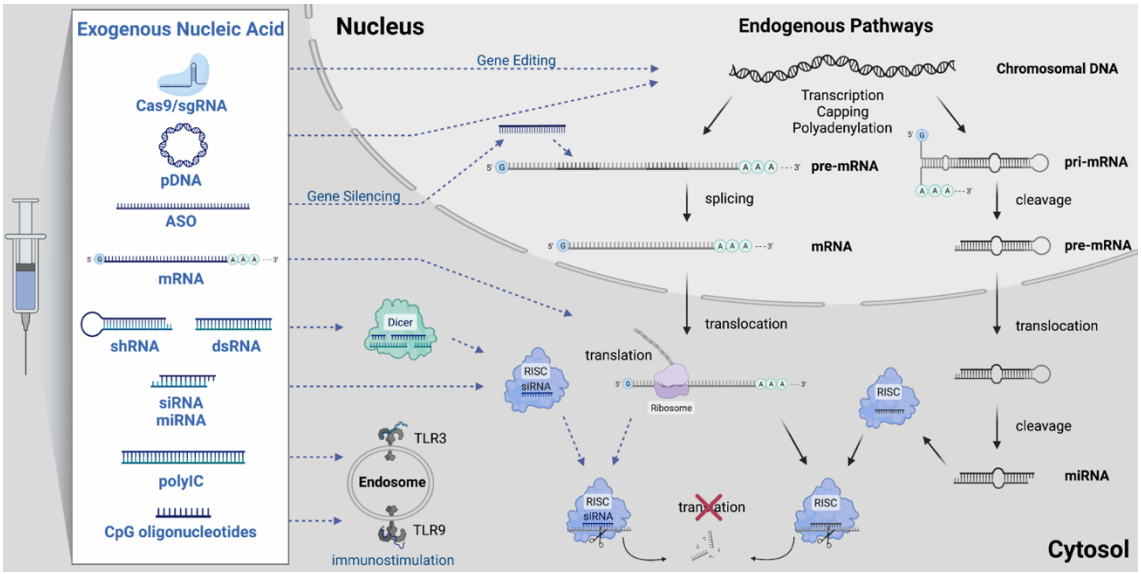

Figure 6. Nucleic acid-based therapeutic strategies acting on different levels of the gene expression cascade. The delivery of exogenous DNA and mRNA enables expression of therapeutic genes, peptides, and proteins. The Cas9/sgRNA system enables gene editing of endogenous DNA (delivery of Cas9 DNA, mRNA, or protein and sgRNA to the nucleus). The expression of specific genes may be suppressed by introduction of antisense oligonucleotides (ASO), double-stranded RNA (dsRNA), short-hairpin RNA (shRNA), short interfering RNA (siRNA) or microRNA (miRNA). polyIC (double-stranded RNA), RIG-I agonists, or CpG oligonucleotides induce endosomal (TLRs) or cytosolic (MDA-5, RIG-I) immunostimulation. Created with BioRender.com.

Table 4. Molecular therapeutic strategies

Therapeutic nucleic acid	Mechanism of action	Polyplex	Major findings	Refs.
pTNF-α	Enhanced tumor accumulation, induction of tumor necrosis, tumor regression by affecting vascularization	(Tf-PEI)/ pDNA	Tumor necrosis and inhibited tumor growth in all tested cell lines (N2A, MethA, M-3); complete tumor regression in a MethA model; no systemic toxicity	[296]
		G3-HD-OEI/DNA LPEI-PEG-GE11/pDNA + doxorubicin	pDNA delivery with polyplexes increased TNF-α mRNA expression in liver and tumor; TNF-α enhanced antitumoral activity of doxorubicin	[360]

pEGFP-hTRAIL	Induction of apoptosis specifically in tumor cells	ANG-CLP/PTX/pDNA + paclitaxel	Efficient co-delivery of pDNA and paclitaxel; combination therapy showed improved antitumor effect and prolonged survival time of U87 MG glioma bearing mice	[262]
		DGL-choline/pDNA + doxorubicin	Enhanced apoptosis in targeted tumor cells	[361]
pING4	Tumor growth supression and induction of apoptosis	DGL-PEG-LNP/pDNA	ING4 expression led to increased apoptosis in gliomas and longest survival time of treated mice compared to control groups	[210]
	I_6P_7 peptide inhibits tumor growth by blocking IL-6/JAK/STAT	I_6P_7-Stp-His/pDNA	Combination of pING4 delivery and IL-6 receptor blocking significantly prolonged survival time of U87 tumor bearing mice	[362]
pNIS	Therapeutic radioiodide accumulation in tumors; non-invasive imaging of carrier distribution and functional gene expression	cMBP2-PEG-Stp/pDNA	NIS expressed in Huh7 cells led to high radioiodide accumulation; three cycles of pNIS-polyplex and ^{131}I application led to reduced tumor growth and prolonged survival time	[37]
		LPEI-PEG-GE11/pDNA	Systemic treatment of spontaneous PDAC mice; ^{131}I administration reduced tumor growth; NIS expression was sufficient to achieve high radioiodide accumulation for imaging and therapeutic effect	[27]

		LPEI-PEG-GE11 + LPEI-PEG-cMBP2/ pDNA	Dual-targeting enabled pNIS delivery to different tumors with varying receptor expression and achieved higher tumor specific NIS expression levels than single-targeted polyplexes	[363]
		Lipo-OAA-PEG24-GE11/pDNA	EGFR-dependent gene expression, radioiodide accumulation, tumor growth reduction and prolonged survival of treated glioblastoma xenograft mice	[364]
pIncRNA MEG3	Inhibition of tumor growth, induction of apoptosis	PAMAM-PEG-EpDT3/ pDNA	lncRNA MEG3 expression inhibited tumor growth; targeted lncRNA MEG3-polyplexes achieved highest tumor suppression effect; no toxicity	[365]
RAF-1 siRNA	RAF-1 silencing leads to tumor cell apoptosis	HK/siRNA	Raf-1 siRNA reduced tumor vascularization and size (by > 50%) after intratumoral injection in tumor bearing mice	[366]
EWS-FLI1 siRNA	Silencing to suppress tumor proliferation	Tf-PEG-CDP/siRNA	Silencing of EWS-FLI1 inhibited tumor growth in a murine model of metastatic Ewing's sarcoma; targeted delivery for therapeutic efficacy	[300]
PTN siRNA	Down-regulation of PTN to inhibit tumor growth	PEI/siRNA	Intraperitoneal or subcutaneous administration led to reduction of PTN levels in tumor cells and inhibited tumor growth; intracranial delivery resulted in antitumoral effects	[367]

RRM2 siRNA	Inhibition of RRM2 has antiproliferative effects in tumor cells	Tf-PEG-CDP/siRNA	Multiple systemic doses showed no severe toxicity or immune responses in non-human primates, demonstrating the safety of the formulation	[301] [368]
			Reduction of RRM2 mRNA and protein compared to pre-dosing tissue in a Phase I study; specific gene inhibition demonstrated	[303]
DANCR siRNA	Antitumoral silencing of lncRNA DANCR	RGD-PEG-ECO/ siDANCR	80-90% DANCR knockdown in vivo reduced TNBC progression, invasion, and regression; DANCR is involved in multiple molecular pathways	[162]
PD-L1 siRNA	Blocking interaction of PD-L1 with its receptor PD-1	POP micelles/ siRNA + PDT	POP micelles induced PD-L1 knockdown and ROS production, stimulating immune responses; combined PD-L1 knockdown and PDT reduced tumor growth	[369]
β-3 integrin siRNA	Blocking integrin β-3 supresses TGF-β mediated EMT/ invasion	ECO-PEG-RGD/siRNA	Effective silencing of β3-integrin reduces TGF- β mediated EMT and invasion in vitro; intravenous injection eased primary tumor burden and inhibited metastasis of TNBC	[161]
PLK1 + VEGFR2 siRNA	Inhibit tumor growth and reduce tumor vascularization	Angiopep-3I-NM/siRNA	Tumor growth reduction and prolonged survival time by PLK1 and VEGFR2 knockdown; reduced vascularization of glioma, extensive necrosis and apoptosis within an orthotopic glioma mouse model	[370]

miR-145 **miR-33a**	miRNA replacement to achieve proapoptotic and antiproliferative effects	PEI/miRNA	Systemic or local application of miRNAs exhibited antitumor effects in mouse xenograft tumors; miR-145 delivery led to knockdown of c-Myc and ERK5; miR-33a reduced Pim-1 expression	[371]
miR-200c		RGD-PEG-ECO/ miR-200c	Systemic administration to mice bearing orthotopic TNBC significantly reduced tumor progression and altered the TME by reducing extradomain B fibronectin expression without toxic side effects	[163]
polyIC	Activation of multiple cell killing mechanisms + bystander effect	Melittin-PEI-PEG-EGF/polyIC	polyIC induced rapid apoptosis of glioblastoma cells, secretion of cytokines and bystander effects; complete regression of intracranial tumors, breast cancer and adenocarcinoma xenografts	[310]
		Melittin-PEI-PEG-EGF/polyIC + PBMCs	Intravenous application of polyIC + intraperitoneal PBMCs into tumor bearing mice with disseminated tumors completely cured mice; neighboring EGFR-negative cells were killed through a strong bystander effect; immune cells significantly homed to tumor	[372]
		LPEI-PEG2kDa-EGF/polyIC	Increased therapeutic efficacy in vitro compared to previous formulation (Shir et al., 2011); efficacy of polyIC polyplexes correlated with glioma cell	[373]

			EGFR levels; well-tolerated, repeated intravenous injection reduced tumor growth in A431 tumor bearing mice	
		PEI-PEG-GE11/polyIC	Strong antitumor effect in vivo and prolonged survival time compared to untreated mice (U87 orthotopic model) after intratumoral injection	[313]
sFlt-1 mRNA	prevents VEGF binding to its receptor, inducing anti-angiogenicity	PEG-PAsp(TEP)-Chol/mRNA	Efficient mRNA expression resulting in significantly reduced tumor growth; cholesterol-stabilized polyplexes were required	[374]

Abbreviations: NIS, sodium iodide symporter; ING4, inhibitor of growth protein 4; RRM2, M2 subunit of ribonucleotide reductase; PDT, photodynamic immunotherapy; POP micelles, PDPA−OEI-C14−PPa; PBMCs, peripheral blood mononuclear cells; MRMI, magnetic resonance molecular imaging; PTN, pleiotrophin; DGL, dendrigraft-poly-L-lysine; sFLT-1, fms-like tyrosine kinase 1; EpDT3, aptamer targeting EpCAM

2.8.1 Therapeutic pDNA polyplexes

The delivery of DNA to tumors is the most obvious strategy to introduce therapeutic genes or replace malfunctioning tumor suppressor genes. Hence, multiple types of pDNA have been intensively investigated for their ability to inhibit tumor growth. The delivery of pDNA encoding for TNF-α (pTNF-α), a cytokine that mediates many antitumor mechanisms, has exhibited great potential for tumor treatment [296, 360]. In tumors, TNF-α induces necrosis, inflammatory processes, and enhanced vasculature permeability, which allows immune cells, but also therapeutic drugs, to extravasate into the tumor. The systemic therapeutic application of TNF-α protein is hampered by its severe systemic toxicity, which requires specific targeting to tumors cells. Thus, TfR- and EGFR-targeted polyplexes encapsulating TNF-α expressing pDNA were developed to allow tumor-specific expression and paracrine activity of the cytokine [296, 360]. The targeted polyplexes led to sustained intratumoral TNF-α expression 48-72 hours after transfection in murine tumor models, resulting in efficient tumor necrosis, growth

reduction, and in some cases even complete tumor regression [296, 360]. The extent of therapeutic efficacy was tumor-type dependent, with tumor necrosis and tumor regressions demonstrated in one model, and retardation of tumor growth in several models [296, 360]. Moreover, Su et al. could show that chemotherapeutic drugs such as liposomal doxorubicin (DOX) could benefit from pTNF-α pre-treatment through the cytokine-mediated enhanced vascular permeability, achieving a more than 35-fold increase in DOX accumulation and its resulting antitumor efficacy [360].

pTRAIL, encoding for the cytokine 'tumor necrosis factor-related apoptosis inducing ligand' has likewise been delivered to tumors *via* targeted polyplexes, leading to distinctive antitumor effects caused by induced apoptotic mechanisms [262]. However, a drawback of pTRAIL is that tumors may gain resistance against the cytokine. Thus, Sun et al. and Li et al. used paclitaxel and doxorubicin, respectively, to enhance the tumor's sensitivity towards the chemokine and overcome potential resistance. *In vivo* trials with both combination therapies led to increased apoptosis, reduced tumor growth, and prolonged survival time of glioma xenograft bearing mice compared to single-therapeutic treated mice [262, 361].

pING4, a pDNA encoding for the inhibitor of growth protein 4, has also exhibited strong suppression of tumor growth and significantly prolonged survival time of glioma tumor models [210, 362]. The antitumor efficacy of ING4 is based on the regulation of multiple pathways essential for oncogenesis and tumor proliferation, including DNA repair, angiogenesis, migration, and transcriptional regulation [375]. Moreover, ING4 has the ability to induce apoptosis by activating a cascade reaction of the mitochondria-induced apoptotic pathway [375]. To increase the pDNA delivery efficiency, BBB penetration and efficacy for glioma treatment, polyplexes were actively targeted with I_6P_7, a ligand for the IL-6 receptor which is overexpressed on the BBB and on glioma cells. Wang et al. revealed that the peptide ligand significantly contributed to tumor cell apoptosis. In addition to enhanced pING4 accumulation in glioma cells, I_6P_7 was able to block the IL-6 mediated JAK/STAT tumor growth pathway. Thus, the I_6P_7-pING4 polyplex exhibited significantly enhanced antitumor efficacy and prolonged survival times in treated mice compared to untargeted pING4 polyplexes [362].

The sodium iodide symporter (NIS) represents a well-characterized theranostic tool that has proven its capacity to specifically accumulate diagnostic (^{123}I) or therapeutic radioiodide (^{131}I) in tumors. Various carriers including c-MET- and EGFR- targeted oligoaminoamide-based polyplexes [27, 37, 363, 364] have proven their ability to deliver NIS encoding pDNA to different non-thyroidal tumor models [37]. Diagnostic imaging allows detailed investigation of the distribution of NIS gene expression by the extent of

iodide accumulation for dosimetric calculations *via* non-invasive imaging through ^{123}I-scintigraphy and ^{124}I-/^{18}F-tetrafluoroborate positron emission tomography. Tumor therapy benefits from the strong bystander effects mediated by β-emitter ^{131}I, which expands its toxic effects to neighboring tumor cells. The delivery of NIS pDNA with targeted polyplexes and therapeutic iodide accumulation in murine hepatocellular [37], pancreatic [27] and glioma tumor models [364] resulted in significantly reduced tumor growth and in most cases prolonged survival time of treated mice [37, 364]. In an Huh7 tumor mouse model, treated by intravenous application with cMBP2-functionalized pNIS polyplexes, ^{123}I gamma camera imaging revealed tumor specific radioiodide accumulation and a 2-fold increase in survival time of pNIS and ^{131}I treated mice compared to the untreated groups. To overcome potential limitations through heterogenous receptor expression on tumor cells and to increase targeting efficiency, dual-targeting strategies with cMBP2 and GE11 ligands have proven to be beneficial [363]. The dual-targeted polyplexes achieved enhanced reduction of tumor growth and prolonged survival time of a treated mice in comparison to the previous single-targeted pNIS polyplexes [363].

Nucleic acid-based cancer vaccines present another type of antitumoral gene therapy [344, 376]. Schreiber et al. applied γ-irradiated melanoma cells, *ex vivo* transfected with a human interleukin-2 (IL-2) construct *via* Tf-pLys targeted transferrinfection as vaccine in a clinical phase I study with patients suffering from advanced stage IV melanoma. This gene-modified irradiated vaccine was able to secrete immunostimulatory IL-2 to trigger anti-melanoma immune responses, as demonstrated in preclinical models [377] and patients. Several patients showed periods of stabilized tumor sizes and regression of single metastases. Also, the mean survival time of patients was increased, demonstrating that nucleic acid-based tumor vaccines may bring benefits for certain patients possibly at earlier tumor stages.

pDNA transfection was also used to express non-coding RNAs. The long noncoding RNA (lncRNA) MEG3 has been proven to be closely related to tumorigenesis as it is expressed by most normal cells, but scarcely found in tumor cells. Tai et al. recently developed a pMEG3 polyplex targeting the epithelial adhesion molecule EpCAM. For targeting the RNA aptamer EpDT3 was applied as ligand. The expressed lncRNA exhibited the capacity to induce apoptosis, reduce proliferation and inhibit DNA synthesis of tumor cells [365]. *In vivo*, systemically administered pMEG3 polyplexes achieved a 60% reduced tumor size without showing systemic toxicity [365].

2.8.2 Therapeutic siRNA polyplexes

siRNA represents a class of gene therapeutics suitable for efficient silencing of tumor-promoting genes. Hence, identification of one or several target mRNAs who function for tumor growth, invasion, and metastasis is critical for tumor regression. As the site of siRNA action is the cytosol and not the nucleus, its anti-tumor effects are more potent but commonly transient. Nevertheless, this makes it a safer potential therapeutic compared to possible genomic interventions of pDNA or genome editing strategies.

Multiple siRNA polyplex formulations directed towards tumor promoting mRNAs have exhibited significant antitumor effects in various tumor types such as breast cancer [366], gliomas [300], and sarcomas [367]. siRAF-1, directed towards mRNA encoding for a cytosolic serine-threonine kinase, siEWS-FLI1 [300], against a chimeric fusion protein found in Ewing's sarcoma, and siPTN [367], against the cytokine pleiotrophin which is especially expressed in brain cancer, are just a few of the investigated siRNAs that have exhibited strong tumor reduction, prolonged survival time and no toxicity after their systemic, polyplex encapsulated application into murine tumor models [366].

siRRM2 was applied by Heidel et al. as a therapeutic siRNA with the capacity to suppress mRNA expression and inhibit tumor growth [368], which was later investigated in a phase I clinical study [303]. RRM2, a ribonucleotide reductase, is an enzyme essential for the production of nucleotides. Hence, RRM2 is a rate-limiting factor for DNA replication and presents a potential target to inhibit tumor growth. To enhance delivery of siRRM2, a cyclodextrin-based and Tf-targeted polyplex-system was employed, whose safety and efficacy in systemic applications was confirmed *in vivo* in mice and in non-human primates [301]. The subsequent phase I clinical study clearly exhibited siRRM2-mediated downregulation of the RRM2 enzyme evidently caused by a site-specific mRNA cleavage that lasted for several weeks after application.

Long noncoding RNAs (lncRNAs) may play a role in multiple oncogenic processes. The lncRNA DANCR (differentiation antagonizing non-coding RNA) regulates the proliferation and progression of various tumor types. Through its influence on tumor development and its well-defined spatial and temporal expression, DANCR presents an ideal target for siRNA-based tumor therapy. siDANCR, encapsulated into ECO-PEG-cRGD polyplexes, has been investigated for its antitumor effect in triple-negative breast cancer (TNBC) [162]. In vitro, siDANCR achieved 80-90% knockdown, resulting in decreased proliferation, invasion, migration, and survival of treated cells. Subsequent studies in a murine TNBC model exhibited the same oncogenic activities leading to significant tumor regression and prolonged survival times. The same setting, applying ECO-PEG-cRGD/siRNA polyplexes to TNBC xenograft mice, was employed to

investigate the efficacy of siβ3, an siRNA designed to suppress the expression of integrin β3 in tumors. siβ3 exhibited the ability to successfully reduce tumor growth, through the inhibition of TGF-β-mediated EMT (epithelial-mesenchymal transition), as well as invasion and metastasis [161].

To further increase antitumor efficacy, siRNA-mediated tumor therapy has also been combined with photodynamic therapy (PDT). PDT induces cytotoxic reactive oxygen species (ROS), generated in the presence of photosensitizers, molecular oxygen, and laser light. Subsequent ROS mediated antitumor immune responses are based on several mechanisms, including the upregulation and secretion of cytokines, and facilitating antigen expression to T-lymphocytes. Tumors may develop resistance against immune therapy, mediated by the immune checkpoint molecules 'programmed cell death receptor 1' (PC-1) and its ligand 'programmed death ligand 1' (PD-L1). Hence, Wang et al. developed an acid-cleavable micelloplex that induced ROS production upon PDT and prevented immune resistance through siPD-1-PD-L1-mediated mRNA degradation. The systemically applied micelloplexes achieved reduced tumor growth and metastasis in a murine tumor model, achieved through the synergistic effects of PDT, which initiated the secretion of cytokines, and the siRNA, which inhibited the interaction of PD-1 with its ligand and thereby prevented immune resistance towards PDT [369].

ROS may not only induce immune reactions but can also be applied to destabilize ROS-responsive nanomedicines. Zheng et al. designed an angiopep-functionalized, stabilized carrier for the co-delivery of siPLK1 (polo-like kinase 1) and siVEGFR (vascular endothelial growth factor receptor) to specifically target and treat well-vascularized glioblastomas. Intravenous injection of the angiopep-functionalized siRNA polyplex efficiently silenced PLK1 and VEGFR mRNA in glioblastoma cells, which resulted in tumor necrosis, reduced vascularization and ultimately in reduced tumor growth and prolonged survival time of an orthotopic glioma mouse model [370].

Taken together, siRNA has proven its potential to inhibit tumor growth in systemic applications. Combination therapies combining several antitumoral siRNA targets optionally with standard chemotherapeutic might provide an encouraging avenue against chemoresistance of cancer.

2.8.3 Therapeutic miRNA polyplexes

Apart from siRNA, RNA interference may also be induced by micro RNAs (miRNAs), 17-25 nucleotide short RNAs that are closely related to siRNA regarding their structure and mRNA-silencing mechanism. However, in contrast to siRNAs, miRNAs occur naturally

and often play a role in the regulation of tumorigenic processes such as tumor invasion, metastasis, and therapeutic resistance. Moreover, miRNA-mRNA binding is commonly not completely complementary but mediated by a 2-8 nucleotide seed-sequence within the miRNA. In many cases this only leads to translation inhibition and less to mRNA degradation. Although siRNA may lead to more efficient knockdown due to its capacity to induce degradation, miRNA has the advantage that its limited binding sequence length allows regulation of more than 100 mRNAs per miRNA molecule.

miR-145 and miR-33a are such natural occurring miRNAs and their presence in cells correlates with proapoptotic and antiproliferative effects. The lack of miR-145 and miR-33a in many tumors leads to the expression of their regulated oncogenes c-Myc and ERK5, and Pim-1, respectively. Therefore, Ibrahim et al. investigated the replacement of miR-145 and miR-33a with systemically injected PEI polyplexes to restore the miRNA-mediated antitumor effects. Polyplex administration achieved specific downregulation of the target mRNA and significantly reduced tumor growth at high biocompatibility.

miR-200c is a well-investigated miRNA whose reduced expression in many tumors has effects on EMT, cell motility, apoptosis resistance, and multi-drug resistance. In TNBC, miR-200c expression levels are closely related to the survival rates of patients [163]. Z.R. Lu et al., who had already successfully delivered the structural related siRNA to TNBC tumor models, investigated the effects of miR-200c delivery to mice bearing orthotopic breast cancer. Systemically delivered miR-200c polyplexes demonstrated the ability to reduce tumor progression and proliferation without signs of toxic effects. Moreover, monitoring the tumor response with non-invasive magnetic resonance molecular imaging (MRMI) and immunohistochemistry revealed that miR-200c altered the TME by reducing extradomain B fibronectin expression.

2.8.4 Other therapeutic RNA polyplexes

mRNA delivery has attracted attention as a strategy to introduce therapeutic peptides [374], proteins [378] or antibodies [379] to tumors. Compared to DNA, mRNA has the advantage that it circumvents insertional mutagenesis and can be applied to non-dividing cells. Compared to direct peptide and protein delivery, mRNA has a more sustainable effect. However, the delivery of single-stranded mRNA to tumor cells is hampered by its instability in blood circulation, requiring stable carriers to protect it from enzymatic degradation.

Nonetheless, first systemically applied mRNA formulations have achieved antitumor effects related to their successful intracellular translation. Uchida et al. achieved high

mRNA transfection efficiency *in vivo* using a PEG-polyaspartate carrier, stabilized with cholesterol. Treatment of pancreatic cancer with an mRNA encoding for the anti-angiogenic peptide 'fms-like tyrosine kinase 1' (sFlt-1), a soluble receptor for VEGF, was investigated. sFlt-1 inhibits VEGF binding to its cellular receptor (VEGFR), which in the study led to a decreased vascular density, revealed by immunohistological staining, and which consequently led to a remarkable inhibition of tumor growth [374].

Outside the class of polyplexes, the great potential of therapeutic mRNA was recently demonstrated by its use as LNP (lipid nanoparticle)-based mRNA vaccines in the COVID-19 pandemic. The fast development of mRNA-based vaccines was in part due to a long-term program focusing on the development of patient-specific cancer vaccination, where mRNA that is designed based on the patient-specific tumor RNA transcriptome is applied to trigger specific antitumor immunity [103, 104, 380, 381].

Alternative immunological strategies employed for cancer treatment include direct intratumoral application of immunostimulatory nucleic acids, including Toll-like receptor (TLR) or retinoic acid-inducible gene I (RIG-I) oligonucleotide agonists [382]. Virus-infected cells frequently express double-stranded RNA that activate pro-apoptotic processes such as the regulation pro-apoptotic protein expression and the secretion of cytokines. For example, polyIC (polyinosinic : polycytidylic acid) is a synthetic double-stranded RNA that has been used to initiate cell-killing mechanisms in tumor cells. Moreover, the delivery of polyIC polyplexes has exhibited a strong bystander effect mediated by its induced secretion of cytokines [372]. The efficacy of polyIC polyplexes to treat tumors has been confirmed by several *in vivo* studies. The administration of EGFR-targeted polyplexes with the immunostimulatory RNA has achieved significant antitumor effects after intracranial administration to gliomas and systemic administration to other EGFR positive tumors, resulting in reduced tumor sizes and prolonged survival times of treated mice [310, 313, 372, 373].

The recent global use of mRNA therapeutics has also attracted attention for their application as gene editing tools, as illustrated by the first clinical *in vivo* studies using CRISPR Cas9 mRNA/sgRNA LNPs [97]. As a possible alternative to gene knock down by RNA interference, genome editing by the CRISPR Cas9/sgRNA has been introduced as potential tool in anticancer therapy [383-386]. From technology perspective, different formats, Cas9 pDNA versus Cas9 mRNA versus Cas9 RNPs, can be delivered [99]. pDNA encoding CRISPR Cas9 and the sgRNA targeting the oncogene survivin has been delivered by heparin/ethanolamine-modified poly(glycidyl methacrylate) polyplexes to treat orthotopic HCC (hepatocellular carcinoma) in mice via tail vein injection, and achieved anti-tumor effects [384]. The therapeutic efficacy of gene editing tools to treat

tumors has mainly been demonstrated using other delivery systems than polyplexes, especially LNPs. The delivery of Cas9 mRNA and sgRNAs against PLK1 (sgPLK1-cLNPs) through intracerebral injection into orthotopic glioblastoma enabled up to 70% gene editing, tumor cell apoptosis, 50% tumor growth inhibition and 30% improved survival. Intraperitoneal administration of EGFR-targeted sgPLK1-cLNPs enabled up to 80% gene editing in an ovarian tumor mouse model, linked with tumor growth inhibition and increased survival of mice [385]. Polymer-formulated CRISPR/Cas9-based RNPs containing a combination of sgRNAs enhanced tumor accumulation after intravenous application and efficient gene editing in targeted tumor cells. A combination of sgRNAs that targets STAT3 and RUNX1 led to effective growth inhibition of a heterogeneous tumor responsive to either STAT3 or RUNX1 knock-out [386].

Taken together, nucleic acid-based tumor therapy has the potential to treat cancer by targeting gene expression at different levels. To develop such potent therapeutics, it is required to understand tumor biology and to identify tumor-essential genes, whose expression or suppression are related to tumorigenesis.

2.9 Conclusion

Systemic delivery of nucleic acid-based polyplexes to tumors is a complex procedure facing multiple extra- and intracellular barriers, all requiring specific polyplex modifications. Stability in blood circulation, formation of protein corona, extravasation, penetration of tumor stroma, tumor specific cellular uptake, endosomal escape, cargo release and finally therapeutic efficacy of the nucleic acid sums up the aspects which require most consideration when developing nucleic acid-based therapeutics. Polyplex modifications may have conflicting effects: cationic surface charges for enhanced cellular uptake may lead to severe side-effects, PEGylation against unspecific interactions may reduce cellular internalization, and high polyplex stability may reduce intracellular nucleic acid release. Here, finding the right balance may be the key for highly efficient polyplexes. Stimuli-responsive formulations with size-switching or charge-switching capacity may present solutions to meet the distinct barrier demands. Moreover, every barrier but also every tumor type and stage due to their distinct morphologies may require specific adaptions. Variations in degree of vascularization, leakiness of tumor blood vessels or composition and density of stroma influence polyplex capacity to penetrate tumor tissue. Regarding the increasing number of preclinical and clinical studies and market products, nucleic acid-based therapeutics are steadily being implemented as a new platform for cancer treatment.

Funding. This work was supported by the German Research Foundation (DFG) SFB1032 (project-ID 201269156) sub-project B4.

Declaration of Competing Interest. The authors declare no competing interests.

Acknowledgements. The authors are greatly thankful for support of their related work by the German Research Foundation (DFG) WA 1648/7-1 and by the UPGRADE (Unlocking Precision Gene Therapy) project that has received funding from the European Union's Horizon 2020 research and innovation program (grant agreement no. 825825).

3 Ionic coating of siRNA polyplexes with cRGD–PEG–hyaluronic acid to modulate serum stability and in vivo performance

Victoria C. Vetter,[a] Mina Yazdi,[a] Irene Gialdini,[b] Jana Pöhmerer,[a] Johanna Seidl,[a] Miriam Höhn,[a] Don C. Lamb,[b,c] and Ernst Wagner [a,c,d,]*

[a] Pharmaceutical Biotechnology, Department of Pharmacy, Ludwig-Maximilians-Universität, Butenandtstraße 5-13, Munich 81377, Germany

[b] Department of Chemistry, Ludwig Maximilians-Universität München, Butenandtstraße 5-13, Munich 81377, Germany

[c] Center for NanoScience (CeNS), Ludwig-Maximilians-Universität, Butenandtstraße 5-13, Munich 81377, Germany

[d] CNATM – Cluster for Nucleic Acid Therapeutics Munich, Würmtalstr. 201, Munich 81377, Germany

[*] Email: ernst.wagner@lmu.de

This chapter is adapted from a research article published in **Biochemistry in March 2025, DOI: https://doi.org/10.1021/acs.biochem.4c00650. [387]**

Table of Contents Figure

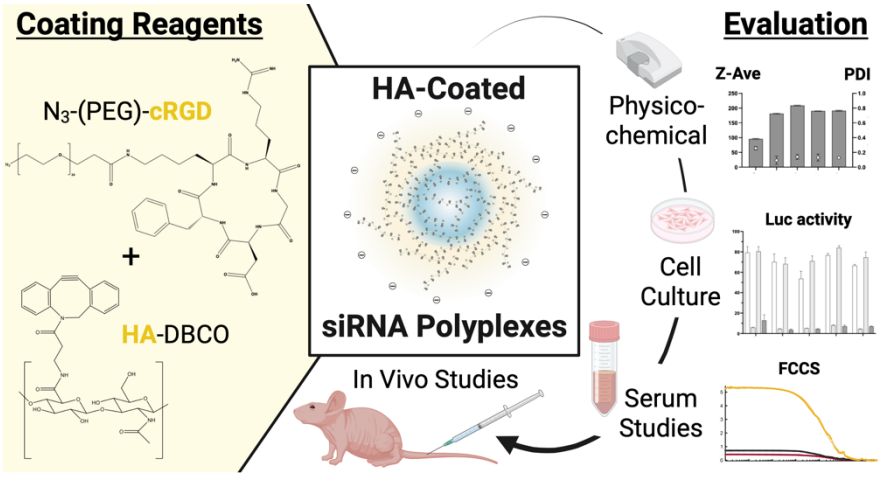

Created with BioRender.com

3.1 Abstract

Efficient delivery of siRNA-based polyplexes to tumors remains a major challenge. Nonspecific interactions in the bloodstream, limited circulation time, and non-targeted biodistribution hamper sufficient tumor accumulation. To address these challenges, we developed an ionic hyaluronic acid (HA) coating to shield sequence-defined oligoaminoamide-based polyplexes. This coating should shield the positive polyplex surface charge, thus reducing nonspecific interactions and enhancing serum stability. Additionally, we modified the HA coating with the cyclic RGDfK (cRGD) peptide to specifically target tumor endothelial cells (TECs). Optionally, a polyethylene glycol (PEG) spacer was also introduced to improve ligand presentation on the polyplex surface. The HA-coated polyplexes exhibited favorable physicochemical properties including a negative zeta potential and effective siRNA retention within the polyplex, which was not adversely affected by PEG and cRGD modification. *In vitro* analyses revealed that these polyplexes not only enhanced tumor cell association and preserved the high transfection efficiency of plain cationic polyplexes but also exhibited coating-dependent cellular internalization, as evidenced by a competitive inhibition experiment. Even in the presence of serum, the HA-coated polyplexes encapsulated siRNA effectively, exhibited suitable particle sizes and maintained a high gene silencing efficiency. *In vivo* studies involving intravenous administration into Neuro2a tumor-bearing mice showed that the HA-coating, particularly when modified with PEG or cRGD, significantly increased the tumor accumulation of polyplexes. HA-PEG-cRGD shielded polyplexes exhibited significantly enhanced *in vivo* gene silencing in tumors compared with plain polyplexes. Collectively, our results indicate a superior performance of HA-coated polyplexes in terms of stability and cellular uptake, both *in vitro and in vivo*.

3.2 Introduction

Small interfering RNA (siRNA) is an emerging class of gene therapeutics with the potential to reversibly silence target genes in a sequence-specific manner through RNA interference (RNAi). This capability has led to the development of several siRNA-based therapeutics on the market and numerous further candidates in clinical trials [2, 388-390]. These therapeutics offer novel treatment options for genetic conditions primarily originating in the liver, which were previously difficult to manage. However, despite decades of research in the field, the bottleneck in the development of novel siRNA therapeutics remains efficient delivery to tissues beyond liver hepatocytes. One of the most compelling applications for siRNA therapeutics is in tumor therapy, where siRNA

would down-regulate genes related to tumor survival and proliferation. Compared to traditional chemotherapeutics, siRNA-based tumor therapy could reduce the side effects associated with chemotherapy due to its specific mechanism of action, degrading only the targeted mRNA, thus decreasing the likelihood of off-target effects.

For effective tumor delivery, siRNA must be administered intravenously, making the use of protective measures such as chemical modifications or nanocarriers essential [86, 90, 391-397], as unprotected siRNA is rapidly degraded and eliminated from the bloodstream. Encapsulation of siRNA into polyplexes–cationic nanocomplexes formed by spontaneous electrostatic interactions between cationic carriers and anionic nucleic acids–is a widely applied strategy to provide for extracellular stability, delivery, intracellular release, and high transfection efficiency [19, 115, 398-401]. However, the challenge associated with these positively charged nanoparticles is their pronounced propensity to interact with blood proteins, leading to inflammatory and innate immune responses and resulting in *in vivo* toxicities [26, 57, 62, 121]. Furthermore, the cationic surface charge of polyplexes promotes nonspecific electrostatic adherence to negatively charged cell membranes, which leads to unintended tissue accumulation rather than targeted delivery.

A favorable strategy to mitigate these adverse effects and to prolong blood circulation involves employing hydrophilic agents such as polyethylene glycol (PEG) and other hydrophilic macromolecules [26, 131, 402-404], such as coating with artificial [405-407] or natural polyanions like hyaluronic acid (HA) [66, 126, 127] to shield the positive surface charge. Due to the beneficial characteristics of HA, including its high biocompatibility and biodegradability, and its lower immunogenicity compared to PEG, this endogenous biopolymer has frequently been applied in nanoparticle design [66, 67, 126, 355, 408]. However, its application in tumor delivery remains underexplored. Besides its potential for shielding, HA acts as a targeting ligand through its binding capacity to the CD44 receptor, which is commonly overexpressed on tumor and tumor endothelial cells (TECs) [354, 409]. Additionally, the presence of hydroxyl, carboxyl, and N-acetyl groups in each disaccharide unit provides several options for chemical modifications of the polyanion.

In our previous work, we designed covalently HA-coated polyplexes for siRNA delivery to tumors [40]. We demonstrated that cationic polyplexes formed with a cationizable sequence-defined lipo-oligoaminoamide (OAA), when covalently coated with HA, showed significantly increased *in vivo* gene silencing in tumor-bearing mice compared to their non-coated equivalent. Given that anionic nanoparticles have commonly proven to reduce serum protein adsorption [410], which improves its performance in blood

circulation and facilitates diffusion through the anionic network in the tumor extracellular matrix (ECM) [269, 411], in the current work, we aimed to develop an ionic HA coating resulting in negatively charged siRNA polyplexes. Based on encouraging previous work [66, 126, 127], we hypothesize that ionically coated polyplexes remain structurally intact even if the weakly-bound HA partly detaches with time.

Because the well-shielded anionic HA polyplexes may hamper tumor accumulation due to the loss of TEC-adhesive positive surface charge, we tuned the HA coating with additional targeting entities. For this, we chose the peptide-ligand cyclic RGDfK (cRGD), which has been shown to enhance tumor delivery in various settings by targeting integrin αvβ3 [86, 172-177]. The integrin αvβ3 receptor is widely expressed in TECs due to its significant role in cell proliferation, metastasis and cell survival. TECs are an ideal target for enhancing tumor accumulation, as they represent the first barrier for tumor-directed polyplexes circulating in the bloodstream. For ligand attachment, we utilized HA modified with DBCO linkage modules (HA-DBCO) to enable facile click chemistry with azido-functionalized targeting ligands (cRGD or PEG–cRGD) through copper-free strain-promoted alkyne–azide cycloaddition (SPAAC) [412].

In this study, we aimed to develop anionic HA-coated siRNA polyplexes to enhance *in vivo* compatibility, blood circulation, and stability compared to their plain cationic counterparts. Additionally, tuning the ionic HA coating with the targeting peptide-ligand cRGD without or with a short PEG spacer aimed to improve TEC adherence, thereby enhancing *in vivo* tumor accumulation and gene silencing efficiency. During development, we first established colloidally stable anionic HA-coated polyplexes by varying the HA to polyplex ratio. Subsequently, these polyplexes were further functionalized with the targeting ligand cRGD by applying covalently coupled HA–cRGD or HA–PEG–cRGD conjugates for ionic coating. Physicochemical evaluations demonstrated that ligand modification did not significantly alter the polyplex characteristics. After confirming consistently high efficiency of both non-coated and HA-coated formulations in cell culture studies, we validated the functionality and stability of these polyplexes after serum incubation by fluorescence (cross-) correlation spectroscopy (FCS/FCCS). Subsequent *in vivo* studies in Neuro2a tumor-bearing mice revealed a clear beneficial effect of the HA coating in tumor biodistribution and gene silencing.

3.3 Materials and Methods

3.3.1 Materials

2-Chlorotrityl resin, Fmoc- α-amino acids, N,N-dimethylformamide (DMF), dichloromethane (DCM), N,N-diisopropylethylamine (DIPEA), trifluoroacetic acid (TFA), and N-methyl-2-pyrrolidone (NMP) were purchased from Iris biotech (Marktredewitz, Germany). 1-Hydroxybenzotriazole (HOBt), triisopropylsilane (TIS), dibenzocyclooctyne-amine (DBCO-amine), dimethyl sulfoxide (DMSO), benzotriazole-1-yl-oxy-trispyrrolidino-phosphonium hexafluorophosphate (PyBOP) and oleic acid were bought from Sigma Aldrich (Munich, Germany). Fmoc-Stp$(Boc)_3$-OH was synthesized in-house according to published protocols [413]. Hyaluronic acid (HA20K; average molecular weight 38 kDa) was obtained from Lifecore Biomedical (Chaska, USA). Polypropylene syringe microreactors for peptide synthesis were purchased from MultiSynTech (Witten, Germany). Control siRNA (siCtrl) [5´-AuGuAuuGGccuGuAuuAGdTsdT-3´ (sense); 5´-CuAAuAcAGGCcAAuAcAUdTsdT-3´(antisense)], eGFP-targeted siRNA (siGFP) [5´-AuAucAuGGccGAcAAGcdTsdT-3´ (sense); 5´-UGCUUGUCGGCcAUGAuAUdTsdT-3´ (antisense)], EG5-targeted siRNA (siEG5) [5´-ucGAGAAucuAAAcuAAcudTsdT-3´(sense); 5´-AGUuAGUUuAGAUUCUCGAdTsdT-3´ (antisense)], Cy5-labeled siRNA (Cy5-siAHA1) [5´-(Cy5)(NHC6)GGAuGAAGuGGAGAuuAGudTsdT-3´ (sense); 5´-ACuAAUCUCcACUUcAUCCdTsdT-3´ (antisense)], and Cy7-labeled siRNA (Cy7-siAHA1) [5´-(Cy7)(NHC6)GGAuGAAGuGGAGAuuAGudTsdT-3´ (sense); 5´-ACuAAUCUCcACUUcAUCCdTsdT-3´ (antisense)] were provided by Roche Kulmbach GmbH (now Axolabs GmbH, Kulmbach, Germany). Atto565-labeled siRNA [5´-(Atto565)AUGUAUUGGCCUGUAUUAGdTsdT-3´ (sense); 5´-CUAAUACAGGCCAAUACAUdTsdT-3´ (antisense)] was purchased from biomers.net GmbH (Ulm, Germany) and VEGFR-2-targeted siRNA (siVEGFR-2, ON-TARGETPlus SMARTpool siRNA) from Dharmacon. The cell culture medium, fetal bovine serum (FBS), trypsin/EDTA, β-mercaptoethanol, 3-(4,5-dimethyl-2-thiazolyl)-2,5-diphenyl-tetrazolium bromide (MTT), antibiotics (penicillin/streptomycin), paraformaldehyde (PFA), 4'-6-diamidino-2-phenylindole (DAPI), adenosine 5′-triphosphate, and coenzyme A were obtained from Sigma Aldrich (Munich, Germany). Rhodamine-phalloidin (Invitrogen) was obtained from Thermo Fisher Scientific (Schwerte, Germany), tissue culture test plates were obtained from TPP (Trasadingen, Switzerland), and cell culture flasks and pipettes were obtained from Sarstedt (Nümbrecht, Germany). All other cell culture consumables were obtained from Faust Lab Science (Klettgau, Germany).

HEPES was purchased from Biomol GmbH (Hamburg, Germany), glucose monohydrate, agarose (NEEO Ultraquality) and GelRed were purchased from VWR (Darmstadt, Germany), and disodium ethylenediaminetetraacetic acid (EDTA) was purchased from Merck (Darmstadt, Germany). Cell culture lysis buffer and D-luciferin sodium salt were obtained from Promega (Mannheim, Germany). cRGDfK-PEG1K-N_3 was purchased from KamulinBiotechco.ltd (Xi'an City, China), N_3-PEG1K-OH from Otto Nordwald GmbH (Hamburg, Germany), and Atto643-N_3 from ATTO-TEC GmbH (Siegen, Germany). All further reagents were purchased from Sigma-Aldrich (Munich, Germany), Iris Biotech (Marktredewitz, Germany), Merck (Darmstadt, Germany), or AppliChem (Darmstadt, Germany).

3.3.2 Methods

3.3.2.1 Synthesis of lipo-oligoaminoamide 1670

The lipo-OAA 1670 (see **Scheme 1A**) was synthesized using standard Fmoc-based solid-phase supported synthesis in syringe reactors, following protocols analogous to previously reported methods [35, 40, 157, 414, 415]. The synthesis consisted of four main steps: loading, coupling, deprotection, and cleavage from the resin. A cysteine-loaded chlorotrityl chloride resin served as a solid support for synthesizing the backbone, utilizing a Syro Wave synthesizer (Biotage, Uppsala, Sweden) with microwave assistance. The side chain was subsequently coupled manually. Due to the presence of oleic acid in the side chain, the cleavage from the resin was performed using an optimized protocol, involving incubation of the resin for 30 min with TFA-TIS-H_2O 95:2.5:2.5 (10 mL/g resin, cooled to 4°C prior to addition), followed by immediate precipitation in 40 mL of precooled methyl tert-butyl ether (MTBE)-n-hexane (1:1) [415].

3.3.2.2 Synthesis of DBCO-modified hyaluronic acid

HA (38 kDa hyaluronic acid, 1 equiv, 0.025 mmol monomers, 5 mg), NHS (N-hydroxysuccinimide, 5 equiv, 0.06 mmol, 6.9 mg), and EDC (3-(ethyliminomethylenamino)-N,N,-dimethylpropan-1-amine, 5 equiv, 0.06 mmol, 11.5 mg) were dissolved in 1.2 mL of activation buffer (0.1 M TES, 2-[[1,3-dihydroxy-2-(hydroxymethyl)propan-2-yl]amino]ethanesulfonic acid) and incubated for 2 h at RT while shaking (700 rpm). Subsequently, 1 equiv of DBCO-amine (0.024 mmol, 6.63 mg) solved in 0.4 mL DMF was added to the reaction mixture, and the pH was adjusted to 7 using NaOH (1 M). After continuous shaking for 18 h at RT, the resulting HA-DBCO was purified by dialysis against deionized water using a 3500 Da cutoff membrane. The

product was then lyophilized, and the degree of DBCO substitution was analyzed using UV-vis spectroscopy at 308 nm (ε = 12,000 M^{-1} cm^{-1}) and confirmed by the ^{1}H NMR spectrum.

3.3.2.3 Synthesis of N_3-cRGDfK

The linear precursor structure H_2N-DfK(N_3)-RG-OH was synthesized using standard manual 9-fluorenyl-methoxycarbonyl solid-phase peptide synthesis (SPPS) on an $_{L}$-Gly-OH-preloaded 2-chlorotrityl resin (loading: 0.22 mmol/g) using the following Fmoc-protected amino acids: Fmoc-$_{L}$-Arg(Pbf)-OH, Fmoc-$_{L}$-Lys(N_3)-OH, Fmoc-$_{D}$-Phe-OH, and Fmoc-Asp(OtBu)-OH [76].To preserve the side chain protecting groups, the peptide was cleaved under mild conditions conducting a DCM/TFA solution (99/1, v/v) for 30 min at RT. Subsequently, the solvent was evaporated under reduced pressure. Additionally, toluene was added to prevent the concentration of TFA from increasing within the mixture upon evaporation. The resulting residue was dried under high vacuum (HV).

The linear peptide was cyclized by forming an amide bond between the N-terminal amino group of aspartic acid and the C-terminal carboxyl group of glycine. This was achieved by dissolving the linear precursor in DCM, followed by the addition of PyBOP (4 eq), HOBt (4 equiv), and DIPEA (8 equiv). The reaction mixture was stirred at RT for 3 days. The resulting cyclic ligand, with side chain protecting groups, was purified by using reverse-phase high-performance liquid chromatography (RP-HPLC) with a Symmetry C18 column and subsequently freeze-dried. The identity of the purified cyclic ligand was confirmed using matrix-assisted laser desorption/ionization-time of flight mass spectrometry (MALDI-TOF-MS).

The side chain-protecting groups were removed by adding a TFA/H_2O/TIS (95/2.5/2.5, v/v/v) solution for 90 min at RT. The cleavage solution was then evaporated under reduced pressure with toluene, and the residue was dried under HV. The residue was dissolved in ethanol and water, and dialyzed (100–500 Da MWCO, Carl Roth) against water for 24 h at 4°C to purify the cyclic ligand. The final product was characterized by MALDI-TOF-MS. Synthesis was kindly performed by Johanna Seidl (Pharmaceutical Biotechnology, LMU Munich).

3.3.2.4 Preparation of HA-ligand conjugates

HA-DBCO and the respective azido ligand (N_3-cRGDfK, N_3-PEG_{1K}-OH, N_3-PEG_{1K}-cRGDfK) were mixed in an Eppendorf tube and incubated for a minimum of 4 h with constant shaking (700 rpm) at RT. The amount of azido ligand was calculated based on

the DBCO substitution degree on HA, with a 20% excess added to ensure complete DBCO functionalization. The resulting HA-ligand conjugates (HA-cRGDfK, HA-PEG_{1K}, HA-PEG_{1K}-cRGDfK) were dialyzed against purified water using a 14 kDa cutoff membrane, followed by lyophilization. Complete reaction of all DBCO groups was verified through UV-vis spectroscopy at 308 nm.

3.3.2.5 siRNA polyplex formation

Oligoaminoamides (OAA) and siRNA were each diluted to 30% of the final polyplex volume using 20 mM HEPES buffered 5% glucose, pH 7.4 (HBG). Equal volumes of the diluted siRNA and OAA solutions were then mixed at a nitrogen-to-phosphate (N/P) ratio of 12, considering only protonatable amines for the N/P calculation (see **Scheme 1A**). This mixture constituted 60% of the total polyplex volume. The solutions were mixed by rapidly pipetting up and down, and the resulting core-polyplexes were incubated for 40 min at RT to allow self-assembly through electrostatic interactions and disulfide bridge formation.

For HA coating, the coating agent (either unmodified HA or HA-ligand conjugate) was diluted in HBG to 40% of the final polyplex volume. The core polyplex (60 % of final volume) was then added to the HA solution, mixed carefully through pipetting, and incubated for 10 min at RT (see **Scheme 1B**). The HA amount was calculated using a ratio of 3 HA units per Stp. Each HA unit corresponds to one disaccharide repeat unit bearing a single negative charge from its carboxy group, while each Stp unit contains one positive charge, contributed by one of its three protonatable amines, which is protonated at pH 7.4. For plain cationic polyplexes, the core polyplex was mixed with an equivalent volume of HBG instead of the HA solution.

3.3.2.6 Agarose gel shift assay

A 2.5% agarose gel was prepared by dissolving agarose in TBE buffer (10.8 g of Trizma base, 5.5 g of boric acid, 0.75 g of disodium EDTA, 1 L of water). After the mixture cooled to approximately 50 °C, GelRed (1/1000 (v/v); Biotum, Heyward, USA) was added to the gel mixture, which was then transferred to the electrophoresis chamber. Formulations containing 500 ng of siRNA were prepared in 20 µL of HBG (25 ng/µL) and supplemented with 4 µL loading buffer (6 mL of glycerol, 1.2 mL of 0.5 M EDTA, 0.02 g of bromophenol blue, 2.8 mL of H_2O). The formulations were then pipetted into the gel pockets, and electrophoresis was conducted for 1 h at 100 V.

3.3.2.7 Particle size and Zeta potential

For dynamic and electrophoretic light scattering (DLS and ELS) measurements, a Zetasizer Nano ZS with backscatter detection (Malvern Instruments, Worcestershire, UK) was used. Twenty µL of polyplexes were prepared containing the indicated amount of siRNA. Before measurement, formulations were diluted with 60 µL HBG and transferred to a folded capillary cell (DTS 1070) for particle size and polydispersity index (PDI) analysis with the settings as follows: 30 s equilibration time, temperature 25 °C, refractive index 1.330, viscosity 0.8872 mPa* s. Each sample was measured three times with six subruns. For zeta potential measurements, the sample was further diluted with 700 µL of 20 mM HEPES. Measurement parameters were identical to those used for size and PDI determination, with an increased equilibration time of 60 s. Each sample was measured 3 times with 15 subruns lasting 10 s. The zeta potential was calculated by using the Smoluchowski equation. All values (size, PDI, and zeta potential) were displayed as the mean ± SD out of these measurements.

3.3.2.8 Cell culture

The human cervix carcinoma KB (wt) and KB eGFP/Luc cells, which stably express the eGFPLuc fusion gene, were used for evaluating the gene silencing effect of siRNA polyplexes, as well as the murine neuroblastoma cells Neuro2a, were cultivated in DMEM low glucose (1 g/L glucose). The human prostate cancer reporter cells DU (wt) and DU145 eGFP/Luc, which also stably express the eGFPLuc fusion gene, were cultivated in RPMI 1640 medium. The murine brain endothelial cells bEnd.3 were grown in DMEM (4.5 g/L glucose). All media were supplemented with 10% (v/v) FBS and antibiotics (100 U/mL penicillin and 100 µg/mL streptomycin). Cells were kept in an incubator at 37°C with 5% CO_2 and a relative humidity of 95%.

3.3.2.9 Cell association by flow cytometry

DU145 and KB cells were seeded in 96-well plates at a density of 5000 cells/well and cultivated for 24 h prior to transfection. Cells were transfected with polyplexes containing 20% Cy5-labeled and 80% unlabeled siRNA at a dose of 62.5 ng/well and incubated at 37°C for time periods ranging from 0.5 to 48 h. Cells treated with HBG served as a negative control. After incubation, cells were washed twice with PBS and were then collected through trypsinization and resuspension in flow cytometry buffer (PBS containing 10% FBS) supplemented with 1 ng/µL DAPI viability dye. The analysis was conducted on viable cells using a CytoFLEX S flow cytometer (Beckman, USA). Cy5-

labeled cells were counted through excitation at 635 nm and detection at 665 nm. The results were evaluated with FlowJo 7.6.5 software (Ashland, Oregon, USA). Cell association was quantified as the percentage of Cy5-positive cells and mean fluorescence intensity (MFI), and presented as the mean of triplicate wells ± SD.

3.3.2.10 Endocytosis inhibition assay

KB cells were seeded in 96-well plates at a density of 10,000 cells/well and cultivated for 24 h prior to treatment. The medium was then replaced with 100 µL of serum-free medium containing various inhibitors (sucrose 450 mM, amiloride 1 mM, nystatin 54 µM) and incubated for 1 h at 37°C. Subsequently, the medium was replaced with 95 µL of fresh medium including 10% FBS and 5 µL of HBG buffer containing polyplexes at a dose of 125 ng siRNA (20% spiked with Cy5-labeled siRNA). Polyplexes were incubated on the cells for 4 h at 37°C. HBG-treated cells served as a negative control. After incubation, the cells were treated with heparin and incubated for 15 min on ice. Finally, the cells were collected, and the mean fluorescence intensity (MFI) was measured by using a flow cytometer following the standard protocol for assessing cell association.

3.3.2.11 Cell internalization by confocal laser scanning microscopy

DU145 cells were seeded in 8-well Ibidi µ-slides (Ibidi GmbH, Germany) at a density of 20,000 cells per well. After 24 h, polyplexes containing 20% Cy5-labeled siRNA were transfected for 48 h at 37°C at a dose of 62.5 ng of siRNA per well. After incubation, the cells were washed twice with PBS and fixed with 4% (w/v) paraformaldehyde (PFA) for 30 min. After re-washing, the actin skeletons were stained with rhodamine-phalloidin (1 µg/mL, Invitrogen) for 1 h, followed by cell nuclei staining with DAPI (1 µg/mL, Sigma-Aldrich) for 20 min. Afterward, cells were rewashed, and wells were filled with PBS for imaging. The images were captured by M. Höhn (Pharmaceutical Biotechnology, LMU Munich) with a Leica-TCS-SP8 confocal microscope with HC PL APO 63 x 1.4 objective (Germany) using Leica LAS X software.

3.3.2.12 Reporter gene silencing study by luciferase assay

Cells expressing the eGFP/Luc reporter gene were seeded in 96-well plates at a density of 5000 cells/well and incubated in 100 µl of a medium containing 10% FBS at 37°C for 24 h prior to the experiment. Cells were transfected with polyplexes at two different doses (62.5 and 250 ng siRNA), containing either siCtrl (control siRNA) or siGFP (GFP-targeted siRNA). After incubation for 48 h at 37 °C, cells were lysed using 100 µL of 0.5× lysis

buffer, followed by 1h of incubation at RT. The luciferase activity of 35 µL of the cell lysates was measured with a Centro LB 960 plate reader luminometer (Berthold Technologies, Bad Wildbad, Germany) using LAR buffer (20 mM glycylglycine, 1 mM MgCl2, 0.1 mM EDTA, 3.3 mM dithiothreitol (DTT), 0.55 mM adenosine 5'-triphosphate (ATP), 0.27 mM coenzyme A, pH 8-8.5) supplemented with 5% (v/v) luciferin solution (10 mM luciferin, 29.4 mM glycylglycerine). The relative light units (RLUs) of samples were calculated as the percentage of HBG-treated control cells, and the luciferase activity of the eGFP/Luc fusion protein was presented as the mean of triplicate wells ± SD.

3.3.2.13 Receptor gene silencing study by flow cytometry

Murine brain endothelial (bEnd.3) cells were seeded in 48-well plates at a density of 10,000 cells per well and incubated for 24 h prior to transfection. Polyplexes containing VEGFR-2-targeted siRNA (siVEGFR-2) were then prepared and transfected at a dose of 500 ng of siRNA/well. The cells were incubated with the polyplexes for 48 h at 37°C. Afterward, cells were washed with PBS, harvested and incubated in flow cytometry buffer containing PE-Vio-conjugated VEGFR-2 mAb for 30 min on ice and in the dark. Subsequently, cells were washed twice, resuspended in flow cytometry buffer containing 0.1% Sytox Blue viability dye (Invitrogen), and acquired by flow cytometry (MACSQuant Analyzer 10, Miltenyi Biotec, Germany). The data was analyzed using FlowJo Software (version 10.1) to determine MFI values. An isotope matched mAb (IgG1, REA293, and Miltenyi Biotec) served as a control to set the threshold. The data are presented as means of duplicate wells ± SD (relative to the HBG control group). The experiment was kindly performed in collaboration with M. Yazdi (Pharmaceutical Biotechnology, LMU Munich) and Dr. A. Bashiri Dezfouli (Department of Otorhinolaryngology, TUM Munich).

3.3.2.14 Cell viability study by MTT assay

KB and DU145 cells were seeded in 96-well plates at a density of 5000 cells/well and incubated in 100 µL of a medium containing 10% FBS at 37 °C for 24 h prior to the experiment. Polyplexes containing siCtrl were transfected in triplicate at doses of 250 and 62.5 ng of siRNA per well. HBG-treated cells served as a negative control. After 48 h of incubation at 37 °C, 10 µL MTT (3-(4,5-dimethylthiazol-2-yl)2,5-diphenyltetrazolium bromide, 5 mg/mL) were added to each well and incubated for an additional 2 h at 37 °C. Subsequently, the supernatant was removed, and the cells were frozen at -80°C overnight. To dissolve the crystals, 100 µL of DMSO was added to each well and the plates were kept at 37 °C for 30 min while shaking. The purple formazan product was

quantified by a microplate reader (Tecan, Switzerland) at 530 nm with a background correction at 630 nm. The relative cell viability was calculated as a percentage of HBG-treated control wells (100%) and is presented as the mean of triplicate wells (± SD).

3.3.2.15 Serum stability of polyplexes

For assessing polyplex stability in 90% fetal bovine serum (FBS), polyplexes were prepared at the *in vivo* relevant concentration of 1.5 µg of siRNA in 10 µL HBG (150 ng/µL). These polyplexes were diluted with 90 µL of 100% FBS to achieve a final concentration of 15 ng of siRNA/µL and 90% FBS, followed by incubation at 37 °C for 2 h. Analogously, polyplexes were also diluted and incubated in HBG as a control. The samples were subsequently used to assess siRNA compaction via agarose gel electrophoresis, size distribution via DLS, and transfection efficiency via a luciferase reporter gene silencing assay. For agarose gel electrophoresis, 20 µL of the diluted samples (containing 300 ng siRNA) was used. For size distribution measurements, 20 µL of the diluted samples was further diluted with 60 µL HBG to a final volume of 80 µL and transferred to a folded capillary cell. Measurement parameters were identical to standard size and PDI measurements. To assess transfection efficiency, cells were treated with the serum and HBG-diluted polyplexes at a dose of 62.5 ng of siRNA. Further procedures were also identical to our previously reported gene silencing studies.

3.3.2.16 Fluorescence (Cross-)Correlation Spectroscopy (FCS, FCCS)

Fluorescently labeled non-coated and HA-coated polyplexes were prepared at a siRNA concentration of 150 ng/µL. 2.5% of the total siRNA was composed of ATTO565-labeled siRNA (1:1 molar ratio of dye per siRNA). The HA coating incorporated 0.5% ATTO643-labeled HA molecules, leading to double-labeled HA-coated polyplexes. The labeling of HA was performed by coupling azido-functionalized ATTO643 to HA-DBCO through SPAAC, followed by dialysis and lyophilization. A HA-DBCO batch containing 1 DBCO module per HA molecule was used for coupling, leading to a 1:1 molar ratio of dye per HA molecule. Before the measurements, the labeled polyplexes were diluted 1:10 in either HBG or FBS (heat inactivated, non-USA origin, Sigma Aldrich, Germany) and 25 µL of each sample was measured in an 8-well LabTek I slide (VWR). Freely diffusing ATTO565 and ATTO643 as well as freely diffusing labeled siRNA and HA were used as controls. The FCS measurements were performed by I. Gialdini (Department of Chemistry, LMU Munich) on an in-house-built laser scanning confocal microscope described elsewhere [416]. Alignment of the setup was routinely checked by measuring

a 10 nM mixture of ATTO565-COOH and ATTO655-COOH in dPBS (Gibco). The experiments were performed with a 60× water immersion objective (Plan Apo 60x WI/NA 1.27, Nikon). A 560 nm pulsed diode laser (LDH-P-FA-560, PicoQuant) was used for the excitation of ATTO565-labeled siRNA and polyplexes, and a 635 nm pulsed diode laser (LDH-P-C-635M, PicoQuant) was used for ATTO643-labeled HA and polyplexes. The power of both lasers was set as 1.2 µW before the objective, the pulse repetition rate was 25 MHz, and the red laser was electronically delayed by ~17 ns to achieve pulsed interleaved excitation (PIE) [417] and thus minimize the spectral cross-talk. The fluorescence emission was recorded for 10-15 min by two avalanche photodiode detectors (SPCM-AQR-14, PerkinElmer, after a 595/50 bandpass emission filter for ATTO565 and Count® Single Photon Counting Module, Laser Components after 635 nm long-pass emission filter for ATTO643). The excitation and emission were synchronized via time-correlated single-photon-counting electronics (TCSPC cards, Becker SPC-150 and Hickl). PIE analysis in MATLAB (PAM) [418] was used for the analyses of the FCS data. Depending on the sample, the autocorrelation functions (ACFs) were fit with a model containing up to three diffusional components. Assuming a 3D Gaussian focus shape, the ACF is given by

$$G(\tau) = \frac{\gamma}{(A_1 + A_2 + A_3)^2}\left\{\left[A_1\left(1+\frac{4D_1\tau}{\omega_r^2}\right)^{-1}\left(1+\frac{4D_1\tau}{\omega_z^2}\right)^{-\frac{1}{2}}\right] + \left[A_2\left(1+\frac{4D_2\tau}{\omega_r^2}\right)^{-1}\left(1+\frac{4D_2\tau}{\omega_z^2}\right)^{-\frac{1}{2}}\right] + \left[A_3\left(1+\frac{4D_3\tau}{\omega_r^2}\right)^{-1}\left(1+\frac{4D_3\tau}{\omega_z^2}\right)^{-\frac{1}{2}}\right]\right\} \quad \text{Eqn [1]}$$

with τ being the time lag of the correlation, D_i the diffusion coefficient of the species *i,* and ω_r and ω_z the lateral and axial focus sizes, respectively. For a 3D Gaussian shape, the geometric factor γ is $2^{-3/2}$. A_i is the relative amplitude of the corresponding fluorescence species within the observation volume. A_i is equal to the particle number N_i only if all of the components have equal brightnesses. With this model, the molecular brightness is equal to the fluorescence intensity divided by the sum of the values of N_i. If the brightnesses are not equal, to make an accurate quantification of N_i, the relative brightness of each species should be included in the analyses [419]. In the case of the cross-correlation analysis, the fluorescence cross-correlation function (CCF) is given by

$$G(\tau) = \frac{\gamma\, A_{YR}}{(A_{YT})(A_{RT})}\left[\left(1+\frac{4D_{YR}\tau}{\omega_r^2}\right)^{-1}\left(1+\frac{4D_{YR}\tau}{\omega_z^2}\right)^{-\frac{1}{2}}\right] \qquad \text{Eqn [2]}$$

where A_{YR} is related to the fraction of double-labeled particles and A_{YT} and A_{RT} represent the total number of yellow-labeled and red-labeled particles respectively.

3.3.2.17 In vitro confocal imaging of single particles and colocalization analyses

Similarly to the FCS experiments, labeled non-coated and HA-coated polyplexes were diluted 1:10 in HBG or FBS and imaged in LabTek I slides by I. Gialdini (Department of Chemistry, LMU Munich) on the same home-built LSCM instrument [416]. For each sample, a movie consisting of 100–200 frames (300 × 300 pixels, 100 × 100 µm) was acquired at a frame time of 1 s. Image postprocessing and colocalization analyses were performed in Fiji software (version 2.14.0/1.54f) [420] with a self-written semiautomated macro. Briefly, each movie was background subtracted and the analysis was performed on every 20th frame: knowing that the diffusion time of the polyplexes is on the order of a few milliseconds, this ensures that the same particle is not counted twice. The segmentation of the particles and the colocalization analyses were performed with DiAna [421], a plugin of ImageJ that evaluates the overlap between objects of two different channels. The integrated density of each analyzed particle was also retrieved as an output of the colocalization analysis with DiAna.

3.3.2.18 Animal experiments

All animal experiments were performed according to the guidelines of the German Animal Welfare Act and were approved by the animal experiments ethical committee of the Government of Upper Bavaria, Germany (accreditation number Gz. ROB-55.2-2532.Vet_02-19-20). For both the ex vivo biodistribution study and the *in vivo* EG5 silencing study, female NMRI-nu (nu/nu) mice (Janvier, Le Genest-Saint-Isl, France) were used. The mice were housed in isolated vented cages under pathogen-free conditions with a 12 h light/dark cycle and free access to water and food ad libitum and were acclimated for at least 7 days prior to experiments. Animals were injected with 1 × 10^6 Neuro2a murine neuroblastoma cells subcutaneously for both the ex vivo biodistribution study, and the *in vivo* EG5 silencing study. The tumor volume was measured by a caliper and calculated as [0.5 × (longest diameter) × (shortest diameter)^2].

3.3.2.19 Ex vivo biodistribution study

When tumors reached a volume of 250–500 mm^3, polyplexes containing siCtrl, spiked with 50% of Cy7-labeled siRNA (Cy7-siAHA1), were prepared in 200 µL of HBG and injected intravenously via the tail vein to NMRI-nu (nu/nu) mice (6–8 weeks of age, n = 4) at a dose of 30 µg siRNA per mouse. After one h, the mice were euthanized by cervical dislocation, and their organs and tumors were harvested for near-infrared (NIR) ex vivo imaging using an *in vivo* optical imaging system (IVIS spectrum, Xenogen, USA). For image evaluation, the fluorescence signal efficiency was analyzed after equalizing the color bar scales using Living Image Software 3.2 (Caliper Life Sciences, Hopkinton, MA, USA). The injection, euthanasia, and harvesting of organs was kindly performed by the veterinarians of our research group, J. Pöhmerer (Pharmaceutical Biotechnology, LMU Munich) and M. Yazdi (Pharmaceutical Biotechnology, LMU Munich).

3.3.2.20 Gene silencing of siEG5 in vivo

Once tumor sizes reached 250–500 mm^3, polyplexes containing either 50 µg of siEG5 or siCtrl were prepared in 250 µl of HBG and injected intravenously via the tail vein into mice (n=5). A second injection was administered after 24 h. After 48 h, the mice were euthanized, and the tumors were harvested and homogenized. Total mRNA was extracted from the tumors using the peqGOLD total RNA Kit (VWR, Leuven, Belgium), and cDNA was synthesized using the qScript cDNA synthesis Kit (Quantabio, Beverly, USA), both according to the manufacturers' protocols. Quantitative RT-PCR was performed in triplicate on a LightCycler 480 system (Roche, Mannheim, Germany) using TaqMan probes and Master Mix for gene expression assays (ThermoFisher Scientific, Waltham, MA, USA), with GAPDH as a housekeeping gene. The sample composition was as follows: 5 µL of Master Mix, 0.5 µL of probe, 4.5 µL of 1:10 diluted cDNA. Results were analyzed by the ΔC_T method. C_T values of GAPDH were subtracted from C_T values of EG5, and the resulting ΔC_T values were calculated as percentage relative to ΔC_T from HBG-treated mice. The injection, euthanasia, and harvesting of tumors was kindly performed by the veterinarians of our research group, J. Pöhmerer (Pharmaceutical Biotechnology, LMU Munich) and M. Yazdi (Pharmaceutical Biotechnology, LMU Munich).

3.3.2.21 Statistical Analysis

Results are presented as mean values (arithmetic mean) of triplicate unless otherwise specified. Error bars display the standard deviation (SD). Statistical analysis of results

(mean ± SD) was evaluated by one-way ANOVA, and the Šidák multiple comparison test. Calculations and graphical presentations were performed with GraphPad Prism version 10.0.3. (GraphPad Software Inc.). ns (not statistically significant) $p > 0.05$; * $p \leq 0.05$; ** $p \leq 0.01$; *** $p \leq 0.001$; **** $p \leq 0.0001$.

3.4 Results and Discussion

3.4.1 Design of a tunable ionic HA coating for siRNA polyplexes

When injected intravenously, cationic polyplexes are prone to various electrostatic interactions with biological components, including nonspecific adherence to cell membranes, the formation of a protein corona, and opsonization. Consequently, cationic polyplexes often accumulate nonspecifically, have an altered chemical identity, and tend to be rapidly cleared from the bloodstream through the reticuloendothelial system (RES). Thus, the circulation time and potential therapeutic efficacy are substantially reduced.

To address these challenges, we aimed to develop an ionic HA coating strategy to shield polyplexes from undesired interactions by switching the polyplex surface charge from positive to negative. Additionally, we incorporated a TEC-targeting ligand into the HA-coating to achieve tumor specific accumulation and compensate for the reduced intrinsic cell adhesion capacity of polyplexes resulting from charge reversal.

For the development of the multifunctional HA-coating, we utilized siRNA polyplexes based on cationizable lipo-OAA ID#1670 **(Scheme 1A**). Lipo-OAA 1670 was synthesized using solid-phase supported synthesis (SPSS), building on a previous similar T-shaped OAA which had been identified as an effective carrier for *in vivo* siRNA delivery [40]. Lipo-OAA 1670 features a symmetric cationic backbone with terminal cysteines, followed by three tyrosines, alternating histidines and succinoyltetraethylenepentamines (Stp), and a central branching lysine, which carries the lipidic branch with two oleic acids (**Scheme 1A**). The disulfide-forming cysteines, the tyrosine tripeptides and a terminal leucine enhance polyplex stability, while the imidazole containing histidines have proven to be beneficial for endosomal escape [19, 42-44].

The initial development step of the ionic coating focused on determining the optimal HA amount per polyplex to achieve the desired size, polydispersity, and negative zeta potential. For this, 1670/siRNA core polyplexes were first prepared through turbulent mixing of equal volumes OAA 1670 and siRNA at a N/P ratio of 12, followed by a 40 min incubation at room temperature (RT) (**Scheme 1A**). These core polyplexes were then combined with varying quantities of HA, enabling anionic HA to form an electrostatic coating around the cationic core polyplex (**Scheme 1B**). HA quantities were calculated

as HA disaccharide repeat units per Stp, which represents one negative charge (one carboxy group of disaccharide repeat unit) per positive charge (one protonated amine of Stp at pH 7.4) and ranged from 0 to 3.5 HA units/Stp.

Scheme 1. Preparation of HA-coated polyplexes.

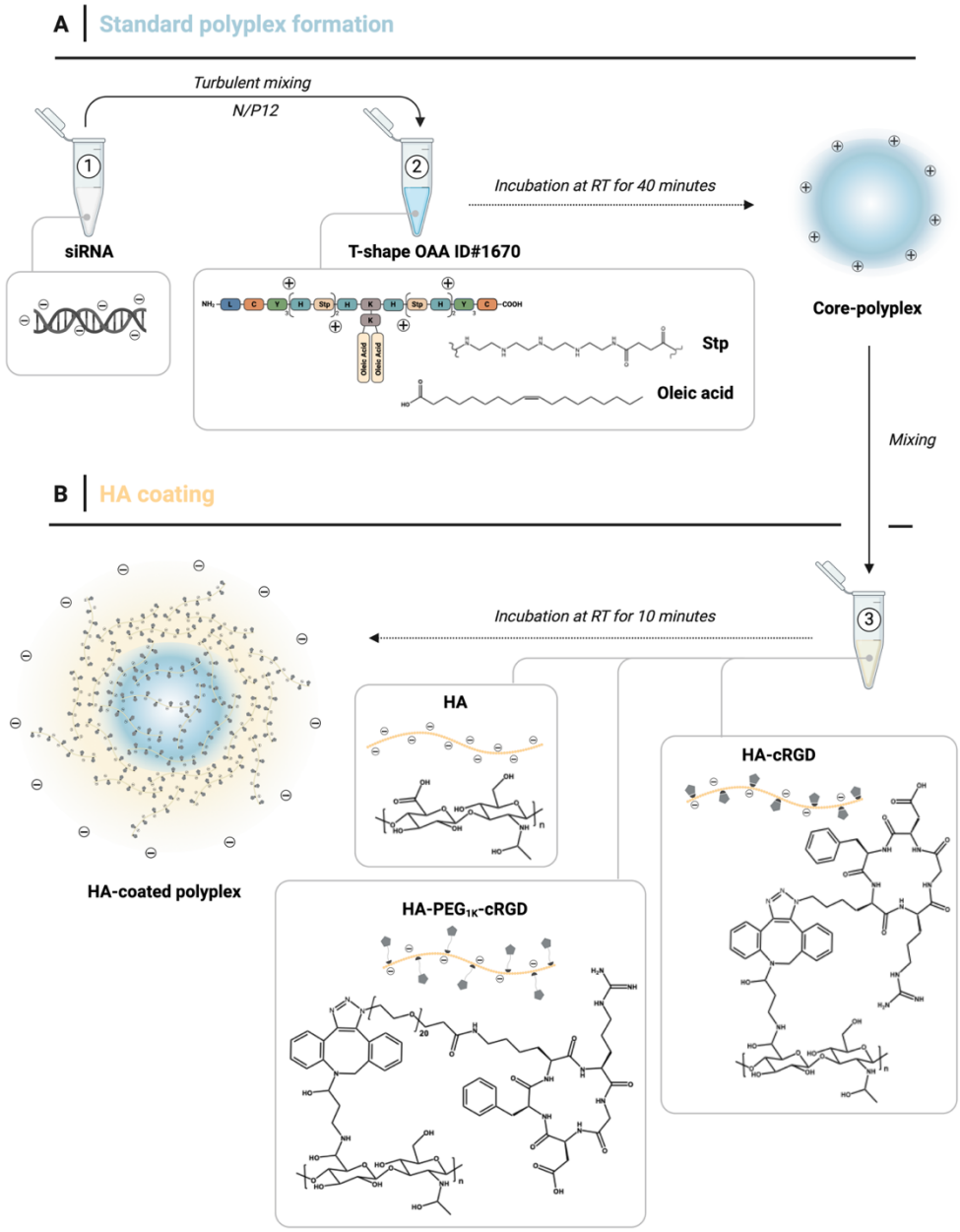

A) Core polyplexes are prepared through turbulent mixing of equal volumes siRNA (1) and T-shape oligoaminoamide ID#1670 at N/P 12 (2) and incubation at room temperature (RT) for 40 minutes. B) For HA-coating, the core polyplex is subsequently added to the hyaluronic acid solution (3) and incubated for further 10 minutes to allow formation of the ionic HA coating, reversing the polyplex surface charge from positive to negative. For coating, either unmodified HA, HA-cRGD or HA-PEG_{1K}-cRGD are used (n = 100 disaccharid repeat units in 38 kDa HA) and the amount of HA is calculated as 3 HA disaccharide repeat units/Stp. In the OAA backbone the following amino acids are incorporated: L, leucin; C, cysteine; Y, tyrosine; H, histidine; Stp, succinoyl tetraethylene pentamine; K, lysine.

DLS and ELS measurements were used to analyze the size (Z-Ave), polydispersity index (PDI), and zeta potential of the coated polyplexes (**Figure 1A**). Zeta potential inversion from positive to negative charge occurred through a minimum of 1 HA unit/Stp, but more than 2 HA units/Stp were needed to achieve optimal sizes (< 300 nm) and PDIs (< 0.2). Besides polyplex size and charge, the ability to quantitatively encapsulate the nucleic acid is of utmost importance for high efficacy. An agarose gel electrophoresis indicated that siRNA was completely complexed regardless of the utilized HA ratio, as evidenced by the absence of bands at the level of the control sample containing only free siRNA (**Figure 1C**). The electrophoresis data also suggest that the anionic coating does not compete with the nucleic acid for binding to the cationic carrier peptide. For further investigations, a ratio of 3 HA units/Stp was determined to be suitable for ionic coating of polyplexes, resulting in hydrodynamic diameters below 300 nm, low PDI values, negative zeta potentials of less than -20 mV, and complete siRNA entrapment.

In the next step, the ionic HA coating was modified with the cyclic RGDfK (cRGD) peptide, a ligand that targets the tumor endothelial cell receptor integrin αvβ3 and was selected based on its previous success in tumor-targeted polyplexes [160-163, 422-424]. Functionalizing HA with the targeting ligand rather than the polyplex itself was intended to simplify and accelerate preparation of the multifunctional polyplexes by allowing the addition of both the shielding and targeting agent in a single formulation step. To incorporate the targeting ligands into the HA, we first modified HA with DBCO units as linkage modules, as described in our previous work [40]. 11–13% of carboxylic acids in HA were modified, as confirmed by UV-vis and ^{1}H-NMR data (**Figures S3 and S4**).

To enable conjugation of cRGD to HA-DBCO via copper-free click chemistry, we utilized targeting ligands functionalized with a terminal azido group (**Schemes 1B and S1**). We compared two strategies for azido-cRGD coupling: (1) direct coupling of N_3–cRGD to HA–DBCO or (2) coupling via a PEG_{1K} spacer: N_3–PEG_{1K}–cRGD. While the PEG-spacer may sterically hinder CD44 targeting through HA, we hypothesize that the hydrophilic spacer supports cRGD presentation on the polyplex surface, reducing internal hiding, compensates for the hydrophobicity of the DBCO linkage module, and potentially adds an additional shielding component. As a control, N_3–PEG_{1K} was tested equivalently in all studies to distinguish it from unspecific effects through the spacer.

For preparation of the click chemistry-coupled HA-ligand conjugates (HA–cRGD, HA–PEG_{1K}–cRGD, and the control HA–PEG_{1K}), HA–DBCO and an excess of the respective azido ligand (1.2 equiv ligand per DBCO [mol/mol]) were incubated for at least 4 h at RT while shaking. Afterward, the conjugates were dialyzed against deionized water for purification and lyophilized. UV-vis data confirmed the quantitative reaction of all DBCO

units, as the absorption at the characteristic wavelength for DBCO (308 nm) decreased to 0 (**Figure S4**). An overview of the final HA and cRGD molar ratios used for polyplex formation is provided in **Table S4**.

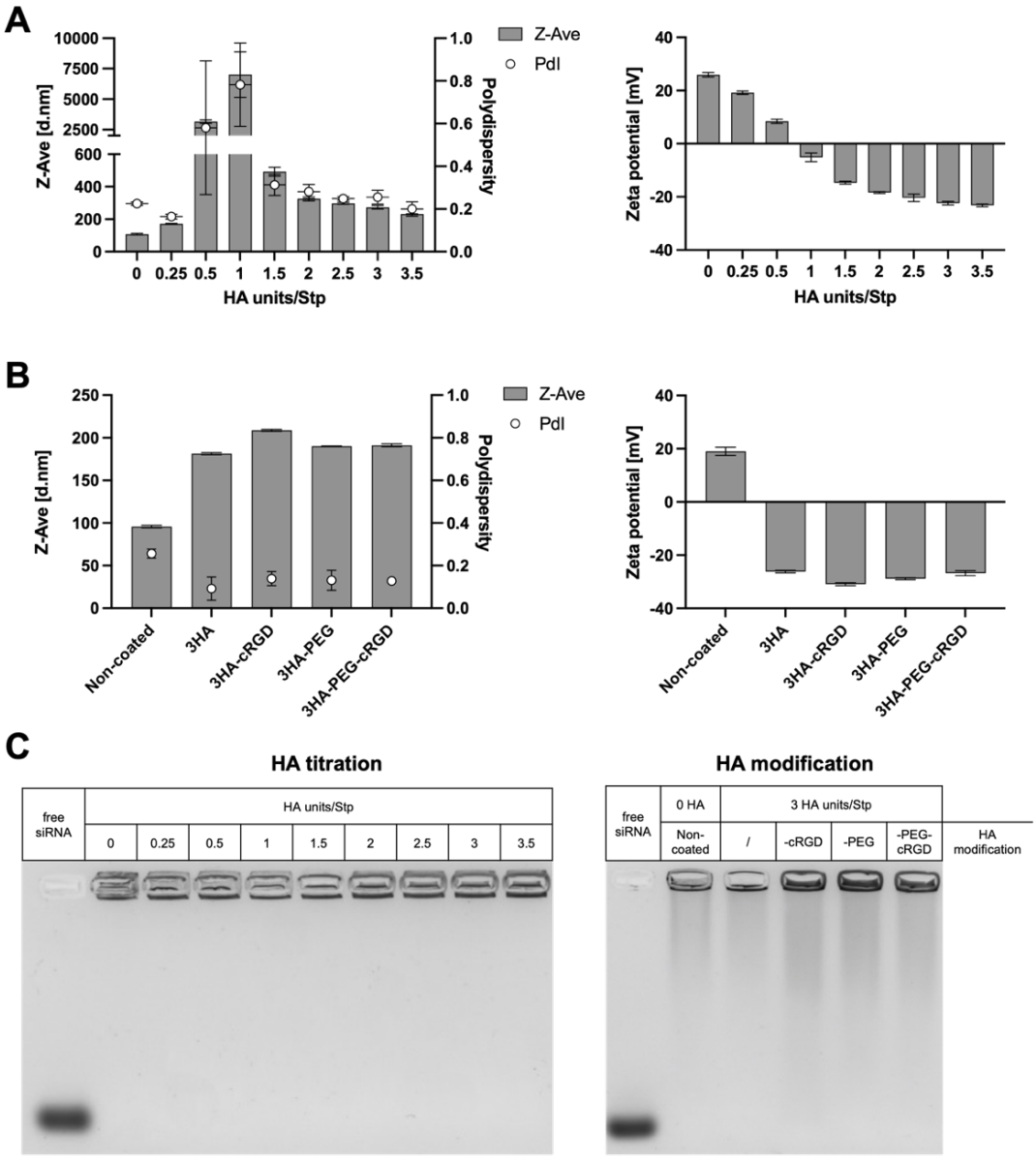

Figure 1. Physicochemical evaluation of HA-coated polyplexes. (A, B) Polyplex sizes (*z*-average by intensity) and polydispersity index (PDI) were determined through dynamic light scattering (DLS) (n = 3, mean ± SD), and zeta potential values were determined through electrophoretic laser light scattering (ELS) (n=3, mean ± SD). Polyplexes were prepared in HBG at a N/P ratio of 12 containing 500 ng siRNA in a total volume of 20 µL. (A) Coating of polyplexes with increasing amounts of HA units/Stp in comparison to non-coated polyplexes (0 HA units/Stp). (B) Coating of polyplexes with unmodified HA (3HA), 3HA–cRGD, 3HA–PEG and 3HA–PEG–cRGD at a ratio of 3 HA units/Stp in comparison to unmodified polyplexes (0 HA units/Stp). (C) siRNA compaction of non-coated and HA-coated polyplexes was determined through agarose gel electrophoresis.

Subsequently, core polyplexes were coated with either unmodified HA or the novel coating conjugates HA–cRGD, HA–PEG, and HA–PEG–cRGD at the established ratio of 3 HA units/Stp (coatings hereafter referred to as 3HA, 3HA–cRGD, 3HA–PEG, and 3HA–PEG–cRGD). Evaluation of physicochemical characteristics was performed using DLS, ELS and an agarose gel shift assay (**Figure 1B**). The data indicated that HA modification with azido ligands did not notably alter the size, PDI, or zeta potential compared to polyplexes coated with unmodified HA. Furthermore, agarose gel electrophoresis demonstrated complete siRNA compaction for all tested formulations (**Figure 1C**).

In summary, the presented physicochemical data indicate that we successfully developed an ionic HA coating functionalized with the targeting ligand cRGD, which enables charge inversion of polyplexes while maintaining suitable sizes, PDIs, and siRNA encapsulation ability.

3.4.2 Cell association and gene silencing efficiency of HA-coated polyplexes

Knowing that cellular internalization is a crucial prerequisite for polyplex efficacy, our initial investigations in cell culture focused on evaluating cell association of the novel HA- and cRGD-modified polyplexes with an integrin αvβ3 and CD44 expressing cell line, specifically the human prostate cancer cells DU145 [425, 426]. The cells were seeded at a density of 5000 cells per well and transfected with polyplexes at a dose of 62.5 ng of siRNA, of which 20% were spiked with Cy5-labeled siRNA. Cell association was evaluated using flow cytometry after different incubation periods ranging from 30 min to 48 h at 37 °C. A range of time points was selected to capture the maximum association of each formulation, considering the possible varying kinetics of the different polyplexes. Over the first 24 h following transfection, the cell association of 3HA-coated polyplexes was highest, followed by non-coated polyplexes (**Figure 2A**). These formulations reached maximum cell association after 24 h, while the MFI continued to increase for 3HA–cRGD, 3HA–PEG, and 3HA–PEG–cRGD polyplexes. After 48 h, 3HA–cRGD polyplexes demonstrated the highest overall cell association, followed by 3HA–PEG–cRGD, 3HA, 3HA–PEG, and non-coated polyplexes.

To further confirm cellular uptake, we performed complementary CLSM after 48 h in DU145 cells using the same formulations and siRNA dose. The images verified that internalization of all formulations occurred after 48 h, eliminating the possibility that polyplexes were solely adhering to the outer cell membrane surface (**Figures 2B and S5**).

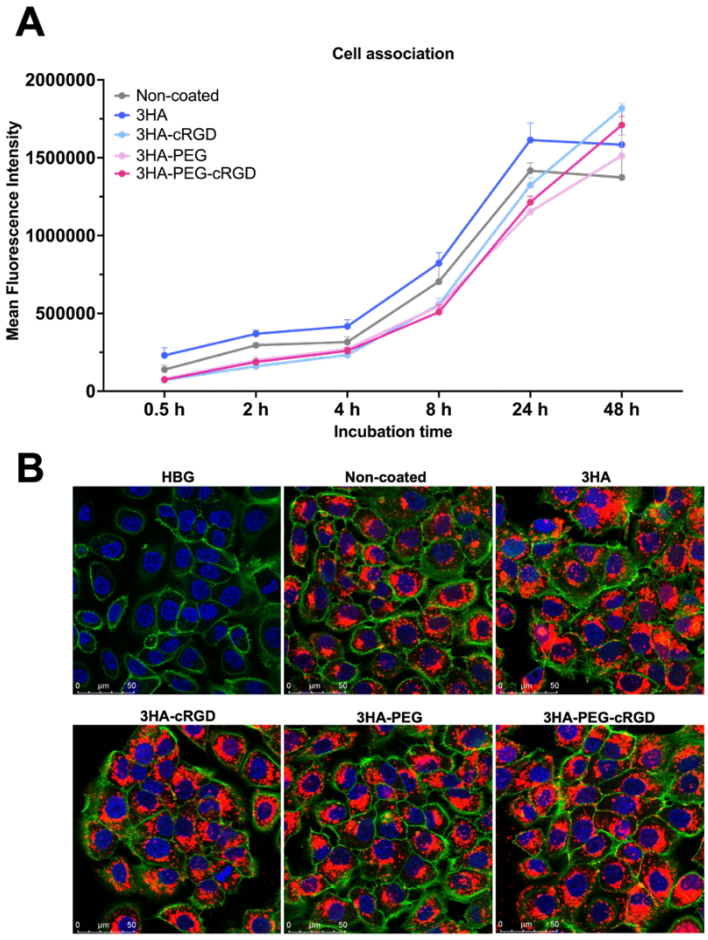

Figure 2. Cell association and cell internalization of HA-coated polyplexes. Non-coated and HA-coated polyplexes containing 20% Cy5-labeled siRNA were transfected in the human prostate cancer cells DU145 at a dose of 62.5 ng of siRNA (5000 cells/well). (A) Cell association was evaluated after different time periods (0.5, 2, 4, 8, 24, 48 h) via flow cytometry. The data are presented as mean fluorescence intensity of Cy5-signal per cell (mean ± SD, n = 3). HBG-treated cells were used as a negative control. (B) Cell internalization of Cy5-labeled polyplexes (red) was imaged by M. Höhn (Pharmaceutical Biotechnology, LMU Munich) using confocal laser scanning microscopy (CLSM) after 48 h of incubation on DU145 cells. The actin skeletons were stained with rhodamine-phalloidin (green) and nuclei with DAPI (blue). The scale bar is 50 µm. Images of each layer (before merge) are presented in **Figure S6**.

The average percentage of Cy5-positive DU145 cells was also evaluated, revealing no significant differences among the tested formulations. All achieved more than 90% Cy5-positive cells at all time points **(Figure S6**). This analysis was extended to a second integrin αvβ3- and CD44-expressing cell line, human cervix carcinoma (KB) cells [425, 426], which consistently showed over 95% Cy5-positivity across all formulations and time points (**Figure S6**).

Cellular uptake was further evaluated in KB cells (**Figure S7A**), along with an endocytosis inhibition assay to investigate the mechanisms underlying polyplex internalization (**Figure S7B**). After incubating the different formulations with the cells for

4 h, 3HA polyplexes exhibited the highest cellular uptake, followed by 3HA–cRGD and non-coated polyplexes. The PEG-containing formulations 3HA–PEG and 3HA–PEG–cRGD showed lower overall MFI values, likely due to the shielding properties of PEG. However, 3HA–PEG–cRGD outperformed 3HA–PEG, suggesting a cRGD-mediated targeting effect.

The endocytosis inhibition assay (**Figure S7B**) revealed clathrin-mediated endocytosis (inhibited by sucrose) and macropinocytosis (inhibited by amiloride) as prominent uptake pathways for non-coated, cationic polyplexes. In contrast, all HA-coated anionic formulations were only partly inhibited by the macropinocytosis inhibitor, with clathrin-mediated endocytosis presenting the main uptake route. This pathway was dominant for the 3HA–cRGD–coated polyplexes. Caveolae-mediated endocytosis (inhibited by nystatin) contributed to the uptake of 3HA–PEG-coated polyplexes only but the contribution was reduced for the other four formulations.

Taken together, in DU145 cells, all formulations exhibited similar high cell association which increase with time. At 24 h high Cy5-positivity was found for all formulations, similar as observed for KB cells. Evaluating uptake in KB cells at a medium 4 h time point suitable for observing differences, the HA coating enhanced, and the HA–PEG coated formulation reduced uptake compared with non-coated nanoparticles. Importantly, incorporation of cRGD significantly enhanced the uptake in the 3HA–PEG–cRGD formulation. Combined with the finding of a primarily clathrin-coated endocytosis and reduced macropinocytosis pathway, data are consistent with receptor-mediated uptake (by either cRGD or HA) and optional PEG shielding.

Next, we assessed gene silencing efficiency of the non-coated and HA-coated polyplexes by conducting a luciferase reporter assay in DU145 eGFP/Luc and KB eGFP/Luc reporter cell lines, which stably express the eGFP-Luciferase reporter gene. Cells were seeded at a density of 5000 cells per well and treated with both high (250 ng/well) and low (62.5 ng/well) doses of siRNA. In comparison to our previous work, where typically 500 ng of siRNA per well was used for transfections [40, 157], we utilized lower doses to discern differences between our novel formulations. A previously conducted dose titration with non-coated polyplexes confirmed sufficiently high gene silencing even at 1/8 of the former standard dose (**Figure S8**). For each formulation, both siCtrl and siGFP containing polyplexes were prepared and transfected to distinguish specific gene silencing (siGFP) from non-specific effects (siCtrl). Luciferase activity of the transfected reporter cells was measured 48 hours post-transfection after the addition of luciferin. Gene silencing efficiency was calculated as the difference between non-

specific gene silencing of siCtrl-containing polyplexes and specific gene silencing of siGFP-polyplexes. A summary of the exact calculated efficiencies is provided in **Tables S1 and S2** for comparison.

In both DU145 and KB eGFP/Luc cells, all tested formulations achieved significant gene silencing at both high and low siRNA doses (**Figure 3A**). Transfections with 250 ng of siRNA per well resulted in indistinguishable gene silencing efficiencies for all formulations in both cell lines, exceeding 50%-60% specific gene silencing in DU145 eGFP/Luc cells, and more than 70% in KB eGFP/Luc cells. Transfections with the lower dose (62.5 ng) siRNA revealed formulation- and cell line-dependent differences in polyplex efficiency. In DU145 cells, transfection efficiency remained high at over 60% for all formulations, with no significant differences, consistent with the observed cell association. In contrast, in KB eGFP/Luc cells, the gene silencing efficiency decreased by 10% to 40% compared to the high dose, depending on the transfected formulation. The transfection efficiency of 3HA, 3HA–cRGD, and 3HA–PEG–cRGD coated polyplexes outperformed both the non-coated and the well-shielded 3HA–PEG coated polyplexes, resulting in the following ranking sorted by gene silencing efficiency: 3HA-cRGD > 3HA > 3HA-PEG-cRGD > non-coated > 3HA-PEG. The higher gene silencing efficiency of HA-coated polyplexes, and the pronounced difference in efficiency between 3HA–PEG- (40%) and 3HA–PEG–cRGD- (56%) coated polyplexes, suggest that both the HA- coating and the modification with the ligand cRGD affect functional activity. These data are also consistent with the cellular uptake study in most aspects, where 3HA and 3HA–cRGD polyplexes outperformed non-coated polyplexes, and a ligand effect was observed when comparing 3HA–PEG with 3HA–PEG–cRGD polyplexes.

As our intention was to enhance *in vivo* efficacy by improving polyplex adherence to TECs, in addition to improving biocompatibility through HA shielding, we evaluated the transfection capacity of all formulations in a subsequent functional assay in the endothelial cell line bEnd.3. Polyplexes containing siVEGFR-2 were prepared and transfected at a dose of 500 ng of siRNA per 10,000 cells, corresponding to the high-dose conditions used in the previous gene silencing studies (250 ng per 5000 cells). The murine brain endothelial cell line bEnd.3 was selected due to its expression of the integrin αvβ3 receptor and VEGFR-2 [76]. After 48 h of incubation, VEGFR-2 knockdown efficiency was assessed using a labeled VEGFR-2 monoclonal antibody (mAb) and flow cytometry. HBG-treated cells, showing the baseline VEGFR-2 expression, were used to calculate the MFI fold change of VEGFR-positive cells treated with HA-coated and non-coated polyplexes. Polyplexes coated with 3HA–cRGD and 3HA–PEG–cRGD were also prepared containing siCtrl to exclude non-specific gene silencing.

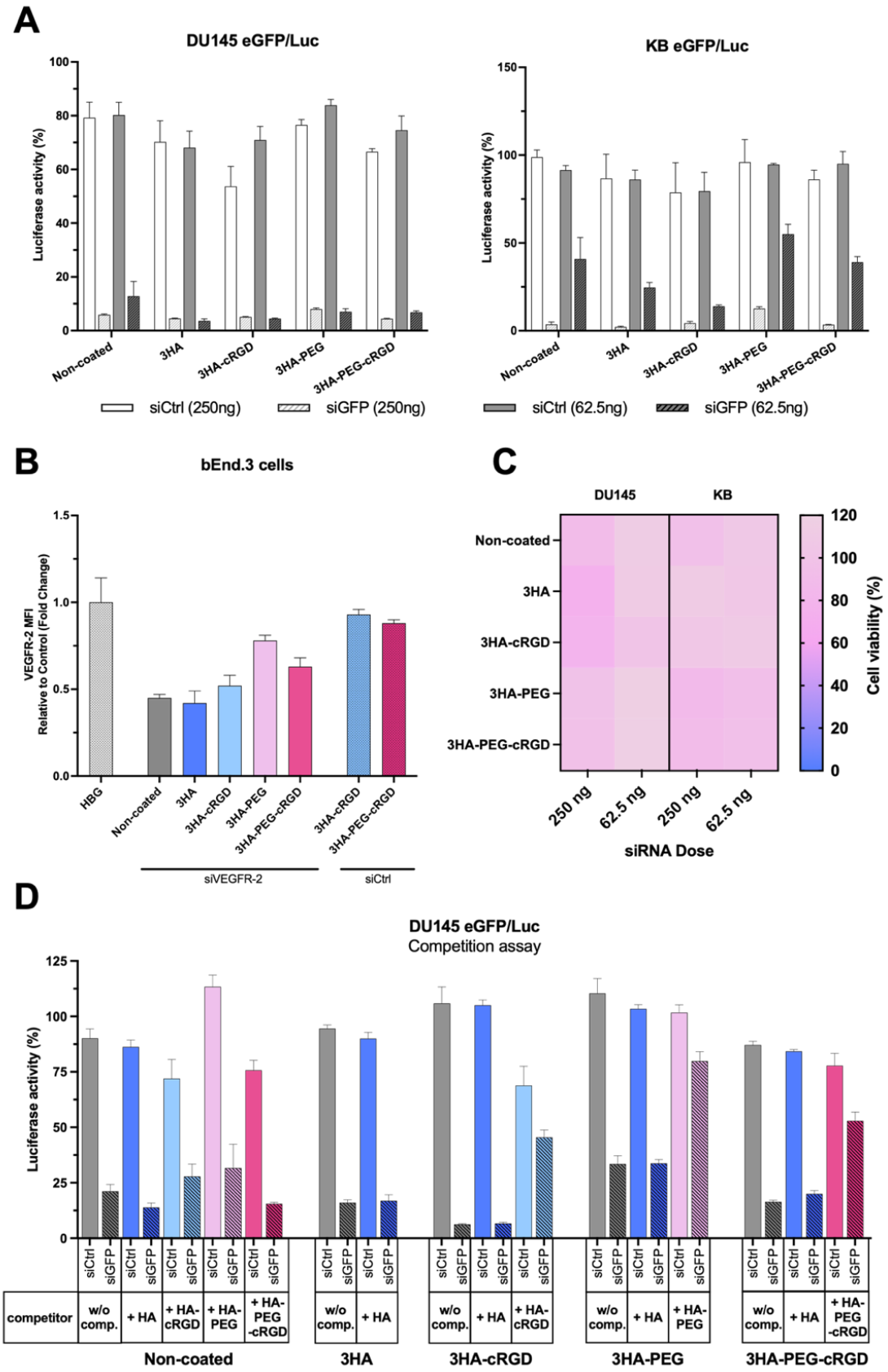

Figure 3. In vitro evaluation of HA-coated polyplexes. (A) Gene silencing efficiency of non-coated (0 HA/Stp) and HA-coated polyplexes (coated with unmodified HA, HA–cRGD, HA–PEG or HA–PEG–cRGD) was assessed in the reporter cell lines DU145 eGFP/Luc and KB eGFP/Luc.

Polyplexes were prepared containing siGFP (siRNA silencing enhanced green fluorescent protein expression) and siCtrl (control siRNA) at both high (250 ng) and low (62.5 ng) siRNA doses (5000 cells/well). After 48 h of incubation, luciferase activity of the eGFP-luciferase (eGFPLuc) fusion protein was evaluated. The luciferase activity is expressed as percentage relative to that of HBG-treated cells (mean ± SD, n = 3). B) Expression of VEGFR-2 in murine brain endothelial bEnd.3 cells was quantified by flow cytometry after 48 h of exposure to non-coated and coated polyplexes containing 500 ng of siVEGFR-2 (per 10,000 cells). 3HA–cRGD and 3HA–PEG–cRGD polyplexes containing siCtrl were used as a negative control. MFI fold change of positive cells was calculated relative to the respective values of HBG-treated cells (mean ± SD, n = 3). Statistical significancy was determined as ns $p > 0.05$; * $p \leq 0.05$; ** $p \leq 0.01$; *** $p \leq 0.001$; **** $p \leq 0.0001$ (ordinary one-way ANOVA, Šidák multiple compaison test; GraphPad Prism 10.0.3). The experiment was performed in collaboration with M. Yazdi (Pharmaceutical Biotechnology, LMU Munich) and Dr. A. Bashiri Dezfouli (Department of Otorhinolaryngology, TUM Munich). (C) Metabolic activity of DU145 and KB cells incubated with non-coated and HA-coated polyplexes containing high (250 ng) and low (62.5 ng) doses of siRNA for 48 h was measured via the MTT assay. Cell viability was calculated as percentage of HBG-treated cells (mean ± SD, n = 3). (D) Gene silencing efficiency of non-coated and HA-coated polyplexes in the presence of excess coating agent for competition was evaluated in the reporter cell line DU145 eGFP/Luc by measuring luciferase activity. Cells were preincubated with a 50-fold excess of HA coatings for 45 min at 37 °C prior to transfection with polyplexes containing 62.5 ng of siGFP, or siCtrl as a negative control (per 5000 cells). Luciferase activity was measured after 48 h of incubation of polyplexes on the cells in the continued presence of the competitors and was calculated as percentage relative to that of HBG-treated cells (mean ± SD, n = 3). As a positive control, all formulations were also transfected without a competitor (gray bars). Non-coated polyplexes were coincubated with all HA-coating types to exclude unspecific competition (colored bars). 3HA-polyplexes were only coincubated with unmodified HA (blue bars), whereas polyplexes coated with 3HA–cRGD, 3HA–PEG, and 3HA–PEG–cRGD were transfected in the continued presence of both the respective HA-coating types [HA–cRGD (green), HA–PEG (light pink), and HA–PEG–cRGD (pink) and unmodified HA (blue)].

The results were generally consistent with those from the luciferase reporter gene silencing assay, aligning with certain findings from both the studies in DU145 and KB eGFP/Luc reporter cells, while also revealing some differences. Overall, all formulations, except for 3HA–PEG polyplexes, achieved significant VEGFR-2 silencing (**Figure 3B**). Non-coated, 3HA- and 3HA–cRGD-polyplexes demonstrated the highest gene silencing efficiency, followed by 3HA–PEG–cRGD polyplexes. The enhanced efficiency of 3HA–PEG–cRGD polyplexes compared with 3HA-PEG polyplexes, as shown in the luciferase assay in KB eGFP/Luc cells, indicated that the ligand cRGD contributes to polyplex efficacy. In contrast to KB cells, but consistent with results from DU145 cells, non-coated polyplexes exhibited similar efficiency to HA-coated polyplexes. Overall, this complementary functional study confirmed the internalization and efficacy of the HA- and cRGD-modified polyplexes in endothelial cells.

Beyond polyplex functionality, the *in vitro* gene silencing studies demonstrated low non-specific side effects, indicating high biocompatibility of all formulations. This finding was corroborated by a subsequent MTT assay, which measured the metabolic activity of cells treated with high and low doses of the non-coated and coated polyplexes after 48 h (**Figure 3C**). Metabolic activity remained high for all formulations in both cell lines, with

minor cell line dependent differences, consistent with the luciferase reporter assay data. In DU145 cells, a slight decrease in cell viability was observed for 3HA- and 3HA–cRGD–coated polyplexes after transfection with 250 ng of siRNA, though cell survival was still adequate. At the low dose, all formulations maintained the same high cell viability. In KB cells, transfection with either high or low doses of siRNA resulted in only marginal differences in metabolic activity, with nearly 100% cell viability observed for all formulations.

To further investigate the role of the specific coating types in the internalization process and functionality, gene silencing of the polyplexes was assessed in the presence of competitive inhibitors. DU145 GFP/Luc cells were chosen as the representative cell line due to their consistent gene silencing efficiency across all formulations in previous experiments, allowing for clearer detection of differences when competitors were introduced. Prior to transfection, cells were preincubated for 45 min at 37 °C with a 50-fold excess of the respective coating agent, including both the specific coating agents and unmodified HA to differentiate from HA-dependent uptake mechanisms. Following preincubation, cells were transfected with 62.5 ng of siRNA per 5000 cells and incubated for 48 h in the continued presence of the competitor. Non-coated polyplexes were coincubated with all coating types as a control to identify nonspecific effects, while coated polyplexes were only coincubated with the specific coating agent and unmodified HA. Gene silencing was assessed by measuring luciferase activity and comparing it to cells transfected with the same formulation, but without a competitor (**Figure 3D**).

Gene silencing efficiency of non-coated polyplexes remained unaffected by the presence of any competitor. Only the competing coatings HA–cRGD and HA–PEG–cRGD induced minor nonspecific gene silencing, which was considered when comparing gene silencing efficiencies of coated polyplexes and is likely attributable to the high concentration used. Similarly, 3HA-coated polyplexes did not show reduced gene silencing activity in the presence of excess unmodified HA, which suggests that CD44-mediated interactions are not the primary mechanism of internalization of these formulations. In contrast, 3HA–cRGD, 3HA–PEG, and 3HA–PEG–cRGD polyplexes exhibited a more than 3-fold reduction in gene silencing when cotreated with the respective coating agent but not with unmodified HA. We primarily attribute the inhibition observed with cRGD-containing formulations to a ligand-mediated effect. This interpretation is supported by the finding that 3HA–cRGD polyplexes exhibit competitive interactions with HA–cRGD but not with unmodified HA.

While achieving sufficient cell uptake and gene silencing is necessary for ensuring the functionality of polyplexes, these requirements are still not sufficient regarding *in vivo*

performance after intravenous injection. *In vivo* functionality relies on numerous unpredictable factors, such as polyplex stability in serum, blood circulation time, physicochemical characteristics, and the behavior in the presence of a protein corona, none of which can be fully replicated *in vitro* [84, 427]. To partially address this, serum studies were conducted to evaluate the *in vivo* compatibility of HA-coated polyplexes, which will be discussed in the following section. Nevertheless, the low cytotoxicity observed at both high and low doses in cell culture indicates that all formulations are suitable candidates for *in vivo* testing without concern.

3.4.3 Physicochemical characteristics and functionality of HA-coated polyplexes after serum incubation

Aiming at improving stability and efficacy upon *in vivo* application, we investigated the ionically HA-coated polyplexes under conditions that partially mimic the *in vivo* environment. This involved assessing siRNA compaction, polyplex size, gene silencing efficiency, and the intactness of ionic HA-coating after dilution in fetal bovine serum (FBS). Polyplexes were prepared at a concentration of 150 ng/µL, which was selected for its relevance to following *in vivo* studies, and subsequently diluted 1:10 in FBS to achieve a final serum concentration of 90%. The polyplexes were then incubated for two h at 37 °C while being shaken to replicate shear stress experienced during intravenous injection and blood circulation.

To evaluate siRNA condensation of the non-coated and HA-coated polyplexes postserum incubation, an agarose gel shift assay was performed with 20 µL of the FBS-diluted samples, containing 300 ng of siRNA (**Figure 4A**). siRNA release was assessed by comparison with the control samples containing the same amount of free siRNA, and siRNA release was subsequently calculated using ImageJ software. To differentiate between serum and dilution effects, 1:10 dilutions were also performed with HBG, followed by incubation at 37 °C for 2 h. After HBG dilution, all formulations retained most of the siRNA, although minor release occurred. This release is likely attributable to the effects of dilution, incubation, or shaking, as our previous gel shift assays without these effects showed that siRNA was fully compacted (**Figure 1C**). The release of siRNA was negligible for non-coated and 3HA-polyplexes but was more pronounced for 3HA-cRGD, 3HA-PEG, and 3HA-PEG-cRGD polyplexes. However, upon serum dilution, non-coated and 3HA-polyplexes exhibited increased siRNA release, showing up to 40% of the initially encapsulated dose becoming free siRNA. In contrast, polyplexes coated with 3HA–cRGD, 3HA–PEG, and 3HA–PEG–cRGD maintained their siRNA compaction

capacity even after dilution in FBS. Notably, formulations incorporating PEG spacers exhibited the lowest siRNA release after FBS dilution. Although the formulations containing cRGD- and PEG-modified HA demonstrated the highest overall stability in serum, all formulations retained substantial amounts of siRNA after being diluted in FBS and incubated for 2 h.

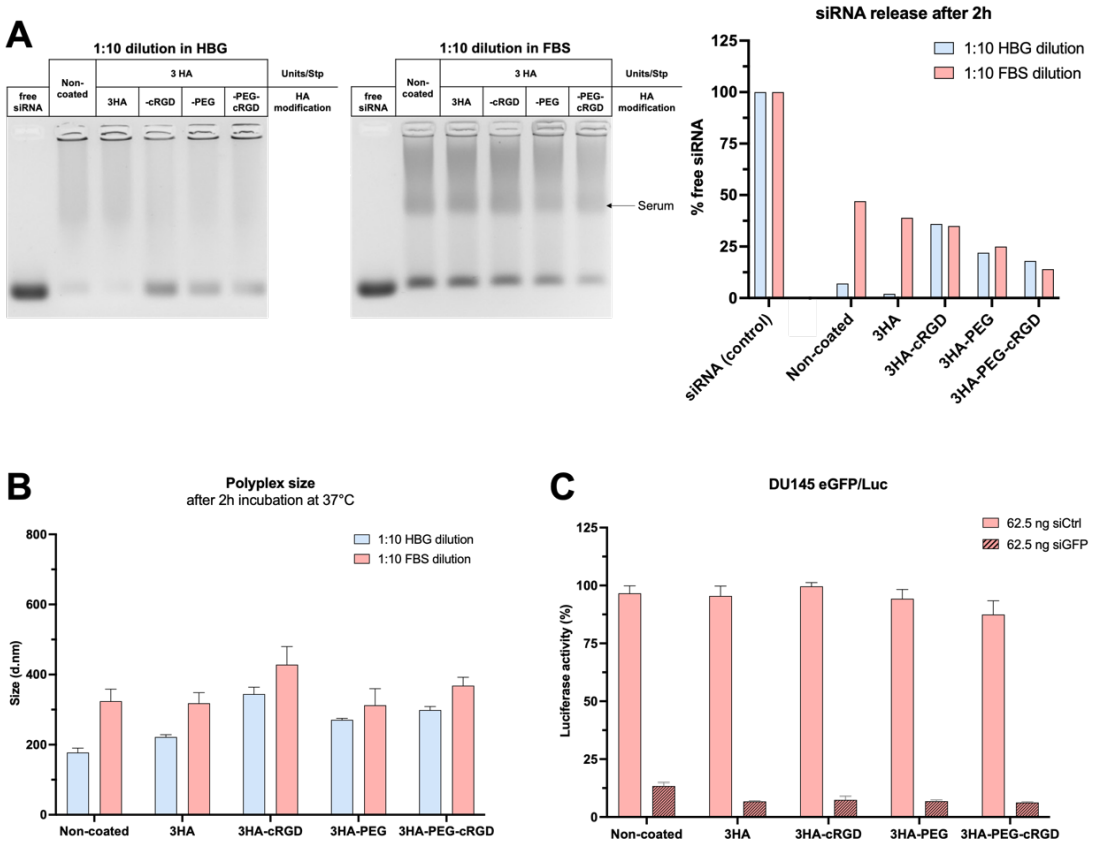

Figure 4. Serum compatibility of HA-coated polyplexes. Polyplexes were prepared at a concentration of 150 ng/µL and diluted 1:10 in HBG or fetal bovine serum (FBS; final FBS concentration: 90%), followed by an incubation for 2 h at 37 °C while shaking. (A) Stability of non-coated and coated polyplexes was determined by an agarose gel electrophoresis. Twenty µL of the diluted samples (containing 300 ng of siRNA) was evaluated. As a positive control, a sample containing 300 ng of free siRNA was used. siRNA release was determined using the ImageJ software and was calculated as a percentage of the positive control (% free siRNA). (B) Hydrodynamic diameters of non-coated and coated polyplexes after 1:10 dilution in HBG and FBS were determined by DLS measurements (mean ± SD, n = 3). (C) Gene silencing efficiency of FBS-diluted polyplexes at a dose of 62.5 ng of siRNA per well. Luciferase activity was measured after a 48 h exposure of polyplexes to the reporter cell line DU145 eGFP/Luc and was calculated as the percentage to the activity of HBG-treated cells. Polyplexes prepared with siCtrl served as a negative control.

The impact of serum incubation on the hydrodynamic size of the polyplexes was subsequently assessed using DLS measurements. Samples were diluted in both FBS and HBG and incubated at 37 °C for 2 h, as in the gel electrophoresis study. Dilution in HBG did not considerably alter the polyplex size compared to previous measurements (**Figure 4B**). In contrast, serum incubation resulted in an increase in size for all

formulations, likely due to the formation of a protein corona, as noted in other studies [428]. The smallest size increase was observed for polyplexes coated with cRGD- and PEG-modified HA, followed by those coated with unmodified HA. Non-coated polyplexes exhibited the largest percentage increase in size (**Figure 4B and S9**).

Following the evaluation of physicochemical characteristics, the functionality of all formulations postserum incubation was evaluated in DU145 eGFP/Luc cells. After serum dilution and incubation for 2 h at 37 °C, cells were transfected with non-coated or HA-coated polyplexes at a dose of 62.5 ng of siRNA. Gene silencing was effective across all formulations, exceeding 80%, and comparable to results obtained under standard transfection conditions (**Figure 4C and Table S3**). HA-coated polyplexes exhibited up to 10% higher gene silencing efficiency compared to non-coated polyplexes, consistent with their superior performance in the previous gel shift assay and DLS study.

To confirm the retention and functionality of the HA-coating postserum incubation, fluorescence correlation and cross-correlation spectroscopy (FCS and FCCS) experiments were employed. FCS examines the intensity fluctuations caused by the diffusion of fluorescently labeled particles through a small observation volume (~ 1 femtoliter) [429]. The intensity fluctuations are analyzed via a temporal autocorrelation function (ACF), the decay of which is related to the diffusion constant of the present fluorescent species. A slower diffusion, caused for instance by a larger molecular size, higher viscosity of the medium or interaction between two or more molecules, will result in a shift of the ACF toward longer time scales. FCCS is the two-color extension of FCS, in which the correlated fluctuations of two differently labeled species are examined simultaneously. In this case, the intensity fluctuations in two detection channels are analyzed via the temporal cross-correlation function (CCF)[430]. If the two species interact, i.e. they diffuse together through the observation volume, the fluorescence fluctuations in both channels will be coordinated and a cross-correlation signal will be present. The higher the amplitude of the CCF, with respect to the amplitude of the ACFs, the higher the number of double-labeled complexes diffusing in solution.

For the F(C)CS measurements, the polyplexes were prepared with a mixture of unlabeled siRNA spiked with 2.5% ATTO565-labeled siRNA (siRNA-ATTO565). The HA-coated polyplexes were prepared with a mixture of labeled and nonlabeled HA. For labeling, an equimolar amount of siRNA-ATTO565 and ATTO643-labeled HA (HA-ATTO643) was used and the remainder of HA needed for coating the particles was unlabeled. Electrostatic coating of polyplexes with unmodified HA only was evaluated as a representative coat for all tested HA- derivatives. Given that only around 11% of the

carboxylic acids of the polyanionic HA are optionally modified with cRGD and/or small amounts of PEG, this is unlikely to reduce the electrostatic interaction with the polyplex. As in the before mentioned serum studies, non-coated and 3HA-coated polyplexes were diluted 1:10 in HBG and FBS and incubated for two h at 37 °C while shaking. FCCS measurements were conducted before and after the 2 h incubation.

Right after dilution, as expected, the double-labeled HA-coated polyplexes showed cross-correlation in both HBG and FBS (**Figure 5A**) indicating that the labeled siRNA and HA are complexed in the polyplexes. Interestingly, after two h in FBS, a cross-correlation signal appeared also for the non-coated polyplexes. As the non-coated polyplexes do not contain any red labels, the cross-correlation is attributed to autofluorescence of the serum itself. FBS alone shows measurable fluctuations as observed in the ACFs but exhibits no cross-correlation amplitude (**Figure S10A**). The positive cross-correlation amplitude observed with the polyplexes suggests that a serum induced protein corona is probably forming around the non-coated particles. For the HA-coated polyplexes, the highest cross-correlation amplitude was recorded under HBG conditions, as expected, indicating a high efficiency of coating. In serum, before and after incubation, the amplitude of the CCF, relative to the ACF of the siRNA-ATTO565 polyplexes, is reduced, suggesting that the number of double-labeled complexes is decreased. This indicates that the polyplexes are partially disassembling and/or releasing some HA, although a considerable number of particles are still present even after two h. To exclude that this effect is caused by dilution or incubation, we performed FCCS after two h in HBG, the result of which nicely recapitulated the initial HBG conditions (**Figure S10B**).

To investigate whether the polyplexes are disassembling, i.e., releasing siRNA, or only losing the coating, i.e. releasing HA, we normalized the “yellow” and “red” ACFs to 1, which allows us to easily inspect the decay of each curve and thus compare the diffusion coefficient (D) of the observed species. The release of either siRNA (D_{FBS} = 64 $\mu m^2/s$, **Table S4**) or HA (D_{FBS} = 20 $\mu m^2/s$, **Table S4**) would result in the presence of a fast-diffusing component in the ACFs. Right after dilution in FBS, the HA-coated polyplexes did not show siRNA release. The ACF was similar to the one measured in HBG, although shifted toward longer time scales, as expected due to the higher viscosity of FBS and the larger size of the polyplexes in serum (**Figure 5B and Figure 4B**). After 2 h in serum, only a minor release of siRNA was detected, indicating that the core polyplex is substantially stable. Similar results were obtained for the non-coated polyplexes (**Figure S10C**). On the other hand, the HA started to be released immediately after dilution in FBS, with a more significant amount released during the two h between measurements

(**Figure 5C**). Altogether, these results indicate that although some HA-coated polyplexes disassemble and release siRNA, the reduced cross-correlation in serum is mostly due to dissociation of HA rather than the release of siRNA.

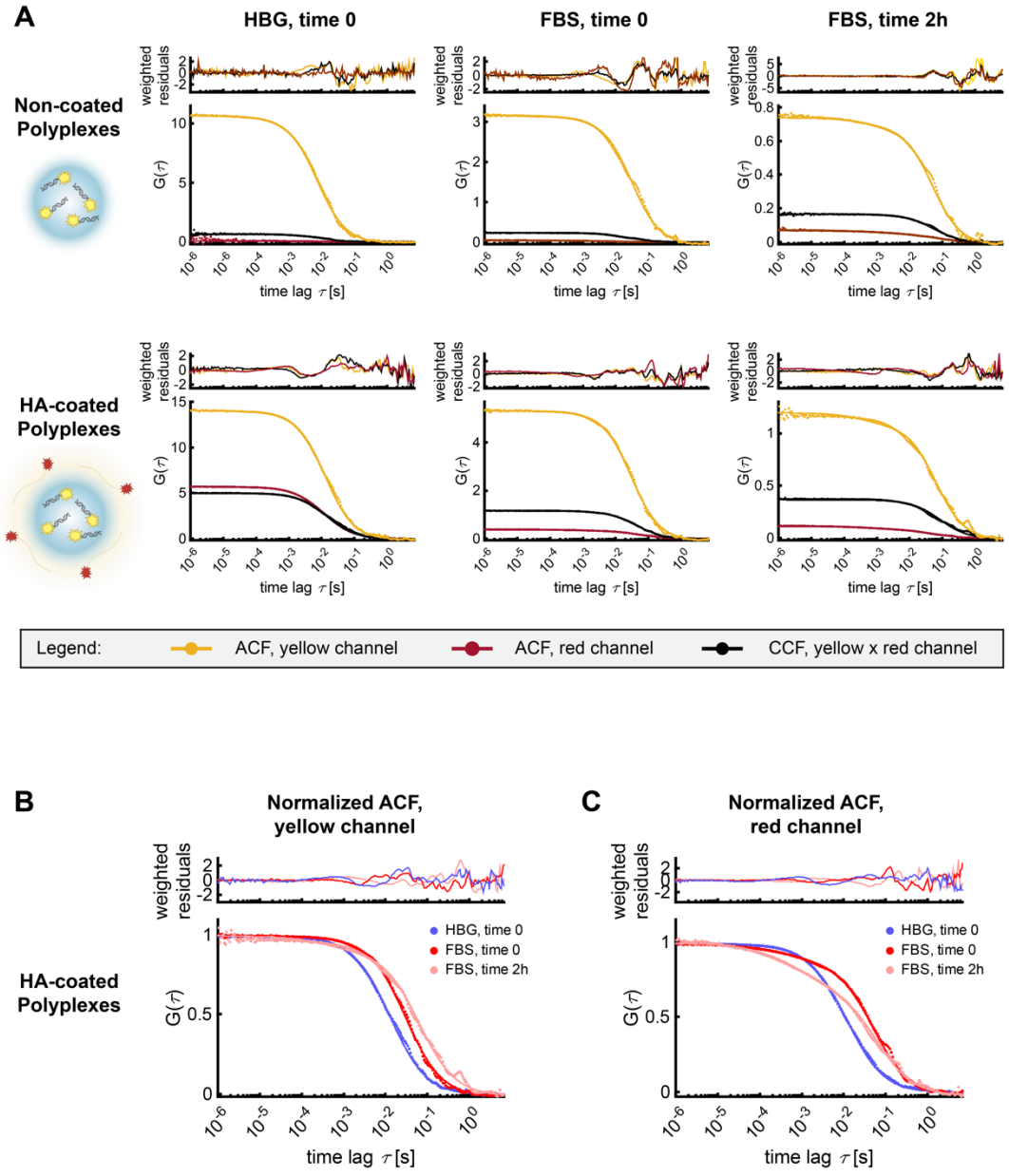

Figure 5. Characterization of polyplexes' stability in HBG and serum via fluorescence (cross-) correlation spectroscopy. (A) Representative autocorrelation functions (ACFs, yellow and red curves) and cross-correlation functions (CCF, black curve) of non-coated and HA-coated polyplexes in HBG and FBS, before and after 2 h of incubation at 37 °C while shaking. The results of the FCCS experiments for two additional independent replicates, are reported in the Supporting Information (**Tables S6 and S7**). The curves depicted here are without normalization, to appreciate the relative CCF amplitude. To better visualize changes in the diffusion of polyplexes in FBS over time, the ACFs of siRNA-ATTO565 (B) and HA-ATTO643 (C) complexed into HA-coated polyplexes were normalized to 1. The experiments were performed in collaboration with I. Gialdini (Department of Chemistry, LMU Munich).

Since an accurate quantification of the number of HA molecules per particle via FCCS is hindered by the high difference in brightness of the diffusing species (**Tables S4–S7**)[431], we analyzed the colocalization between siRNA-ATTO565 and HA-ATTO643 at the single particle level to determine whether some HA molecules are still retained within the polyplexes (**Figure 6A**). For both non-coated and HA-coated polyplexes, the overall number of particles detected in HBG and in FBS right after dilution remains unaffected, albeit with a high standard deviation resulting from batch-to-batch variability. After two h in serum, the number of detected non-coated particles decreased to 10% of the initial values in FBS, while 40% of HA-coated polyplexes were still present (**Figure 6B**).

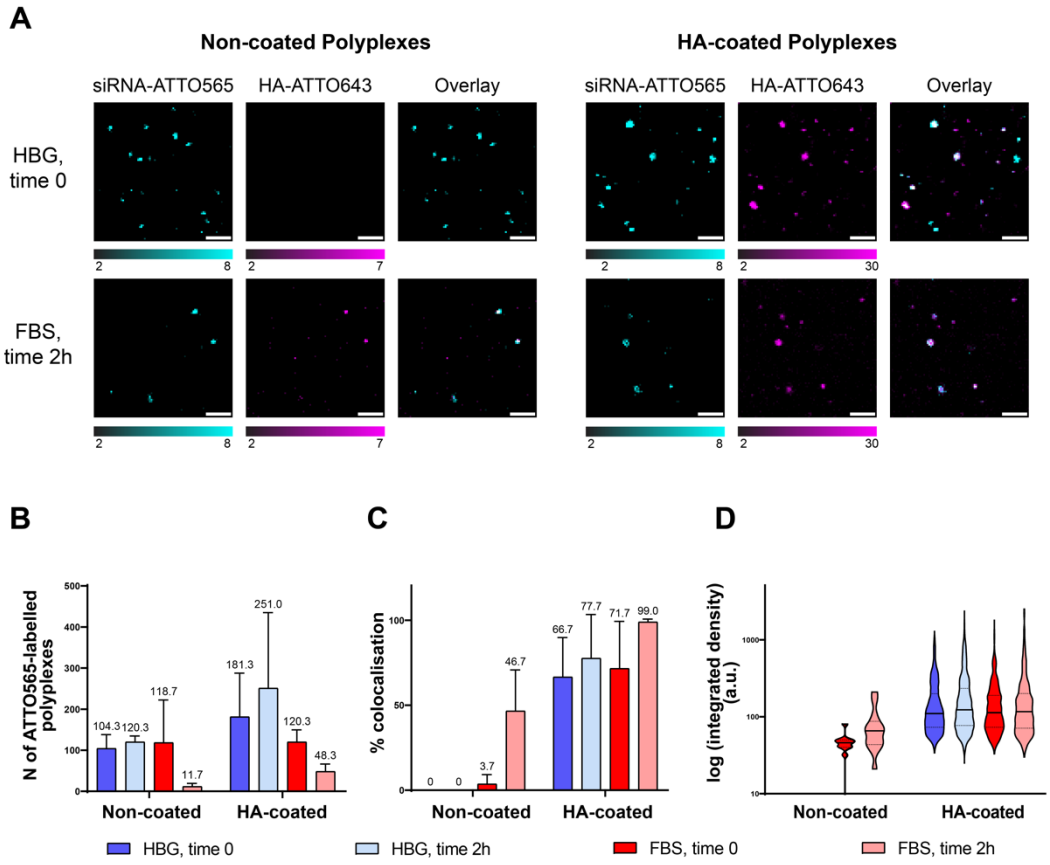

Figure 6. Colocalization between the HA coating and siRNA-ATTO565 core polyplexes in HBG and FBS. (A) Representative confocal images of non-coated and HA-coated nanoparticles in HBG and after 2 h of incubation in serum at 37 °C with shaking. The core of the polyplex is labeled via internalization of siRNA-ATTO565 (cyan), and the HA is labeled with ATTO643 (magenta). The scale bar is 5 µm. (B) Average number of non-coated and HA-coated siRNA-ATTO565 polyplexes detected in HBG and FBS are shown both before and after incubation. The results of three independent experiments are reported as mean ± SD. (C) Percentage of siRNA-ATTO565 core polyplexes colocalizing with serum protein (non-coated polyplexes) or HA-ATTO643 (coated polyplexes). The results of three independent experiments are reported as mean ± SD. (D) Particle-wise brightness in the red channel, corresponding to the fluorescence of serum protein (non-coated polyplexes) or HA-ATTO643 (coated polyplexes). The integrated density (i.e. intensity) of each detected particle was extracted with ImageJ and plotted on a logarithmic scale. The violin plots were compiled from 3 independent experimental replicates. The experiments were performed in collaboration with I. Gialdini (Department of Chemistry, LMU Munich).

In HBG and right after dilution in serum, ~70% of the HA-coated particles showed colocalization between siRNA-ATTO565 and HA-ATTO643, indicating that, despite a high coating efficiency, some particles without the HA layer exist. Interestingly, after two h in FBS, 99% of the polyplexes showed colocalization, possibly indicating that those particles that were initially present in HBG without proper HA coating, are degraded by prolonged incubation in FBS (**Figure 6C**). This result suggests that not only the HA coating is retained on the particles even in the presence of serum, but that also the HA shields the polyplexes from the serum proteins and is necessary to prevent the degradation of the nanocarriers. Consistent with the FCCS results, the non-coated polyplexes were undetectable in the red channel in HBG, but some red signal was visible in serum. Also in this case, we attribute the signal to the autofluorescence of the FBS components. The percentage of detected non-coated polyplexes that colocalize with serum proteins increases from 4% to 47% after two h of incubation, consistent with a progressive development of the protein corona around non-coated polyplexes (**Figure 6C**). The quantification of single-particle brightness in the red channel supported this observation, as the brightness increased after two hours of serum incubation (**Figure 6D**). In addition, the brightness of the non-coated polyplexes remained much lower compared to the HA-ATTO643-coated particles. This suggests that the signal obtained for the non-coated particles indeed originates from FBS autofluorescence as ATTO643-labeled particles showed higher brightness. This finding does not exclude the possibility of the formation of the protein corona around the HA-coated polyplexes. However, the higher brightness of HA-ATTO643 compared to FBS may hide the protein corona effect in these experiments. As a control, the single-particle brightness was also evaluated in the yellow channel; i.e., the brightness of siRNA-ATTO565 polyplexes was quantified. In this case, both non-coated and HA-coated polyplexes showed substantially unaltered brightness during serum incubation, indicating that the particles that remain in serum are intact. The HA-coated particles showed overall higher siRNA brightness than the non-coated polyplexes, consistent with their larger diameter (**Figure S11**).

Taken together, these results indicate that (i) HA-coated nanoparticles do contain siRNA and HA, and (ii) although some polyplexes may disassemble during incubation in serum, a substantial proportion of HA is retained with the particles, which improves the stability of the polyplexes, and potentially improves blood circulation *in vivo*.

In summary, the HA-coating modulates the physicochemical properties, performance, and stability of polyplexes upon serum dilution. Both the gel shift assay and F(C)CS study confirmed the stability of the core polyplexes, with minimal siRNA release from both non-coated and HA-coated polyplexes after two h of exposure to serum. Notably,

in the gel shift assay, HA-coated polyplexes, particularly those with PEG modifications, showed enhanced siRNA compaction capacity in FBS. Subsequent DLS measurements revealed that HA-coated polyplexes experienced a smaller size increase in serum, indicating reduced protein corona formation. A functional assay further supported these observations, demonstrating that HA-coated polyplexes maintained higher gene silencing efficiency compared to non-coated polyplexes in DU145 eGFP/Luc cells following FBS dilution. Importantly, the FCCS study finally confirmed that a substantial portion of the ionic HA coating remained associated with the polyplexes after serum incubation, indicating that the beneficial effects observed with the HA formulations can be attributed to the coating. This implies that since the ligands are attached to the polyplex solely through the HA, they too remain associated, which may further contribute to the efficacy of the polyplexes. Overall, these findings highlight the critical role of HA-coating in enhancing polyplex stability and performance in serum, paving the way for enhanced efficacy *in vivo* compared to non-coated polyplexes.

3.4.4 *In vivo* biodistribution of HA-coated polyplexes

Analogous to the dependency of the *in vitro* gene silencing efficiency on cell association, the *in vivo* efficacy relies on efficient accumulation of the therapeutic at the target site. To this end, we assessed the biodistribution of non-coated and HA-coated polyplexes containing 50% Cy7-labeled siRNA. Polyplexes were prepared at a concentration of 150 ng/µL and administered intravenously via the tail vein into Neuro2a tumor-bearing NMRI mice at a dose of 30 µg siRNA (n = 4). One hour postinjection, organs and tumors were harvested and imaged ex vivo using an IVIS imaging system (**Figure 7A**). The average fluorescence efficiency in each organ and tumor was quantified using living image software (**Figure 7B**).

No significant changes in accumulation were visible in the brain, heart, kidneys and liver for any of the applied formulations. However, differences in accumulation were noted in the lung, spleen and tumor. In the lung, accumulation decreased in the order of non-coated > 3HA > 3HA–cRGD > 3HA–PEG > 3HA–PEG–cRGD polyplexes (**Figure 7**). This trend suggests that increasing the shielding properties through HA coating and additional modifications with cRGD, PEG, or both reduces lung retention. In the spleen, accumulation was comparable across all formulations, with the exception of 3HA-PEG polyplexes, which exhibited higher spleen accumulation in comparison to all other formulations. Notably, the most significant observation was an increased tumor accumulation of specific formulations coated with HA. Polyplexes coated with 3HA-PEG-

cRGD demonstrated significantly (*) increased tumor accumulation compared to non-coated polyplexes (**Figure 7B**). Coating with unmodified 3HA also enhanced accumulation, although it was not statistically significant.

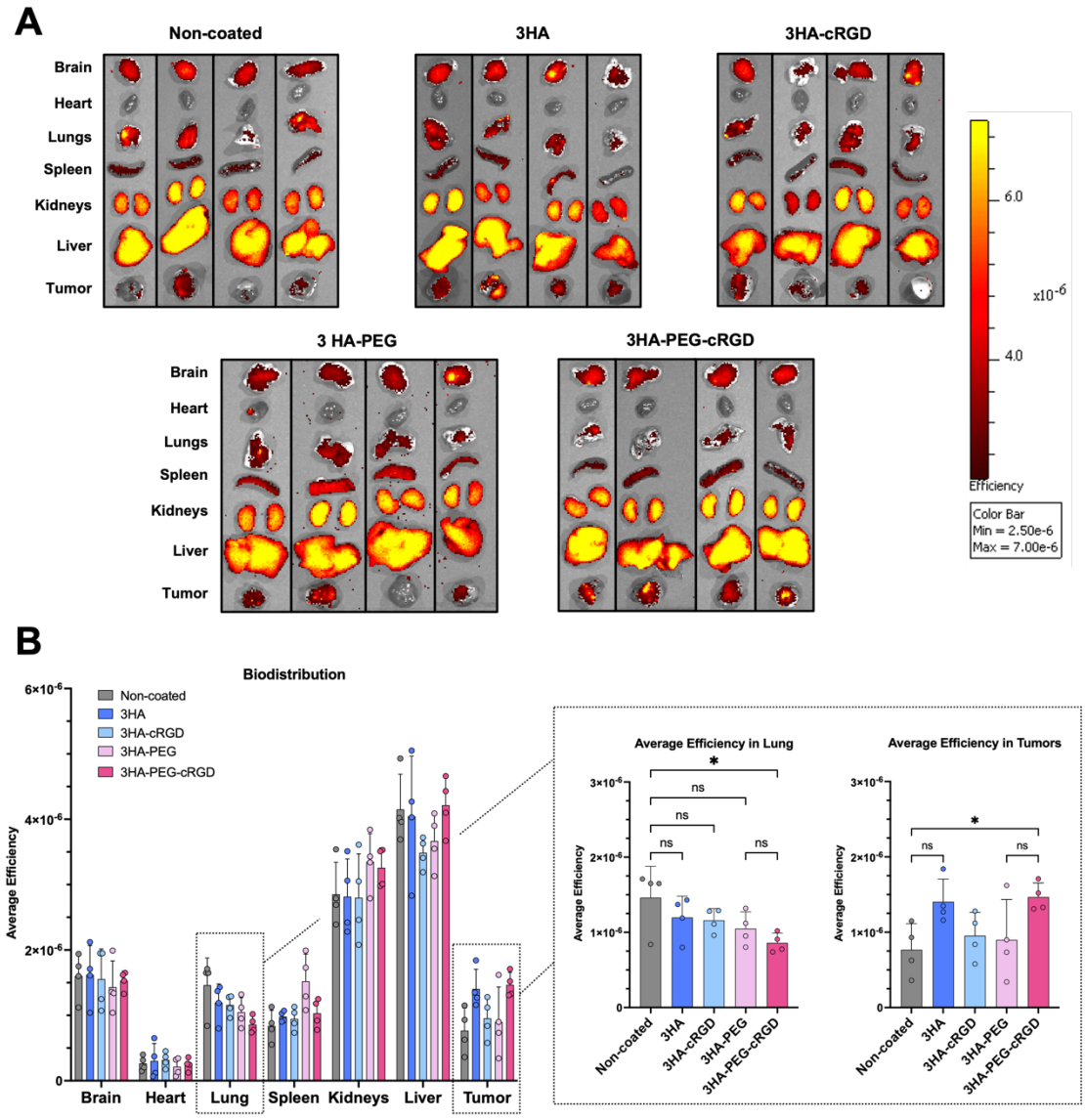

Figure 7. Biodistribution of Cy7-labeled polyplexes *in vivo*. Polyplexes were prepared at a concentration of 150 ng/µL containing 50% Cy7-labeled siRNA and 50% unlabeled siCtrl. Polyplexes encapsulating 30 µg of siRNA were injected intravenously into the tail vein of Neuro2a tumor bearing NMRI mice. (A) Organs and tumors were imaged ex vivo with an IVIS imaging system one hour post injection (n = 4) of the non-coated and HA-coated polyplexes (unmodified HA, HA–cRGD, HA–PEG, or HA–PEG–cRGD). (B) Average efficiency in organs and tumors was quantified using the Living Image Software (mean ± SD, n = 4). Statistical significance was determined as: ns $p > 0.05$; * $p \leq 0.05$ (ordinary one-way ANOVA, Šidák multiple comparison test; GraphPad Prism 10.0.3). The injections, euthanasia and organ collection were performed by the veterinarians of our research group, J. Pöhmerer (Pharmaceutical Biotechnology, LMU Munich) and M. Yazdi (Pharmaceutical Biotechnology, LMU Munich).

IVIS images revealed that polyplexes coated with 3HA–PEG–cRGD consistently increased the intensity of the Cy7 signal in the tumors of all four injected mice (**Figure 7A**). Mice treated with 3HA-polyplexes also showed observable signals in all tumors, though with greater variability and overall lower intensity. In contrast, 3HA–cRGD and 3HA–PEG polyplexes only achieved an efficiency comparable to non-coated polyplexes, despite some individual tumors showing enhanced accumulation.

The finding that only 3HA–PEG–cRGD polyplexes showed significantly enhanced tumor accumulation suggests that HA-mediated CD44 targeting may be inhibited by DBCO- and ligand- modifications, as indicated by other studies [432, 433]. Therefore, 3HA–PEG–cRGD polyplexes may achieve tumor accumulation via integrin targeting. The lack of accumulation of 3HA-cRGD polyplexes could be attributed to the direct conjugation of cRGD to HA via the hydrophobic DBCO anchor, which may compromise the ligand functionality. This hypothesis is supported by our initial concept that a PEG spacer might be necessary for effective cRGD functionality. Taken together, the biodistribution study indicates that certain anionic HA-coated polyplexes achieve significantly higher tumor accumulation compared with plain cationic polyplexes, which is crucial for enhancing polyplex efficacy, as assessed in the subsequent study.

3.4.5 *In vivo* gene silencing efficiency

After confirming tumor accumulation for specific HA-coated polyplexes, we assessed their *in vivo* gene silencing efficacy. Polyplexes were prepared at a concentration of 200 ng/µL, containing EG5-targeted siRNA (siEG5), which silences the motor protein EG5, an essential protein in mitosis. Prior to administration, polyplexes were characterized via DLS and ELS to confirm their suitability for *in vivo* administration at this higher concentration (**Figure S12**). NMRI mice bearing Neuro2a tumors were injected intravenously into the tail vein. Each formulation containing 50 µg of siEG5 was administered twice, on day 1 (t_{0h}) and day 2 (t_{24h}), to ensure an effective *in vivo* dose. Tumors were harvested on day 3 (t_{48h}) to allow sufficient time for siRNA activity. To control for nonspecific gene silencing, 3HA-coated polyplexes containing 50 µg of siCtrl were also administered accordingly.

Following tumor collection, total mRNA was extracted, and cDNA was synthesized using reverse transcriptase. Quantitative PCR (qPCR) was employed to quantify the expression levels of EG5 and the housekeeping gene GAPDH. The ΔC_T values were calculated by subtracting C_T values of GAPDH from those of EG5 and were normalized to the ΔC_T of HBG-treated mice. Interestingly, the gene silencing results only partially

correlated with the biodistribution data. Consistent with the biodistribution study, 3HA–PEG–cRGD polyplexes outperformed all other formulations, except for 3HA–cRGD polyplexes, exhibiting significantly higher gene silencing than both non-coated polyplexes ($p \leq 0.01$; **) and the 3HA–PEG control group ($p \leq 0.0001$, ****) lacking the targeting ligand cRGD (**Figure 8**).

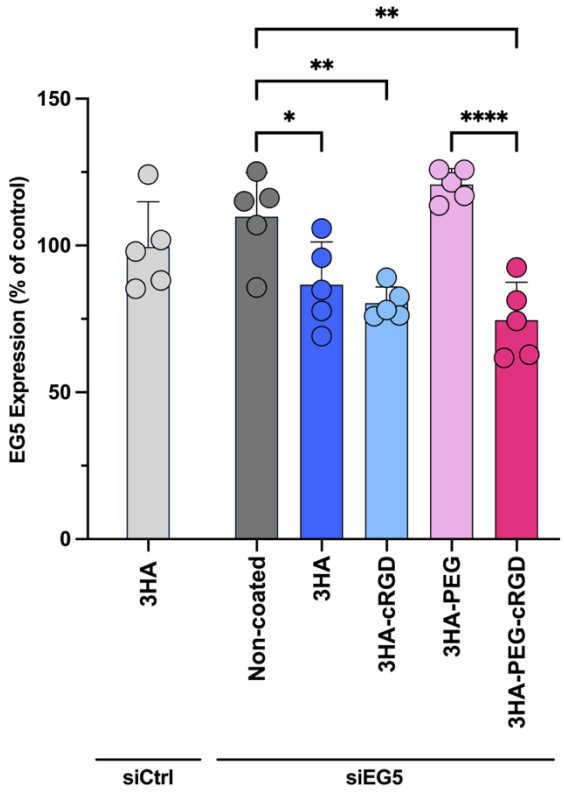

Figure 8. *In vivo* gene silencing efficiency of non-coated cationic and HA-coated polyplexes (coated with unmodified HA, HA–cRGD, HA–PEG, or HA–PEG–cRGD). Each formulation was prepared at a concentration of 200 ng/µL and injected intravenously into the tail vein of Neuro2a tumor-bearing NMRI mice at a dose of 50 µg of siEG5 (n = 5). Injections were performed twice for every formulation: on day 1 (t_{0h}) and on day 2 (t_{24h}); on day 3 (t_{48h}), mice were sacrificed. 3HA-coated polyplexes containing siCtrl served as a negative control. For evaluation of gene silencing efficiency, tumors were collected after scarification. Their total mRNA was extracted and used for cDNA synthesis by reverse transcriptase. EG5 and GAPDH expression were quantified using qRCR. EG5 expression of mice was analyzed by the ΔC_T method. C_T values of GAPDH were subtracted from C_T values of EG5. ΔC_T values of treated animals were calculated as percentage of HBG-treated control animals. Statistical significance was determined as: ns $p > 0.05$; * $p \leq 0.05$; ** $p \leq 0.01$; **** $p \leq 0.0001$ (ordinary one-way ANOVA, Šidák multiple comparison test; GraphPad Prism 10.0.3). The injections, euthanasia and organ collection were performed by the veterinarians of our research group, J. Pöhmerer (Pharmaceutical Biotechnology, LMU Munich) and M. Yazdi (Pharmaceutical Biotechnology, LMU Munich).

Additionally, 3HA-coated polyplexes showed significantly higher efficacy than plain polyplexes ($p \leq 0.01$, *), following the same trend as observed in the biodistribution study. However, unlike the biodistribution results, 3HA-cRGD polyplexes also showed significantly increased gene silencing compared to the non-coated polyplexes, despite

not demonstrating increased accumulation in the biodistribution study. The EG5 gene silencing activity refers to all cell types within the tumor beyond the TECs. An absolute EG5 gene silencing of 25% reflects that achieving effective gene silencing is challenging as it involves multiple critical steps beyond TEC adherence, such as migration through the extracellular matrix (ECM), cellular uptake by tumor cells, intracellular trafficking, and endosomal escape [86].

In summary, the data suggest that HA–PEG–cRGD coating significantly enhances *in vivo* gene silencing efficiency compared to non-coated or HA–PEG-coated polyplexes. The poor performance of the well-shielded 3HA-PEG control formulation, which lacks the targeting ligand, suggests that active cRGD targeting mechanisms contribute to both tumor accumulation and efficacy. While the HA and cRGD may facilitate initial retention of the polyplexes at the tumor site, HA shielding may improve biodistribution and tissue migration. Ultimately, both cRGD-containing formulations achieve comparable, significantly ($p \leq 0.01$; **) better *in vivo* efficacy than non-coated cationic polyplexes, despite the discrepancy in their tumor accumulation.

From our FCCS study, we assume that a substantial proportion of the ionic HA coating, which also carries the targeting ligand cRGD, remains bound to the polyplexes after intravenous injection, contributing to the observed beneficial effects. Reflecting on the *in vitro* results, we conclude that these data were only partially predictive of the final *in vivo* performance, consistent with findings from other studies [160]. Although uptake and reporter gene silencing assays indicated a general benefit of the HA coating, they did not allow us to clearly identify a superior *in vivo* formulation. In contrast to *in vitro* studies, where ligand-targeted nanoparticles can easily find and bind their cell surface receptors, upon intravenous delivery nanoparticles need to survive intact in the bloodstream, escape clearance by RES, avoid protein corona formation that may block receptor ligands, and need to overcome several pharmacological delivery barriers before they meet their cellular target. The partial *in vitro* - *in vivo* discrepancies as also observed in the current study highlight the need for more predictive assays for further optimization of tumor-targeted nanoparticles.

3.5 Conclusions

siRNA therapeutics hold the potential to treat a variety of diseases, but their efficacy in tumor treatment is limited by challenges in effectively delivering the therapeutic agent to tumors. While cationic polyplexes have demonstrated high efficacy as siRNA carriers *in vitro*, their *in vivo* performance is compromised by their strongly positive charge. Our strategy employs an ionic coating with hyaluronic acid (HA) along with the incorporation of cRGD as a TEC-targeting ligand via a PEG spacer. Stability and functional assays performed after FBS dilution of polyplexes demonstrated that the HA coating is retained on the polyplex after prolonged exposure to serum but also that the coating conferred greater stability, higher transfection efficiency, and a lower increase in polyplex size. *In vivo* testing finally revealed significantly enhanced tumor accumulation and gene silencing of HA–PEG–cRGD coated polyplexes.

Associated Content

Supporting Information

The supporting information includes analytical methods, tables with calculated gene silencing efficiencies, additional data obtained from FCS measurements, and relevant molar ratios for polyplex formation, as well as additional figures and schemes.

Author Contributions

Conceptualization, VV and EW; methodology, VV, MY, IG, JP, JS, MH; investigation, VV, MY, IG, JP, JS, MH; data curation, VV, IG, EW; formal analysis, VV, MY, IG, DL, EW; validation, VV, MY, IG, JP, JS, MH, DL, EW; visualization, VV, IG, MH, EW; writing - original draft, VV, IG, EW; writing - review and editing, VV, MY, IG, DL, EW; funding acquisition, project administration, resources, supervision, DL, EW. All authors have read and agreed to the submitted version of the manuscript.

Conflicts of interest

There are no conflicts to declare.

Acknowledgments

The authors thankfully acknowledge the financial support of the Deutsche Forschungsgemeinschaft (DFG, German Research Foundation) – Project-ID 201269156 – SFB 1032 Projects B03 (D.C.L) and B04 (E.W.), and BMBF Cluster for Future “CNATM – Cluster for Nucleic Acid Therapeutics Munich” – project-ID 03ZU1201AA (E.W.). D.C.L acknowledges funding from the Federal Ministry of Education and Research (BMBF) and the Free State of Bavaria under the Excellence Strategy of the Federal Government and the Länder through the ONE MUNICH Project Munich Multiscale Biofabrication as well as financial support of the Ludwig-Maximilians-Universität München via the Department of Chemistry, the Center for NanoScience (CeNS) and the LMUinnovativ program BioImaging Network (BIN). They thank Profs. Biel and Fürst for providing the IVIS imaging system, Dr. Ali Bashiri Dezfouli for measuring VEGFR-2 silencing via flow cytometry, Melina Grau and Tobias Burghardt for MALDI-TOF measurements, and Wolfgang Rödl and Olga Brück for technical and organizational support. Figures were created in BioRender. Vetter, V. (2024) BioRender.com/k90p780

4 Summary

Over the past few decades, nucleic acid-based therapeutics have revolutionized the treatment of genetic disorders. Notably, this therapeutic modality also holds immense potential in tumor therapy, addressing the need for more targeted and effective treatment options. Among nucleic acid-based approaches, siRNA is particularly promising due to its ability to selectively silence tumor-promoting genes, enhancing therapeutic efficacy while minimizing the systemic side effects commonly associated with conventional chemotherapy. However, despite its remarkable potential, the clinical translation of siRNA for tumor therapy remains challenging, primarily due to difficulties in achieving efficient delivery to tumor cells.

To address these challenges, sophisticated delivery systems such as viral and non-viral vectors are essential to protect nucleic acids from degradation in the bloodstream and facilitate cellular uptake. While viral vectors currently dominate the market, there is a growing shift toward non-viral vectors given their advantages, including higher encapsulation efficiency and reduced immunogenicity. Among these, polyplexes, alongside lipoplexes and lipid nanoparticles (LNPs), show particular promise for siRNA delivery, offering high stability, efficient cellular uptake, and effective endosomal escape. However, their positively charged surface, while beneficial for siRNA binding and cellular interaction, promotes non-specific interactions *in vivo*, leading to immune system activation, reduced tumor specificity, and potential toxicity. Thus, developing strategies such as surface shielding and tumor-specific targeting is crucial to overcome these limitations and realize the full therapeutic potential of siRNA polyplexes.

In this thesis, shielding and targeting strategies were developed to enhance the delivery of oligoaminoamide (OAA)-based siRNA polyplexes to tumor cells. For shielding, polyplexes were ionically coated with hyaluronic acid (HA) to mask their positive surface charge, thereby reducing adverse effects and extending blood circulation time. Additionally, the natural affinity of HA for CD44 receptors was intended to enable targeting of tumor endothelial cells (TECs).

Physicochemical studies demonstrated that the HA-to-polyplex ratio significantly influenced key particle characteristics, particularly the surface charge, which progressively shifted from positive to negative with increasing HA amounts. An optimal ionic coating was achieved with a molar ratio of three HA disaccharide units per succinoyl tetraethylene pentamine (Stp), the protonatable building block of the OAA. These 3HA-coated polyplexes exhibited favorable size, negative zeta potential, and complete siRNA complexation, confirmed by DLS measurements and a gel shift assay.

To further enhance TEC specificity, the peptide ligand cRGD, which targets integrin $\alpha v\beta_3$—a receptor commonly overexpressed on TECs—was conjugated to the HA coating using SPAAC chemistry. This functionalization required azido modification of the cRGD ligand, either directly (3HA-cRGD) or via a short PEG spacer (3HA-PEG-cRGD), along with the incorporation of DBCO modules into HA. As a control, HA was modified with a PEG spacer only (3HA-PEG). Notably, functionalization with cRGD or PEG did not significantly alter the physicochemical properties of the polyplexes.

In vitro studies showed that HA coating enhanced polyplex association with cells and improved gene silencing efficiency across various cell lines. Additional cRGD functionalization increased these effects under certain conditions, suggesting targeted delivery. This hypothesis was further explored through a competition assay, where the gene silencing efficiency of cRGD-functionalized polyplexes, particularly 3HA-cRGD polyplexes, was significantly reduced when excess coating agent was present, confirming receptor-mediated uptake. In contrast, non-coated and 3HA-coated polyplexes remained unaffected. An endocytosis inhibition assay further revealed distinct internalization mechanisms among the formulations. HA-coated polyplexes, especially 3HA-cRGD polyplexes, predominantly utilized clathrin-mediated endocytosis, whereas non-coated polyplexes relied equally on clathrin-mediated endocytosis and macropinocytosis. Importantly, all formulations exhibited low cytotoxicity *in vitro*, as determined by an MTT assay.

Experiments in the presence of serum further highlighted the advantages of HA-coated polyplexes under physiological conditions. Polyplexes coated with ligand-modified HA exhibited superior siRNA complexation. Moreover, HA coating minimized particle size increase in serum while preserving high transfection efficiency. Notably, fluorescence cross-correlation spectroscopy (FCCS) confirmed that the HA coating remained stably associated with the polyplexes during serum incubation, contributing directly to these enhanced properties.

Ultimately, the developed shielding and targeting strategy markedly enhanced the *in vivo* performance of siRNA polyplexes. Biodistribution and gene silencing experiments performed in Neuro2A-tumor-bearing mice demonstrated that 3HA-PEG-cRGD-coated polyplexes achieved significantly higher tumor accumulation and superior gene silencing efficiency compared to non-coated polyplexes following systemic administration.

In conclusion, these findings demonstrate that modifying polyplex surfaces with shielding and targeting moieties such as HA and cRGD can significantly modulate the stability, tumor accumulation, and gene silencing efficiency of siRNA-based therapeutics *in vivo*.

5 Appendix

5.1 Supplementary information

5.1.1 Analytical methods

5.1.1.1 ^{1}H NMR spectroscopy

^{1}H NMR (nuclear magnetic resonance) spectra were recorded using a Bruker Avance III HD 400 (400 MHz). Signals were calibrated to the residual, non-deuterated signal of the solvent used as an internal standard (D_2O 4.79 ppm). Chemical shifts (δ) were reported in parts per million (ppm). The spectra were analyzed using MestreNova software (MestReLab Research x64). Integration was performed manually.

5.1.1.2 MALDI-TOF mass spectrometry

MALDI-TOF (matrix assisted laser desorption ionization – time of flight) MS was conducted using an Autoflex II mass spectrometer (Bruker Daltonics, Germany). As matrix, a solution of 10 mg/ml super-DHB (9/1 (w/w) mixture of 2,5-dihydroxybenzoic acid and 2-hydroxy-5-methoxybenzoic acid) in 69.93/30/0.07 (v/v/v) H_2O/ACN/TFA was used. 1 µl of matrix solution was spotted on a MTP AnchorChip (Bruker Daltonics, Germany). Subsequently, 1 µl of sample solution, dissolved in H_2O at a concentration of 1 mg/ml, was added onto the matrix, co-crystallized and analyzed. Spectra were recorded in positive or negative ion mode. Measurements were kindly performed by T. Burghardt (Pharmaceutical Biotechnology, LMU Munich) and M. Grau (Pharmaceutical Biotechnology, LMU Munich).

5.1.1.3 Lyophilization

Lyophilization of the synthesis products was conducted using a Freeze-dryer ALPHA 3-4 LSCbasic (Martin Christ Gefriertrocknungsanlagen GmbH, Osterode am Harz, Germany). The condenser temperature was set to -105°C at 0.050 mbar.

5.1.1.4 UV-vis spectroscopy

UV/vis spectra were recorded on an Agilent Cary 3500 UV-Vis Multicell Peltier spectrophotometer using micro-UV-cuvettes (Brand GmbH & Co. KG, Wertheim, Germany). Absorption was recorded either as scan from 200 to 800 nm or at the distinct wavelength of 308 nm for detection of DBCO units. For click reaction monitoring, both unfunctionalized HA-DBCO and HA-ligand conjugates were assessed. 10 mg/ml stocks were diluted 1:100.

5.1.2 Supporting tables

Table S1. Calculated gene silencing efficiency of non-coated and HA-coated polyplexes at a dose of 250 ng siRNA.

	250 ng siRNA/well					
	Luciferase activity (%)				Gene silencing efficiency (%)	P value
	siCtrl		siGFP			
Formulation	Mean	SD	Mean	SD		
DU145 eGFP/Luc						
Non-coated	79,26	5,79	5,88	0,30	**73,39**	****
3HA	70,20	7,88	4,50	0,20	**65,71**	***
3HA-cRGD	53,71	7,39	5,08	0,18	**48,63**	***
3HA-PEG	76,56	1,98	8,01	0,47	**68,55**	****
3HA-PEG-cRGD	66,59	1,14	4,41	0,20	**62,18**	****
KB eGFP/Luc						
Non-coated	98,84	39,90	3,62	1,44	**95,23**	****
3HA	86,73	13,71	2,15	0,46	**84,57**	***
3HA-cRGD	78,77	16,93	4,32	0,98	**74,45**	**
3HA-PEG	96,07	12,84	12,64	1,08	**83,42**	***
3HA-PEG-cRGD	86,19	5,26	3,43	0,24	**82,76**	****

The cell lines DU145 eGFP/Luc and KB eGFP/Luc, which both stably express the enhanced green fluorescent protein-luciferase (eGFP/Luc) fusion protein, were transfected with all formulations at a dose of 250 ng eGFP-targeted siRNA (siGFP) and control siRNA (siCtrl). The data are taken from **Figure 3A**. The luciferase activity was calculated as percentage relative to HBG-treated cells (mean ± SD, n = 3). Gene silencing efficiency (%) represents the difference in luciferase activity of siCtrl- and siGFP-transfected cells. Statistical significance was determined as ns (statistically not significant) $p > 0.05$; * $p \leq 0.05$; ** $p \leq 0.01$; *** $p \leq 0.001$; **** $p \leq 0.0001$.

Table S2. Calculated gene silencing efficiency of non-coated and HA-coated polyplexes at a dose of 62.5 ng siRNA.

	62.5 ng siRNA/well					
	Luciferase activity (%)				Gene silencing efficiency (%)	P value
	siCtrl		siGFP			
Formulation	Mean	SD	Mean	SD		
DU145 eGFP/Luc						
Non-coated	80,27	4,70	12,82	5,48	**67,45**	****
3HA	68,10	6,10	3,66	0,74	**64,44**	****
3HA-cRGD	70,97	5,03	4,48	0,21	**66,49**	****
3HA-PEG	83,92	2,10	7,05	1,14	**76,88**	****
3HA-PEG-cRGD	74,60	5,30	6,85	0,53	**67,75**	****
KB eGFP/Luc						
Non-coated	91,50	2,56	40,85	12,23	**50,65**	*
3HA	86,14	5,37	24,62	2,89	**61,52**	****
3HA-cRGD	79,47	10,77	13,94	0,75	**65,53**	***
3HA-PEG	94,61	0,76	54,95	5,64	**39,66**	***
3HA-PEG-cRGD	95,11	6,95	39,06	3,14	**56,05**	***

The cell lines DU145 eGFP/Luc and KB eGFP/Luc, which both stably express the eGFP/Luc fusion protein, were transfected with all formulations containing 62.5 ng siGFP and siCtrl. The data are taken from **Figure 3A**. The luciferase activity was calculated as percentage relative to HBG-treated cells (mean ± SD, n = 3). Gene silencing efficiency (%) represents the difference in luciferase activity of siCtrl- and siGFP-transfected cells. Statistical significance was determined as ns (statistically not significant) $p > 0.05$; * $p \leq 0.05$; ** $p \leq 0.01$; *** $p \leq 0.001$; **** $p \leq 0.0001$.

Table S3. Calculated gene silencing efficiency of non-coated and HA-coated polyplexes at a dose of 62.5 ng siRNA after 1:10 dilution in FBS.

	62.5 ng siRNA/well					
	Luciferase activity (%)				Gene silencing efficiency (%)	P value
	siCtrl		siGFP			
Formulation	Mean	SD	Mean	SD		
DU145 eGFP/Luc						
Non-coated	96,56	3,22	13,41	1,52	**83,15**	****
3HA	95,42	4,29	6,75	0,29	**88,67**	****
3HA-cRGD	99,61	1,58	7,42	1,58	**92,19**	****
3HA-PEG	94,25	4,00	6,86	0,48	**87,39**	****
3HA-PEG-cRGD	87,40	5,97	6,25	0,34	**81,15**	****

HA-coated and non-coated polyplexes were prepared at a concentration of 150 ng/µl and diluted 1:10 with FBS. Subsequently, diluted polyplexes were incubated for 2 hours at 37°C while shaking. Afterwards, the cell line DU145 eGFP/Luc, which stably expresses the eGFP/Luc fusion protein, was transfected with the polyplexes at a dose of 62.5 ng siRNA. Polyplexes were prepared with both siGFP and siCtrl. The data are taken from **Figure 4C**. The luciferase activity was calculated as percentage relative to HBG-treated cells (mean ± SD, n = 3). Gene silencing efficiency (%) represents the difference in luciferase activity of siCtrl- and siGFP-transfected cells. Statistical significance was determined as ns (statistically not significant) $p > 0.05$; * $p \leq 0.05$; ** $p \leq 0.01$; *** $p \leq 0.001$; **** $p \leq 0.0001$.

Table S4. FCS control measurements: values obtained from fitting the ACFs related to the yellow channel (i.e. with 560 nm excitation).

	ε (kHz)	A_1	A_2	D_1 (μm²/s)	D_2 (μm²/s)
FBS	0.92	1.00	-	29.51	-
ATTO565 in HBG	4.91	1.00	-	359.95	-
siRNA-ATTO565 in HBG	5.01	1.00	-	92.07	-
ATTO565 in FBS	2.81	0.77	0.23	214.32	29.51 (fixed as FBS)
siRNA-ATTO565 in FBS	5.45	0.56	0.44	64.16	214.32 (fixed as ATTO565 in FBS)

The autocorrelation function of the yellow channel (i.e. with 560 nm excitation) was analyzed using a one or two-component diffusion model (Eqn [1], main text). The average molecular brightness (ε) is reported. The parameters A_1 and A_2 represent the relative amplitudes of the species with diffusion coefficients D_1 and D_2 respectively. FCCS measurements were performed by I. Gialdini (Department of Chemistry, LMU Munich).

Table S5. FCS control measurements: values obtained from fitting the ACFs related to the red channel (i.e. with 635 nm excitation)

	ε (kHz)	A_1	A_2	D_1 (μm²/s)	D_2 (μm²/s)
FBS	1.70	1.00	-	28.28	-
ATTO643 in HBG	8.49	1.00	-	280.78	-
HA-ATTO643 in HBG	13.04	0.84	0.16	23.12	280.78 (fixed as ATTO643 in HBG)
ATTO643 in FBS	8.09	0.85	0.15	221.93	28.28 (fixed as FBS)
HA-ATTO643 in FBS	15.16	0.72	0.28	20.46	221.93 (fixed as ATTO643 in FBS)

The autocorrelation function of the red channel (i.e. with 635 nm excitation) was analyzed using a one or two-component diffusion model (Eqn [1], main text). The average molecular brightness (ε) is reported. The parameters A_1 and A_2 represent the relative amplitudes of the species with diffusion coefficients D_1 and D_2 respectively. FCCS measurements were performed by I. Gialdini (Department of Chemistry, LMU Munich).

Table S6. FCS polyplexes measurements: values obtained from fitting the ACFs related to the yellow channel (i.e. with 560 nm excitation).

	Mean ε (kHz) ± SD	**Mean A_1 ± SD**	**Mean A_2 ± SD**	**Mean D_1 ($\mu m^2/s$) ± SD**	**Mean D_2 ($\mu m^2/s$) ± SD**
Non-coated Polyplexes in HBG at time 0	332.17 ± 109.34	0.99 ± 0.01	0.01 ± 0.01	2.77 ± 0.31	92 (fixed as siRNA-ATTO565 in HBG)
Non-coated Polyplexes in HBG at time 2h	323.09 ± 55.55	0.97 ± 0.02	0.03 ± 0.02	2.11 ± 0.41	
Non-coated Polyplexes in FBS at time 0	81.70 ± 55.55	0.98 ± 0.02	0.02 ± 0.02	1.14 ± 0.41	64 (fixed as siRNA-ATTO565 in FBS)
Non-coated Polyplexes in FBS at time 2h	30.39 ± 16.39	0.88 ± 0.12	0.12 ± 0.12	0.81 ± 0.43	
HA-coated Polyplexes in HBG at time 0	432.71 ± 11.55	0.97 ± 0.02	0.03 ± 0.02	1.77 ± 0.12	92 (fixed as siRNA-ATTO565 in HBG)
HA-coated Polyplexes in HBG at time 2h	504.06±314.62	0.99 ± 0.02	0.01 ± 0.02	1.82 ± 0.82	
HA-coated Polyplexes	149.67 ± 137.62	0.99 ± 0.01	0.01 ± 0.01	0.93 ± 0.33	64 (fixed as

in FBS at time 0					siRNA-ATTO565 in FBS)
HA-coated Polyplexes in FBS at time 2h	42.02 ± 36.92	0.89 ± 0.07	0.11 ± 0.07	0.39 ± 0.06	

The autocorrelation function of the yellow channel (i.e. with 560 nm excitation) was analyzed using a one or two-component diffusion model (Eqn [1], main text). The average molecular brightness (ε) is reported. The parameters A1 and A2 represent the relative amplitudes of the species with diffusion coefficients D1 and D2 respectively. The reported values represent the mean ± SD of three independent FCS experiments. The high standard deviation is caused by the batch-to-batch variability, typical of polyplex preparation. FCCS measurements were performed by I. Gialdini (Department of Chemistry, LMU Munich).

Table S7. FCS polyplexes measurements: values obtained from fitting the ACFs related to the red channel (i.e. with 635 nm excitation).

	Mean ε (kHz) ± SD	Mean A_1 ± SD	Mean A_2 ± SD	Mean A_3 ± SD	Mean D_1 ($\mu m^2/s$) ± SD	Mean D_2 ($\mu m^2/s$) ± SD	Mean D_3 ($\mu m^2/s$) ± SD
Non-coated Polyplexes in HBG at time 0	0.19 ± 0.09	1.0	-	-	2.58 ± 1.02	-	-
Non-coated Polyplexes in HBG at time 2h	0.30 ± 0.14	1.0	-	-	2.29± 1.22	-	-
Non-coated Polyplexes in FBS at time 0	3.52 ± 1.43	0.44 ± 0.26	0.56 ± 0.26	-	0.95 ± 0.08	28.28 (fixed as FBS)	-

Non-coated Polyplexes in FBS at time 2h	7.10 ± 3.61	0.68 ± 0.16	0.32 ± 0.16	-	0.58 ± 0.28		-
HA-coated Polyplexes in HBG at time 0	582.30 ± 301.33	0.96 ± 0.02	0.04 ± 0.02	-	1.85 ± 0.15	23.12 (fixed as HA-ATTO643 in HBG)	-
HA-coated Polyplexes in HBG at time 2h	788.23 ± 318.76	0.96 ± 0.02	0.04 ± 0.02	-	1.42 ± 0.68		-
HA-coated Polyplexes in FBS at time 0	88.34 ± 62.62	0.75 ± 0.32	0.15 ± 0.16	0.13 ± 0.13	0.72 ± 0.40	20.46 (fixed as HA-ATTO643 in FBS)	221 (Fixed as free ATTO643 in FBS)
HA-coated Polyplexes in FBS at time 2h	51.25 ± 21.97	0.65 ± 0.21	0.25 ± 0.03	0.14 ± 0.15	0.30 ± 0.13		

The autocorrelation function of the red channel (i.e. with 635 nm excitation) was analyzed using a one or two-component diffusion model (Eqn [1], main text). The average molecular brightness (ε) is reported. The parameters A1 and A2 represent the relative amplitudes of the species with diffusion coefficients D1 and D2 respectively. The reported values represent the mean ± SD of three independent FCS experiments. The high standard deviation is caused by the batch-to-batch variability, typical of polyplex preparation. FCCs measurements were performed by I. Gialdini (Department of Chemistry, LMU Munich).

Table S8. Overview of relevant molar ratios used for polyplex preparation.

	mol/mol	Relevant formulations
N/P ratio	12	all
Stp/OAA	4	all
Protonated amines per Stp at pH 7.4	1	all
HA units/HA 38kDa	100.13	3HA 3HA-cRGD 3HA-PEG 3HA-PEG-cRGD
HA units/Stp	3	3HA 3HA-cRGD 3HA-PEG 3HA-PEG-cRGD
HA molecules/OAA	0.12	3HA 3HA-cRGD 3HA-PEG 3HA-PEG-cRGD
DBCO/HA	11-13 (HA-DBCO batch dependent)	3HA 3HA-cRGD 3HA-PEG 3HA-PEG-cRGD
cRGD/OAA	1.32-1.56 (HA-DBCO batch dependent)	3HA-cRGD 3HA-PEG-cRGD
PEG/OAA	1.6-1.8	3HA-PEG 3HA-PEG-cRGD

5.1.3 Supporting figures and schemes

Scheme S1. Functionalization of HA-DBCO with azido-functionalized cRGD

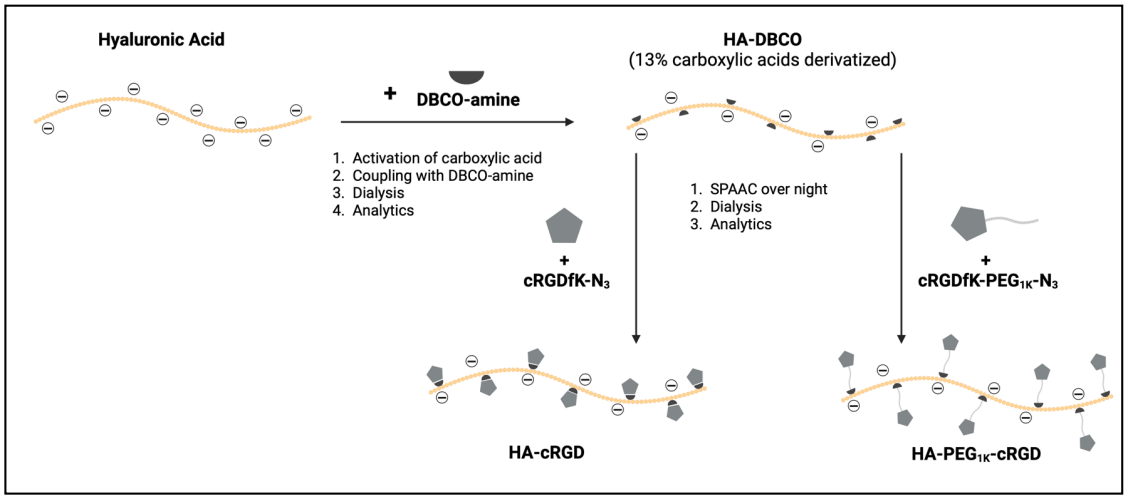

Hyaluronic acid (HA) was functionalized with the targeting ligand cRGD utilizing strain-promoted azide-alkyne cycloaddition (SPAAC). Initially, carboxylic acids contained in the HA units were modified with DBCO-amine. After purification by dialysis and subsequent lyophilization, DBCO was quantified by UV-vis spectroscopy. In the resulting HA-DBCO approximately 13% of carboxylic acids were derivatized. HA-DBCO was then coupled to the cRGD-ligands cRGDfK-N_3 or cRGDfK-PEG_{1K}-N_3 overnight. Afterwards, the conjugates were dialyzed for purification, lyophilized, and complete DBCO reaction was monitored via UV-vis spectroscopy.

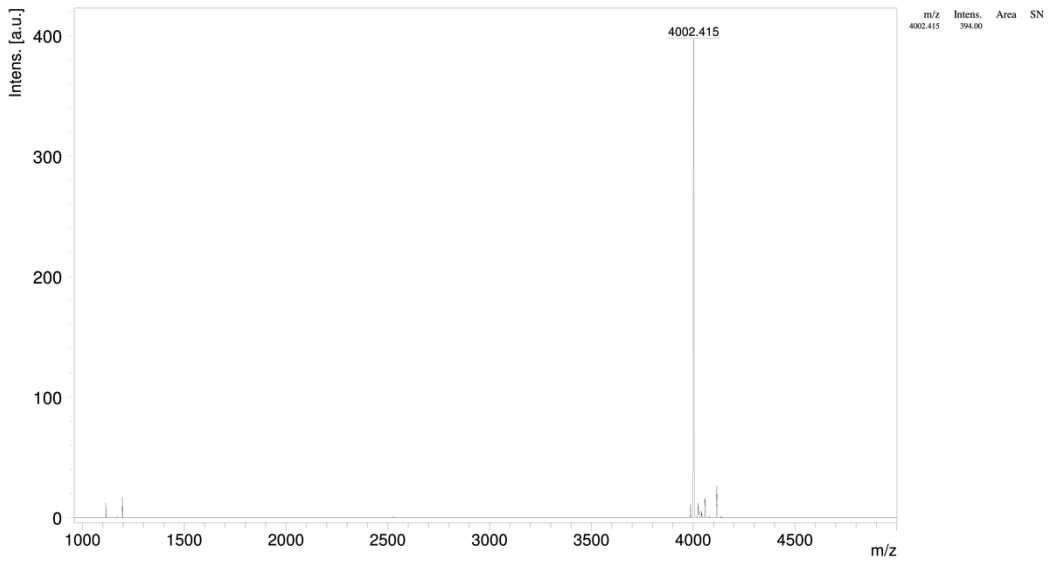

Figure S1. MALDI-TOF-MS spectrum of OAA 1670. [M+H+] calculated: 4007.33. [M+H+] found: 4002.42. Measurements were performed by T. Burghardt (Pharmaceutical Biotechnology, LMU Munich) and M. Grau (Pharmaceutical Biotechnology, LMU Munich).

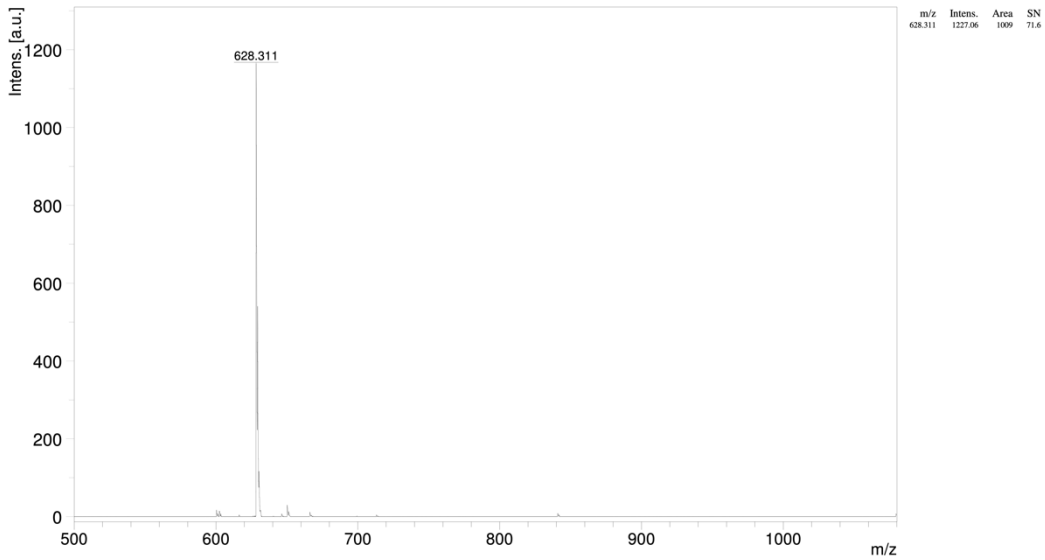

Figure S2. MALDI-TOF-MS spectrum of cRGDfK-N3. [M+H+] calculated: 629.3. [M+H+] found: 628.311. Measurements were performed by T. Burghardt (Pharmaceutical Biotechnology, LMU Munich) and M. Grau (Pharmaceutical Biotechnology, LMU Munich).

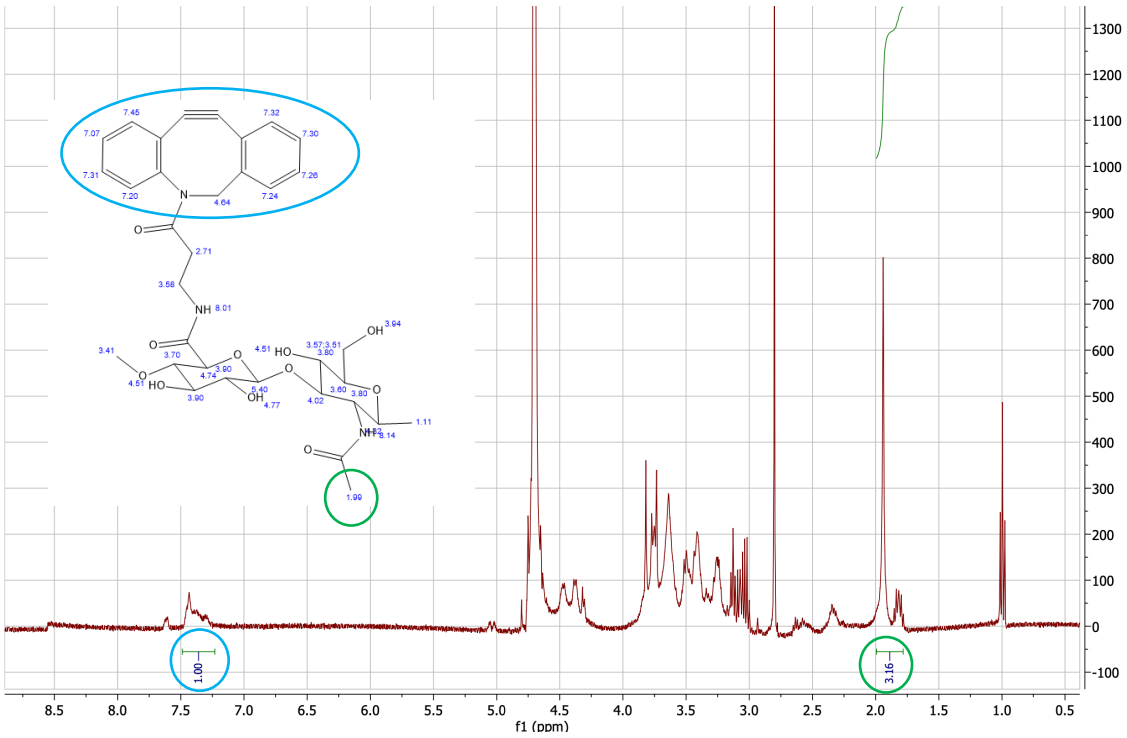

Figure S3. ^{1}H-NMR of HA-DBCO in D_2O for calculation of DBCO/HA ratio. DBCO/HA ratio was calculated based on the integrated DBCO (∂ (ppm) = 7.07-7.45) and CH_3- (∂ (ppm) = 1.99) signals.

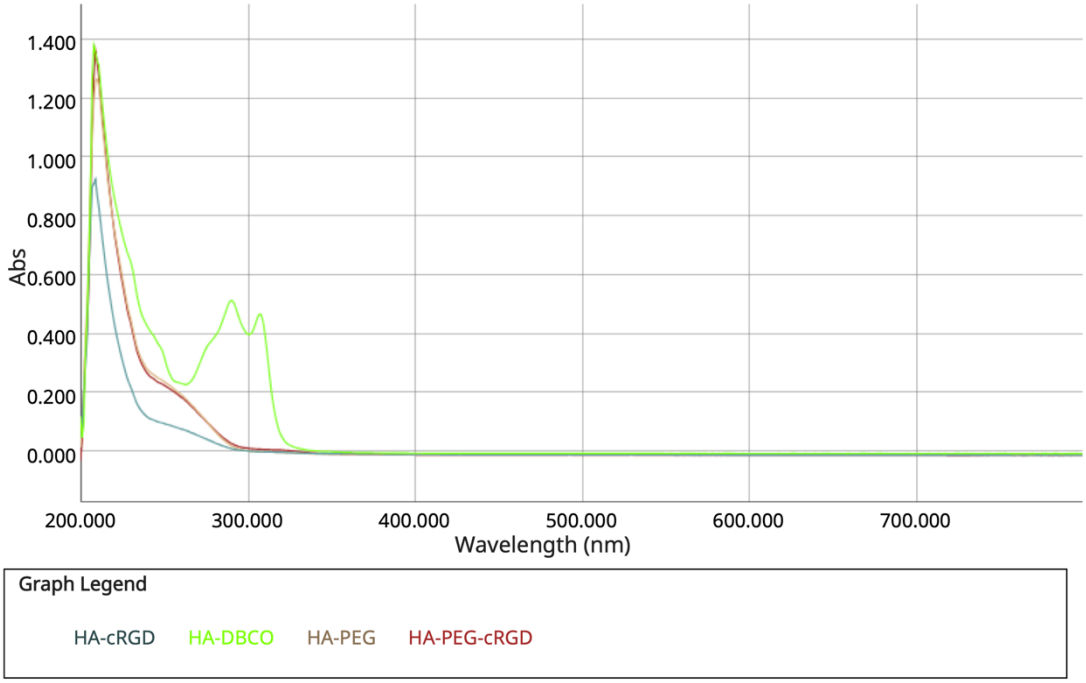

Wavelength scan (2024-05-28 10:23:26 (+02:00))

Sample	308,00 nm
	Abs
HA-PEG-cRGD	0,008
HA-PEG	0,000
HA-cRGD	0,000
HA-DBCO	0,467

Figure S4. UV-Vis wavelength scan of HA-DBCO, HA-cRGD, HA-PEG and HA-PEG-cRGD. The successful click chemistry reaction of HA-DBCO and N_3-cRGD, N_3-PEG, and N_3-PEG-cRGD was investigated by measuring the absorbance at 308 nm. HA-DBCO showed absorbance proportionally to the amount of DBCO groups. Quantitative click chemistry reaction reduced absorbance at 308 nm due to decreased number of free DBCO groups.

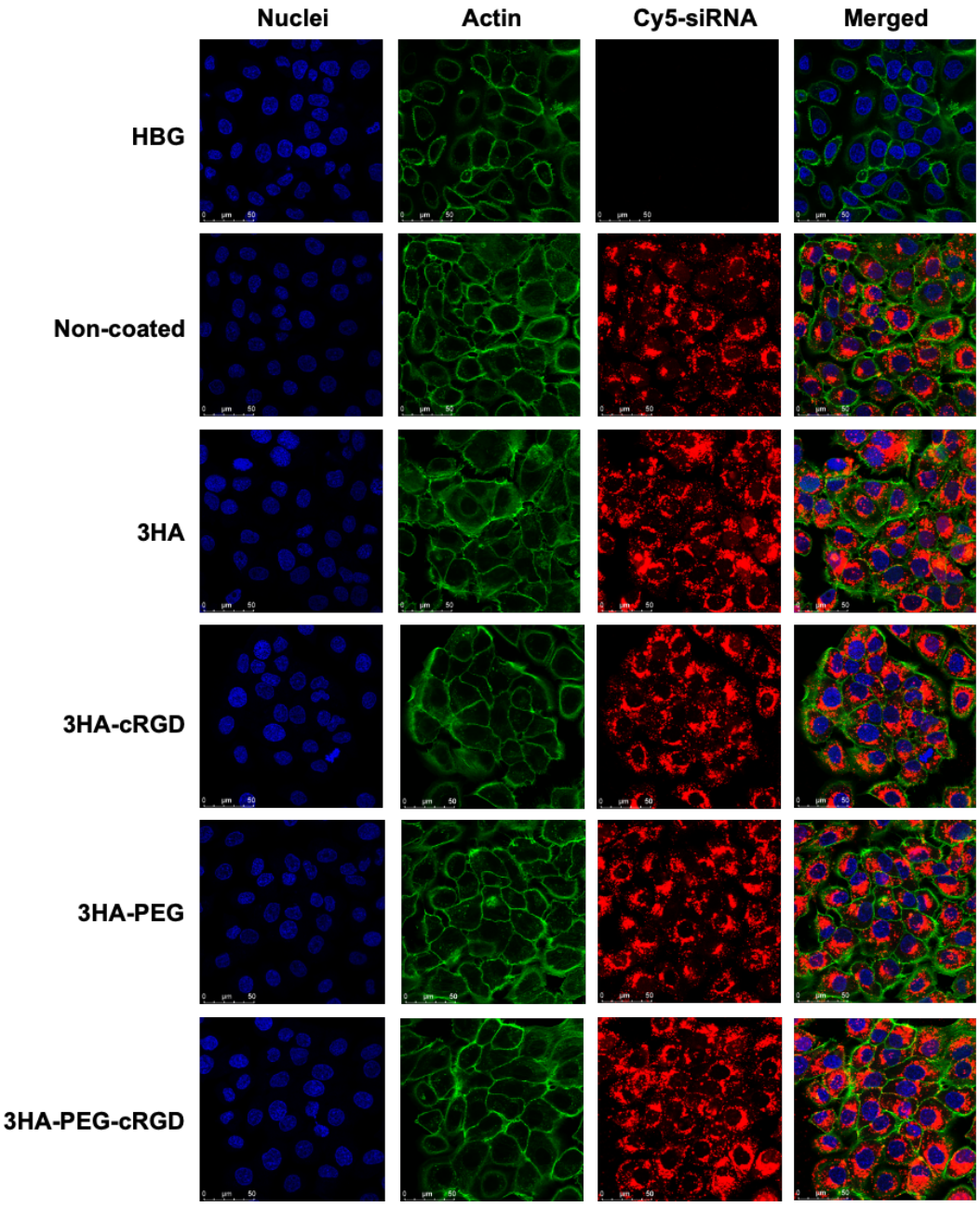

Figure S5. CLSM images of Cy5-labeled HA-coated polyplexes in DU145 cells. Plain and HA-coated polyplexes were prepared containing 20% Cy5-labeled siRNA and transfected in human prostate cancer cells DU145 at a dose of 62.5 ng siRNA (20,000 cells/well). HBG-treated cells were used as a negative control. Cell internalization of Cy5-labeled polyplexes (red) was imaged by M. Höhn (Pharmaceutical Biotechnology, LMU Munich) using confocal laser scanning microscopy (CLSM) after 48 hours incubation on DU145 cells. The actin skeletons were stained with rhodamine-phalloidin (green) and nuclei with DAPI (blue). The scale bar is 50 µm.

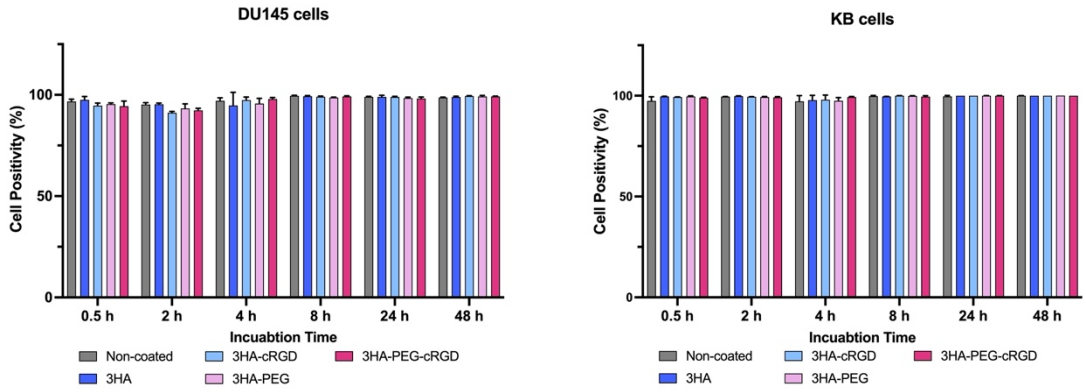

Figure S6. Percentage of Cy5-positive cells. Cell association of non-coated and HA-coated polyplexes containing 20% Cy5-labeled siRNA was evaluated after transfection in the human cervix carcinoma cells KB and human prostate cancer cells DU145 at a dose of 62.5 ng siRNA (5000 cells/well). Cell association was evaluated after different time periods (0.5 h, 2 h, 4 h, 8 h, 24 h, 48 h) via flow cytometry (mean ± SD, n = 3). HBG-treated cells were used as a negative control.

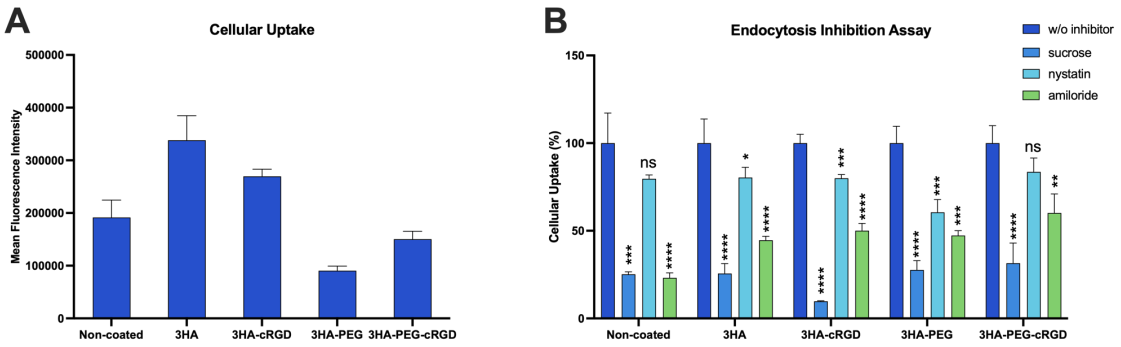

Figure S7. Results from a cellular uptake study (A) and endocytosis inhibition assay (B) with different inhibitors on KB cells. KB cells were treated with polyplexes at a dose of 125 ng siRNA (20% spiked with Cy5-labeled siRNA) and incubated for 4h. Before measuring the MFI of cells with a flow cytometer, the cells were incubated with heparin for 15 min on ice. For the inhibition assay (panel B), cells were treated with inhibitors for 1h at 37°C prior to transfection. The following inhibitors were used: sucrose 450 mM (clathrin-mediated endocytosis); nystatin 54 µM (caveolin-mediated endocytosis); amiloride 1mM (macropinocytosis). Cellular uptake was normalized to cells treated without inhibitor. Statistical significance was determined as: ns $p > 0.05$; * $p \leq 0.05$; ** $p \leq 0.01$; *** $p \leq 0.001$; **** $p \leq 0.0001$ (ordinary one-way ANOVA, Dunnett's multiple comparisons test; GraphPad Prism 10.0.3.

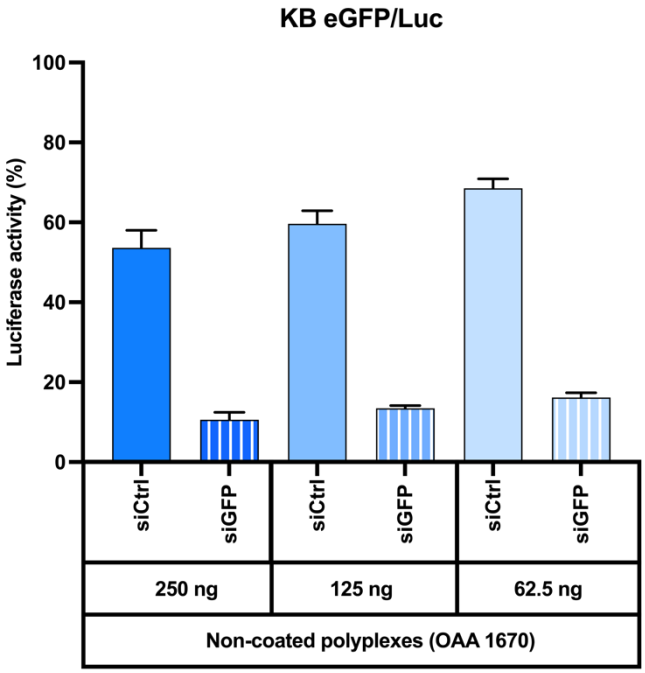

Figure S8. Transfection efficiency of plain 1670-based polyplexes at different doses. KB eGFP/Luc cells which stably express the eGFP/Luc fusion gene were transfected with non-coated 1670-based polyplexes at three doses of siRNA (250 ng, 125 ng, 62.5 ng). Polyplexes were prepared with both siGFP and also siCtrl (for identification of non-specific reduction of gene expression). Luciferase activity of treated cells was measured 48 hours after transfection and was calculated as percentage relative to HBG-treated cells (mean ± SD, n = 3).

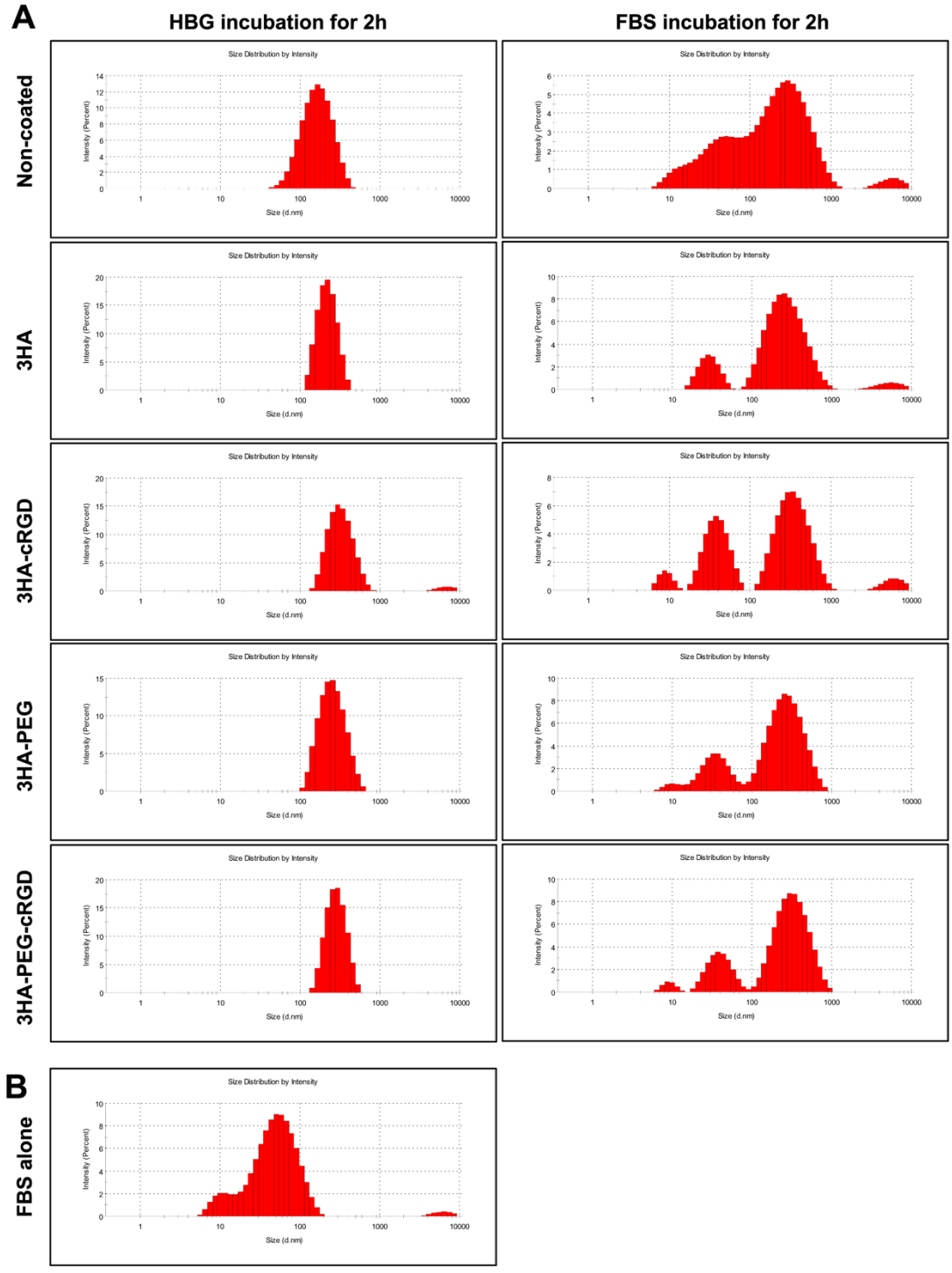

Figure S9. Size distribution of polyplexes after serum dilution. A) Size distribution (size distribution by intensity) of non-coated and HA-coated polyplexes after dilution and incubation in 90% FBS (left) and HBG (right) for 2 h at 37°C, determined by DLS measurements. For size measurement, 20 µl of the FBS- or HBG-diluted polyplexes were further diluted with 60 µl HBG to a final volume of 80 µl and transferred to a folded capillary cell. B) Size measurement of FBS alone, which was treated analogously to diluted polyplex samples before measurement.

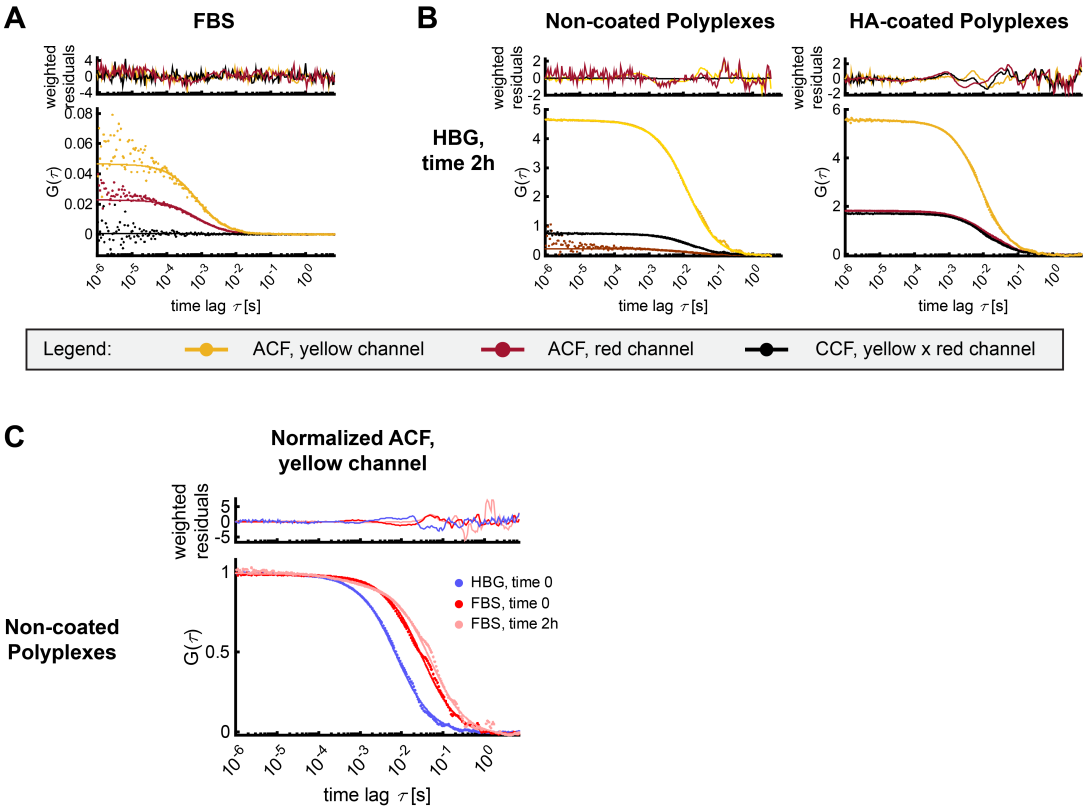

Figure S10. Non-coated and HA-coated polyplex stability in HBG after two hours of incubation at 37 °C with shaking. A) Yellow and red ACFs (in yellow and red respectively) and the CCF (black curve) of pure FBS alone. B) Representative ACFs (yellow and red curves) and CCF (black curve) of polyplexes after two hours of incubation in HBG. The results of the fit, as well as the F(C)CS results for two additional independent replicates, are reported in the supplementary information (Table S6 and S7). The curves are here depicted without normalization, to appreciate the relative CCF amplitude. C) Representative amplitude normalized ACFs of siRNA-ATTO565 complexed into non-coated polyplexes, in HBG and FBS before and after two hours of incubation. Experiment was performed in collaboration with I. Gialdini (Department of Chemistry, LMU Munich).

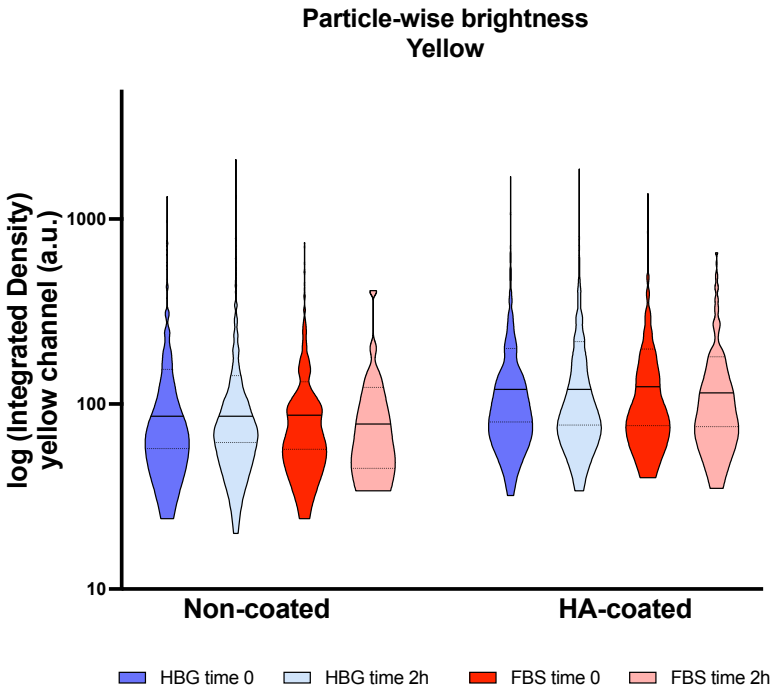

Figure S11. Particle-wise brightness in the yellow channel, corresponding to siRNA-ATTO565 fluorescence in polyplexes. The integrated density of each detected particle was extracted with ImageJ and plotted on a logarithmic scale (see Figure 6). The violin plots were compiled from 3 independent experimental replicates. Experiment was performed in collaboration with I. Gialdini (Department of Chemistry, LMU Munich).

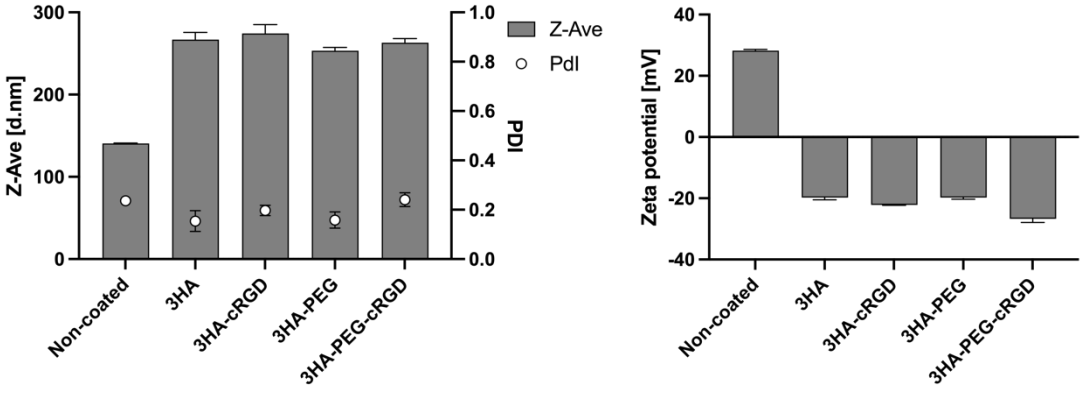

Figure S12. Polyplex size and zeta potential of *in vivo* injected polyplexes. DLS and ELS measurements of injected formulations in the *in vivo* EG5 gene silencing study. The average size, polydispersity and zeta potential of polyplexes prepared at a concentration of 50 µg per 250 µl (200 ng/µl) for the *in vivo* gene silencing experiment were measured just before injections.

5.2 Abbreviations

°C	Degree Celsius
µg, µl	Microgram(s), microliter(s)
AAV	Adeno-associated virus
AChR	Acetylcholin receptor
ANG	Angiopep
ASO	Antisense oligonucleotide
ATTO565, ATTO643	ATTO fluorescent dyes
bEnd.3	Murine brain endothelial cell line
CCD	Cyclic PAsp(-N=C-PEG)-PCys-PAsp(DETA)
cDNA	Complementary DNA
CDP	β-cyclodextrin
CLSM	Confocal Laser Scanning Microscopy
COVID-19	Coronavirus disease 2019
CPP	Cell penetrating peptide
cRGD	Cyclic RGDfK
Ctrl	Control
Cy5, Cy7	Cyanine 5, Cyanine 7
DAB	3-diaminobutyric polypropylenimine
DAPI	4',6-diamidino-2-phenylindole
DCBO	Dibenzocyclooctyne
DCM	Dichloromethane
DGL	Dendrigraft poly-L-lysine
DLS	Dynamic light scattering
DMEM	Dulbecco's Modified Eagle's Medium
DMSO	Dimethyl sulfoxide
DNA	Deoxyribonucleic acid
DoE	Design of Experiments
DU145	Human prostate cancer cell line
ECO	(1-aminoethyl)-iminobis[N-oleicylcysteinyl-1-aminoethyl)propionamide]
EDTA	Ethylenediaminetetraacetic acid
eGFP	Enhanced green fluorescent protein
EGF	Epidermal growth factor
EGFR	Epidermal growth factor receptor
ELS	Electrophoretic light scattering
FBS	Fetal bovine serum
F(C)CS	Fluorescence (Cross-)Correlation Spectroscopy
FDA	U.S. Food and Drug Administration

Fmoc	Fluorenylmethoxycarbonyl
FR	Folate receptor
HA	Hyaluronic acid
HBG	HEPES buffered glucose
HEPES	N-(2-hydroxyethyl)piperazine-N'(2-ethansulfonic acid)
HK	Histidine-lysine
IBFP	3-(2-(2-(vinylsulfonyl)ethylthio)ethyl)quinazoline-2,4(1H,3H)-dione
i.v.	Intravenous
KB	Human cervix carcinoma cell line
kDa	Kilodalton
LA	Lauric acid
LAR buffer	Luciferase Assay Reagent buffer
LfR	Lactoferrin receptor
LGA	lactic-co-glycolic acid
LLHH	Endosomal escape segment
LNP	Lipid nanoparticle
LNP	Nuclear translocation signal sequence of the LIM Kinase 2 protein
LRP-1	Low-density lipoprotein receptor-related protein
Luc	Luciferase
MALDI	Matrix-assisted laser desorption/ionization
MFI	Mean Fluorescent Intensity
mg, ml	Milligram(s), milliliter(s)
miRNA	Micro RNA
mRNA	Messenger RNA
MS	Mass spectrometry
MSLN	Mesothelin
MTBE	Methyl tert-butyl ether
MTT	3-(4,5-dimethylthiazol-2-yl)-2,5-diphenyltetrazolium bromide
MTX	Methotrexate
mV	Millivolt
n	Number of samples
N/P	Carrier nitrogen to nucleic acid phosphate ratio
nm	Nanometer
NRP-1	Neuropilin-1
ns	Not significant
nM	Nanomolar
OAA	Oligoaminoamide
OEI	Oligoethylenimine
ODN	Oligodeoxynucleotides

OleA	Oleic acid
PAMAM	Polyamidoamine
PAsp(DET)	Poly(N′-[N-(2-aminoethyl)-2-aminoethyl]aspartamide)
PBS	Phosphate buffered saline
PCL	Polycaprolactone
PEI	Polyethylenimine
PLI	mPEG-b-PLL-g-(ss-lPEI)
PLL	Poly-L-lysine
pDNA	Plasmid deoxyribonucleic acid
PDP	Pullulan-desoxycholin acid-PEI
PEG	Polyethylene glycol
PFA	Paraformaldehyde
PF14	CPP PepFect 14
Ph.D.	Doctor of Philosophy
PIC	Polyion complex
PMDM	mal-PEGMA-b-PDPA-b-PDMA
polyIC	Polyinosine/cytosine
PPFR	poly(citric acid)-polymine-folic acid-rhodamine
qPCR	Quantitative polymerase chain reaction
RES	Reticuloendothelial system
reTfR	Retroenantio transferrin receptor targeting peptide
RNA	Ribonucleic acid
rpm	Rounds per minute
RT	Room temperature
RVG9R	RVG-arginine nonamer
SD	Standard deviation
siRNA	Small interfering RNA
shRNA	Short hairpin RNA
SMCC	N-succinimidyl-4-(maleimidomethyl)-cyclohexancarboxylate
SPPP	N-succinimidyl-3-(2-pyridyldithio)proprionate
SPSS	Solid phase supported synthesis
Stp	Succinoyltetraethylenepentaamine
TBE	Tris-boric acid EDTA buffer
TCP	Targeted combinatorial polyplex
TFA	Trifluoroacetic acid
TIS	Triisopropylsilane
TfR	Transferrin receptor
TLP	Targeted lipoplexes
TMC-SH	thiolated trimethylated chitosan

TOF	Time of flight
TPN	Tumor-penetrating nanocomplex

6 References

1. Friedmann T and Roblin R. Gene therapy for human genetic disease? Science. 1972. 175(4025): p. 949-55.

2. ASGCT and Citeline, Gene, Cell, + RNA Therapy Landscape Report, Q4 2024 Quarterly Data Report. 2024: https://asgct.org/publications/landscape-report.

3. Fire A, Xu S, Montgomery MK, Kostas SA, Driver SE, and Mello CC. Potent and specific genetic interference by double-stranded RNA in Caenorhabditis elegans. Nature. 1998. 391(6669): p. 806-11.

4. Elbashir SM, Harborth J, Lendeckel W, Yalcin A, Weber K, and Tuschl T. Duplexes of 21-nucleotide RNAs mediate RNA interference in cultured mammalian cells. Nature. 2001. 411(6836): p. 494-498.

5. Rivas FV, Tolia NH, Song JJ, Aragon JP, Liu J, Hannon GJ, and Joshua-Tor L. Purified Argonaute2 and an siRNA form recombinant human RISC. Nat Struct Mol Biol. 2005. 12(4): p. 340-9.

6. Zamore PD, Tuschl T, Sharp PA, and Bartel DP. RNAi: Double-Stranded RNA Directs the ATP-Dependent Cleavage of mRNA at 21 to 23 Nucleotide Intervals. Cell. 2000. 101(1): p. 25-33.

7. Hammond SM, Bernstein E, Beach D, and Hannon GJ. An RNA-directed nuclease mediates post-transcriptional gene silencing in Drosophila cells. Nature. 2000. 404(6775): p. 293-296.

8. Taghdiri M and Mussolino C. Viral and Non-Viral Systems to Deliver Gene Therapeutics to Clinical Targets. Int J Mol Sci. 2024. 25(13).

9. Zhang C and Zhang B. RNA therapeutics: updates and future potential. Sci China Life Sci. 2023. 66(1): p. 12-30.

10. Egli M and Manoharan M. Chemistry, structure and function of approved oligonucleotide therapeutics. Nucleic Acids Res. 2023. 51(6): p. 2529-2573.

11. Adams D, Gonzalez-Duarte A, O'Riordan WD, Yang CC, Ueda M, Kristen AV, Tournev I, Schmidt HH, Coelho T, Berk JL, Lin KP, Vita G, Attarian S, Plante-Bordeneuve V, Mezei MM, Campistol JM, Buades J, Brannagan TH, 3rd, Kim BJ, Oh J, Parman Y, Sekijima Y, Hawkins PN, Solomon SD, Polydefkis M, Dyck PJ, Gandhi PJ, Goyal S, Chen J, Strahs AL, Nochur SV, Sweetser MT, Garg PP, Vaishnaw AK, Gollob JA, and Suhr OB. Patisiran, an RNAi Therapeutic, for Hereditary Transthyretin Amyloidosis. N Engl J Med. 2018. 379(1): p. 11-21.

12. Polack FP, Thomas SJ, Kitchin N, Absalon J, Gurtman A, Lockhart S, Perez JL, Marc GP, Moreira ED, Zerbini C, Bailey R, Swanson KA, Roychoudhury S, Koury K, Li P, Kalina WV, Cooper D, Frenck RW, Hammitt LL, Türeci Ö, Nell H, Schaefer A, Ünal S, Tresnan DB, Mather S, Dormitzer PR, Şahin U, Jansen KU, and Gruber WC. Safety and Efficacy of the BNT162b2 mRNA Covid-19 Vaccine. New England Journal of Medicine. 2020. 383(27): p. 2603-2615.

13. Baden LR, Sahly HME, Essink B, Kotloff K, Frey S, Novak R, Diemert D, Spector SA, Rouphael N, Creech CB, McGettigan J, Khetan S, Segall N, Solis J, Brosz A, Fierro C, Schwartz H, Neuzil K, Corey L, Gilbert P, Janes H, Follmann D, Marovich M, Mascola J, Polakowski L, Ledgerwood J, Graham BS, Bennett H, Pajon R, Knightly C, Leav B, Deng W, Zhou H, Han S, Ivarsson M, Miller J, and Zaks T. Efficacy and Safety of the mRNA-1273 SARS-CoV-2 Vaccine. New England Journal of Medicine. 2021. 384(5): p. 403-416.

14. Edouard Mathieu HR, Lucas Rodés-Guirao, Cameron Appel, Daniel Gavrilov, Charlie Giattino, Joe Hasell, Bobbie Macdonald, Saloni Dattani, Diana Beltekian, Esteban Ortiz-Ospina and Max Roser Coronavirus (COVID-19) Vaccinations. 2020; Available from: OurWorldinData.org/covid-vaccinations.

15. Ibba ML, Ciccone G, Esposito CL, Catuogno S, and Giangrande PH. Advances in mRNA non-viral delivery approaches. Advanced Drug Delivery Reviews. 2021. 177: p. 113930.

16. Ferhan AR, Park S, Park H, Tae H, Jackman JA, and Cho N-J. Lipid Nanoparticle Technologies for Nucleic Acid Delivery: A Nanoarchitectonics Perspective. Advanced Functional Materials. 2022. 32(37): p. 2203669.

17. Mendes BB, Conniot J, Avital A, Yao D, Jiang X, Zhou X, Sharf-Pauker N, Xiao Y, Adir O, Liang H, Shi J, Schroeder A, and Conde J. Nanodelivery of nucleic acids. Nature Reviews Methods Primers. 2022. 2(1): p. 24.

18. Raemdonck K, Naeye B, Buyens K, Vandenbroucke RE, Høgset A, Demeester J, and De Smedt SC. Biodegradable Dextran Nanogels for RNA Interference: Focusing on Endosomal Escape and Intracellular siRNA Delivery. Advanced Functional Materials. 2009. 19(9): p. 1406-1415.

19. Lachelt U and Wagner E. Nucleic Acid Therapeutics Using Polyplexes: A Journey of 50 Years (and Beyond). Chem Rev. 2015. 115(19): p. 11043-78.

20. Felgner PL BY, Behr JP, Cheng SH, Cullis P, Huang L, Jessee JA, Seymour L, Szoka F, Thierry AR, Wagner E, Wu G. Nomenclature for Synthetic Gene Delivery Systems. Hum Gene Ther. 1997(8(5)): p. 511.

21. Wu GY and Wu CH. Receptor-mediated in vitro gene transformation by a soluble DNA carrier system. Journal of Biological Chemistry. 1987. 262(10): p. 4429-4432.

22. Wagner E, Ogris, M., & Zauner, W. Polylysine-based transfection systems utilizing receptor-mediated delivery. Advanced drug delivery reviews. 1998. 30(1-3): p. 97–113.

23. Wagner E, Zenke, M. Cotten, M., Beug, H., Birnstiel, M. L. Transferrin-polycation conjugates as carriers for DNA uptake into cells. Proceedings of the National Academy of Sciences. 1990. 87: p. 3410-3414.

24. Boussif O, Lezoualc'h F, Zanta MA, Mergny MD, Scherman D, Demeneix B, and Behr JP. A versatile vector for gene and oligonucleotide transfer into cells in culture and in vivo: polyethylenimine. Proc.Natl.Acad.Sci.U.S.A. 1995. 92(16): p. 7297-7301.

25. Wightman L, Kircheis R, Rossler V, Carotta S, Ruzicka R, Kursa M, and Wagner E. Different behavior of branched and linear polyethylenimine for gene delivery in vitro and in vivo. J Gene Med. 2001. 3(4): p. 362-72.

26. Ogris M, Brunner S, Schuller S, Kircheis R, and Wagner E. PEGylated DNA/Transferrin-PEI Complexes: Reduced Interaction with Blood Components, Extended Circulation in Blood and Potential for Systemic Gene Delivery. Gene Ther. 1999. 6(4): p. 595-605.

27. Schmohl KA, Gupta A, Grunwald GK, Trajkovic-Arsic M, Klutz K, Braren R, Schwaiger M, Nelson PJ, Ogris M, Wagner E, Siveke JT, and Spitzweg C. Imaging and targeted therapy of pancreatic ductal adenocarcinoma using the theranostic sodium iodide symporter (NIS) gene. Oncotarget. 2017. 8(20): p. 33393-33404.

28. Uchida H, Miyata K, Oba M, Ishii T, Suma T, Itaka K, Nishiyama N, and Kataoka K. Odd-even effect of repeating aminoethylene units in the side chain of N-substituted polyaspartamides on gene transfection profiles. J Am Chem Soc. 2011. 133(39): p. 15524-32.

29. Verbaan FJ, Oussoren C, Snel CJ, Crommelin DJ, Hennink WE, and Storm G. Steric stabilization of poly(2-(dimethylamino)ethyl methacrylate)-based polyplexes mediates prolonged circulation and tumor targeting in mice. J Gene Med. 2004. 6(1): p. 64-75.

30. Novo L, Rizzo LY, Golombek SK, Dakwar GR, Lou B, Remaut K, Mastrobattista E, van Nostrum CF, Jahnen-Dechent W, Kiessling F, Braeckmans K, Lammers T, and Hennink WE. Decationized polyplexes as stable and safe carrier systems for improved biodistribution in systemic gene therapy. J Control Release. 2014. 195: p. 162-175.

31. Cheng Y, Yumul RC, and Pun SH. Virus-Inspired Polymer for Efficient In Vitro and In Vivo Gene Delivery. Angew Chem Int Ed Engl. 2016. 55(39): p. 12013-7.

32. Dufes C, Uchegbu IF, and Schatzlein AG. Dendrimers in gene delivery. Adv Drug Deliv Rev. 2005. 57(15): p. 2177-202.

33. Chen C, Posocco P, Liu X, Cheng Q, Laurini E, Zhou J, Liu C, Wang Y, Tang J, Col VD, Yu T, Giorgio S, Fermeglia M, Qu F, Liang Z, Rossi JJ, Liu M, Rocchi P, Pricl S, and Peng L. Mastering Dendrimer Self-Assembly for Efficient siRNA Delivery: From Conceptual Design to In Vivo Efficient Gene Silencing. Small. 2016. 12(27): p. 3667-76.

34. Wang K, Hu Q, Zhu W, Zhao M, Ping Y, and Tang G. Structure-Invertible Nanoparticles for Triggered Co-Delivery of Nucleic Acids and Hydrophobic Drugs for Combination Cancer Therapy. Advanced Functional Materials. 2015. 25(22): p. 3380-3392.

35. Schaffert D, Troiber C, Salcher EE, Frohlich T, Martin I, Badgujar N, Dohmen C, Edinger D, Klager R, Maiwald G, Farkasova K, Seeber S, Jahn-Hofmann K, Hadwiger P, and Wagner E. Solid-Phase Synthesis of Sequence-Defined T-, i-, and U-Shape Polymers for pDNA and siRNA Delivery. Angew Chem Int Ed Engl. 2011. 50(38): p. 8986-9.

36. Schaffert D, Naresh B, and Wagner E. Novel Fmoc-Polyamino Acids for Solid-Phase Synthesis of Defined Polyamidoamines. Organic Letters. 2011. 13 (7): p. 1586-1589.

37. Urnauer S, Morys S, Krhac Levacic A, Muller AM, Schug C, Schmohl KA, Schwenk N, Zach C, Carlsen J, Bartenstein P, Wagner E, and Spitzweg C. Sequence-defined cMET/HGFR-targeted Polymers as Gene Delivery Vehicles for the Theranostic Sodium Iodide Symporter (NIS) Gene. Mol Ther. 2016. 24(8): p. 1395-404.

38. Levacic AK, Morys S, Kempter S, Lachelt U, and Wagner E. Minicircle Versus Plasmid DNA Delivery by Receptor-Targeted Polyplexes. Hum Gene Ther. 2017. 28(10): p. 862-874.

39. Frohlich T, Edinger D, Klager R, Troiber C, Salcher E, Badgujar N, Martin I, Schaffert D, Cengizeroglu A, Hadwiger P, Vornlocher HP, and Wagner E. Structure-activity relationships of siRNA carriers based on sequence-defined oligo (ethane amino) amides. J Control Release. 2012. 160(3): p. 532-41.

40. Luo J, Schmaus J, Cui M, Hörterer E, Wilk U, Höhn M, Däther M, Berger S, Benli-Hoppe T, Peng L, and Wagner E. Hyaluronate siRNA Nanoparticles with Positive Charge Display Rapid Attachment to Tumor Endothelium and Penetration into Tumors. Journal of Controlled Release. 2021. 329: p. 919-933.

41. Lächelt U, Kos P, Mickler FM, Herrmann A, Salcher EE, Rödl W, Badgujar N, Bräuchle C, and Wagner E. Fine-tuning of proton sponges by precise diaminoethanes and histidines in pDNA polyplexes. Nanomedicine: Nanotechnology, Biology and Medicine. 2014. 10(1): p. 35-44.

42. Troiber C, Edinger D, Kos P, Schreiner L, Kläger R, Herrmann A, and Wagner E. Stabilizing Effect of Tyrosine Trimers on pDNA and siRNA Polyplexes. Biomaterials. 2013. 34(5): p. 1624-1633.

43. Leng Q, Scaria P, Zhu J, Ambulos N, Campbell P, and Mixson AJ. Highly Branched HK Peptides are Effective Carriers of siRNA. J Gene Med. 2005. 7(7): p. 977-986.

44. Stevenson M, Ramos-Perez V, Singh S, Soliman M, Preece JA, Briggs SS, Read ML, and Seymour LW. Delivery of siRNA Mediated by Histidine-Containing Reducible Polycations. J Control Release. 2008. 130(1): p. 46-56.

45. Dellian M, Yuan F, Trubetskoy VS, Torchilin VP, and Jain RK. Vascular permeability in a human tumour xenograft: molecular charge dependence. Br J Cancer. 2000. 82(9): p. 1513-8.

46. Thurston G, McLean, J. W., Rizen, M., Baluk, P., Haskell, A., Murphy, T. J., Hanahan, D., & McDonald, D. M. . Cationic liposomes target angiogenic endothelial cells in tumors and chronic inflammation in mice. he Journal of clinical investigation. 1998: p. 1401–1413.

47. Campbell RB, Fukumura D, Brown EB, Mazzola LM, Izumi Y, Jain RK, Torchilin VP, and Munn LL. Cationic charge determines the distribution of liposomes between the vascular and extravascular compartments of tumors. Cancer Res. 2002. 62(23): p. 6831-6.

48. Kos P, Lachelt U, Herrmann A, Mickler FM, Doblinger M, He D, Krhac Levacic A, Morys S, Brauchle C, and Wagner E. Histidine-rich stabilized polyplexes for cMet-directed tumor-targeted gene transfer. Nanoscale. 2015. 7(12): p. 5350-62.

49. Grau M and Wagner E. Strategies and mechanisms for endosomal escape of therapeutic nucleic acids. Curr Opin Chem Biol. 2024. 81: p. 102506.

50. Gao H, Jia H, Dong J, Yang X, Li H, and Ouyang D. Integrated in silico formulation design of self-emulsifying drug delivery systems. Acta Pharmaceutica Sinica B. 2021. 11(11): p. 3585-3594.

51. Loecher A, Bruyns-Haylett M, Ballester PJ, Borros S, and Oliva N. A machine learning approach to predict cellular uptake of pBAE polyplexes. Biomater Sci. 2023. 11(17): p. 5797-5808.

52. S NP, Colombo P, Colombo G, and D MR. Design of experiments (DoE) in pharmaceutical development. Drug Dev Ind Pharm. 2017. 43(6): p. 889-901.

53. Eurostat, Causes of death statistics. 2024; Available from: https://ec.europa.eu/eurostat/statistics-explained/index.php?title=Causes_of_death_statistics#Major_causes_of_death_in_the_EU_in_2021.

54. Kochanek KDM, Sherry L.;Xu, Jiaquan;Arias, Elizabeth;. Mortality in the United States, 2022. NCHS Data Briefs. 2022.

55. Think globally about cancer. Nat Med. 2019. 25(3): p. 351.

56. Ferlay J, Colombet M, Soerjomataram I, Mathers C, Parkin DM, Pineros M, Znaor A, and Bray F. Estimating the global cancer incidence and mortality in 2018: GLOBOCAN sources and methods. Int J Cancer. 2019. 144(8): p. 1941-1953.

57. Hall A, Lachelt U, Bartek J, Wagner E, and Moghimi SM. Polyplex Evolution: Understanding Biology, Optimizing Performance. Mol Ther. 2017. 25(7): p. 1476-1490.

58. Osada K, Christie RJ, and Kataoka K. Polymeric micelles from poly(ethylene glycol)-poly(amino acid) block copolymer for drug and gene delivery. J R Soc Interface. 2009. 6 Suppl 3(Suppl 3): p. S325-39.

59. Kircheis R, Wightman L, Kursa M, Smrekar B, Ostermann E, and Wagner E. Surface-shielded polycation-based systems targeting reporter and therapeutic genes to distant tumors Review Article. 2004.

60. Lieleg O, Baumgärtel RM, and Bausch AR. Selective filtering of particles by the extracellular matrix: an electrostatic bandpass. Biophys J. 2009. 97(6): p. 1569-77.

61. Cabral H, Matsumoto Y, Mizuno K, Chen Q, Murakami M, Kimura M, Terada Y, Kano MR, Miyazono K, Uesaka M, Nishiyama N, and Kataoka K. Accumulation of sub-100 nm polymeric micelles in poorly permeable tumours depends on size. Nature Nanotechnology. 2011. 6(12): p. 815-823.

62. Plank C, Mechtler K, Szoka F, and Wagner E. Activation of the Complement System by Synthetic DNA Complexes: A Potential Barrier for Intravenous Gene Delivery. Human gene therapy. 1996. 7: p. 1437-46.

63. Uchida S, Itaka K, Chen Q, Osada K, Ishii T, Shibata MA, Harada-Shiba M, and Kataoka K. PEGylated polyplex with optimized PEG shielding enhances gene introduction in lungs by minimizing inflammatory responses. Mol Ther. 2012. 20(6): p. 1196-203.

64. Uchida S, Lau CYJ, Oba M, and Miyata K. Polyplex designs for improving the stability and safety of RNA therapeutics. Advanced Drug Delivery Reviews. 2023. 199: p. 114972.

65. Luo J, Schmaus J, Cui M, Horterer E, Wilk U, Hohn M, Dather M, Berger S, Benli-Hoppe T, Peng L, and Wagner E. Hyaluronate siRNA nanoparticles with positive charge display rapid attachment to tumor endothelium and penetration into tumors. J Control Release. 2020.

66. Dillinger AE, Guter M, Froemel F, Weber GR, Perkumas K, Stamer WD, Ohlmann A, Fuchshofer R, and Breunig M. Intracameral Delivery of Layer-by-Layer Coated siRNA Nanoparticles for Glaucoma Therapy. Small. 2018. 14(50): p. e1803239.

67. Andretto V, Repellin M, Pujol M, Almouazen E, Sidi-Boumedine J, Granjon T, Zhang H, Remaut K, Jordheim LP, Briancon S, Keil IS, Vascotto F, Walzer KC, Sahin U, Haas H, Kryza D, and Lollo G. Hybrid Core-Shell Particles for mRNA Systemic Delivery. J Control Release. 2023 Jan(353): p. 1037-1049.

68. Nabar N, Dacoba TG, Covarrubias G, Romero-Cruz D, and Hammond PT. Electrostatic adsorption of polyanions onto lipid nanoparticles controls uptake, trafficking, and transfection of RNA and DNA therapies. Proc Natl Acad Sci U S A. 2024. 121(11): p. e2307809121.

69. Correa S, Boehnke N, Barberio AE, Deiss-Yehiely E, Shi A, Oberlton B, Smith SG, Zervantonakis I, Dreaden EC, and Hammond PT. Tuning Nanoparticle Interactions with Ovarian Cancer through Layer-by-Layer Modification of Surface Chemistry. ACS Nano. 2020. 14(2): p. 2224-2237.

70. Jain RK. Transport of molecules across tumor vasculature. Cancer Metastasis Rev. 1987: p. 559-593.

71. Hansen AE, Petersen AL, Henriksen JR, Boerresen B, Rasmussen P, Elema DR, af Rosenschold PM, Kristensen AT, Kjaer A, and Andresen TL. Positron Emission Tomography Based Elucidation of the Enhanced Permeability and Retention Effect in Dogs with Cancer Using Copper-64 Liposomes. ACS Nano. 2015. 9(7): p. 6985-95.

72. Yuan F, Dellian, M., Fukumura, D., Leunig, M., Berk, D. A., Torchilin, V. P., & Jain, R. K. . Vascular permeability in a human tumor xenograft: molecular size dependence and cutoff size. Cancer research. 1995. 55: p. 3752–3756.

73. Roberts WG and Palade GE. Neovasculature induced by vascular endothelial growth factor is fenestrated. Cancer Res. 1997. 57(4): p. 765-72.

74. Matsumura Y and Maeda H. A New Concept for Macromolecular Therapeutics in Cancer Chemotherapy: Mechanism of Tumoritropic Accumulation of Proteins and the Antitumor Agent Smancs. Cancer Research. 1986. 46(12 Part 1): p. 6387-6392.

75. Benli-Hoppe T, Gol Ozturk S, Ozturk O, Berger S, Wagner E, and Yazdi M. Transferrin Receptor Targeted Polyplexes Completely Comprised of Sequence-Defined Components. Macromol Rapid Commun. 2021: p. e2100602.

76. Yazdi M, Pohmerer J, Hasanzadeh Kafshgari M, Seidl J, Grau M, Hohn M, Vetter V, Hoch CC, Wollenberg B, Multhoff G, Bashiri Dezfouli A, and Wagner E. In Vivo Endothelial Cell Gene Silencing by siRNA-LNPs Tuned with Lipoamino Bundle Chemical and Ligand Targeting. Small. 2024: p. e2400643.

77. Ramishetti S, Kedmi R, Goldsmith M, Leonard F, Sprague AG, Godin B, Gozin M, Cullis PR, Dykxhoorn DM, and Peer D. Systemic Gene Silencing in Primary T Lymphocytes Using Targeted Lipid Nanoparticles. ACS Nano. 2015. 9(7): p. 6706-16.

78. Buschle M, Cotten M, Kirlappos H, Mechtler K, Schaffner G, Zauner W, Birnstiel ML, and Wagner E. Receptor-mediated gene transfer into human T lymphocytes via binding of DNA/CD3 antibody particles to the CD3 T cell receptor complex. Hum Gene Ther. 1995. 6(6): p. 753-61.

79. Zenke M, Steinlein P, Wagner E, Cotten M, Beug H, and Birnstiel ML. Receptor-mediated endocytosis of transferrin-polycation conjugates: an efficient way to introduce DNA into hematopoietic cells. Proc Natl Acad Sci U S A. 1990. 87(10): p. 3655-9.

80. Anraku Y, Kuwahara H, Fukusato Y, Mizoguchi A, Ishii T, Nitta K, Matsumoto Y, Toh K, Miyata K, Uchida S, Nishina K, Osada K, Itaka K, Nishiyama N, Mizusawa H, Yamasoba T, Yokota T, and Kataoka K. Glycaemic control boosts glucosylated nanocarrier crossing the BBB into the brain. Nature Communications. 2017. 8(1): p. 1001.

81. Plank C, Zatloukal K, Cotten M, Mechtler K, and Wagner E. Gene transfer into hepatocytes using asialoglycoprotein receptor mediated endocytosis of DNA complexed with an artificial tetra-antennary galactose ligand. Bioconjug Chem. 1992. 3(6): p. 533-9.

82. Uehara K, Harumoto T, Makino A, Koda Y, Iwano J, Suzuki Y, Tanigawa M, Iwai H, Asano K, Kurihara K, Hamaguchi A, Kodaira H, Atsumi T, Yamada Y, and Tomizuka K. Targeted delivery to macrophages and dendritic cells by chemically modified mannose ligand-conjugated siRNA. Nucleic Acids Res. 2022. 50(9): p. 4840-4859.

83. Berger S, Krhac Levacic A, Horterer E, Wilk U, Benli-Hoppe T, Wang Y, Ozturk O, Luo J, and Wagner E. Optimizing pDNA Lipo-polyplexes: A Balancing Act between Stability and Cargo Release. Biomacromolecules. 2021. 22(3): p. 1282-1296.

84. Berger S, Berger M, Bantz C, Maskos M, and Wagner E. Performance of nanoparticles for biomedical applications: The in vitro/in vivo discrepancy. Biophysics Reviews. 2022. 3(1): p. 011303.

85. Metwally AA, Nayel AA, and Hathout RM. In silico prediction of siRNA ionizable-lipid nanoparticles In vivo efficacy: Machine learning modeling based on formulation and molecular descriptors. Front Mol Biosci. 2022. 9: p. 1042720.

86. Vetter VC and Wagner E. Targeting Nucleic Acid-Based Therapeutics to Tumors: Challenges and Strategies for Polyplexes. J Control Release. 2022. 346: p. 110-135.

87. American Society of Gene + Cell Therapy; Gene, Cell & RNA Therapy Landscape Report, https://asgct.org/research/landscape-report

88. Nabel GJ, Nabel EG, Yang ZY, Fox BA, Plautz GE, Gao X, Huang L, Shu S, Gordon D, and Chang AE. Direct gene transfer with DNA-liposome complexes in melanoma: expression, biologic activity, and lack of toxicity in humans. Proc Natl Acad Sci U S A. 1993. 90(23): p. 11307-11.

89. Zuckerman JE and Davis ME. Clinical experiences with systemically administered siRNA-based therapeutics in cancer. Nat Rev Drug Discov. 2015. 14(12): p. 843-56.

90. Kim HJ, Kim A, Miyata K, and Kataoka K. Recent Progress in Development of siRNA Delivery Vehicles for Cancer Therapy. Adv Drug Deliv Rev. 2016. 104: p. 61-77.

91. Mainini F and Eccles MR. Lipid and Polymer-Based Nanoparticle siRNA Delivery Systems for Cancer Therapy. Molecules (Basel, Switzerland). 2020. 25(11): p. 2692.

92. Zhang MM, Bahal R, Rasmussen TP, Manautou JE, and Zhong XB. The growth of siRNA-based therapeutics: Updated clinical studies. Biochem Pharmacol. 2021. 189: p. 114432.

93. Debacker AJ, Voutila J, Catley M, Blakey D, and Habib N. Delivery of Oligonucleotides to the Liver with GalNAc: From Research to Registered Therapeutic Drug. Mol Ther. 2020. 28(8): p. 1759-1771.

94. Kormann MS, Hasenpusch G, Aneja MK, Nica G, Flemmer AW, Herber-Jonat S, Huppmann M, Mays LE, Illenyi M, Schams A, Griese M, Bittmann I, Handgretinger R, Hartl D, Rosenecker J, and Rudolph C. Expression of therapeutic proteins after delivery of chemically modified mRNA in mice. Nat Biotechnol. 2011. 29(2): p. 154-7.

95. Kowalski PS, Rudra A, Miao L, and Anderson DG. Delivering the Messenger: Advances in Technologies for Therapeutic mRNA Delivery. Mol Ther. 2019. 27(4): p. 710-728.

96. Haabeth OAW, Blake TR, McKinlay CJ, Tveita AA, Sallets A, Waymouth RM, Wender PA, and Levy R. Local Delivery of Ox40l, Cd80, and Cd86 mRNA Kindles Global Anticancer Immunity. Cancer Res. 2019. 79(7): p. 1624-1634.

97. Gillmore JD, Gane E, Taubel J, Kao J, Fontana M, Maitland ML, Seitzer J, O'Connell D, Walsh KR, Wood K, Phillips J, Xu Y, Amaral A, Boyd AP, Cehelsky JE, McKee MD, Schiermeier A, Harari O, Murphy A, Kyratsous CA, Zambrowicz B, Soltys R, Gutstein DE, Leonard J, Sepp-Lorenzino L, and

Lebwohl D. CRISPR-Cas9 In Vivo Gene Editing for Transthyretin Amyloidosis. N Engl J Med. 2021. 385(6): p. 493-502.

98. Song X, Liu C, Wang N, Huang H, He S, Gong C, and Wei Y. Delivery of CRISPR/Cas systems for cancer gene therapy and immunotherapy. Adv Drug Deliv Rev. 2021. 168: p. 158-180.

99. Lin Y, Wagner E, and Lächelt U. Non-viral delivery of the CRISPR/Cas system: DNA versus RNA versus RNP. Biomater Sci. 2022.

100. Schoenmaker L, Witzigmann D, Kulkarni JA, Verbeke R, Kersten G, Jiskoot W, and Crommelin DJA. mRNA-lipid nanoparticle COVID-19 vaccines: Structure and stability. Int J Pharm. 2021. 601: p. 120586.

101. Sahin U, Muik A, Vogler I, Derhovanessian E, Kranz LM, Vormehr M, Quandt J, Bidmon N, Ulges A, Baum A, Pascal KE, Maurus D, Brachtendorf S, Lörks V, Sikorski J, Koch P, Hilker R, Becker D, Eller AK, Grützner J, Tonigold M, Boesler C, Rosenbaum C, Heesen L, Kühnle MC, Poran A, Dong JZ, Luxemburger U, Kemmer-Brück A, Langer D, Bexon M, Bolte S, Palanche T, Schultz A, Baumann S, Mahiny AJ, Boros G, Reinholz J, Szabó GT, Karikó K, Shi PY, Fontes-Garfias C, Perez JL, Cutler M, Cooper D, Kyratsous CA, Dormitzer PR, Jansen KU, and Türeci Ö. BNT162b2 vaccine induces neutralizing antibodies and poly-specific T cells in humans. Nature. 2021. 595(7868): p. 572-577.

102. Baden LR, El Sahly HM, Essink B, Kotloff K, Frey S, Novak R, Diemert D, Spector SA, Rouphael N, Creech CB, McGettigan J, Khetan S, Segall N, Solis J, Brosz A, Fierro C, Schwartz H, Neuzil K, Corey L, Gilbert P, Janes H, Follmann D, Marovich M, Mascola J, Polakowski L, Ledgerwood J, Graham BS, Bennett H, Pajon R, Knightly C, Leav B, Deng W, Zhou H, Han S, Ivarsson M, Miller J, and Zaks T. Efficacy and Safety of the mRNA-1273 SARS-CoV-2 Vaccine. N Engl J Med. 2021. 384(5): p. 403-416.

103. Kranz LM, Diken M, Haas H, Kreiter S, Loquai C, Reuter KC, Meng M, Fritz D, Vascotto F, Hefesha H, Grunwitz C, Vormehr M, Husemann Y, Selmi A, Kuhn AN, Buck J, Derhovanessian E, Rae R, Attig S, Diekmann J, Jabulowsky RA, Heesch S, Hassel J, Langguth P, Grabbe S, Huber C, Tureci O, and Sahin U. Systemic RNA delivery to dendritic cells exploits antiviral defence for cancer immunotherapy. Nature. 2016. 534(7607): p. 396-401.

104. Diken M, Kranz LM, Kreiter S, and Sahin U. mRNA: A Versatile Molecule for Cancer Vaccines. Curr Issues Mol Biol. 2017. 22: p. 113-128.

105. Felgner PL, Gadek TR, Holm M, Roman R, Chan HW, Wenz M, Northrop JP, Ringold GM, and Danielsen M. Lipofection: A highly efficient, lipid mediated DNA-transfection procedure. Proc Natl Acad Sci U S A. 1987. 84: p. 7413-7417.

106. Behr JP, Demeneix B, Loeffler JP, and Perez-Mutul J. Efficient gene transfer into mammalian primary endocrine cells with lipopolyamine-coated DNA 6. Proc.Natl.Acad.Sci.U.S.A. 1989. 86(18): p. 6982-6986.

107. Radler JO, Koltover I, Salditt T, and Safinya CR. Structure of DNA-cationic liposome complexes: DNA intercalation in multilamellar membranes in distinct interhelical packing regimes. Science. 1997. 275: p. 810-814.

108. Wang Y, Miao L, Satterlee A, and Huang L. Delivery of oligonucleotides with lipid nanoparticles. Adv Drug Deliv Rev. 2015. 87: p. 68-80.

109. Li S and Huang L. In vivo gene transfer via intravenous administration of cationic lipid-protamine-DNA (LPD) complexes 39. Gene Ther. 1997. 4(9): p. 891-900.

110. Pichon C, Billiet L, and Midoux P. Chemical vectors for gene delivery: uptake and intracellular trafficking. Curr Opin Biotechnol. 2010. 21(5): p. 640-5.

111. Cullis PR and Hope MJ. Lipid Nanoparticle Systems for Enabling Gene Therapies. Mol Ther. 2017. 25(7): p. 1467-1475.

112. Pack DW, Hoffman AS, Pun S, and Stayton PS. Design and development of polymers for gene delivery. Nat Rev Drug Discov. 2005. 4(7): p. 581-93.

113. Schaffert D and Wagner E. Gene therapy progress and prospects: synthetic polymer-based systems. Gene Therapy. 2008. 15(16): p. 1131-1138.

114. Cabral H, Miyata K, Osada K, and Kataoka K. Block Copolymer Micelles in Nanomedicine Applications. Chemical Reviews. 2018. 118(14): p. 6844-6892.

115. Kumar R, Santa Chalarca CF, Bockman MR, Bruggen CV, Grimme CJ, Dalal RJ, Hanson MG, Hexum JK, and Reineke TM. Polymeric Delivery of Therapeutic Nucleic Acids. Chem Rev. 2021. 121(18): p. 11527-11652.

116. van den Berg AIS, Yun CO, Schiffelers RM, and Hennink WE. Polymeric delivery systems for nucleic acid therapeutics: Approaching the clinic. J Control Release. 2021. 331: p. 121-141.

117. Blanco E, Shen H, and Ferrari M. Principles of nanoparticle design for overcoming biological barriers to drug delivery. Nat Biotechnol. 2015. 33(9): p. 941-51.

118. Wagner E. Programmed drug delivery: nanosystems for tumor targeting. Expert.Opin.Biol Ther. 2007. 7(5): p. 587-593.

119. Huang L, Chen F, Lai Y, Xu Z, and Yu H. Engineering Nanorobots for Tumor-Targeting Drug Delivery: From Dynamic Control to Stimuli-Responsive Strategy. Chembiochem. 2021. 22(24): p. 3369-3380.

120. Sun M, Wang K, and Oupický D. Advances in Stimulus-Responsive Polymeric Materials for Systemic Delivery of Nucleic Acids. Advanced Healthcare Materials. 2018. 7(4): p. 1701070.

121. Merkel OM, Urbanics R, Bedocs P, Rozsnyay Z, Rosivall L, Toth M, Kissel T, and Szebeni J. In Vitro and In Vivo Complement Activation and Related Anaphylactic Effects Associated with Polyethylenimine and Polyethylenimine-Graft-Poly(ethylene glycol) Block Copolymers. Biomaterials. 2011. 32(21): p. 4936-42.

122. Alberg I, Kramer S, Schinnerer M, Hu Q, Seidl C, Leps C, Drude N, Mockel D, Rijcken C, Lammers T, Diken M, Maskos M, Morsbach S, Landfester K, Tenzer S, Barz M, and Zentel R. Polymeric Nanoparticles with Neglectable Protein Corona. Small. 2020. 16(18): p. e1907574.

123. Wang H-X, Zuo Z-Q, Du J-Z, Wang Y-C, Sun R, Cao Z-T, Ye X-D, Wang J-L, Leong KW, and Wang J. Surface charge critically affects tumor penetration and therapeutic efficacy of cancer nanomedicines. Nano Today. 2016. 11(2): p. 133-144.

124. Chollet P, Favrot MC, Hurbin A, and Coll JL. Side-effects of a systemic injection of linear polyethylenimine-DNA complexes. J Gene Med. 2002. 4(1): p. 84-91.

125. Gabizon A and Papahadjopoulos D. Liposome formulations with prolonged circulation time in blood and enhanced uptake by tumors. Proceedings of the National Academy of Sciences. 1988. 85(18): p. 6949-6953.

126. Dreaden EC, Morton SW, Shopsowitz KE, Choi JH, Deng ZJ, Cho NJ, and Hammond PT. Bimodal Tumor-Targeting from Microenvironment Responsive Hyaluronan Layer-by-Layer (LbL) Nanoparticles. ACS Nano. 2014. 8(8): p. 8374-82.

127. Sato T, Nakata M, Yang Z, Torizuka Y, Kishimoto S, and Ishihara M. In vitro and in vivo gene delivery using chitosan/hyaluronic acid nanoparticles: Influences of molecular mass of hyaluronic acid and lyophilization on transfection efficiency. J Gene Med. 2017. 19(8): p. e2968.

128. Hatakeyama H, Akita H, and Harashima H. A multifunctional envelope type nano device (MEND) for gene delivery to tumours based on the EPR effect: a strategy for overcoming the PEG dilemma. Adv Drug Deliv Rev. 2011. 63(3): p. 152-60.

129. Walker GF, Fella C, Pelisek J, Fahrmeir J, Boeckle S, Ogris M, and Wagner E. Toward synthetic viruses: endosomal pH-triggered deshielding of targeted polyplexes greatly enhances gene transfer in vitro and in vivo. Mol Ther. 2005. 11(3): p. 418-25.

130. Hatakeyama H, Akita H, Kogure K, Oishi M, Nagasaki Y, Kihira Y, Ueno M, Kobayashi H, Kikuchi H, and Harashima H. Development of a novel systemic gene delivery system for cancer therapy with a tumor-specific cleavable PEG-lipid. Gene Ther. 2007. 14(1): p. 68-77.

131. Beckert L, Kostka L, Kessel E, Krhac Levacic A, Kostkova H, Etrych T, Lachelt U, and Wagner E. Acid-Labile pHPMA Modification of Four-Arm Oligoaminoamide pDNA Polyplexes Balances Shielding and Gene Transfer Activity In Vitro and In Vivo. Eur J Pharm Biopharm. 2016. 105: p. 85-96.

132. Schöttler S, Becker G, Winzen S, Steinbach T, Mohr K, Landfester K, Mailänder V, and Wurm FR. Protein adsorption is required for stealth effect of poly(ethylene glycol)- and poly(phosphoester)-coated nanocarriers. Nat Nanotechnol. 2016. 11(4): p. 372-7.

133. Maeda H. The link between infection and cancer: tumor vasculature, free radicals, and drug delivery to tumors via the EPR effect. Cancer Sci. 2013. 104(7): p. 779-89.

134. Maeda H. Polymer therapeutics and the EPR effect. J Drug Target. 2017. 25(9-10): p. 781-785.

135. Maeda H. The 35th Anniversary of the Discovery of EPR Effect: A New Wave of Nanomedicines for Tumor-Targeted Drug Delivery-Personal Remarks and Future Prospects. J Pers Med. 2021. 11(3): p. 229.

136. Shi Y, van der Meel R, Chen X, and Lammers T. The EPR effect and beyond: Strategies to improve tumor targeting and cancer nanomedicine treatment efficacy. Theranostics. 2020. 10(17): p. 7921-7924.

137. Schnitzer JE. gp60 is an albumin-binding glycoprotein expressed by continuous endothelium involved in albumin transcytosis. The American journal of physiology. 1992. 262: p. H246–H254.

138. Oh P, Testa JE, Borgstrom P, Witkiewicz H, Li Y, and Schnitzer JE. In vivo proteomic imaging analysis of caveolae reveals pumping system to penetrate solid tumors. Nat Med. 2014. 20(9): p. 1062-8.

139. Liu Y, Huo Y, Yao L, Xu Y, Meng F, Li H, Sun K, Zhou G, Kohane DS, and Tao K. Transcytosis of Nanomedicine for Tumor Penetration. Nano Lett. 2019. 19(11): p. 8010-8020.

140. de Lázaro I, Mooney, D.J. A nanoparticle's pathway into tumours. Nat Mater. 2020. 19(5): p. 481-482.

141. Pandit S, Dutta D, and Nie S. Active transcytosis and new opportunities for cancer nanomedicine. Nat Mater. 2020. 19(5): p. 478-480.

142. Belykh E, Shaffer KV, Lin C, Byvaltsev VA, Preul MC, and Chen L. Blood-Brain Barrier, Blood-Brain Tumor Barrier, and Fluorescence-Guided Neurosurgical Oncology: Delivering Optical Labels to Brain Tumors. Front Oncol. 2020. 10: p. 739.

143. Lammers T. Drug delivery research in Europe. J Control Release. 2012. 161(2): p. 151.

144. Martins JP, das Neves J, de la Fuente M, Celia C, Florindo H, Gunday-Tureli N, Popat A, Santos JL, Sousa F, Schmid R, Wolfram J, Sarmento B, and Santos HA. The solid progress of nanomedicine. Drug Deliv Transl Res. 2020. 10(3): p. 726-729.

145. Miura S, Suzuki H, and Bae YH. A Multilayered Cell Culture Model for Transport Study in Solid Tumors: Evaluation of Tissue Penetration of Polyethyleneimine Based Cationic Micelles. Nano Today. 2014. 9(6): p. 695-704.

146. Xiao K, Li Y, Luo J, Lee JS, Xiao W, Gonik AM, Agarwal RG, and Lam KS. The effect of surface charge on in vivo biodistribution of PEG-oligocholic acid based micellar nanoparticles. Biomaterials. 2011. 32(13): p. 3435-46.

147. Igarashi K, Cabral H, Hong T, Anraku Y, Mpekris F, Stylianopoulos T, Khan T, Matsumoto A, Kataoka K, Matsumoto Y, and Yamasoba T. Vascular Bursts Act as a Versatile Tumor Vessel Permeation Route for Blood-Borne Particles and Cells. Small. 2021. 17(42): p. e2103751.

148. Matsumoto Y, Nichols JW, Toh K, Nomoto T, Cabral H, Miura Y, Christie RJ, Yamada N, Ogura T, Kano MR, Matsumura Y, Nishiyama N, Yamasoba T, Bae YH, and Kataoka K. Vascular bursts enhance permeability of tumour blood vessels and improve nanoparticle delivery. Nat Nanotechnol. 2016. 11(6): p. 533-538.

149. Chen N, Brachmann C, Liu X, Pierce DW, Dey J, Kerwin WS, Li Y, Zhou S, Hou S, Carleton M, Klinghoffer RA, Palmisano M, and Chopra R. Albumin-bound nanoparticle (nab) paclitaxel exhibits enhanced paclitaxel tissue distribution and tumor penetration. Cancer Chemother Pharmacol. 2015. 76(4): p. 699-712.

150. Sindhwani S, Syed AM, Ngai J, Kingston BR, Maiorino L, Rothschild J, MacMillan P, Zhang Y, Rajesh NU, Hoang T, Wu JLY, Wilhelm S, Zilman A, Gadde S, Sulaiman A, Ouyang B, Lin Z, Wang L, Egeblad M, and Chan WCW. The entry of nanoparticles into solid tumours. Nat Mater. 2020. 19(5): p. 566-575.

151. Jamieson JJ, Searson PC, and Gerecht S. Engineering the human blood-brain barrier in vitro. Journal of biological engineering. 2017. 11: p. 37-37.

152. Banks WA. From blood-brain barrier to blood-brain interface: new opportunities for CNS drug delivery. Nat Rev Drug Discov. 2016. 15(4): p. 275-92.

153. Pardridge WM. Blood-brain barrier delivery. Drug Discov Today. 2007. 12(1-2): p. 54-61.

154. Chinot OL, Wick W, Mason W, Henriksson R, Saran F, Nishikawa R, Carpentier AF, Hoang-Xuan K, Kavan P, Cernea D, Brandes AA, Hilton M, Abrey L, and Cloughesy T. Bevacizumab plus Radiotherapy–Temozolomide for Newly Diagnosed Glioblastoma. New England Journal of Medicine. 2014. 370(8): p. 709-722.

155. Pardridge WM. The blood-brain barrier: bottleneck in brain drug development. NeuroRx. 2005. 2(1): p. 3-14.

156. Liu X, Lin P, Perrett I, Lin J, Liao YP, Chang CH, Jiang J, Wu N, Donahue T, Wainberg Z, Nel AE, and Meng H. Tumor-penetrating peptide enhances transcytosis of silicasome-based chemotherapy for pancreatic cancer. J Clin Invest. 2017. 127(5): p. 2007-2018.

157. Klein PM, Kern S, Lee DJ, Schmaus J, Hohn M, Gorges J, Kazmaier U, and Wagner E. Folate Receptor-Directed Orthogonal Click-Functionalization of siRNA Lipopolyplexes for Tumor Cell Killing In Vivo. Biomaterials. 2018. 178: p. 630-642.

158. Carlisle RC, Read ML, Wolfert MA, and Seymour LW. Self-assembling poly(l-lysine)/DNA complexes capable of integrin-mediated cellular uptake and gene expression. Colloids and Surfaces B: Biointerfaces. 1999. 16(1): p. 261-272.

159. Erbacher P, Remy JS, and Behr JP. Gene transfer with synthetic virus-like particles via the integrin-mediated endocytosis pathway. Gene Therapy. 1999. 6(1): p. 138-145.

160. Schiffelers RM, Ansari A, Xu J, Zhou Q, Tang Q, Storm G, Molema G, Lu PY, Scaria PV, and Woodle MC. Cancer siRNA Therapy by Tumor Selective Delivery with Ligand-Targeted Sterically Stabilized Nanoparticle. Nucleic Acids Res. 2004. 32(19): p. e149.

161. Parvani JG, Gujrati MD, Mack MA, Schiemann WP, and Lu Z-R. Silencing β3 Integrin by Targeted ECO/siRNA Nanoparticles Inhibits EMT and Metastasis of Triple-Negative Breast Cancer. Cancer research. 2015. 75(11): p. 2316-2325.

162. Vaidya AM, Sun Z, Ayat N, Schilb A, Liu X, Jiang H, Sun D, Scheidt J, Qian V, He S, Gilmore H, Schiemann WP, and Lu ZR. Systemic Delivery of Tumor-Targeting siRNA Nanoparticles against an Oncogenic LncRNA Facilitates Effective Triple-Negative Breast Cancer Therapy. Bioconjug Chem. 2019. 30(3): p. 907-919.

163. Schilb AL, Ayat NR, Vaidya AM, Hertz LM, Hall RC, Scheidt JH, Sun D, Sun Z, Gopalakrishnan R, and Lu ZR. Efficacy of Targeted ECO/miR-200c Nanoparticles for Modulating Tumor Microenvironment and Treating Triple Negative Breast Cancer as Non-invasively Monitored by MR Molecular Imaging. Pharm Res. 2021. 38(8): p. 1405-1418.

164. Chen Q, Osada K, Ge Z, Uchida S, Tockary TA, Dirisala A, Matsui A, Toh K, Takeda KM, Liu X, Nomoto T, Ishii T, Oba M, Matsumoto Y, and Kataoka K. Polyplex micelle installing intracellular self-processing functionalities without free catiomers for safe and efficient systemic gene therapy through tumor vasculature targeting. Biomaterials. 2017. 113: p. 253-265.

165. Ge Z, Chen Q, Osada K, Liu X, Tockary TA, Uchida S, Dirisala A, Ishii T, Nomoto T, Toh K, Matsumoto Y, Oba M, Kano MR, Itaka K, and Kataoka K. Targeted gene delivery by polyplex micelles with crowded PEG palisade and cRGD moiety for systemic treatment of pancreatic tumors. Biomaterials. 2014. 35(10): p. 3416-3426.

166. Zhou G, Xu Y, Chen M, Cheng D, and Shuai X. Tumor-penetrating peptide modified and pH-sensitive polyplexes for tumor targeted siRNA delivery. Polymer Chemistry. 2016. 7(23): p. 3857-3863.

167. Ren Y, Cheung HW, von Maltzhan G, Agrawal A, Cowley GS, Weir BA, Boehm JS, Tamayo P, Karst AM, Liu JF, Hirsch MS, Mesirov JP, Drapkin R, Root DE, Lo J, Fogal V, Ruoslahti E, Hahn WC, and Bhatia SN. Targeted tumor-penetrating siRNA nanocomplexes for credentialing the ovarian cancer oncogene ID4. Sci Transl Med. 2012. 4(147): p. 147ra112.

168. Leng Q and Mixson AJ. The neuropilin-1 receptor mediates enhanced tumor delivery of H2K polyplexes. J Gene Med. 2016. 18(7): p. 134-44.

169. Moffatt S, Wiehle S, and Cristiano RJ. Tumor-Specific Gene Delivery Mediated by a Novel Peptide–Polyethylenimine–DNA Polyplex Targeting Aminopeptidase N/CD13. Human Gene Therapy. 2005. 16(1): p. 57-67.

170. Son S, Singha K, and Kim WJ. Bioreducible BPEI-SS-PEG-cNGR polymer as a tumor targeted nonviral gene carrier. Biomaterials. 2010. 31(24): p. 6344-6354.

171. Lu ZX, Liu LT, and Qi XR. Development of small interfering RNA delivery system using PEI-PEG-APRPG polymer for antiangiogenic vascular endothelial growth factor tumor-targeted therapy. Int J Nanomedicine. 2011. 6: p. 1661-73.

172. Arap W, Pasqualini R, and Ruoslahti E. Cancer Treatment by Targeted Drug Delivery to Tumor Vasculature in a Mouse Model. Science. 1998. 279(5349): p. 377-380.

173. Ellerby HM, Arap W, Ellerby LM, Kain R, Andrusiak R, Rio GD, Krajewski S, Lombardo CR, Rao R, Ruoslahti E, Bredesen DE, and Pasqualini R. Anti-Cancer Activity of Targeted Pro-Apoptotic Peptides. Nature Medicine. 1999. 5(9): p. 1032-1038.

174. Murphy EA, Majeti BK, Barnes LA, Makale M, Weis SM, Lutu-Fuga K, Wrasidlo W, and Cheresh DA. Nanoparticle-Mediated Drug Delivery to Tumor Vasculature Suppresses Metastasis. Proc Natl Acad Sci U S A. 2008. 105(27): p. 9343-8.

175. Sakurai Y, Hatakeyama H, Sato Y, Hyodo M, Akita H, Ohga N, Hida K, and Harashima H. RNAi-Mediated Gene Knockdown and Anti-Angiogenic Therapy of RCCs Using a Cyclic RGD-Modified Liposomal-siRNA System. Journal of Controlled Release. 2014. 173: p. 110-118.

176. Sakurai Y, Hada T, Kato A, Hagino Y, Mizumura W, and Harashima H. Effective Therapy Using a Liposomal siRNA that Targets the Tumor Vasculature in a Model Murine Breast Cancer with Lung Metastasis. Mol Ther Oncolytics. 2018. 11: p. 102-108.

177. Khabazian E, Vakhshiteh F, Norouzi P, Fatahi Y, Dinarvand R, and Atyabi F. Cationic Liposome Decorated with Cyclic RGD Peptide for Targeted Delivery of anti-STAT3 siRNA to Melanoma Cancer Cells. Journal of Drug Targeting. 2021: p. 1-34.

178. Martinez-Jothar L, Barendrecht AD, de Graaff AM, Oliveira S, van Nostrum CF, Schiffelers RM, Hennink WE, and Fens M. Endothelial Cell Targeting by cRGD-Functionalized Polymeric Nanoparticles under Static and Flow Conditions. Nanomaterials (Basel). 2020. 10(7): p. 1353.

179. Rios De La Rosa JM, Spadea A, Donno R, Lallana E, Lu Y, Puri S, Caswell P, Lawrence MJ, Ashford M, and Tirelli N. Microfluidic-assisted preparation of RGD-decorated nanoparticles: exploring integrin-facilitated uptake in cancer cell lines. Sci Rep. 2020. 10(1): p. 14505.

180. Sugahara KN, Teesalu T, Karmali PP, Kotamraju VR, Agemy L, Girard OM, Hanahan D, Mattrey RF, and Ruoslahti E. Tissue-penetrating delivery of compounds and nanoparticles into tumors. Cancer Cell. 2009. 16(6): p. 510-20.

181. Ruoslahti E. Tumor penetrating peptides for improved drug delivery. Adv Drug Deliv Rev. 2017. 110-111: p. 3-12.

182. Teesalu T, Sugahara KN, Kotamraju VR, and Ruoslahti E. C-end rule peptides mediate neuropilin-1-dependent cell, vascular, and tissue penetration. Proc Natl Acad Sci U S A. 2009. 106(38): p. 16157-62.

183. Alberici L, Roth L, Sugahara KN, Agemy L, Kotamraju VR, Teesalu T, Bordignon C, Traversari C, Rizzardi G-P, and Ruoslahti E. De Novo Design of a Tumor-Penetrating Peptide. Cancer Research. 2013. 73(2): p. 804-812.

184. Negussie AH, Miller JL, Reddy G, Drake SK, Wood BJ, and Dreher MR. Synthesis and in vitro evaluation of cyclic NGR peptide targeted thermally sensitive liposome. Journal of controlled release : official journal of the Controlled Release Society. 2010. 143(2): p. 265-273.

185. Chen Y, Wu JJ, and Huang L. Nanoparticles targeted with NGR motif deliver c-myc siRNA and doxorubicin for anticancer therapy. Mol Ther. 2010. 18(4): p. 828-34.

186. Roth L, Agemy L, Kotamraju VR, Braun G, Teesalu T, Sugahara KN, Hamzah J, and Ruoslahti E. Transtumoral targeting enabled by a novel neuropilin-binding peptide. Oncogene. 2012. 31(33): p. 3754-63.

187. Porkka K, Laakkonen P, Hoffman JA, Bernasconi M, and Ruoslahti E. A fragment of the HMGN2 protein homes to the nuclei of tumor cells and tumor endothelial cells in vivo. Proceedings of the National Academy of Sciences. 2002. 99(11): p. 7444-7449.

188. Hu Q, Gao X, Kang T, Feng X, Jiang D, Tu Y, Song Q, Yao L, Jiang X, Chen H, and Chen J. CGKRK-modified nanoparticles for dual-targeting drug delivery to tumor cells and angiogenic blood vessels. Biomaterials. 2013. 34(37): p. 9496-508.

189. Sugahara KN, Teesalu T, Karmali PP, Kotamraju VR, Agemy L, Greenwald DR, and Ruoslahti E. Coadministration of a tumor-penetrating peptide enhances the efficacy of cancer drugs. Science. 2010. 328(5981): p. 1031-5.

190. Simón-Gracia L, Hunt H, Scodeller P, Gaitzsch J, Kotamraju VR, Sugahara KN, Tammik O, Ruoslahti E, Battaglia G, and Teesalu T. iRGD peptide conjugation potentiates intraperitoneal tumor delivery of paclitaxel with polymersomes. Biomaterials. 2016. 104: p. 247-57.

191. Gomes-da-Silva LC, Santos AO, Bimbo LM, Moura V, Ramalho JS, Pedroso de Lima MC, Simões S, and Moreira JN. Toward a siRNA-containing nanoparticle targeted to breast cancer cells and the tumor microenvironment. Int J Pharm. 2012. 434(1-2): p. 9-19.

192. Elsabahy M, Shrestha R, Clark C, Taylor S, Leonard J, and Wooley KL. Multifunctional hierarchically assembled nanostructures as complex stage-wise dual-delivery systems for coincidental yet differential trafficking of siRNA and paclitaxel. Nano letters. 2013. 13(5): p. 2172-2181.

193. Pasqualini R, Koivunen E, Kain R, Lahdenranta J, Sakamoto M, Stryhn A, Ashmun RA, Shapiro LH, Arap W, and Ruoslahti E. Aminopeptidase N is a receptor for tumor-homing peptides and a target for inhibiting angiogenesis. Cancer Res. 2000. 60(3): p. 722-7.

194. Oku N, Asai T, Watanabe K, Kuromi K, Nagatsuka M, Kurohane K, Kikkawa H, Ogino K, Tanaka M, Ishikawa D, Tsukada H, Momose M, Nakayama J, and Taki T. Anti-neovascular therapy using novel peptides homing to angiogenic vessels. Oncogene. 2002. 21(17): p. 2662-2669.

195. Koide H, Asai T, Kato H, Yonenaga N, Yokota M, Ando H, Dewa T, Nango M, Maeda N, and Oku N. Susceptibility of PTEN-positive metastatic tumors to small interfering RNA targeting the mammalian target of rapamycin. Nanomedicine : nanotechnology, biology, and medicine. 2014. 11.

196. Ando H, Asai T, Koide H, Okamoto A, Maeda N, Tomita K, Dewa T, Minamino T, and Oku N. Advanced cancer therapy by integrative antitumor actions via systemic administration of miR-499. J Control Release. 2014. 181: p. 32-9.

197. Maeda N, Takeuchi Y, Takada M, Sadzuka Y, Namba Y, and Oku N. Anti-neovascular therapy by use of tumor neovasculature-targeted long-circulating liposome. J Control Release. 2004. 100(1): p. 41-52.

198. Huang RQ, Qu YH, Ke WL, Zhu JH, Pei YY, and Jiang C. Efficient gene delivery targeted to the brain using a transferrin-conjugated polyethyleneglycol-modified polyamidoamine dendrimer. FASEB J. 2007. 21(4): p. 1117-25.

199. Kuang Y, An S, Guo Y, Huang S, Shao K, Liu Y, Li J, Ma H, and Jiang C. T7 peptide-functionalized nanoparticles utilizing RNA interference for glioma dual targeting. Int J Pharm. 2013. 454(1): p. 11-20.

200. Somani S, Robb G, Pickard BS, and Dufès C. Enhanced gene expression in the brain following intravenous administration of lactoferrin-bearing polypropylenimine dendriplex. Journal of Controlled Release. 2015. 217: p. 235-242.

201. Kumar P, Wu H, McBride JL, Jung KE, Kim MH, Davidson BL, Lee SK, Shankar P, and Manjunath N. Transvascular delivery of small interfering RNA to the central nervous system. Nature. 2007. 448(7149): p. 39-43.

202. Liu Y, Huang R, Han L, Ke W, Shao K, Ye L, Lou J, and Jiang C. Brain-targeting gene delivery and cellular internalization mechanisms for modified rabies virus glycoprotein RVG29 nanoparticles. Biomaterials. 2009. 30(25): p. 4195-202.

203. Hwang DW, Son S, Jang J, Youn H, Lee S, Lee D, Lee YS, Jeong JM, Kim WJ, and Lee DS. A brain-targeted rabies virus glycoprotein-disulfide linked PEI nanocarrier for delivery of neurogenic microRNA. Biomaterials. 2011. 32(21): p. 4968-75.

204. Gong C, Li X, Xu L, and Zhang YH. Target delivery of a gene into the brain using the RVG29-oligoarginine peptide. Biomaterials. 2012. 33(12): p. 3456-63.

205. Huo H, Gao Y, Wang Y, Zhang J, Wang ZY, Jiang T, and Wang S. Polyion complex micelles composed of pegylated polyasparthydrazide derivatives for siRNA delivery to the brain. J Colloid Interface Sci. 2015. 447: p. 8-15.

206. Ke W, Shao K, Huang R, Han L, Liu Y, Li J, Kuang Y, Ye L, Lou J, and Jiang C. Gene delivery targeted to the brain using an Angiopep-conjugated polyethyleneglycol-modified polyamidoamine dendrimer. Biomaterials. 2009. 30(36): p. 6976-6985.

207. Huang S, Li J, Han L, Liu S, Ma H, Huang R, and Jiang C. Dual targeting effect of Angiopep-2-modified, DNA-loaded nanoparticles for glioma. Biomaterials. 2011. 32(28): p. 6832-8.

208. An S, He D, Wagner E, and Jiang C. Peptide-like Polymers Exerting Effective Glioma-Targeted siRNA Delivery and Release for Therapeutic Application. Small. 2015. 11(38): p. 5142-50.

209. Srimanee A, Arvanitidou M, Kim K, Hällbrink M, and Langel Ü. Cell-penetrating peptides for siRNA delivery to glioblastomas. Peptides. 2018. 104: p. 62-69.

210. Yao H, Wang K, Wang Y, Wang S, Li J, Lou J, Ye L, Yan X, Lu W, and Huang R. Enhanced blood–brain barrier penetration and glioma therapy mediated by a new peptide modified gene delivery system. Biomaterials. 2015. 37: p. 345-352.

211. Wang T, Meng Z, Kang Z, Ding G, Zhao B, Han Z, Zheng Z, Wang C, and Meng Q. Peptide Gene Delivery Vectors for Specific Transfection of Glioma Cells. ACS Biomater Sci Eng. 2020. 6(12): p. 6778-6789.

212. Min HS, Kim HJ, Naito M, Ogura S, Toh K, Hayashi K, Kim BS, Fukushima S, Anraku Y, Miyata K, and Kataoka K. Systemic Brain Delivery of Antisense Oligonucleotides across the Blood-Brain Barrier with a Glucose-Coated Polymeric Nanocarrier. Angew Chem Int Ed Engl. 2020. 59(21): p. 8173-8180.

213. Béduneau A, Saulnier P, and Benoit J-P. Active targeting of brain tumors using nanocarriers. Biomaterials. 2007. 28(33): p. 4947-4967.

214. Nishioka T, Oda Y, Seino Y, Yamamoto T, Inagaki N, Yano H, Imura H, Shigemoto R, and Kikuchi H. Distribution of the Glucose Transporters in Human Brain Tumors. Cancer Research. 1992. 52(14): p. 3972-3979.

215. Du D, Chang N, Sun S, Li M, Yu H, Liu M, Liu X, Wang G, Li H, Liu X, Geng S, Wang Q, and Peng H. The role of glucose transporters in the distribution of p-aminophenyl-α-d-mannopyranoside modified liposomes within mice brain. J Control Release. 2014. 182: p. 99-110.

216. Xie F, Yao N, Qin Y, Zhang Q, Chen H, Yuan M, Tang J, Li X, Fan W, Zhang Q, Wu Y, Hai L, and He Q. Investigation of glucose-modified liposomes using polyethylene glycols with different chain lengths as the linkers for brain targeting. Int J Nanomedicine. 2012. 7: p. 163-75.

217. Singh I, Swami R, Jeengar MK, Khan W, and Sistla R. p-Aminophenyl-α-D-mannopyranoside engineered lipidic nanoparticles for effective delivery of docetaxel to brain. Chem Phys Lipids. 2015. 188: p. 1-9.

218. Ying X, Wen H, Lu WL, Du J, Guo J, Tian W, Men Y, Zhang Y, Li RJ, Yang TY, Shang DW, Lou JN, Zhang LR, and Zhang Q. Dual-targeting daunorubicin liposomes improve the therapeutic efficacy of brain glioma in animals. J Control Release. 2010. 141(2): p. 183-92.

219. Tang W, Fan W, Lau J, Deng L, Shen Z, and Chen X. Emerging blood-brain-barrier-crossing nanotechnology for brain cancer theranostics. Chem Soc Rev. 2019. 48(11): p. 2967-3014.

220. Karlsson J, Rui Y, Kozielski KL, Placone AL, Choi O, Tzeng SY, Kim J, Keyes JJ, Bogorad MI, Gabrielson K, Guerrero-Cazares H, Quinones-Hinojosa A, Searson PC, and Green JJ. Engineered nanoparticles for systemic siRNA delivery to malignant brain tumours. Nanoscale. 2019. 11(42): p. 20045-20057.

221. Zorko M and Langel U. Cell-penetrating peptides: mechanism and kinetics of cargo delivery. Adv Drug Deliv Rev. 2005. 57(4): p. 529-45.

222. Chen Y and Liu L. Modern methods for delivery of drugs across the blood-brain barrier. Adv Drug Deliv Rev. 2012. 64(7): p. 640-65.

223. Gupta B, Levchenko TS, and Torchilin VP. TAT peptide-modified liposomes provide enhanced gene delivery to intracranial human brain tumor xenografts in nude mice. Oncol Res. 2007. 16(8): p. 351-9.

224. Han L, Zhang A, Wang H, Pu P, Jiang X, Kang C, and Chang J. Tat-BMPs-PAMAM conjugates enhance therapeutic effect of small interference RNA on U251 glioma cells in vitro and in vivo. Hum Gene Ther. 2010. 21(4): p. 417-26.

225. Oller-Salvia B, Sanchez-Navarro M, Giralt E, and Teixido M. Blood-brain barrier shuttle peptides: an emerging paradigm for brain delivery. Chem Soc Rev. 2016. 45(17): p. 4690-707.

226. Tosi G, Costantino L, Rivasi F, Ruozi B, Leo E, Vergoni AV, Tacchi R, Bertolini A, Vandelli MA, and Forni F. Targeting the central nervous system: in vivo experiments with peptide-derivatized nanoparticles loaded with Loperamide and Rhodamine-123. J Control Release. 2007. 122(1): p. 1-9.

227. Höbel S, Appeldoorn CC, Gaillard PJ, and Aigner A. Targeted CRM197-PEG-PEI/siRNA Complexes for Therapeutic RNAi in Glioblastoma. Pharmaceuticals (Basel). 2011. 4(12): p. 1591-1606.

228. Duffy KR and Pardridge WM. Blood-brain barrier transcytosis of insulin in developing rabbits. Brain Res. 1987. 420(1): p. 32-8.

229. Choudhury H, Pandey M, Chin PX, Phang YL, Cheah JY, Ooi SC, Mak K-K, Pichika MR, Kesharwani P, Hussain Z, and Gorain B. Transferrin receptors-targeting nanocarriers for efficient targeted delivery and transcytosis of drugs into the brain tumors: a review of recent advancements and emerging trends. Drug delivery and translational research. 2018. 8(5): p. 1545-1563.

230. Jefferies WA, Brandon MR, Hunt SV, Williams AF, Gatter KC, and Mason DY. Transferrin receptor on endothelium of brain capillaries. Nature. 1984. 312(5990): p. 162-163.

231. Fishman JB, Rubin JB, Handrahan JV, Connor JR, and Fine RE. Receptor-mediated transcytosis of transferrin across the blood-brain barrier. J Neurosci Res. 1987. 18(2): p. 299-304.

232. Widera A, Norouziyan F, and Shen WC. Mechanisms of TfR-mediated transcytosis and sorting in epithelial cells and applications toward drug delivery. Adv Drug Deliv Rev. 2003. 55(11): p. 1439-66.

233. Tortorella S and Karagiannis TC. Transferrin receptor-mediated endocytosis: a useful target for cancer therapy. J Membr Biol. 2014. 247(4): p. 291-307.

234. Wagner E, Curiel, D. and Cotten, M. Delivery of drugs, proteins and genes into cells using transferrin as a ligand for receptor-mediated endocytosis. Adv. Drug Del. Rev. 1994. 14: p. 113-136.

235. Santi M, Maccari G, Mereghetti P, Voliani V, Rocchiccioli S, Ucciferri N, Luin S, and Signore G. Rational Design of a Transferrin-Binding Peptide Sequence Tailored to Targeted Nanoparticle Internalization. Bioconjugate Chemistry. 2017. 28(2): p. 471-480.

236. Huo T, Yang Y, Qian M, Jiang H, Du Y, Zhang X, Xie Y, and Huang R. Versatile hollow COF nanospheres via manipulating transferrin corona for precise glioma-targeted drug delivery. Biomaterials. 2020. 260: p. 120305.

237. Li J, Feng L, Fan L, Zha Y, Guo L, Zhang Q, Chen J, Pang Z, Wang Y, Jiang X, Yang VC, and Wen L. Targeting the brain with PEG-PLGA nanoparticles modified with phage-displayed peptides. Biomaterials. 2011. 32(21): p. 4943-50.

238. Prades R, Oller-Salvia B, Schwarzmaier SM, Selva J, Moros M, Balbi M, Grazú V, de La Fuente JM, Egea G, Plesnila N, Teixidó M, and Giralt E. Applying the retro-enantio approach to obtain a peptide capable of overcoming the blood-brain barrier. Angew Chem Int Ed Engl. 2015. 54(13): p. 3967-72.

239. Xia H, Anderson B, Mao Q, and Davidson BL. Recombinant human adenovirus: targeting to the human transferrin receptor improves gene transfer to brain microcapillary endothelium. J Virol. 2000. 74(23): p. 11359-66.

240. Lee JH, Engler JA, Collawn JF, and Moore BA. Receptor mediated uptake of peptides that bind the human transferrin receptor. Eur J Biochem. 2001. 268(7): p. 2004-12.

241. Zhang Y, Zhang YF, Bryant J, Charles A, Boado RJ, and Pardridge WM. Intravenous RNA interference gene therapy targeting the human epidermal growth factor receptor prolongs survival in intracranial brain cancer. Clin Cancer Res. 2004. 10(11): p. 3667-77.

242. Chen L, Fu C, Zhang Q, He C, Zhang F, and Wei Q. The role of CD44 in pathological angiogenesis. The FASEB Journal. 2020. 34(10): p. 13125-13139.

243. Zhang Y, Boado RJ, and Pardridge WM. In vivo knockdown of gene expression in brain cancer with intravenous RNAi in adult rats. J Gene Med. 2003. 5(12): p. 1039-45.

244. Zhang Y, Jeong Lee H, Boado RJ, and Pardridge WM. Receptor-mediated delivery of an antisense gene to human brain cancer cells. J Gene Med. 2002. 4(2): p. 183-94.

245. Zhang Y, Boado RJ, and Pardridge WM. Marked enhancement in gene expression by targeting the human insulin receptor. J Gene Med. 2003. 5(2): p. 157-63.

246. Zhang Y, Zhu C, and Pardridge WM. Antisense gene therapy of brain cancer with an artificial virus gene delivery system. Mol Ther. 2002. 6(1): p. 67-72.

247. Chang J, Paillard A, Passirani C, Morille M, Benoit JP, Betbeder D, and Garcion E. Transferrin adsorption onto PLGA nanoparticles governs their interaction with biological systems from blood circulation to brain cancer cells. Pharm Res. 2012. 29(6): p. 1495-505.

248. Porru M, Zappavigna S, Salzano G, Luce A, Stoppacciaro A, Balestrieri ML, Artuso S, Lusa S, De Rosa G, Leonetti C, and Caraglia M. Medical treatment of orthotopic glioblastoma with transferrin-conjugated nanoparticles encapsulating zoledronic acid. Oncotarget. 2014. 5(21): p. 10446-59.

249. Lam FC, Morton SW, Wyckoff J, Vu Han TL, Hwang MK, Maffa A, Balkanska-Sinclair E, Yaffe MB, Floyd SR, and Hammond PT. Enhanced efficacy of combined temozolomide and bromodomain inhibitor therapy for gliomas using targeted nanoparticles. Nat Commun. 2018. 9(1): p. 1991.

250. Huwyler J, Wu D, and Pardridge WM. Brain drug delivery of small molecules using immunoliposomes. Proceedings of the National Academy of Sciences of the United States of America. 1996. 93(24): p. 14164-14169.

251. Huang RQ, Ke WL, Qu YH, Zhu JH, Pei YY, and Jiang C. Characterization of lactoferrin receptor in brain endothelial capillary cells and mouse brain. J Biomed Sci. 2007. 14(1): p. 121-8.

252. Drappatz J, Brenner A, Wong ET, Eichler A, Schiff D, Groves MD, Mikkelsen T, Rosenfeld S, Sarantopoulos J, Meyers CA, Fielding RM, Elian K, Wang X, Lawrence B, Shing M, Kelsey S, Castaigne JP, and Wen PY. Phase I Study of GRN1005 in Recurrent Malignant Glioma. Clinical Cancer Research. 2013. 19(6): p. 1567-1576.

253. Demeule M, Currie JC, Bertrand Y, Ché C, Nguyen T, Régina A, Gabathuler R, Castaigne JP, and Béliveau R. Involvement of the low-density lipoprotein receptor-related protein in the transcytosis of the brain delivery vector angiopep-2. J Neurochem. 2008. 106(4): p. 1534-44.

254. Lillis AP, Van Duyn LB, Murphy-Ullrich JE, and Strickland DK. LDL receptor-related protein 1: unique tissue-specific functions revealed by selective gene knockout studies. Physiol Rev. 2008. 88(3): p. 887-918.

255. Demeule M, Beaudet N, Régina A, Besserer-Offroy É, Murza A, Tétreault P, Belleville K, Ché C, Larocque A, Thiot C, Béliveau R, Longpré JM, Marsault É, Leduc R, Lachowicz JE, Gonias SL, Castaigne JP, and Sarret P. Conjugation of a brain-penetrant peptide with neurotensin provides antinociceptive properties. J Clin Invest. 2014. 124(3): p. 1199-213.

256. Ché C, Yang G, Thiot C, Lacoste M-C, Currie J-C, Demeule M, Régina A, Béliveau R, and Castaigne J-P. New Angiopep-Modified Doxorubicin (ANG1007) and Etoposide (ANG1009) Chemotherapeutics With Increased Brain Penetration. Journal of Medicinal Chemistry. 2010. 53(7): p. 2814-2824.

257. Zhu Y, Jiang Y, Meng F, Deng C, Cheng R, Zhang J, Feijen J, and Zhong Z. Highly efficacious and specific anti-glioma chemotherapy by tandem nanomicelles co-functionalized with brain tumor-targeting and cell-penetrating peptides. Journal of Controlled Release. 2018. 278: p. 1-8.

258. Xin H, Sha X, Jiang X, Zhang W, Chen L, and Fang X. Anti-glioblastoma efficacy and safety of paclitaxel-loading Angiopep-conjugated dual targeting PEG-PCL nanoparticles. Biomaterials. 2012. 33(32): p. 8167-76.

259. Régina A, Demeule M, Ché C, Lavallée I, Poirier J, Gabathuler R, Béliveau R, and Castaigne JP. Antitumour activity of ANG1005, a conjugate between paclitaxel and the new brain delivery vector Angiopep-2. British journal of pharmacology. 2008. 155(2): p. 185-197.

260. Zou Y, Sun X, Wang Y, Yan C, Liu Y, Li J, Zhang D, Zheng M, Chung RS, and Shi B. Single siRNA Nanocapsules for Effective siRNA Brain Delivery and Glioblastoma Treatment. Adv Mater. 2020. 32(24): p. e2000416.

261. Yang ZZ, Li JQ, Wang ZZ, Dong DW, and Qi XR. Tumor-targeting dual peptides-modified cationic liposomes for delivery of siRNA and docetaxel to gliomas. Biomaterials. 2014. 35(19): p. 5226-39.

262. Sun X, Pang Z, Ye H, Qiu B, Guo L, Li J, Ren J, Qian Y, Zhang Q, Chen J, and Jiang X. Co-delivery of pEGFP-hTRAIL and paclitaxel to brain glioma mediated by an angiopep-conjugated liposome. Biomaterials. 2012. 33(3): p. 916-24.

263. Sakamoto K, Shinohara T, Adachi Y, Asami T, and Ohtaki T. A novel LRP1-binding peptide L57 that crosses the blood brain barrier. Biochemistry and biophysics reports. 2017. 12: p. 135-139.

264. Rodrigues JP, Prajapati N, DeCoster MA, Poh S, and Murray TA. Efficient LRP1-Mediated Uptake and Low Cytotoxicity of Peptide L57 In Vitro Shows Its Promise as CNS Drug Delivery Vector. J Pharm Sci. 2021. 110(2): p. 824-832.

265. Schlachetzki F, Zhang Y, Boado RJ, and Pardridge WM. Gene therapy of the brain. The trans-vascular approach. 2004. 62(8): p. 1275-1281.

266. Mathupala SP. Delivery of small-interfering RNA (siRNA) to the brain. Expert opinion on therapeutic patents. 2009. 19(2): p. 137-140.

267. Lu CT, Zhao YZ, Wong HL, Cai J, Peng L, and Tian XQ. Current approaches to enhance CNS delivery of drugs across the brain barriers. Int J Nanomedicine. 2014. 9: p. 2241-57.

268. Turley SJ, Cremasco V, and Astarita JL. Immunological hallmarks of stromal cells in the tumour microenvironment. Nature Reviews Immunology. 2015. 15(11): p. 669-682.

269. Jain RK and Stylianopoulos T. Delivering nanomedicine to solid tumors. Nat Rev Clin Oncol. 2010. 7(11): p. 653-64.

270. Dai Q, Wilhelm S, Ding D, Syed AM, Sindhwani S, Zhang Y, Chen YY, MacMillan P, and Chan WCW. Quantifying the Ligand-Coated Nanoparticle Delivery to Cancer Cells in Solid Tumors. ACS Nano. 2018. 12(8): p. 8423-8435.

271. Khawar IA, Kim JH, and Kuh HJ. Improving drug delivery to solid tumors: priming the tumor microenvironment. J Control Release. 2015. 201: p. 78-89.

272. Wang J, Byrne JD, Napier ME, and DeSimone JM. More effective nanomedicines through particle design. Small. 2011. 7(14): p. 1919-31.

273. Dreher MR, Liu W, Michelich CR, Dewhirst MW, Yuan F, and Chilkoti A. Tumor vascular permeability, accumulation, and penetration of macromolecular drug carriers. J Natl Cancer Inst. 2006. 98(5): p. 335-44.

274. Nance E, Zhang C, Shih TY, Xu Q, Schuster BS, and Hanes J. Brain-penetrating nanoparticles improve paclitaxel efficacy in malignant glioma following local administration. ACS Nano. 2014. 8(10): p. 10655-64.

275. Ito T, Yoshihara C, Hamada K, and Koyama Y. DNA/polyethyleneimine/hyaluronic acid small complex particles and tumor suppression in mice. Biomaterials. 2010. 31(10): p. 2912-8.

276. Joyce JA and Pollard JW. Microenvironmental regulation of metastasis. Nature Reviews Cancer. 2009. 9(4): p. 239-252.

277. Smrekar B, Wightman L, Wolschek MF, Lichtenberger C, Ruzicka R, Ogris M, Rödl W, Kursa M, Wagner E, and Kircheis R. Tissue-dependent factors affect gene delivery to tumors in vivo. Gene Ther. 2003. 10(13): p. 1079-88.

278. Zhang YR, Lin R, Li HJ, He WL, Du JZ, and Wang J. Strategies to improve tumor penetration of nanomedicines through nanoparticle design. Wiley Interdiscip Rev Nanomed Nanobiotechnol. 2019. 11(1): p. e1519.

279. Sun Q, Ojha T, Kiessling F, Lammers T, and Shi Y. Enhancing Tumor Penetration of Nanomedicines. Biomacromolecules. 2017. 18(5): p. 1449-1459.

280. Zhou Q, Shao S, Wang J, Xu C, Xiang J, Piao Y, Zhou Z, Yu Q, Tang J, Liu X, Gan Z, Mo R, Gu Z, and Shen Y. Enzyme-activatable polymer-drug conjugate augments tumour penetration and treatment efficacy. Nat Nanotechnol. 2019. 14(8): p. 799-809.

281. Netti PA, Berk DA, Swartz MA, Grodzinsky AJ, and Jain RK. Role of extracellular matrix assembly in interstitial transport in solid tumors. Cancer research. 2000. 60(9): p. 2497–2503.

282. Brown E, McKee T, diTomaso E, Pluen A, Seed B, Boucher Y, and Jain RK. Dynamic imaging of collagen and its modulation in tumors in vivo using second-harmonic generation. Nature medicine. 2003. 9(6): p. 796–800.

283. Gong H, Chao Y, Xiang J, Han X, Song G, Feng L, Liu J, Yang G, Chen Q, and Liu Z. Hyaluronidase To Enhance Nanoparticle-Based Photodynamic Tumor Therapy. Nano Letters. 2016. 16(4): p. 2512-2521.

284. Zhou H, Fan Z, Deng J, Lemons PK, Arhontoulis DC, Bowne WB, and Cheng H. Hyaluronidase Embedded in Nanocarrier PEG Shell for Enhanced Tumor Penetration and Highly Efficient Antitumor Efficacy. Nano Letters. 2016. 16(5): p. 3268-3277.

285. Tong RT, Boucher Y, Kozin SV, Winkler F, Hicklin DJ, and Jain RK. Vascular normalization by vascular endothelial growth factor receptor 2 blockade induces a pressure gradient across the vasculature and improves drug penetration in tumors. Cancer Res. 2004. 64(11): p. 3731-6.

286. Liu J, Liao S, Diop-Frimpong B, Chen W, Goel S, Naxerova K, Ancukiewicz M, Boucher Y, Jain RK, and Xu L. TGF-β blockade improves the distribution and efficacy of therapeutics in breast carcinoma by normalizing the tumor stroma. Proc Natl Acad Sci U S A. 2012. 109(41): p. 16618-23.

287. von Gersdorff K, Sanders NN, Vandenbroucke R, De Smedt SC, Wagner E, and Ogris M. The internalization route resulting in successful gene expression depends on both cell line and polyethylenimine polyplex type. Mol Ther. 2006. 14(5): p. 745-53.

288. Maeda H, Sawa T, and Konno T. Mechanism of tumor-targeted delivery of macromolecular drugs, including the EPR effect in solid tumor and clinical overview of the prototype polymeric drug SMANCS. Journal of Controlled Release. 2001. 74(1-3): p. 47-61.

289. Yoo J, Park C, Yi G, Lee D, and Koo H. Active Targeting Strategies Using Biological Ligands for Nanoparticle Drug Delivery Systems. Cancers (Basel). 2019. 11(5).

290. Cotten M, Langle-Rouault F, Kirlappos H, Wagner E, Mechtler K, Zenke M, Beug H, and Birnstiel ML. Transferrin-polycation-mediated introduction of DNA into human leukemic cells: stimulation by agents that affect the survival of transfected DNA or modulate transferrin receptor levels. Proc.Natl.Acad.Sci.U.S.A. 1990. 87(11): p. 4033-4037.

291. Wagner E, Zatloukal K, Cotten M, Kirlappos H, Mechtler K, Curiel DT, and Birnstiel ML. Coupling of adenovirus to transferrin-polylysine/DNA complexes greatly enhances receptor-mediated gene delivery and expression of transfected genes. Proc.Natl.Acad.Sci.U.S.A. 1992. 89(13): p. 6099-6103.

292. Wagner E, Plank C, Zatloukal K, Cotten M, and Birnstiel ML. Influenza virus hemagglutinin HA-2 N-terminal fusogenic peptides augment gene transfer by transferrin-polylysine-DNA complexes: toward a synthetic virus-like gene-transfer vehicle. Proc.Natl.Acad.Sci.U.S.A. 1992. 89(17): p. 7934-7938.

293. Kircheis R, Kichler A, Wallner G, Kursa M, Ogris M, Felzmann T, Buchberger M, and Wagner E. Coupling of cell-binding ligands to polyethylenimine for targeted gene delivery. Gene Therapy. 1997. 4(5): p. 409-418.

294. Kircheis R, Wightman L, Schreiber A, Robitza B, Rossler V, Kursa M, and Wagner E. Polyethylenimine/DNA complexes shielded by transferrin target gene expression to tumors after systemic application. Gene Ther. 2001. 8(1): p. 28-40.

295. Kircheis R, Schuller S, Brunner S, Ogris M, Heider KH, Zauner W, and Wagner E. Polycation-based DNA complexes for tumor-targeted gene delivery in vivo. J Gene Med. 1999. 1(2): p. 111-20.

296. Kircheis R, Ostermann E, Wolschek MF, Lichtenberger C, Magin-Lachmann C, Wightman L, Kursa M, and Wagner E. Tumor-targeted gene delivery of tumor necrosis factor-alpha induces tumor necrosis and tumor regression without systemic toxicity. Cancer Gene Ther. 2002. 9(8): p. 673-80.

297. Kursa M, Walker GF, Roessler V, Ogris M, Roedl W, Kircheis R, and Wagner E. Novel shielded transferrin-polyethylene glycol-polyethylenimine/DNA complexes for systemic tumor-targeted gene transfer. Bioconjug Chem. 2003. 14(1): p. 222-31.

298. Tietze N, Pelisek J, Philipp A, Roedl W, Merdan T, Tarcha P, Ogris M, and Wagner E. Induction of apoptosis in murine neuroblastoma by systemic delivery of transferrin-shielded siRNA polyplexes for downregulation of Ran. Oligonucleotides. 2008. 18(2): p. 161-74.

299. Bellocq NC, Pun SH, Jensen GS, and Davis ME. Transferrin-Containing, Cyclodextrin Polymer-Based Particles for Tumor-Targeted Gene Delivery. Bioconjugate Chemistry. 2003. 14(6): p. 1122-1132.

300. Hu-Lieskovan S, Heidel JD, Bartlett DW, Davis ME, and Triche TJ. Sequence-specific knockdown of EWS-FLI1 by targeted, nonviral delivery of small interfering RNA inhibits tumor growth in a murine model of metastatic Ewing's sarcoma. Cancer Res. 2005. 65(19): p. 8984-92.

301. Heidel JD, Yu Z, Liu JY, Rele SM, Liang Y, Zeidan RK, Kornbrust DJ, and Davis ME. Administration in non-human primates of escalating intravenous doses of targeted nanoparticles containing ribonucleotide reductase subunit M2 siRNA. Proc Natl Acad Sci U S A. 2007. 104(14): p. 5715-21.

302. Davis ME. The first targeted delivery of siRNA in humans via a self-assembling, cyclodextrin polymer-based nanoparticle: from concept to clinic. Mol Pharm. 2009. 6(3): p. 659-68.

303. Davis ME, Zuckerman JE, Choi CH, Seligson D, Tolcher A, Alabi CA, Yen Y, Heidel JD, and Ribas A. Evidence of RNAi in humans from systemically administered siRNA via targeted nanoparticles. Nature. 2010. 464(7291): p. 1067-70.

304. Zhang W, Rödl W, He D, Döblinger M, Lächelt U, and Wagner E. Combination of sequence-defined oligoaminoamides with transferrin-polycation conjugates for receptor-targeted gene delivery. J Gene Med. 2015. 17(8-9): p. 161-72.

305. Zhang W, Muller K, Kessel E, Reinhard S, He D, Klein PM, Hohn M, Rodl W, Kempter S, and Wagner E. Targeted siRNA Delivery Using a Lipo-Oligoaminoamide Nanocore with an Influenza Peptide and Transferrin Shell. Adv Healthc Mater. 2016. 5(12): p. 1493-504.

306. Chen J, Gamou S, Takayanagi A, and Shimizu N. A novel gene delivery system using EGF receptor-mediated endocytosis. FEBS Lett. 1994. 338(2): p. 167-9.

307. Xu B, Wiehle S, Roth JA, and Cristiano RJ. The contribution of poly-L-lysine, epidermal growth factor and streptavidin to EGF/PLL/DNA polyplex formation. Gene Therapy. 1998. 5(9): p. 1235-1243.

308. Blessing T, Kursa M, Holzhauser R, Kircheis R, and Wagner E. Different strategies for formation of pegylated EGF-conjugated PEI/DNA complexes for targeted gene delivery. Bioconjug Chem. 2001. 12(4): p. 529-37.

309. Wolschek MF, Thallinger C, Kursa M, Rossler V, Allen M, Lichtenberger C, Kircheis R, Lucas T, Willheim M, Reinisch W, Gangl A, Wagner E, and Jansen B. Specific systemic nonviral gene

delivery to human hepatocellular carcinoma xenografts in SCID mice. Hepatology. 2002. 36(5): p. 1106-14.

310. Shir A, Ogris M, Wagner E, and Levitzki A. EGF Receptor-Targeted Synthetic Double-Stranded RNA Eliminates Glioblastoma, Breast Cancer, and Adenocarcinoma Tumors in Mice. PLOS Medicine. 2005. 3(1): p. e6.

311. Schafer A, Pahnke A, Schaffert D, van Weerden WM, de Ridder CM, Rodl W, Vetter A, Spitzweg C, Kraaij R, Wagner E, and Ogris M. Disconnecting the yin and yang relation of epidermal growth factor receptor (EGFR)-mediated delivery: a fully synthetic, EGFR-targeted gene transfer system avoiding receptor activation. Hum Gene Ther. 2011. 22(12): p. 1463-73.

312. Mickler FM, Möckl L, Ruthardt N, Ogris M, Wagner E, and Bräuchle C. Tuning Nanoparticle Uptake: Live-Cell Imaging Reveals Two Distinct Endocytosis Mechanisms Mediated by Natural and Artificial EGFR Targeting Ligand. Nano Letters. 2012. 12(7): p. 3417-3423.

313. Abourbeh G, Shir A, Mishani E, Ogris M, Rodl W, Wagner E, and Levitzki A. PolyIC GE11 polyplex inhibits EGFR-overexpressing tumors. IUBMB Life. 2012. 64(4): p. 324-30.

314. Muller K, Klein PM, Heissig P, Roidl A, and Wagner E. EGF receptor targeted lipo-oligocation polyplexes for antitumoral siRNA and miRNA delivery. Nanotechnology. 2016. 27(46): p. 464001.

315. Steinborn B, Truebenbach I, Morys S, Lachelt U, Wagner E, and Zhang W. Epidermal growth factor receptor targeted methotrexate and small interfering RNA co-delivery. J Gene Med. 2018. 20(7-8): p. e3041.

316. Morys S, Urnauer S, Spitzweg C, and Wagner E. EGFR Targeting and Shielding of pDNA Lipopolyplexes via Bivalent Attachment of a Sequence-Defined PEG Agent. Macromol Biosci. 2018. 18(1).

317. Truebenbach I, Zhang W, Wang Y, Kern S, Hohn M, Reinhard S, Gorges J, Kazmaier U, and Wagner E. Co-delivery of pretubulysin and siEG5 to EGFR overexpressing carcinoma cells. Int J Pharm. 2019. 569: p. 118570.

318. Wang Y, Luo J, Truebenbach I, Reinhard S, Klein PM, Hohn M, Kern S, Morys S, Loy DM, Wagner E, and Zhang W. Double Click-Functionalized siRNA Polyplexes for Gene Silencing in Epidermal Growth Factor Receptor-Positive Tumor Cells. ACS Biomater Sci Eng. 2020. 6(2): p. 1074-1089.

319. Citro G, Szczylik C, Ginobbi P, Zupi G, and Calabretta B. Inhibition of leukaemia cell proliferation by folic acid-polylysine-mediated introduction of c-myb antisense oligodeoxynucleotides into HL-60 cells. Br J Cancer. 1994. 69(3): p. 463-7.

320. Mislick KA, Baldeschwieler JD, Kayyem JF, and Meade TJ. Transfection of Folate-Polylysine DNA Complexes: Evidence for Lysosomal Delivery. Bioconjugate Chemistry. 1995. 6(5): p. 512-515.

321. Leamon CP, Weigl D, and Hendren RW. Folate Copolymer-Mediated Transfection of Cultured Cells. Bioconjugate Chemistry. 1999. 10(6): p. 947-957.

322. Benns JM, Maheshwari A, Furgeson DY, Mahato RI, and Kim SW. Folate-PEG-folate-graft-polyethylenimine-based gene delivery. J Drug Target. 2001. 9(2): p. 123-39.

323. Hwa Kim S, Hoon Jeong J, Chul Cho K, Wan Kim S, and Gwan Park T. Target-specific gene silencing by siRNA plasmid DNA complexed with folate-modified poly(ethylenimine). J Control Release. 2005. 104(1): p. 223-32.

324. Dohmen C, Edinger D, Fröhlich T, Schreiner L, Lächelt U, Troiber C, Rädler J, Hadwiger P, Vornlocher HP, and Wagner E. Nanosized Multifunctional Polyplexes for Receptor-mediated siRNA delivery. ACS nano. 2012. 6: p. 5198–5208.

325. Li J-M, Zhang W, Su H, Wang Y-Y, Tan C-P, Ji L-N, and Mao Z-W. Reversal of multidrug resistance in MCF-7/Adr cells by codelivery of doxorubicin and BCL2 siRNA using a folic acid-conjugated polyethylenimine hydroxypropyl-β-cyclodextrin nanocarrier. International journal of nanomedicine. 2015. 10: p. 3147-3162.

326. Liu L, Zheng M, Librizzi D, Renette T, Merkel OM, and Kissel T. Efficient and Tumor Targeted siRNA Delivery by Polyethylenimine-graft-polycaprolactone-block-poly(ethylene glycol)-folate (PEI-PCL-PEG-Fol). Mol Pharm. 2016. 13(1): p. 134-43.

327. Lee DJ, He D, Kessel E, Padari K, Kempter S, Lachelt U, Radler JO, Pooga M, and Wagner E. Tumoral gene silencing by receptor-targeted combinatorial siRNA polyplexes. J Control Release. 2016. 244(Pt B): p. 280-291.

328. Lee DJ, Kessel E, Lehto T, Liu X, Yoshinaga N, Padari K, Chen YC, Kempter S, Uchida S, Radler JO, Pooga M, Sheu MT, Kataoka K, and Wagner E. Systemic Delivery of Folate-PEG siRNA Lipopolyplexes with Enhanced Intracellular Stability for In Vivo Gene Silencing in Leukemia. Bioconjug Chem. 2017. 28(9): p. 2393-2409.

329. Chen L, Qian M, Zhang L, Xia J, Bao Y, Wang J, Guo L, and Li Y. Co-delivery of doxorubicin and shRNA of Beclin1 by folate receptor targeted pullulan-based multifunctional nanomicelles for combinational cancer therapy. RSC Advances. 2018. 8(32): p. 17710-17722.

330. Wang M, Guo Y, Xue Y, Niu W, Chen M, Ma PX, and Lei B. Engineering multifunctional bioactive citric acid-based nanovectors for intrinsical targeted tumor imaging and specific siRNA gene delivery in vitro/in vivo. Biomaterials. 2019. 199: p. 10-21.

331. Liu Q, Jin Z, Huang W, Sheng Y, Wang Z, and Guo S. Tailor-made ternary nanopolyplexes of thiolated trimethylated chitosan with pDNA and folate conjugated cis-aconitic amide-polyethylenimine for efficient gene delivery. International Journal of Biological Macromolecules. 2020. 152: p. 948-956.

332. Hou L, Song Z, Xu Z, Wu Y, and Shi W. Folate-Mediated Targeted Delivery of siPLK1 by Leucine-Bearing Polyethylenimine. International journal of nanomedicine. 2020. 15: p. 1397-1408.

333. Oba M, Fukushima S, Kanayama N, Aoyagi K, Nishiyama N, Koyama H, and Kataoka K. Cyclic RGD Peptide-Conjugated Polyplex Micelles as a Targetable Gene Delivery System Directed to Cells Possessing αvβ3 and αvβ5 Integrins. Bioconjugate Chemistry. 2007. 18(5): p. 1415-1423.

334. Oba M, Aoyagi K, Miyata K, Matsumoto Y, Itaka K, Nishiyama N, Yamasaki Y, Koyama H, and Kataoka K. Polyplex Micelles with Cyclic RGD Peptide Ligands and Disulfide Cross-Links Directing to the Enhanced Transfection via Controlled Intracellular Trafficking. Molecular Pharmaceutics. 2008. 5(6): p. 1080-1092.

335. Merdan T, Callahan J, Petersen H, Kunath K, Bakowsky U, Kopečková P, Kissel T, and Kopeček J. Pegylated Polyethylenimine−Fab‘ Antibody Fragment Conjugates for Targeted Gene Delivery to Human Ovarian Carcinoma Cells. Bioconjugate Chemistry. 2003. 14(5): p. 989-996.

336. Chiu S-J, Ueno NT, and Lee RJ. Tumor-targeted gene delivery via anti-HER2 antibody (trastuzumab, Herceptin®) conjugated polyethylenimine. Journal of Controlled Release. 2004. 97(2): p. 357-369.

337. Strehblow C, Schuster M, Moritz T, Kirch H-C, Opalka B, and Petri JB. Monoclonal antibody–polyethyleneimine conjugates targeting Her-2/neu or CD90 allow cell type-specific nonviral gene delivery. Journal of Controlled Release. 2005. 102(3): p. 737-747.

338. Li J, Cheng D, Yin T, Chen W, Lin Y, Chen J, Li R, and Shuai X. Copolymer of poly(ethylene glycol) and poly(l-lysine) grafting polyethylenimine through a reducible disulfide linkage for siRNA delivery. Nanoscale. 2014. 6(3): p. 1732-1740.

339. Saqafi B and Rahbarizadeh F. Polyethyleneimine-polyethylene glycol copolymer targeted by anti-HER2 nanobody for specific delivery of transcriptionally targeted tBid containing construct. Artificial Cells, Nanomedicine, and Biotechnology. 2019. 47(1): p. 501-511.

340. Lü J-M, Liang Z, Liu D, Zhan B, Yao Q, and Chen C. Two Antibody-Guided Lactic-co-Glycolic Acid-Polyethylenimine (LGA-PEI) Nanoparticle Delivery Systems for Therapeutic Nucleic Acids. Pharmaceuticals. 2021. 14(9): p. 841.

341. Kim T, Hyun HN, Heo R, Nam K, Yang K, Kim YM, Lee YS, An JY, Park JH, Choi KY, and Roh YH. Dual-targeting RNA nanoparticles for efficient delivery of polymeric siRNA to cancer cells. Chem Commun (Camb). 2020. 56(49): p. 6624-6627.

342. Liu S, Deng S, Li X, and Cheng D. Size- and Surface- Dual Engineered Small Polyplexes for Efficiently Targeting Delivery of siRNA. Molecules. 2021. 26(11): p. 3238.

343. Daniels TR, Bernabeu E, Rodriguez JA, Patel S, Kozman M, Chiappetta DA, Holler E, Ljubimova JY, Helguera G, and Penichet ML. The transferrin receptor and the targeted delivery of therapeutic agents against cancer. Biochim Biophys Acta. 2012. 1820(3): p. 291-317.

344. Schreiber S, Kampgen E, Wagner E, Pirkhammer D, Trcka J, Korschan H, Lindemann A, Dorffner R, Kittler H, Kasteliz F, Kupcu Z, Sinski A, Zatloukal K, Buschle M, Schmidt W, Birnstiel M, Kempe RE, Voigt T, Weber HA, Pehamberger H, Mertelsmann R, Brocker EB, Wolff K, and Stingl G. Immunotherapy of metastatic malignant melanoma by a vaccine consisting of autologous interleukin 2-transfected cancer cells: outcome of a phase I study. Hum Gene Ther. 1999. 10(6): p. 983-93.

345. Miyajima Y, Nakamura H, Kuwata Y, Lee JD, Masunaga S, Ono K, and Maruyama K. Transferrin-loaded nido-carborane liposomes: tumor-targeting boron delivery system for neutron capture therapy. Bioconjug Chem. 2006. 17(5): p. 1314-20.

346. Sasaki K, Kogure K, Chaki S, Nakamura Y, Moriguchi R, Hamada H, Danev R, Nagayama K, Futaki S, and Harashima H. An artificial virus-like nano carrier system: enhanced endosomal escape of nanoparticles via synergistic action of pH-sensitive fusogenic peptide derivatives. Anal Bioanal Chem. 2008. 391(8): p. 2717-27.

347. Tang J, Wang Q, Yu Q, Qiu Y, Mei L, Wan D, Wang X, Li M, and He Q. A stabilized retro-inverso peptide ligand of transferrin receptor for enhanced liposome-based hepatocellular carcinoma-targeted drug delivery. Acta Biomater. 2019. 83: p. 379-389.

348. Kim H and Muller WJ. The role of the epidermal growth factor receptor family in mammary tumorigenesis and metastasis. Exp Cell Res. 1999. 253(1): p. 78-87.

349. Nguyen PV, Allard-Vannier E, Chourpa I, and Hervé-Aubert K. Nanomedicines functionalized with anti-EGFR ligands for active targeting in cancer therapy: Biological strategy, design and quality control. International Journal of Pharmaceutics. 2021. 605: p. 120795.

350. Cristiano RJ and Roth JA. Epidermal growth factor mediated DNA delivery into lung cancer cells via the epidermal growth factor receptor. Cancer Gene Ther. 1996. 3(1): p. 4-10.

351. Li Z, Zhao R, Wu X, Sun Y, Yao M, Li J, Xu Y, and Gu J. Identification and characterization of a novel peptide ligand of epidermal growth factor receptor for targeted delivery of therapeutics. FASEB J. 2005. 19(14): p. 1978-85.

352. Xia W and Low PS. Folate-targeted therapies for cancer. J Med Chem. 2010. 53(19): p. 6811-24.

353. Park EK, Kim SY, Lee SB, and Lee YM. Folate-conjugated methoxy poly(ethylene glycol)/poly(epsilon-caprolactone) amphiphilic block copolymeric micelles for tumor-targeted drug delivery. J Control Release. 2005. 109(1-3): p. 158-68.

354. Griffioen AW, Coenen MJH, Damen CA, Hellwig SMM, van Weering DHJ, Vooys W, Blijham GH, and Groenewegen G. CD44 Is Involved in Tumor Angiogenesis; an Activation Antigen on Human Endothelial Cells. Blood. 1997. 90(3): p. 1150-1159.

355. Masjedi A, Ahmadi A, Atyabi F, Farhadi S, Irandoust M, Khazaei-Poul Y, Ghasemi Chaleshtari M, Edalati Fathabad M, Baghaei M, Haghnavaz N, Baradaran B, Hojjat-Farsangi M, Ghalamfarsa G, Sabz G, Hasanzadeh S, and Jadidi-Niaragh F. Silencing of IL-6 and STAT3 by siRNA Loaded Hyaluronate-N,N,N-trimethyl Chitosan Nanoparticles Potently Reduces Cancer Cell Progression. Int J Biol Macromol. 2020. 149: p. 487-500.

356. Sun Y, Li X, Zhang L, Liu X, Jiang B, Long Z, and Jiang Y. Cell Permeable NBD Peptide-Modified Liposomes by Hyaluronic Acid Coating for the Synergistic Targeted Therapy of Metastatic Inflammatory Breast Cancer. Mol Pharm. 2019. 16(3): p. 1140-1155.

357. Espinosa-Cano E, Huerta-Madroñal M, Cámara-Sánchez P, Seras-Franzoso J, Schwartz S, Abasolo I, San Román J, and Aguilar MR. Hyaluronic acid (HA)-coated naproxen-nanoparticles selectively target breast cancer stem cells through COX-independent pathways. Materials Science and Engineering: C. 2021. 124: p. 112024.

358. Yao H, Sun L, Li J, Zhou X, Li R, Shao R, Zhang Y, and Li L. A Novel Therapeutic siRNA Nanoparticle Designed for Dual-Targeting CD44 and Gli1 of Gastric Cancer Stem Cells. Int J Nanomedicine. 2020. 15: p. 7013-7034.

359. Nie Y, Schaffert D, Rödl W, Ogris M, Wagner E, and Günther M. Dual-targeted polyplexes: One step towards a synthetic virus for cancer gene therapy. Journal of Controlled Release. 2011. 152(1): p. 127-134.

360. Su B, Cengizeroglu A, Farkasova K, Viola JR, Anton M, Ellwart JW, Haase R, Wagner E, and Ogris M. Systemic TNFalpha gene therapy synergizes with liposomal doxorubicine in the treatment of metastatic cancer. Mol Ther. 2013. 21(2): p. 300-8.

361. Li J, Guo Y, Kuang Y, An S, Ma H, and Jiang C. Choline transporter-targeting and co-delivery system for glioma therapy. Biomaterials. 2013. 34(36): p. 9142-8.

362. Wang S, Reinhard S, Li C, Qian M, Jiang H, Du Y, Lachelt U, Lu W, Wagner E, and Huang R. Antitumoral Cascade-Targeting Ligand for IL-6 Receptor-Mediated Gene Delivery to Glioma. Mol Ther. 2017. 25(7): p. 1556-1566.

363. Urnauer S, Schmohl KA, Tutter M, Schug C, Schwenk N, Morys S, Ziegler S, Bartenstein P, Clevert D-A, Wagner E, and Spitzweg C. Dual-targeted NIS polyplexes—a theranostic strategy toward tumors with heterogeneous receptor expression. Gene Therapy. 2019. 26(3): p. 93-108.

364. Spellerberg R, Benli-Hoppe T, Kitzberger C, Berger S, Schmohl KA, Schwenk N, Yen H-Y, Zach C, Schilling F, Weber WA, Kälin RE, Glass R, Nelson PJ, Wagner E, and Spitzweg C. Selective sodium iodide symporter (NIS) genetherapy of glioblastoma mediatedby EGFR-targeted lipopolyplexes. Molecular Therapy - Oncolytics. 2021. 23: p. 432-446.

365. Tai Z, Ma J, Ding J, Pan H, Chai R, Zhu C, Cui Z, Chen Z, and Zhu Q. Aptamer-Functionalized Dendrimer Delivery of Plasmid-Encoding lncRNA MEG3 Enhances Gene Therapy in Castration-Resistant Prostate Cancer. International journal of nanomedicine. 2020. 15: p. 10305-10320.

366. Leng Q and Mixson AJ. Small Interfering RNA Targeting Raf-1 Inhibits Tumor Growth In Vitro and In Vivo. Cancer Gene Ther. 2005. 12(8): p. 682-90.

367. Grzelinski M, Urban-Klein B, Martens T, Lamszus K, Bakowsky U, Hobel S, Czubayko F, and Aigner A. RNA interference-mediated gene silencing of pleiotrophin through polyethylenimine-complexed small interfering RNAs in vivo exerts antitumoral effects in glioblastoma xenografts. Hum.Gene Ther. 2006. 17(7): p. 751-766.

368. Heidel JD, Liu JY, Yen Y, Zhou B, Heale BS, Rossi JJ, Bartlett DW, and Davis ME. Potent siRNA inhibitors of ribonucleotide reductase subunit RRM2 reduce cell proliferation in vitro and in vivo. Clin Cancer Res. 2007. 13(7): p. 2207-15.

369. Wang D, Wang T, Liu J, Yu H, Jiao S, Feng B, Zhou F, Fu Y, Yin Q, Zhang P, Zhang Z, Zhou Z, and Li Y. Acid-Activatable Versatile Micelleplexes for PD-L1 Blockade-Enhanced Cancer Photodynamic Immunotherapy. Nano Lett. 2016. 16(9): p. 5503-13.

370. Zheng M, Liu Y, Wang Y, Zhang D, Zou Y, Ruan W, Yin J, Tao W, Park JB, and Shi B. ROS-Responsive Polymeric siRNA Nanomedicine Stabilized by Triple Interactions for the Robust Glioblastoma Combinational RNAi Therapy. Adv Mater. 2019. 31(37): p. e1903277.

371. Ibrahim AF, Weirauch U, Thomas M, Grunweller A, Hartmann RK, and Aigner A. MicroRNA replacement therapy for miR-145 and miR-33a is efficacious in a model of colon carcinoma. Cancer Res. 2011. 71(15): p. 5214-24.

372. Shir A, Ogris M, Roedl W, Wagner E, and Levitzki A. EGFR-Homing dsRNA Activates Cancer-Targeted Immune Response and Eliminates Disseminated EGFR-Overexpressing Tumors in Mice. Clin Cancer Res. 2011. 17(5): p. 1033-43.

373. Schaffert D, Kiss M, Rodl W, Shir A, Levitzki A, Ogris M, and Wagner E. Poly(I:C)-mediated tumor growth suppression in EGF-receptor overexpressing tumors using EGF-polyethylene glycol-linear polyethylenimine as carrier. Pharm Res. 2011. 28(4): p. 731-41.

374. Uchida S, Kinoh H, Ishii T, Matsui A, Tockary TA, Takeda KM, Uchida H, Osada K, Itaka K, and Kataoka K. Systemic delivery of messenger RNA for the treatment of pancreatic cancer using polyplex nanomicelles with a cholesterol moiety. Biomaterials. 2016. 82: p. 221-228.

375. Li X, Cai L, Chen H, Zhang Q, Zhang S, Wang Y, Dong Y, Cheng H, and Qi J. Inhibitor of growth 4 induces growth suppression and apoptosis in glioma U87MG. Pathobiology. 2009. 76(4): p. 181-92.

376. Wang W, Saeed M, Zhou Y, Yang L, Wang D, and Yu H. Non-viral gene delivery for cancer immunotherapy. J Gene Med. 2019. 21(7): p. e3092.

377. Zatloukal K, Schmidt W, Cotten M, Wagner E, Stingl G, and Birnstiel ML. Somatic gene therapy for cancer: the utility of transferrinfection in generating 'tumor vaccines'. Gene. 1993. 135(1-2): p. 199-207.

378. Abbasi S, Uchida S, Toh K, Tockary TA, Dirisala A, Hayashi K, Fukushima S, and Kataoka K. Co-encapsulation of Cas9 mRNA and guide RNA in polyplex micelles enables genome editing in mouse brain. Journal of Controlled Release. 2021. 332: p. 260-268.

379. Rybakova Y, Kowalski PS, Huang Y, Gonzalez JT, Heartlein MW, DeRosa F, Delcassian D, and Anderson DG. mRNA Delivery for Therapeutic Anti-HER2 Antibody Expression In Vivo. Molecular Therapy. 2019. 27(8): p. 1415-1423.

380. Grabbe S, Haas H, Diken M, Kranz LM, Langguth P, and Sahin U. Translating nanoparticulate-personalized cancer vaccines into clinical applications: case study with RNA-lipoplexes for the treatment of melanoma. Nanomedicine (Lond). 2016. 11(20): p. 2723-2734.

381. Zhang H, You X, Wang X, Cui L, Wang Z, Xu F, Li M, Yang Z, Liu J, Huang P, Kang Y, Wu J, and Xia X. Delivery of mRNA vaccine with a lipid-like material potentiates antitumor efficacy through Toll-like receptor 4 signaling. Proceedings of the National Academy of Sciences. 2021. 118(6): p. e2005191118.

382. Yoo YJ, Lee CH, Park SH, and Lim YT. Nanoparticle-based delivery strategies of multifaceted immunomodulatory RNA for cancer immunotherapy. J Control Release. 2022. 343: p. 564-583.

383. Ho T-C, Kim HS, Chen Y, Li Y, LaMere MW, Chen C, Wang H, Gong J, Palumbo CD, Ashton JM, Kim H-W, Xu Q, Becker MW, and Leong KW. Scaffold-mediated CRISPR-Cas9 delivery system for acute myeloid leukemia therapy. Science advances. 2021. 7(21): p. eabg3217.

384. Nie JJ, Liu Y, Qi Y, Zhang N, Yu B, Chen DF, Yang M, and Xu FJ. Charge-reversal nanocomolexes-based CRISPR/Cas9 delivery system for loss-of-function oncogene editing in hepatocellular carcinoma. J Control Release. 2021. 333: p. 362-373.

385. Rosenblum D, Gutkin A, Kedmi R, Ramishetti S, Veiga N, Jacobi AM, Schubert MS, Friedmann-Morvinski D, Cohen ZR, Behlke MA, Lieberman J, and Peer D. CRISPR-Cas9 genome editing using targeted lipid nanoparticles for cancer therapy. Sci Adv. 2020. 6(47).

386. Liu Q, Cai J, Zheng Y, Tan Y, Wang Y, Zhang Z, Zheng C, Zhao Y, Liu C, An Y, Jiang C, Shi L, Kang C, and Liu Y. NanoRNP Overcomes Tumor Heterogeneity in Cancer Treatment. Nano Lett. 2019. 19(11): p. 7662-7672.

387. Vetter V, Yazdi M, Gialdini I, Pöhmerer J, Seidl J, Miriam Höhn, Lamb D, and Wagner E. Ionic Coating of siRNA Polyplexes with cRGD−PEG−Hyaluronic Acid to Modulate Serum Stability and In Vivo Performance. Biochemistry. 2025. DOI: https://doi.org/10.1021/acs.biochem.4c00650

388. Friedrich M and Aigner A. Therapeutic siRNA: State-of-the-Art and Future Perspectives. BioDrugs. 2022. 36(5): p. 549-571.

389. Narasipura EA, VanKeulen-Miller R, Ma Y, and Fenton OS. Ongoing Clinical Trials of Nonviral siRNA Therapeutics. Bioconjug Chem. 2023. 34(7): p. 1177-1197.

390. Sehgal I, Eells K, and Hudson I. A Comparison of Currently Approved Small Interfering RNA (siRNA) Medications to Alternative Treatments by Costs, Indications, and Medicaid Coverage. Pharmacy (Basel). 2024. 12(2): p. 58.

391. Leng Q and Mixson AJ. Small interfering RNA targeting Raf-1 inhibits tumor growth in vitro and in vivo. Cancer Gene Ther. 2005. 12(8): p. 682-690.

392. Leng Q, Anand A, and Mixson AJ. A Facile and Promising Delivery Platform for siRNA to Solid Tumors. Molecules. 2024. 29(23): p. 5541.

393. Yang Y, Li J, Liu F, and Huang L. Systemic Delivery of siRNA via LCP Nanoparticle Efficiently Inhibits Lung Metastasis. Mol Ther. 2012. 20(3): p. 609-15.

394. Lee DJ, Kessel E, Edinger D, He D, Klein PM, Voith von Voithenberg L, Lamb DC, Lachelt U, Lehto T, and Wagner E. Dual Antitumoral Potency of EG5 siRNA Nanoplexes Armed with Cytotoxic Bifunctional Glutamyl-Methotrexate Targeting Ligand. Biomaterials. 2016. 77: p. 98-110.

395. Rosenblum D, Joshi N, Tao W, Karp JM, and Peer D. Progress and Challenges Towards Targeted Delivery of Cancer Therapeutics. Nat Commun. 2018. 9(1): p. 1410.

396. Karimov M, Schulz M, Kahl T, Noske S, Kubczak M, Gockel I, Thieme R, Büch T, Reinert A, Ionov M, Bryszewska M, Franke H, Krügel U, Ewe A, and Aigner A. Tyrosine-modified Linear PEIs for Highly Efficacious and Biocompatible siRNA Delivery In Vitro and In Vivo. Nanomedicine. 2021. 36: p. 102403.

397. Deshayes S, Konate K, Rydström A, Crombez L, Godefroy C, Milhiet PE, Thomas A, Brasseur R, Aldrian G, Heitz F, Muñoz-Morris MA, Devoisselle JM, and Divita G. Self-Assembling Peptide-Based Nanoparticles for siRNA Delivery in Primary Cell Lines. Small. 2012. 8(14): p. 2184-8.

398. Felgner PL, Barenholz Y, Behr JP, Cheng SH, Cullis P, Huang L, Jessee JA, Seymour L, Szoka F, Thierry AR, Wagner E, and Wu G. Nomenclature for Synthetic Gene Delivery Systems. Hum Gene Ther. 1997. 8(5): p. 511-2.

399. Wagner E. Polymers for siRNA Delivery: Inspired by Viruses to be Targeted, Dynamic, and Precise. Acc Chem Res. 2012. 45(7): p. 1005-13.

400. Feldmann DP, Cheng Y, Kandil R, Xie Y, Mohammadi M, Harz H, Sharma A, Peeler DJ, Moszczynska A, Leonhardt H, Pun SH, and Merkel OM. In Vitro and In Vivo Delivery of siRNA via VIPER Polymer System to Lung Cells. J Control Release. 2018. 276: p. 50-58.

401. Berger S, Lachelt U, and Wagner E. Dynamic Carriers for Therapeutic RNA Delivery. Proc Natl Acad Sci U S A. 2024. 121(11): p. e2307799120.

402. Oupicky D, Ogris M, Howard KA, Dash PR, Ulbrich K, and Seymour LW. Importance of Lateral and Steric Stabilization of Polyelectrolyte Gene Delivery Vectors for Extended Systemic Circulation. Mol Ther. 2002. 5(4): p. 463-472.

403. Fella C, Walker GF, Ogris M, and Wagner E. Amine-Reactive Pyridylhydrazone-Based PEG Reagents for pH-Reversible PEI Polyplex Shielding. Eur J Pharm Sci. 2008. 34(4-5): p. 309-20.

404. Klein PM, Klinker K, Zhang W, Kern S, Kessel E, Wagner E, and Barz M. Efficient Shielding of Polyplexes Using Heterotelechelic Polysarcosines. Polymers (Basel). 2018. 10(6): p. 689.

405. Finsinger D, Remy JS, Erbacher P, Koch C, and Plank C. Protective Copolymers for Nonviral Gene Vectors: Synthesis, Vector Characterization and Application in Gene Delivery. Gene Ther. 2000. 7(14): p. 1183-1192.

406. Sethuraman VA, Na K, and Bae YH. pH-Responsive Sulfonamide/PEI System for Tumor Specific Gene Delivery: An In Vitro Study. Biomacromolecules. 2006. 7(1): p. 64-70.

407. Egorova A, Chepanov S, Selkov S, Kogan I, and Kiselev A. Targeted Gene Delivery to Muscle Cells In Vitro and In Vivo Using Electrostatically Stabilized DNA—Peptide Complexes. Scientia Pharmaceutica. 2024. 92(3): p. 51.

408. Tang Z, You X, Xiao Y, Chen W, Li Y, Huang X, Liu H, Xiao F, Liu C, Koo S, Kong N, and Tao W. Inhaled mRNA Nanoparticles Dual-Targeting Cancer Cells and Macrophages in the Lung for Effective Transfection. Proc Natl Acad Sci U S A. 2023. 120(44): p. e2304966120.

409. Chen L, Fu C, Zhang Q, He C, Zhang F, and Wei Q. The Role of CD44 in Pathological Angiogenesis. FASEB J. 2020. 34(10): p. 13125-13139.

410. Almalik A, Benabdelkamel H, Masood A, Alanazi IO, Alradwan I, Majrashi MA, Alfadda AA, Alghamdi WM, Alrabiah H, Tirelli N, and Alhasan AH. Hyaluronic Acid Coated Chitosan Nanoparticles Reduced the Immunogenicity of the Formed Protein Corona. Sci Rep. 2017. 7(1): p. 10542.

411. Tomasetti L and Breunig M. Preventing Obstructions of Nanosized Drug Delivery Systems by the Extracellular Matrix. Adv Healthc Mater. 2018. 7(3): p. 1700739.

412. Agard NJ, Prescher JA, and Bertozzi CR. A Strain-Promoted [3 + 2] Azide-Alkyne Cycloaddition for Covalent Modification of Biomolecules in Living Systems. J Am Chem Soc. 2004. 126(46): p. 15046-7.

413. Thalmayr S, Grau M, Peng L, Pohmerer J, Wilk U, Folda P, Yazdi M, Weidinger E, Burghardt T, Hohn M, Wagner E, and Berger S. Molecular Chameleon Carriers for Nucleic Acid Delivery: The Sweet Spot between Lipoplexes and Polyplexes. Adv Mater. 2023. 35(25): p. e2211105.

414. Schaffert D, Badgujar N, and Wagner E. Novel Fmoc-Polyamino Acids for Solid-Phase Synthesis of Defined Polyamidoamines. Org Lett. 2011. 13(7): p. 1586-9.

415. Reinhard S, Zhang W, and Wagner E. Optimized Solid-Phase-Assisted Synthesis of Oleic Acid Containing siRNA Nanocarriers. ChemMedChem. 2017. 12(17): p. 1464-1470.

416. Hendrix J, Baumgärtel V, Schrimpf W, Ivanchenko S, Digman MA, Gratton E, Kräusslich HG, Müller B, and Lamb DC. Live-Cell Observation of Cytosolic HIV-1 Assembly Onset Reveals RNA-Interacting Gag Oligomers. J Cell Biol. 2015. 210(4): p. 629-46.

417. Müller BK, Zaychikov E, Brauchle C, and Lamb DC. Pulsed Interleaved Excitation. Biophys J. 2005. 89(5): p. 3508-22.

418. Schrimpf W, Barth A, Hendrix J, and Lamb DC. PAM: A Framework for Integrated Analysis of Imaging, Single-Molecule, and Ensemble Fluorescence Data. Biophys J. 2018. 114(7): p. 1518-1528.

419. Ivanchenko S and Lamb DC. Fluorescence Correlation Spectroscopy: Principles and Developments. in Supramolecular Structure and Function 10. 2011. Dordrecht: Springer Netherlands.

420. Schindelin J, Arganda-Carreras I, Frise E, Kaynig V, Longair M, Pietzsch T, Preibisch S, Rueden C, Saalfeld S, Schmid B, Tinevez JY, White DJ, Hartenstein V, Eliceiri K, Tomancak P, and Cardona A. Fiji: An Open-Source Platform for Biological-Image Analysis. Nat Methods. 2012. 9(7): p. 676-82.

421. Gilles JF, Dos Santos M, Boudier T, Bolte S, and Heck N. DiAna, An ImageJ Tool for Object-Based 3D Co-localization and Distance Analysis. Methods. 2017. 115: p. 55-64.

422. Wang X-L, Xu R, Wu X, Gillespie D, Jensen R, and Lu Z-R. Targeted Systemic Delivery of a Therapeutic siRNA with a Multifunctional Carrier Controls Tumor Proliferation in Mice. Molecular Pharmaceutics. 2009. 6(3): p. 738-746.

423. Martin I, Dohmen C, Mas-Moruno C, Troiber C, Kos P, Schaffert D, Lachelt U, Teixido M, Gunther M, Kessler H, Giralt E, and Wagner E. Solid-Phase-Assisted Synthesis of Targeting Peptide-PEG-Oligo(ethane amino)amides for Receptor-Mediated Gene Delivery. Org Biomol Chem. 2012. 10(16): p. 3258-68.

424. Yi Y, Kim HJ, Mi P, Zheng M, Takemoto H, Toh K, Kim BS, Hayashi K, Naito M, Matsumoto Y, Miyata K, and Kataoka K. Targeted Systemic Delivery of siRNA to Cervical Cancer Model Using Cyclic RGD-Installed Unimer Polyion Complex-Assembled Gold Nanoparticles. J Control Release. 2016. 244(Pt B): p. 247-256.

425. Jin H, Zhang C, Zwahlen M, von Feilitzen K, Karlsson M, Shi M, Yuan M, Song X, Li X, Yang H, Turkez H, Fagerberg L, Uhlén M, and Mardinoglu A. Systematic Transcriptional Analysis of Human Cell Lines for Gene Expression Landscape and Tumor Representation. Nat Commun. 2023. 14(1): p. 5417.

426. Human Protein Atlas 2024-08-20]; Available from: proteinatlas.org.

427. Berger S, Krhač Levačić A, Hörterer E, Wilk U, Benli-Hoppe T, Wang Y, Öztürk Ö, Luo J, and Wagner E. Optimizing pDNA Lipo-polyplexes: A Balancing Act between Stability and Cargo Release. Biomacromolecules. 2021. 22(3): p. 1282-1296.

428. Sikora A, Shard AG, and Minelli C. Size and Zeta-Potential Measurement of Silica Nanoparticles in Serum Using Tunable Resistive Pulse Sensing. Langmuir. 2016. 32(9): p. 2216-24.

429. Magde D, Elson E, and Webb WW. Thermodynamic Fluctuations in a Reacting System—Measurement by Fluorescence Correlation Spectroscopy. Phys. Rev. Lett. 1972. 29(11): p. 705-708.

430. Schwille P, Meyer-Almes F, and Rigler R. Dual-Color Fluorescence Cross-Correlation Spectroscopy for Multicomponent Diffusional Analysis in Solution. Biophys J. 1997. 72: p. 1878-1886.

431. Kim SA, Heinze KG, Bacia K, Waxham MN, and Schwille P. Two-Photon Cross-Correlation Analysis of Intracellular Reactions with Variable Stoichiometry. Biophys J. 2005. 88(6): p. 4319-36.

432. Bhattacharya D, Svechkarev D, Souchek JJ, Hill TK, Taylor MA, Natarajan A, and Mohs AM. Impact of Structurally Modifying Hyaluronic Acid on CD44 Interaction. J Mater Chem B. 2017. 5(41): p. 8183-8192.

433. Kwon MY, Wang C, Galarraga JH, Pure E, Han L, and Burdick JA. Influence of Hyaluronic Acid Modification on CD44 Binding towards the Design of Hydrogel Biomaterials. Biomaterials. 2019. 222: p. 119451.

7 Publications

7.1 Review article

Vetter VC, Wagner E, *Targeting nucleic acid-based therapeutics to tumors: Challenges and strategies for polyplexes*, J Control Release (2022), 346, 110-135

7.2 Research articles

Yazdi M, Pöhmerer J, Hasanzadeh Kafshgari M, Seidl J, Grau M, Höhn M, **Vetter V**, Hoch CC, Wollenberg B, Multhoff G, Bashiri Dezfouli A, Wagner E. *In Vivo Endothelial Cell Gene Silencing by siRNA-LNPs Tuned with Lipoamino Bundle Chemical and Ligand Targeting*, Small (2024), 20, e2400643.

Vetter VC, Yazdi M, Gialdini I, Pöhmerer J, Seidl J, Höhn M, Lamb DC, Wagner E. *Ionic Coating of siRNA Polyplexes with cRGD-PEG-Hyaluronic Acid to Modulate Serum Stability and In Vivo Performance*, Biochemistry (2025), DOI: https://doi.org/10.1021/acs.biochem.4c00650.

8 Acknowledgments

First and foremost, I would like to express my deepest gratitude to my supervisor, Prof. Dr. Ernst Wagner, for granting me the opportunity to join his research group and for his invaluable guidance throughout this thesis. His profound expertise in nucleic acid delivery, combined with his enthusiasm and insightful feedback, has been essential to my growth as a researcher and to the progression of this work.

I am also immensely grateful to my colleagues for their unwavering support, engaging discussions, fruitful collaborations, and always motivating each other. Ricarda, Franzi, Johanna, Melina, Eric, Paul, and Sophie – you were incredible teammates and have also become true friends. I will genuinely miss the time we spent together in the lab, in the tea kitchen, and at events like *Skilager*, *Wandertag*, and *Wiesn*, as well as our *Büro-Einweihungsfeier*, Franzi's office haircuts and lava lamp nights at Buena Vista bar. It was a fun and unforgettable experience with all of you.
Special thanks go to Mina, the best office partner I could have asked for. Your collaborative spirit, generosity, and frequent supply of chocolate were invaluable, but most of all, I sincerely appreciated your constant support and motivation. To Jana, thank you for your exceptional work in managing our mouse facility and coordinating our *in vivo* experiments, which made large parts of this research possible. I greatly appreciated your and Mina's dedication, even during holiday and weekend shifts.
I would also like to thank Simone, Janin, Anni, Tobi, Alex, Teo, and all other members of AK Wagner. Your inspiring discussions, valuable collaborations, and the positive, supportive environment you helped create made my time in the lab truly rewarding. A heartfelt thank you also goes to Wolfgang, Lorina, Miriam, Olga and Melinda, whose dedication behind the scenes ensured the smooth running of our lab. Your hard work and reliability have been invaluable.

Finally, I cannot express enough gratitude to my family and friends. To my parents, thank you for your unconditional support, encouraging words, and belief in me. Without you, I would not have made it this far. And to Ben, thank you for being by my side through it all – for enduring the ups and downs and for being one of my greatest supporters in everything I do. I am genuinely grateful to have you in my life.